Distinct dorsal and ventral basal ganglia contributions to value-based decision-making in health and parkinsonism

Milesa Simic

université de BORDEAUX

THÈSE PRÉSENTÉE

POUR OBTENIR LE GRADE DE

DOCTEUR DE

L'UNIVERSITÉ DE BORDEAUX

ÉCOLE DOCTORALE : SCIENCES DE LA VIE ET DE LA SANTE

SPÉCIALITÉ : NEUROSCIENCES

Par Milesa SIMIC

Rôle des circuits dorsal et ventral des ganglions de la base dans les processus décisionnels en conditions saine et parkinsonienne

Sous la direction de : Marc DEFFAINS

Soutenue le 6 mai 2026

Membres du jury :

Mme Yulia WORBE	Professeure des universités - praticienne hospitalière, Institut du Cerveau (Paris)	Rapporteure
M. David THURA	Chargé de recherche, Centre de Recherche en Neurosciences de Lyon (Bron)	Rapporteur
Mme Shauna PARKES	Directrice de recherche, Institut de Neurosciences Cognitives et Intégratives d'Aquitaine (Bordeaux)	Examinatrice, Présidente du jury
M. Jérôme MUNUERA	Chargé de recherche, Institut du Cerveau (Paris)	Examinateur

Abstracts in french and in english

Rôle des circuits dorsal et ventral des ganglions de la base dans les processus décisionnels en conditions saine et parkinsonienne

Résumé

La prise de décision basée sur la valeur repose sur des processus qui évaluent les options, guident la sélection et l'exécution des actions, puis en évaluent les conséquences en comparant les résultats attendus et obtenus pour ajuster les choix. Ces processus reposent sur des réseaux cérébraux distribués incluant les ganglions de la base (GB). Les GB sont des structures sous-corticales interconnectées modulées par la dopamine du mésencéphale et organisées en circuits cortico-sous-corticaux partiellement parallèles le long d'un axe dorso-ventral. Le circuit dorsal est associé au contrôle moteur et cognitif alors que le ventral est impliqué dans l'évaluation des options/résultats et la motivation. Des dysfonctionnements de ces circuits ont été impliqués dans les déficits décisionnels de la maladie de Parkinson (MP). Cependant, leur rôle dans la prise de décision en conditions saines et pathologiques reste mal compris.

Pour répondre à cette question, nous avons réalisé des enregistrements électrophysiologiques avant et après induction de la MP dans plusieurs noyaux clés des GB (noyau caudé, noyau accumbens (NAc), globus pallidus externe et pallidum ventral) chez des primates non humains réalisant une tâche de décision basée sur la valeur, où les valeurs attendues (VA) dépendaient de la magnitude et de la probabilité de récompense pouvant correspondre à des gains ou pertes. Le comportement variait en fonction de la VA: les options avec des VA élevées étaient choisies plus fréquemment, entraînaient moins d'omissions et des décisions plus rapides. Les enregistrements unitaires ont révélé un gradient fonctionnel: les régions dorsales encodaient préférentiellement les paramètres liés à l'action, alors que l'encodage de la valeur augmentait ventralement. Les représentations de la VA étaient non linéaires avec une sensibilité maximale à la transition entre pertes et gains. L'analyse de population a révélé des dynamiques de trajectoires neuronales dépendantes de la VA, particulièrement dans les régions ventrales, tandis que les signaux spatiaux étaient plus ségrégés dorsalement. L'analyse de décodage a confirmé cette dissociation: la VA était mieux décodée par les populations ventrales et les paramètres spatiaux par les dorsales.

Pour examiner les déficits décisionnels dans la MP, nous avons induit une déplétion dopaminergique progressive par traitement chronique à faible dose de MPTP et comparé les stades sain, précoce et tardif de la maladie. La perte de dopamine a entraîné un désengagement dans la tâche et une diminution de la vigueur motrice, accompagnés de modifications de l'encodage neuronal malgré des capacités décisionnelles préservées. Les effets les plus marqués ont été observés dans le striatum ventral avec une réduction de la fraction de neurones codant la valeur dans le NAc au stade tardif, tandis que les représentations pallidales des variables décisionnelles restaient largement intactes. L'analyse des variations d'amplitude de réponse

neuronale (gain neuronal) a révélé une co-variation entre le désengagement et l'augmentation d'états neuronaux de faible gain similaires à ceux des omissions. La déplétion dopaminergique pourrait déplacer l'état neuronal global du réseau d'un état engagé vers un état désengagé plutôt qu'altérer l'évaluation des options.

Ce travail met en évidence une organisation fonctionnelle des GB dans la décision basée sur la valeur: les circuits ventraux encodent préférentiellement la valeur, avec une sensibilité à la transition entre les pertes et les gains tandis que les circuits dorsaux encodent davantage les variables liées au choix. La perte de dopamine affecte principalement la motivation et l'engagement via des modifications des états neuronaux globaux et une vulnérabilité sélective du striatum ventral, tandis que les populations pallidales pourraient contribuer au maintien des performances décisionnelles, en maintenant les représentations des variables de décision pertinentes pour la tâche.

Mots clés: **ganglions de la base, prise de décision, valeur, électrophysiologie, primate non humain, maladie de Parkinson**

Distinct dorsal and ventral basal ganglia contributions to value-based decision-making in health and parkinsonism

Abstract

Value-based decision-making (DM) relies on processes that evaluate options by assigning them a subjective value, guide action selection and execution, and evaluate consequences by comparing expected and obtained outcomes to update decisions. These processes rely on coordinated activity within distributed brain networks including the basal ganglia (BG). The BG comprise interconnected nuclei modulated by midbrain dopamine and organized into partially overlapping cortico-subcortical circuits along a dorsal-ventral axis. Dorsal circuits are associated with motor and cognitive control, while ventral circuits are linked to valuation/evaluation and motivation. Dysfunctions of these circuits have been implicated in DM deficits observed in Parkinson's disease (PD). However, their distinct contribution to value-based DM in healthy and pathological conditions remains unclear.

To address this question, we performed electrophysiological recordings before and after PD induction in key BG nuclei (caudate nucleus, nucleus accumbens (NAc), external globus pallidus and ventral pallidum) in non-human primates performing a value-based DM task in which expected values (EVs) varied with reward magnitude and probability. We examined how decision variables (value- and action-related signals) associated with losses and gains are encoded and organized across BG structures. Behavior scaled with EV: higher EV options were chosen more accurately, elicited fewer omissions and were associated with faster decision times, linking valuation to behavioral engagement and vigor. Single-unit recordings revealed a functional gradient across structures: dorsal regions preferentially encoded action-related parameters, while value encoding increased ventrally. EV representations were non-linear with maximal

sensitivity at the loss-gain transition. Population-level neural dynamics revealed distinct neural trajectory geometries across EVs, particularly at this transition in ventral regions, where trajectory separation and divergence increased, while spatial signals were more segregated dorsally. Decoding analyses supported this dissociation: EV was best decoded from ventral populations, whereas spatial parameters were most accurately decoded from dorsal populations. Thus, representation of value and action signals across BG structures is distributed but organized.

To examine DM deficits in PD, we induced progressive dopaminergic depletion using chronic low-dose 1-methyl-4-phenyl-1,2,3,6-tetrahydropyridine (MPTP) and compared healthy, early, and late disease stages. Dopamine loss led to marked task disengagement and reduced movement vigor, accompanied by changes in neuronal encoding despite preserved decision performance. The most pronounced alterations occurred in the ventral striatum, including a late-stage decrease in value encoding in NAc neurons, while pallidal representations of decision variables were largely intact. Analysis of cue-evoked changes in neural response magnitude (neural gain) showed maintained differentiation between performed and omitted trials and revealed systematic co-shifts between disengagement and the increasing prevalence of omission-like low-gain neural states across disease stages. Dopamine depletion may therefore shift global network states (from engaged to disengaged) rather than abolish valuation.
Together, this work supports a functional organization of the BG during value-based DM in which ventral circuits preferentially encode value, including non-linear loss-gain sensitivity, while dorsal circuits preferentially encode action-related variables. Dopaminergic depletion primarily affects motivation and task engagement through shifts in global neural states and selective vulnerability of ventral striatal circuits, while pallidal populations may help sustain accurate decision performance by maintaining representations of task-relevant decision variables.

Keywords: basal ganglia, decision-making, value, electrophysiology, non-human primate, Parkinson's disease

Institut des Maladies Neurodégénératives

IMN, CNRS UMRS5293, Centre Broca, 146 rue Léo Saignat, 33076 Bordeaux cedex

Dedication

In loving memory of my mother, Ljiljana.

Acknowledgments

First of all, I would like to warmly thank the members of my jury, Pr. Yulia Worbe, Dr. David Thura, Dr. Shauna Parkes, and Dr. Jérôme Munuera, for agreeing to evaluate my work. I am very grateful for your time and for accommodating this defense in your busy schedules. I also hope you will forgive the length of this manuscript.

I would also like to acknowledge the institutions that made this work financially possible: the *Agence Nationale de la Recherche*, which funded the first three years of my PhD, and *France Parkinson*, which generously supported a fourth-year extension.

This work was carried out at the Institut des Maladies Neurodégénératives (CNRS UMR 5293). I would like to thank the director of the institute, Thomas Boraud, for his support and scientific input. Thank you as well for accompanying me to my first SfN meeting, and, more personally, for not firing me and thus sparing me from one of my nightmares.

I am especially grateful to my supervisor, Marc Deffains, for giving me the opportunity to work on a topic I am truly passionate about. Thank you for your trust, patience, support, and understanding throughout this journey. I am also deeply thankful for the many hours you dedicated to revising this manuscript, your corrections and suggestions significantly improved its quality.

I would like to thank Team 4 and its directors, Nicolas Mallet and Arthur Leblois, for providing such a stimulating and supportive research environment. Nicolas, I will miss your galette des rois, and Arthur, your gatherings were always memorable. I am also grateful to all past and present members of the team. A special thanks to Dominique Guehl for our valuable interactions, Carmen Guerrero for your kind words, and to Aude Retailleau, although no longer officially part of the team, you are still very much present (and not just because your office is down the hallway). Thank you for the shared moments and your support.

I would like to give special thanks to the “monkey team”: Hugues Orignac, Tho Hai Nguyen, and Yasmin Guerra, for your essential help during surgeries and for taking such great care of the animals. Thank you also for making this work enjoyable, even during the more challenging times. Yasmin, I wish you all the best for the rest of your PhD, you will do great (better than me).

I cannot name everyone who has supported me outside of work, but I would like to thank, among others, Miloš, Maya, Magali, Thomas. You know me well enough to know that I am not the most expressive, but your support has meant a great deal to me. A special thanks goes to my dog, Oscar, who, although probably unaware of it, helped me stay sane during the writing process, especially through our walks in the forest.

Thanks also to all the people I met throughout my studies and professional experiences who, in one way or another, helped shape the path that brought me here, notably Masato, Serge, Carole, Sandrine, Atika, Angélique, Aziz, and many more — some of whom became much more than colleagues over time. I would also like to mention Damien, Emma, and Julie, whose friendship has accompanied me throughout this journey.

Finally, I would like to thank the monkeys I worked with, Havane, Fanélie, Chouros, and France, without whom this work would not have been possible.

I am writing these acknowledgments just before submitting the manuscript, and I am sure I have unintentionally omitted some people. I sincerely apologize for any omissions and thank everyone who contributed, directly or indirectly, to this work.

Table of contents

List of abbreviations

ACC: anterior cingulate cortex

BG: basal ganglia
BOLD: blood-oxygen-level dependent

CBG: cortico-basal ganglia
CD: caudate nucleus
CR: calretinin
CT: computed tomography

DA: dopamine
DAB: 3,3'-diaminobenzidine
dACC: dorsal anterior cingulate cortex
DAN: dopaminergic neuron
DBS: deep brain stimulation
dCD: dorsal caudate
dGPe: dorsal external globus pallidus
dlPFC: dorsolateral prefrontal cortex
DLS: dorsolateral striatum
DM: decision-making
dmPFC: dorsomedial prefrontal cortex
DMS: dorsomedial striatum
DRT: dopamine replacement therapy
DS: dorsal striatum
DT: decision time

EV: expected value

fMRI: functional magnetic resonance imaging
FR: firing rate
FSI: fast-spiking interneurons

GABA: gamma-aminobutyric acid
GPe: external globus pallidus
GPi: internal globus pallidus

HFD: high-frequency discharge
HRP: horseradish peroxidase

LDA: linear discriminant analysis
LFD: low-frequency discharge
LFP: local field potential
lOFC: lateral orbitofrontal cortex
lPFC: lateral prefrontal cortex
LTS: low-threshold spiking

M1: primary motor cortex
MLR: multiple linear regression
mOFC: medial orbitofrontal cortex
MPTP: 1-methyl-4-phenyl-1,2,3,6-tetrahydropyridine
MRI: magnetic resonance imaging
MSN: medium spiny neuron
MT: movement time
MUA: multi-unit activity

NAc: nucleus accumbens
NHP: non-human primate

OFC: orbitofrontal cortex

PBS: phosphate-buffered saline
PC: principal component
PCA: principal component analysis
PD: Parkinson's disease
PFC: prefrontal cortex
PV: parvalbumin

RL: reinforcement learning
RPE: reward prediction error
RPV: refractory period violation
RT: reaction time

SMA: supplementary motor area
SNc: substantia nigra pars compacta
SNr: substantia nigra pars reticulata
SNR: signal-to-noise ratio
SOM: somatostatin
SPN: striatal projection neuron
STN: subthalamic nucleus
SUA: single-unit activity

TAN: tonically active neuron
TH: tyrosine hydroxylase

vCD: ventral caudate
vGPe: ventral external globus pallidus
VIF: variance inflation factor
vmPFC: ventromedial prefrontal cortex
VP: ventral pallidum
VS: ventral striatum
VTA: ventral tegmental area

List of tables

List of figures

Part 1 Introduction

Chapter 1 Basal ganglia anatomy

Denny-Brown was the first to define the basal ganglia (BG) as an independent motor control system in 1946 (Denny-Brown, 1946). He proposed a framework in which two parallel systems control movement: the pyramidal and the extrapyramidal tracts. The pyramidal system, composed of direct projections form the motor cortex to the spinal motor neurons which then transfers information down to the distal limbs, was believed to be responsible for the control and execution of voluntary and accurate movements. The extrapyramidal tract, composed of indirect projections to the spinal cord through the BG and the cerebellum, running parallel to the pyramidal system, was thought to be in charge of the control of postural and automatic non-voluntary movements. His work set the basis for our modern understanding of the BG's role which is more than just a purely motor system as previously believed.

1.1 Definition and localization

The BG are paired subcortical structures lying deep in the brain composed of several nuclei namely the striatum, the pallidum, the subthalamic nucleus (STN) and the substantia nigra which can be distinguished based on their morphology and electrophysiological properties (Albin *et al.*, 1989; Parent & Hazrati, 1995a, 1995b; Lanciego *et al.*, 2012; Young *et al.*, 2023). The localization of the BG nuclei in the primate brain are shown in Figure 1-1. The BG have been conserved throughout vertebrate evolution for over 500 million years, from lampreys and fish to amphibians, reptiles, birds, and mammals. Although these nuclei are less clearly individualized in non-mammalian species, they share similar organizational and functional characteristics with the mammalian BG (Reiner *et al.*, 1998).

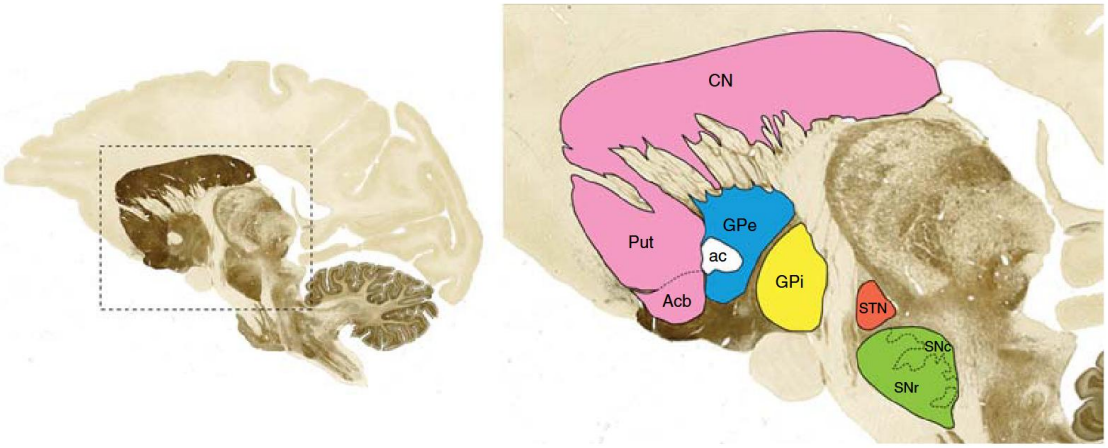

Figure 1-1. The monkey basal ganglia anatomy.

Parasagittal section of a monkey brain showing the localization of the different basal ganglia (BG) nuclei. In pink, the striatum encompassing the caudate nucleus (CN), the putamen (Put) and the nucleus accumbens (Acb); in blue, the external globus pallidus (GPe) with its ventral extension below the anterior commissure (ac) corresponding to the ventral pallidum; in yellow, the internal globus pallidus (GPi); in orange the subthalamic nucleus (STN) and in green the substantia nigra composed of the substantia nigra pars compacta (SNc) and the substantia nigra pars reticulata (SNr). Figure taken from (Lanciego et al., 2012).

1.1.1 The striatum

The striatum, located in the telencephalon, is formed by more than one nucleus in most mammals (Albin *et al.*, 1989; Parent & Hazrati, 1995a; Lanciego *et al.*, 2012):

- the putamen, a rounded structure sitting most laterally (Parent & Hazrati, 1995a; Ghandili & Munakomi, 2023);
- the caudate nucleus (CD), a C-shaped nucleus running alongside the lateral ventricle with a large head located in the floor of the anterior horn of the lateral ventricle, a body following the curvature of the lateral ventricle and a thin tail located in the roof of the inferior horn. It forms the medial part of the striatum (Parent & Hazrati, 1995a; Driscoll *et al.*, 2023);
- the nucleus accumbens (NAc) which connects to the head of the CD and the ventromedial putamen, and can be further subdivided into a core and shell region (Zahm & Heimer, 1988; Meredith *et al.*, 1996; Groenewegen *et al.*, 1999). Together with the olfactory tubercule extending anteriorly, they belong to the ventral striatum (VS).

The putamen and the CD are separated by a dense white matter structure called the internal capsule containing fibers coming from and going to all regions of the cerebral cortex. Putamen and CD connect through caudolenticular grey bridges. Unlike in primates, the rodent CD and the putamen are not anatomically separated but form instead a continuous dorsal striatum (DS). It is functionally divided into a dorsolateral striatum (DLS) which is homologous to the putamen and a dorsomedial striatum (DMS) homologous to the CD (Balleine & O'Doherty, 2010; Alegre-Cortés *et al.*, 2021).

Histochemical studies have revealed that both DS and VS are not homogeneous structures as they appear under the microscope but are rather compartmentalized into striosomes (or patches) and matrix (Graybiel & Ragsdale, 1978; Voorn *et al.*, 1989; Groenewegen *et al.*, 1999; Graybiel & Matsushima, 2023). The striosomes represents 10 to 20% of the total striatum and is characterized by a low activity of the acetylcholinesterase enzyme and express high levels of μ-opioid receptor, enkephalin and substance P neuropeptides (Graybiel & Ragsdale, 1978; Graybiel *et al.*, 1981, 1986; Herkenham & Pert, 1981; Gerfen, 1984). By contrast, the matrix, in which striosomes are embedded, is enriched with acetylcholinesterase, somatostatin (SOM) and calbindin (Graybiel & Ragsdale, 1978; Graybiel *et al.*, 1981, 1986; Herkenham & Pert, 1981; Gerfen, 1984). This compartmentalization is believed to hold differential processing of limbic and sensorimotor information especially in the DS. Indeed, although each cortical area innervates both compartments, motor and sensory cortical regions are found to principally innervate the matrix compartment whereas cortical limbic inputs are preferentially found in striosomes (Ragsdale & Graybiel, 1981; Gerfen, 1984; Donoghue & Herkenham, 1986; Eblen & Graybiel, 1995). The compartmentalization in the VS is less sharply delineated with the particularity of the NAc division into a core domain, enriched in calbindin, and shell domain, poor in calbindin, in addition to the compartmentalization (Groenewegen *et al.*, 1999). The differential innervation is less obvious in the VS in which both striosomes and matrix receive limbic information (Voorn *et al.*, 1989; Groenewegen *et al.*, 1999).

At the cellular level in both primates and rodents, the striatum is further subdivided into a population of projection neurons representing approximately 85-95% of total striatal neurons, called medium spiny neurons (MSNs), and 5-15% of interneurons (Graveland & Difiglia, 1985; Yelnik *et al.*, 1991; Del Rey *et al.*, 2022). Although all the MSNs are inhibitory neurons utilizing gamma-aminobutyric acid (GABA) as their neurotransmitter to reduce the discharge rate of their postsynaptic target neurons (Ribak *et al.*, 1979; Oertel & Mugnaini, 1984), they can be subdivided into two main populations depending on the dopamine (DA) receptor they express (Gerfen *et al.*, 1990) :

- the D1-MSN type, expressing the DA receptor subtype 1 and the neuropeptides substance P and dynorphin (Graybiel, 1990; Parent & Hazrati, 1995a);
- the D2-MSN type, expressing the DA receptor subtype 2 and the neuropeptide enkephalin (Graybiel, 1990; Parent & Hazrati, 1995a).

Although this dichotomy is well established, a small proportion of MSNs has also been found to coexpress both D1 and D2 receptors (Surmeier *et al.*, 1996; Aizman *et al.*, 2000; Bonnavion *et al.*, 2024) and will be discussed in the section “The different models of the basal ganglia / Updated “box-and-arrow” model” of this chapter, pages 18-21.

The striatal interneurons on the other hand have a local modulating action on MSNs and are classified into four groups (Kawaguchi, 1993; Kawaguchi *et al.*, 1995; Tepper & Bolam, 2004):

- the cholinergic interneurons which use acetylcholine as their neurotransmitter, also called tonically active neurons (TANs);
- the GABA-ergic interneurons expressing the calcium-binding protein parvalbumin (PV) or PV-interneurons, also called fast-spiking interneurons (FSIs);
- the GABA-ergic interneurons expressing the calcium-binding protein calretinin (CR) or CR-interneurons;
- the GABA-ergic interneurons which use nitric oxide and neuropeptide Y as their neurotransmitter and express SOM or SOM-interneurons, also called low-threshold spiking (LTS) interneurons.

1.1.2 The globus pallidus

The globus pallidus, located medially to the putamen and posterolaterally to the head of the CD is subdivided into two segments: an external segment (GPe) siting most laterally and an adjacent internal segment (GPi) located medially (Parent & Hazrati, 1995b; Kita, 2007; Nambu, 2007). In rodents, the endopeduncular nucleus is the homologous to the primate GPi while the GPe is referred to as the globus pallidus. Although functionally analogous to its primate homologue, the entopeduncular nucleus is anatomically separated from the globus pallidus and is embedded in the fiber tract of the internal capsule. The ventral pallidum (VP) is the ventral extension of the globus pallidus (Switzer *et al.*, 1982; Haber & Nauta, 1983; Haber & Knutson, 2010). The primate VP is a crescent-shaped structure ventral to the anterior commissure (Zahm & Heimer, 1988). Based on the rodent immunoreactivity, the VP can be subdivided in 3 parts, the ventromedial VP reactive to neurotensin, receiving inputs from the shell of the NAc, the dorsolateral VP, reactive to calbindin, receiving inputs from the core of the NAc and the ventrolateral VP exhibiting little

to no reactivity to both markers, described as finger-like extensions dorsal to the olfactory tubercule and ventral to the NAc (Zahm & Heimer, 1988, 1990; Root *et al.*, 2015).

At the cellular level, although there are rare GABAergic interneurons in the pallidum, the vast majority of pallidal neurons are GABA-ergic projections neurons, providing inhibitory output to their downstream targets (Penney & Young, 1981; Difiglia *et al.*, 1982). Within the rodent GABAergic GPe projection neurons, two populations have been identified based on their projection targets and molecular markers: the prototypic neurons expressing PV, Nkx2-1 and Lhx6 and arkypallidal neurons expressing proenkephalin, Npas1 and FoxP2 (Mallet *et al.*, 2012; Abdi *et al.*, 2015). Prototypic neurons represent approximately 75% of the GPe neuronal population while the arkypallidal neurons account for the remaining 25%. Although this cellular dichotomy has been clearly established in rodents, its direct correspondence in primates remains uncertain. Nevertheless, electrophysiological studies in non-human primates (NHPs) have identified two major classes of GPe neurons distinguished by high- and low-frequency discharge (HFD and LFD) patterns (see "Electrophysiological properties" section of this chapter, pages 36-37). However, based on the molecular markers expressed, other studies have shown that there are probably more than just two subpopulations in rodents (Cui *et al.*, 2021). VP is also a highly heterogeneous structure with GABAergic projection neurons but also cholinergic and glutamatergic neurons (Root *et al.*, 2015). Glutamatergic neurons are primarily present in the rostral ventromedial VP.

1.1.3 The subthalamic nucleus

The STN is a small fusiform nucleus located in the ventral diencephalon, sitting ventrally to the thalamus and is adjacent to the substantia nigra (Parent & Hazrati, 1995b; Bevan, 2016). Unlike the other BG nuclei, the vast majority of neurons in this structure are glutamatergic and use glutamate as their neurotransmitter to increase the discharge rate of their postsynaptic target neurons (Smith & Parent, 1988). The STN is therefore the only excitatory structure within the BG. However, this structure is not homogeneous, as neuronal populations differ according to their anteroposterior and dorsoventral location and exhibit distinct molecular profiles. In the human STN, PV-expressing neurons are predominantly found in dorsal regions, whereas neurons expressing the transcription factor NKX2.1 are preferentially located in the ventral STN (Prasad & Wallén-Mackenzie, 2024). In addition to these principal glutamatergic projection neurons, the STN contains a small population of local GABAergic interneurons, further contributing to its cellular and functional heterogeneity.

1.1.4 The substantia nigra

The substantia nigra pars reticulata (SNr) and the substantia nigra pars compacta (SNc) together form the substantia nigra, a small nucleus located medial to the cerebral peduncles of the ventral mesencephalon (also referred to as the midbrain). The SNr is located ventrally and is separated from the GPi by the cerebral peduncles, whereas the SNc lies dorsally (Parent & Hazrati, 1995a). The SNr is composed predominantly of GABAergic projection neurons and constitutes a major

inhibitory output structure of the BG. Although GPi and SNr contain cytologically similar neurons, recent evidence indicates that SNr neurons are heterogeneous and can be subdivided into genetically distinct subclasses corresponding to segregated BG output pathways (Yelnik *et al.*, 1984, 1987; Mendelsohn *et al.*, 2025). Medial to the SNr is lying the ventral tegmental area (VTA). SNc and VTA both contain dopaminergic neurons (DANs), and are referred to as the mesencephalic (or midbrain) dopaminergic system. Multiple DAN types exist in both the VTA and the SNc depending on the markers they express (Gaertner *et al.*, 2022; Fitzgerald & Day, 2025). Moreover, SNc and VTA are more heterogeneous than simple DANs. Indeed, some glutamatergic, GABAergic neurons also exist in the VTA as well as neurons co-expressing DA with GABA, DA with glutamate, glutamate with GABA and all 3 neurotransmitters together (Fitzgerald & Day, 2025), whereas GABAergic projection neurons and interneurons have been found in the SNc (Gaertner *et al.*, 2022).

1.2 The different models of the basal ganglia

Several models of the BG have been proposed over the years. Each revolutionary technique, from tracing markers to computer science, has brought evidence for new connections and new ways of thinking the function of the BG.

1.2.1 D1/D2 direct and indirect pathways “box-and-arrow” model

Based on the neuroanatomical, pharmacological and physiological data obtained from animal and post-mortem human studies, Albin, Young and Penney were the first to provide a functional model of the healthy BG in an attempt to explain movement disorders in neurodegenerative diseases and other lesions to the BG (Albin *et al.*, 1989). They were followed soon after by other groups (Alexander & Crutcher, 1990; Bergman *et al.*, 1990; Gerfen *et al.*, 1990) leading to the first 2-pathway “box-and-arrow” model of the BG (Figure 1-2).

Importantly, in this model, the striatum alone is the input structure of the BG which receives excitatory projections from virtually all cortical areas (Kemp & Powell, 1970; Künzle, 1975, 1977; Goldman & Nauta, 1977; Cospito & Kultas-Ilinsky, 1981; McGeorge & Faull, 1989) and from the thalamus (Powell & Cowan, 1956; Jones & Leavitt, 1974; Parent *et al.*, 1983; Giménez-Amaya *et al.*, 1995). The striatum also receives massive modulatory dopaminergic projections from the SNc projecting to the DS and from the VTA projecting to the ventromedial striatum as demonstrated by fluorescent retrograde tracing among other neuroanatomical and neurochemical techniques (Andén *et al.*, 1964, 1966; Arluison *et al.*, 1978; Beckstead *et al.*, 1979; Parent *et al.*, 1983; Schmued & Fallon, 1986; Gerfen *et al.*, 1990). Neuronal tracing experiments have shown that the striatum sends projections to the GPe but also to the GPi and SNr (Fox & Rafols, 1976; Féger & Crossman, 1984; Gerfen, 1985; Giménez-Amaya & Graybiel, 1990; Bolam & Smith, 1992). Moreover, combined with D1, D2, enkephalin, substance P and dynorphin mRNA detection in the striatum, Gerfen and colleagues used retrograde tracing techniques to show that the MSNs projecting to the GPi/SNr were expressing the dopaminergic D1 receptor and the peptide

substance P and dynorphin whereas the ones projecting to the GPe were mainly expressing the D2 receptor together with the enkephalin peptide (Gerfen *et al.*, 1990). Importantly, these neurons are from matrix origin. In contrast, D1- and D2-MSNs from striosomes send their projections back to the SNc, directly or indirectly through the central GPe, respectively (Gerfen *et al.*, 1987; Lazaridis *et al.*, 2024). VP GABAergic but also glutamatergic neurons projecting to the VTA have also been described (Zahm, 1989; Root *et al.*, 2015; Ottenheimer, Wang, *et al.*, 2020). In addition, it has been shown that the GPe sends inhibitory GABAergic projections to the STN (Carter & Fibiger, 1978; Carpenter *et al.*, 1981). The STN has been shown to send excitatory glutamatergic projections to the GPi and the SNr which are the output structures of the BG (Carpenter & Strominger, 1967; Nauta & Cole, 1978; Van Der Kooy & Hattori, 1980; Carpenter *et al.*, 1981; Kita & Kitai, 1987). Finally, these output nuclei project primarily to the thalamus, which in turn sends projections back to the cortex, thereby closing the cortico-BG (CBG)-thalamo-cortical loop (Carpenter & Strominger, 1967; Clavier *et al.*, 1976; Schell & Strick, 1984; Schmued & Fallon, 1986). In addition to these thalamic projections, BG output structures also target several subcortical nuclei, including the lateral habenula, the pedunculopontine nucleus, and the superior colliculus (Hopkins & Niessen, 1976; Carter & Fibiger, 1978; Parent & De Bellefeuille, 1982; François *et al.*, 1988). In the rodents, the SNr constitutes the dominant output structure of the BG whereas in primates both the GPi and SNr serve as major output nuclei (Parent & Hazrati, 1995a).

The model, shown in Figure 1-2 (left model corresponds to work obtained from primate studies and right, the model confirmed by Gerfen and colleagues on rodents, see also Figure 1-3 for a clearer representation) describes two non-overlapping and antagonistic pathways originating from the striatum and running through the BG to control movement: one direct and one indirect pathway.

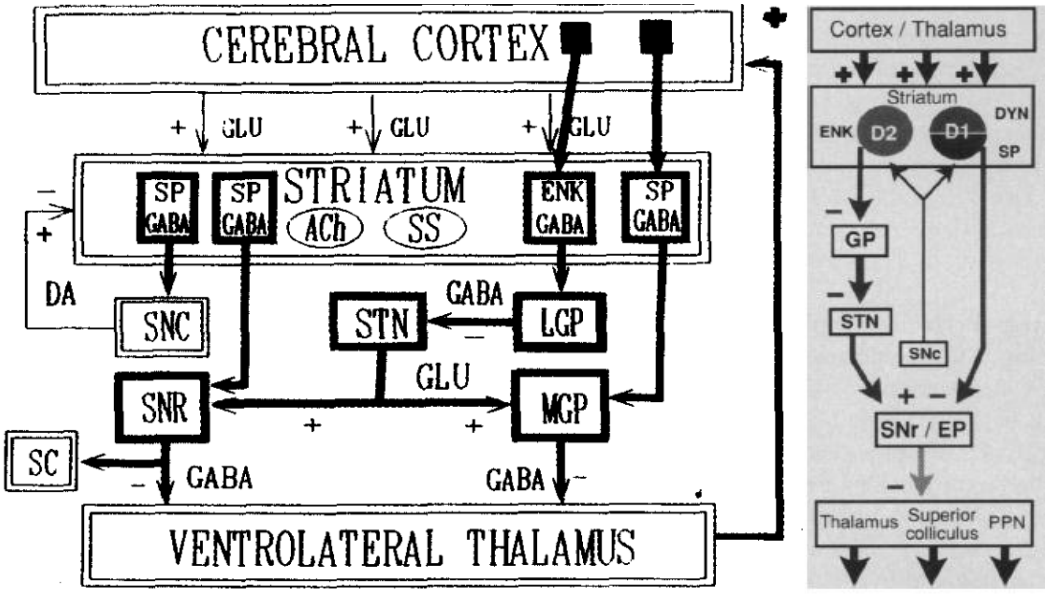

Figure 1-2. D1/D2 direct/indirect pathways "box-and-arrow" model of the basal ganglia.

The left panel is based on primate data and the right panel on rodent data. Taken from (Albin et al., 1989; Gerfen et al., 1990). In the primate model (left), LGP and MGP refer to the lateral and medial globus pallidus, corresponding to the external (GPe) and internal (GPi) segments, respectively. ACh (acetylcholine) and SS (somatostatin) label striatal interneuron populations (cholinergic and low-threshold spiking interneurons respectively). DA (dopamine) from the

substantia nigra pars compacta (SNc) exerts modulatory effects, facilitating D1-expressing neurons and inhibiting D2-expressing neurons (represented by both (+) and (-) signs). SC denotes the superior colliculus. In both models, SP (substance P) identifies D1 medium spiny neurons (MSNs; also expressing dynorphin, DYN, in the rodent model), while ENK (enkephalin) identifies D2 MSNs. STN: subthalamic nucleus; SNr: substantia nigra pars reticulata. Excitatory glutamatergic (GLU) projections are indicated by (+), and inhibitory GABAergic projections by (−). The direct (D1) pathway inhibits basal ganglia output structures (GPi/SNr), leading to disinhibition of the thalamus and facilitation of movement ("Go" pathway). In contrast, the indirect (D2) pathway increases the activity of GPi/SNr via the GPe-STN circuit, resulting in enhanced inhibition of the thalamus and suppression of movement ("No-Go" pathway).

D1 direct pathway:

In the D1 direct pathway, the glutamatergic cortex excites striatal D1-MSNs which in turn inhibit the GPi/SNr neurons. The inhibition of the output structures of the BG leads to the disinhibition of the thalamus which in turn can excite downstream targets including the motor cortex leading to movement. Thus, the D1 direct pathway facilitates movement and is referred to as the "Go" pathway.

D2 indirect pathway:

In the D2 indirect pathway, the glutamatergic cortex excites striatal D2-MSNs which in turn inhibit the GPe neurons. However, GPe neurons normally inhibit STN excitatory neurons projecting to GPi/SNr output structures. Thus, the inhibition of GPe leads to a disinhibition of the STN which in turn excites GPi/SNr. This excitation results in the inhibition of the thalamus which no longer excites the motor cortex leading to movement suppression. Thus, the D2 indirect pathway suppresses movement and is referred to as the "No-Go" pathway.

D1/D2 pathway modulation:

These pathways are modulated by the DA neurotransmitter originating from the midbrain SNc to promote movement (Albin *et al.*, 1989; Gerfen *et al.*, 1990). Depending on the receptor type present on the cell, DA is either excitatory or inhibitory. Indeed, DA is excitatory to D1-MSNs and thus promotes movement by enhancing the direct pathway whereas it is inhibitory to D2-MSNs and promotes movement by suppressing the indirect pathway (Cepeda *et al.*, 1993; Gonon, 1997; West & Grace, 2002). Therefore depletion of DA, observed in Parkinson's disease (PD) for example, provokes an imbalance of BG circuits by a reduced excitation of the D1-direct MSNs which no longer inhibit the output structures and by an increased inhibitory action of the D2-indirect MSNs on GPe which no longer inhibits the STN enabling it to stimulate the output structures. Disinhibition by D1-MSNs and stimulation by the STN of output structures leads to the increase of the inhibitory output to the thalamus resulting in difficulties in movement initiation and vigor.

1.2.2 Updated "box-and-arrow" model

However, several biochemical, anatomical and electrophysiological studies have challenged this first model which does not consider the complexity of the network. The Figure 1-3 compares the classical model (left model) to the updated model (right model) considering the different aspects described below.

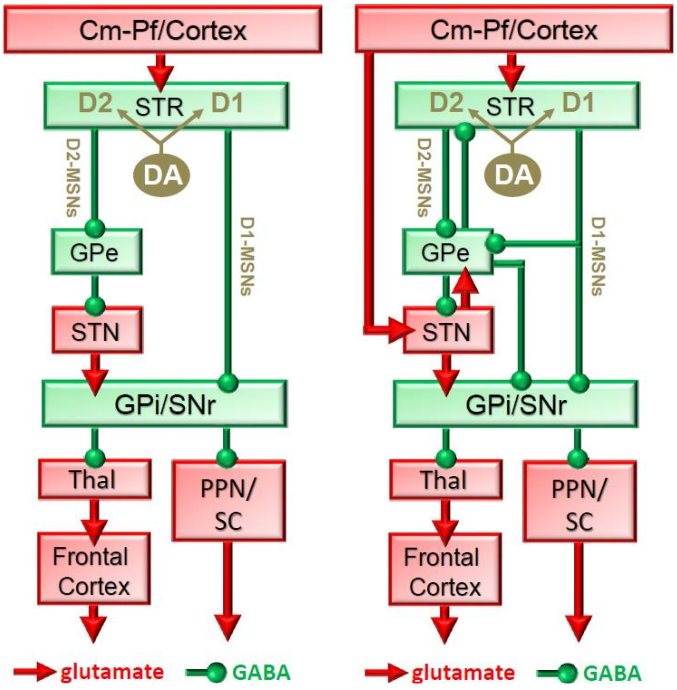

Figure 1-3. Direct and indirect "box-and-arrow" model and updated model.

The left panel shows the first D1/D2 direct/indirect pathways "box-and-arrow" model (as in Figure 1-2), while the right panel illustrates the updated model. The first model is reproduced alongside the updated version using the same color code and layout to facilitate comparison. Red arrows indicate excitatory (glutamatergic) projections, green arrows indicate inhibitory (GABAergic) projections and gold arrows indicate dopaminergic (DA) modulatory effects on D1 and D2 medium spiny neurons (MSNs). The updated model incorporates several key features, including strong excitatory cortical inputs to the subthalamic nucleus (STN), reciprocal connections between the external globus pallidus (GPe) and both the striatum and STN, projections from the GPe to output structures, and collateral projections from D1-MSNs to the GPe.

Striatal D1 direct MSNs also project to the GPe. Indeed, looking at the morphology of the MSNs and where their axons project, Parent and colleagues, in the monkey and Kawaguchi and colleagues in the rat, identified 3 types of striatal projection neurons (SPNs): the type I which projects exclusively to the GPe, the type IIa which projects to the SNr and sends collaterals to the GPi first then to the GPe and type IIb which projects to the SNr and sends collaterals to the GPe (Parent *et al.*, 1984; Kawaguchi *et al.*, 1990). Moreover, using biotin dextran amine to label SPNs in rats, Wu and colleagues confirmed these results and found that type I cells represented 36.4% of labeled MSNs while the remaining cells targeting SNr and/or GPi additionally sent collaterals to the GPe (Wu *et al.*, 2000).

D1- and D2-MSNs interact via local GABAergic collateral connections. Indeed, the work of Wilson and Groves, confirmed later by Kawaguchi and colleagues has shown that MSNs send GABAergic collaterals to other MSNs (Wilson & Groves, 1980; Kawaguchi *et al.*, 1990). More precisely, in a study led by Taverna and colleagues looking at MSN forming connection pairs in the rat striatum, D1- and D2-MSNs pairs were found to form unidirectional synapses on other D1- and D2-MSNs respectively (26 and 36% of pairs analyzed, respectively) (Taverna *et al.*, 2008). Alternatively,

some D2-MSNs pairs were commonly found to form synapses on D1 MSNs (27% of pairs) and only a small number of D1-MSNs were forming synapses on D2-MSNs (6% of pairs). Another study performed by Czubayko and Plenz, showed direct evidence of electrophysiological synaptic transmission between MSN pairs (Czubayko & Plenz, 2002). Together, these findings indicate that neurons of the direct and indirect pathways are not independent but can inhibit each other through local striatal circuitry. Although MSN-MSN inhibition is sparse and weak at the level of individual synapses, it is nonetheless critical at the population level. Indeed, pharmacological blockade of $GABA_A$ receptors with bicuculline abolishes the structured dynamics of striatal cell assemblies in vitro, demonstrating that lateral inhibition is required for the emergence and switching of MSN assemblies (Carrillo-Reid *et al.*, 2008).

In the classical model, activation of the direct pathway facilitates movement, whereas activation of the indirect pathway inhibits movement, suggesting functional segregated and opposite roles. However, in a study led by Cui and colleagues using transgenic mice performing an operant task and in which the specific activities of D1 direct and D2 indirect pathways were measured, authors found that both D1 and D2 pathways were co-active during action initiation (Cui *et al.*, 2013). Moreover, although the amplitude of the response is different, both pathways were found to modulate their activity in response to movement initiation, sensory stimuli and reward cues, and showed correlated activities. Extending these findings, recent calcium imaging data indicate that during ongoing movements, population activity in both D1- and D2-MSNs increases around peak force generation, with significant modulation observed in each cell type (Rodrigues-Vaz *et al.*, 2025). Consistent with this view, inhibition of either the D1 or the D2 pathway was found to disrupt movement initiation (Tecuapetla *et al.*, 2016). These studies show that there is a coactivation and complex coordination of D1 direct and D2 indirect pathways.

Another finding that challenged the idea that D1- and D2-MSNs are divided into separate, not overlapping populations of neurons is the presence of D1 and D2 receptor in the same striatal MSNs obtained by single cell mRNA detection or immunohistochemistry experiments (Surmeier *et al.*, 1996; Aizman *et al.*, 2000). A recent study notably identified a third population of MSNs that coexpress D1 and D2 receptors representing approximately 7% of total MSNs and which exclusively projects to the GPe (Bonnavion *et al.*, 2024).

Moreover, anatomical studies demonstrated the existence of massive feedforward GABAergic projections from the GPe to BG output nuclei in both rodents and primates (Hazrati *et al.*, 1990; Kita & Kita, 1994; Smith *et al.*, 1994; Parent & Hazrati, 1995a; Sato *et al.*, 2000). These direct GPe projections to the GPi and SNr allow the GPe to influence BG output independently of the STN, in contrast to the classical model. In addition, a distinct population of GABAergic neurons in the GPe, named arkypallidal neurons, sends feedback projections to the striatum in rodents (Spooren *et al.*, 1996; Bevan *et al.*, 1998; Bolam *et al.*, 2000; Mallet *et al.*, 2012; Abdi *et al.*, 2015).

STN projects back to the GPe (feedback loop) placing this nucleus not as a simple relay structure between the striatum and the output structures of the BG (Carpenter & Strominger, 1967; Van Der Kooy & Hattori, 1980; Carpenter *et al.*, 1981; Kita & Kitai, 1987; Kita & Kita, 1994; Parent & Hazrati, 1995a, 1995b). In addition, the classical model does not consider the direct inputs from

motor and premotor cortex to the STN (Monakow *et al.*, 1978; Kitai & Deniau, 1981; Afsharpour, 1985; Ryan & Clark, 1991; Fujimoto & Kita, 1993; Féger *et al.*, 1994; Nambu *et al.*, 1996; Nambu, 2004; Haynes & Haber, 2013). As a result, it underestimates the importance of the widespread cortical inputs and the rapid transfer of information from the cortex directly to the output structures, described as the hyperdirect pathway (Nambu *et al.*, 2000; Nambu, Tokuno, *et al.*, 2002).

In the classical model, GPe is inhibited through the indirect pathway leading to disinhibition of the STN and increased excitation of GPi. This suggests that GPe and GPi have opposite activity patterns. Accordingly, when GPe activity is reduced, GPi activity should be increased and vice versa. However, Deffains and colleagues found that both GPe and GPi neurons increased their firing rates (FRs) on average in response to conditioned cues and during delay period (Deffains *et al.*, 2016). This similar activity pattern could be explained by the fact that cue presentation strongly engages sensory and associative cortex, leading to parallel recruitment of both D1- and D2-MSNs, which receive common excitatory glutamatergic cortical input under baseline or low-DA conditions. The convergence of striatal inhibition, cortical excitation, and STN drive may result in correlated increases in firing across pallidal populations. In learning or reward prediction for example, when higher levels of DA are needed, DA is released by the SNc leading to anticorrelated pallidal discharge patterns. Thus, D1 and D2 pathways may operate in either cooperative or opponent modes depending on cortical drive and DA state, dynamics that are not captured by the classical BG model.

1.2.3 From pathway-based models to the three-layer framework

Originally, the BG were thought to be responsible for movement initiation and generation. Another model proposed by John Mink and later extended by Atsushi Nambu's work on the hyperdirect pathway, places the BG as a system selecting one specific action to perform while suppressing the unwanted ones in response to competing sensory stimuli leading to competing actions (Mink, 1996). Accordingly, a multitude of possible actions to perform are triggered by the sensory stimuli and the BG evaluate and select which action to perform. In Mink's model, specific action selection is mediated by the direct pathway through focused inhibition of a specific subset of GPi/SNr neurons, resulting in disinhibition of their thalamocortical targets and enabling the transmission of a selected motor program. In parallel, the indirect pathway broadly excites the GPi/SNr via the STN, which is disinhibited by reduced activity in the GPe, thereby suppressing competing motor output alternatives. Thus, the indirect pathway inhibits all unwanted motor programs except the wanted one activated by the direct pathway. Because the indirect pathway is multisynaptic and therefore the transmission of information along it is slow, the hyperdirect pathway, as proposed by Nambu, can be recruited to provide a fast inhibitory influence on thalamocortical activity via rapid excitation of GPi/SNr by the STN (Nambu, 2004). The direct pathway subsequently disinhibits the selected motor program and the STN is inhibited through the indirect pathway. The hyperdirect pathway is viewed as the brake of the system.

The Mink and Nambu models describe BG function in terms of direct, indirect, and hyperdirect pathways organized in a largely feedforward manner. However, anatomical and physiological evidence indicates that BG nuclei, particularly the GPe and STN, are embedded in recurrent circuits, suggesting that this pathway-based organization is incomplete. Rather than replacing the action-selection framework of Mink and Nambu, a simplified three-layer "box-and-arrow" model reorganizes it at the circuit level by describing BG function in terms of distinct functional layers rather than discrete pathways (Figure 1-4). In this model, the STN is placed as an input structure of the BG alongside with the striatum, rather than solely as a relay nucleus in the indirect pathway as previously described. Moreover, the GPe becomes a central integrative structure of the BG which receives inhibitory inputs from D2-MSNs and excitatory inputs from the STN and projects back to both structures and to the output structures. In parallel, D1-MSNs directly project to the output structures with a subset also sending collaterals to the GPe. Finally, cortical inputs additionally reach the output nuclei through the hyperdirect pathway via the STN.

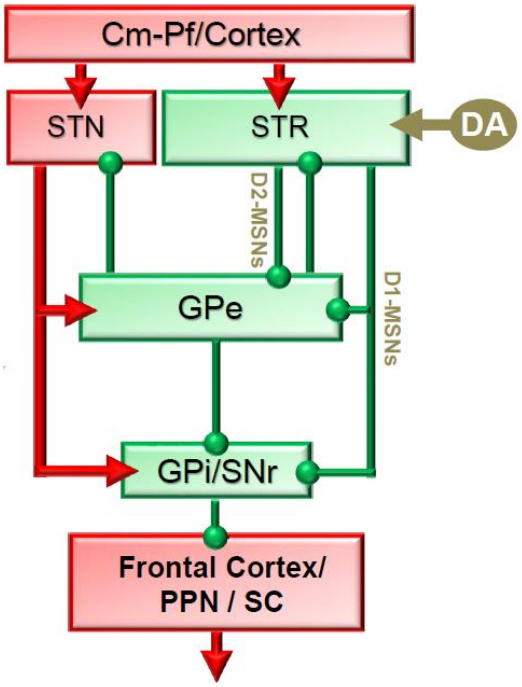

Figure 1-4. Three-layer basal ganglia "box-and-arrow" model.

This simplified model incorporates key features of updated basal ganglia (BG) organization. In particular it accounts for the massive innervation of the cortex to the subthalamic nucleus (STN) and its role as a fast excitatory pathway to the output structures providing rapid inhibition of the thalamocortical circuits. It places the STN as an input structure of the BG and not just as a relay structure in the indirect pathway. This model also places the external globus pallidus (GPe) as the central integrative structure of the BG, forming reciprocal connections with the STN and sending projections back to the striatum, and through which the indirect pathway modulates the output structures.

1.2.4 Actor/Critic reinforcement learning model: main axis vs modulator

Although the simplified three-layer model accounts for the major anatomical connections of the BG, it does not capture their computational dynamics nor the role of DA in corticostriatal plasticity. To address these aspects, reinforcement learning (RL) models of BG have been

developed (Schultz *et al.*, 1997; Sutton & Barto, 1998; Bar-Gad *et al.*, 2003; Goldberg & Bergman, 2011; Parush *et al.*, 2011; Gurney *et al.*, 2015). In RL, each time an agent interacts with the environment, by performing an action or selecting an option, the result, provided by the environment as rewards (positive rewards) or punishments (negative rewards) is used to adjust the agent's future behavior (Sutton & Barto, 1998). The rules that are used to select the optimal behavior in a given state of the environment are referred to as the policy. The goal of RL is to use the policy that will maximize future positive rewards and minimize punishments over time.

A common way to achieve this goal is the actor-critic model of RL. In this model, the agent is divided into two functionally and cooperative sub-systems:

- The actor, which selects and executes actions based on the current policy.
- The critic, which evaluates the results of the actions performed by the actor. It compares the expected value (EV) of the current state to the value updated by the obtained outcome and generates a prediction error which corresponds to the difference between the expectation and reality. This prediction error is then used by the critic to update the value representation and adjust the actor's behavioral policy.

Two situations can occur:

- the prediction error is positive (the outcome is better than expected): the behavior is reinforced.
- the prediction error is negative (the outcome is worse than expected): the policy is adjusted and the behavior is changed.

Interestingly, BG network can be depicted as an actor-critic RL model (Schultz *et al.*, 1997; Sutton & Barto, 1998; Joel *et al.*, 2002; Bar-Gad *et al.*, 2003; Goldberg & Bergman, 2011; Parush *et al.*, 2011; Gurney *et al.*, 2015; Dunovan & Verstynen, 2016). On the one hand, the BG main axis, composed of the different BG structures that connect thalamo-cortical fields (encoding subject's current state) and the brain motor centers, corresponds to the actor and would therefore implement state-to-action mapping. On the other hand, the BG neuromodulators, and more specifically midbrain DANs, correspond to the critic and provide a prediction error signal to the BG main axis, thereby adjusting its activity by modulating the efficacy of cortico-striatal transmission (Reynolds *et al.*, 2001; Shen *et al.*, 2008; Deffains & Bergman, 2015).

<u>Actor:</u>

The mechanisms by which the BG main axis maintains and uses state information remain relatively unexplored. However, Deffains and colleagues demonstrated that persistent, task-related activity during prolonged delays between sensory perception and action execution (when sensory information is no longer available) is not unique to frontal and other cortical areas (Goldman-Rakic, 1995; Curtis & Lee, 2010), but can also be observed along the BG main axis (Deffains *et al.*, 2016). This sustained modulation carries information about the current task state in the absence of sensory cues, indicating that the BG can maintain state representations over time. These findings show that the BG main axis is not limited to immediate action control, but also supports state-action coupling when actions are delayed. Importantly, activity along the BG main axis is not homogeneous. Electrophysiological recordings have revealed a marked

heterogeneity of neuronal responses in the GPe, GPi, and SNr, with neurons exhibiting diverse and largely independent firing patterns during task performance (Joshua, Adler, Prut, *et al.*, 2009). Such diversity suggests that the BG main axis operates in a high-dimensional regime, which is conducive to a large information capacity (Bar-Gad *et al.*, 2003). At the computational level, the combination of persistent state-related activity and heterogeneous population responses is consistent with the implementation of an actor that represents and selects actions based on internal state, corresponding to a policy in RL models.

Dopaminergic critic:

In the actor-critic framework, DANs are thought to act as a critic by signaling reward prediction errors (RPEs). This idea was first demonstrated by Schultz and colleagues who recorded midbrain dopaminergic activity in NHP performing a conditioning task in which an auditory cue was associated to a palatable reward and showed that unexpected rewards elicited phasic increases in firing, whereas fully predicted rewards did not (Schultz *et al.*, 1997; Schultz, 1998). As learning progressed, phasic dopaminergic responses shifted from reward delivery to reward-predicting cues, indicating that DANs encode predictions rather than reward per se. Conversely, omission of an expected reward resulted in a transient decrease in dopaminergic activity at the predicted reward time, signaling an outcome worse than expected. This framework was later extended to show that DANs signal prediction errors not only in reward occurrence but also in reward timing, with increased activity at unpredicted reward times and reduced activity at the expected reward time when reward delivery was delayed (Hollerman & Schultz, 1998). Subsequent work by Bayer and Glimcher provided the first quantification of this signal in NHP performing a saccadic timing task with variable reward magnitudes, demonstrating that DANs encode a graded RPE proportional to the difference between expected and obtained outcomes, particularly for outcomes better than expected (Bayer & Glimcher, 2005). This view was further expanded by Fiorillo and colleagues, who showed that DANs also encode reward probability and uncertainty (Fiorillo *et al.*, 2003). In a Pavlovian task in monkeys, phasic dopaminergic responses to reward scaled inversely with reward probability, while a slower, sustained increase in activity during the delay period was maximal at intermediate reward probabilities, corresponding to maximal uncertainty. Moreover, this dopaminergic signal is homogeneous as demonstrated by the skewed distribution of response correlation values towards positive values favoring a unified global information (Joshua, Adler, Prut, *et al.*, 2009). Together, these findings establish DANs as providers of a teaching signal that updates the actor's policy. This interpretation has been confirmed and extended by more recent studies which have examined the scope and limits of dopaminergic prediction error signaling. Farell and colleagues showed that DANs encode RPEs not only during discrete conditioning tasks but also during ongoing, goal-directed behavior (Farrell *et al.*, 2022). Indeed, using a virtual-reality navigation task requiring continuous state estimation, authors observed that DAN activity exhibited gradual ramping as rats approached reward, a pattern that could be explained as temporally distributed RPEs and that predicted subsequent learning. Complementing these findings, Mah and colleagues showed that phasic DA release in the striatum conveys prediction errors independently of adaptive learning rates used

by behavior, indicating that dopaminergic signals encode the error term and not the full learning update (Mah *et al.*, 2024). Finally, dopaminergic prediction error signals have been shown to extend beyond reward outcomes to include errors in predicting task-relevant sensory events. In a sensory preconditioning paradigm, DAN activity was observed when an unexpected neutral cue followed a previously learned neutral cue-cue association, despite the absence of reward (Costa *et al.*, 2025).

Complementary critics:

Although midbrain DANs robustly encode positive and negative RPEs, other neuromodulatory systems contribute complementary evaluative signals within the BG. For example, cholinergic interneurons in the striatum (presumably TANs) have been shown to respond phasically and synchronously to reward-predictive stimuli and outcomes (Kimura *et al.*, 1984; Aosaki *et al.*, 1994; Apicella *et al.*, 1997; Joshua, Adler, Prut, *et al.*, 2009). Importantly, TAN responses are not restricted to appetitive reinforcement. They are also elicited by aversive outcomes and other motivationally salient events, often with limited valence specificity, indicating that TANs convey a salience signal rather than a signed value code (Ravel *et al.*, 1999; Joshua *et al.*, 2008). In addition, TAN activity is strongly shaped by behavioral context and temporal predictability: responses are enhanced when outcome timing is uncertain or irregular and attenuated when events become temporally predictable, consistent with signaling surprise, uncertainty, or the need to update task structure (Apicella *et al.*, 1997; Apicella, 2002, 2007). TANs also show robust modulation at outcome omission, reflecting violations of expected event timing and trial completion rather than encoding a signed negative prediction error (Morris *et al.*, 2004; Joshua *et al.*, 2008). This response is highly homogeneous across TANs, as demonstrated by positively skewed correlation distributions and clustering of TAN activity into a single dominant response pattern (Joshua *et al.*, 2008; Joshua, Adler, Prut, *et al.*, 2009; Adler *et al.*, 2012). The main feature of this modulation is the pause in firing, often preceded by a brief excitation and followed by a rebound increase in activity, which contrasts with the phasic dopaminergic bursts observed in response to rewarding events (Joshua *et al.*, 2008). Moreover, TANs are preferentially located near the borders of striosomal and matrix compartments, allowing them to influence striosome-SNc interactions (Graybiel *et al.*, 1986, 1994). Importantly, TAN activity is tightly coordinated with dopaminergic signaling: pauses in TAN firing are temporally aligned with phasic dopaminergic bursts, indicating coordinated but distinct neuromodulatory signals (Graybiel *et al.*, 1994; Morris *et al.*, 2004; Joshua *et al.*, 2008). Taken together, these findings support the view that cholinergic interneurons complement dopaminergic teaching signals by providing context- and timing-dependent gating signals that regulate when corticostriatal plasticity is engaged and under which contextual conditions learning occurs (Deffains & Bergman, 2015). Thus, alongside the dopaminergic critic that carries signed prediction errors, TANs provide a complementary "critic-like" signal emphasizing salience, predictability, and temporal structure, shaping when striatal circuits interpret and apply dopaminergic teaching signals.

Other studies have demonstrated the role for serotonin and histamine as critics in the BG. Indeed, in their study, Cohen and colleagues showed that serotonin is linked to punishment prediction and demonstrated a differential modulation of activity between punished and rewarded trials in rodents (Cohen *et al.*, 2015). Histamine on the other hand has been linked to attention. Indeed, histaminergic neurons show a higher activity during increased attention (Takahashi *et al.*, 2006).

Beyond these neuromodulatory signals, recent studies indicate that the critic function of the BG is embedded within a broader circuit that includes feedback from striatal and pallidal structures. As described above, striosomal D1- and D2-MSNs project back to the SNc. Recent studies demonstrated that they likely influence motivation for learning and action though an D1 direct mediated inhibitory and D2 indirect mediated excitatory action on the SNc (Lazaridis *et al.*, 2024). In addition, VP neurons can be classified into critic-like and actor-like assemblies (Kaplan et al. 2020; Ottenheimer et al. 2020). Indeed, critic-like neurons that transiently modulate their activity show correlated activity and homogeneous response. Moreover VP glutamate and GABAergic neurons project to the VTA directly or indirectly through the lateral habenula and can drive negative or positive reinforcement through avoidance or approach behavior (Faget *et al.*, 2018).

1.3 Information processing in the basal ganglia

1.3.1 Convergence and divergence in the basal ganglia

There is a long-standing debate concerning information processing along the BG main axis. One view posits that the BG main axis functions as a unified system that receives convergent but sparse input from state-encoding thalamo-cortical fields and channels this information to brain motor centers, while also exhibiting divergence at specific stages of the network.

1.3.1.1 Cortico-striatal divergence and sparsity

Quantitative anatomical studies show that cortico-striatal projections are spatially divergent but sparse at the level of individual neurons. In rats, a single cortical axon can spread widely across the striatum while contacting only a small fraction of MSNs, and neighboring MSNs share very few common cortical inputs (Kincaid *et al.*, 1998; Zheng & Wilson, 2002). As a result, each MSN integrates a unique combination of cortical information, supporting a distributed representation of cortical state. Such precise anatomical studies are missing in the primate but the broad cortico-striatal projections and their partial overlap have been established (Parent & Parent, 2006).

1.3.1.2 Striatal convergence onto basal ganglia output nuclei

Quantitative anatomical studies indicate a drastic and progressive reduction in both volume and neuronal number along the BG main axis, from the striatum to pallidal and nigral output nuclei. Compared to the striatum, the globus pallidus and substantia nigra contain a few hundred times

fewer neurons and occupy substantially smaller volumes across species (rats, monkeys and humans), reflecting a strong convergence of information from input to output structures (Harman & Carpenter, 1950; Percheron *et al.*, 1984, 1994; Oorschot, 1996; Hardman *et al.*, 2002; Yelnik, 2002; Frey *et al.*, 2011; Salvesen *et al.*, 2015; Pauli *et al.*, 2018). Individual MSNs form numerous synaptic contacts onto downstream pallidal and nigral targets, whereas each pallidal or nigral neuron receives inputs from a very large population of MSNs (Kawaguchi *et al.*, 1990; Wu *et al.*, 2000; Yelnik, 2002; Lévesque & Parent, 2005). This numerical and volumetric compression strongly supports the idea that striatal output converges onto a limited set of downstream neurons, enabling integration of distributed striatal representations.

1.3.1.3 Integration of information in pallidal and nigral neurons

Pallidal and nigral neurons are anatomically well suited to integrate convergent information. In particular, neurons in the monkey pallidum exhibit large, broad discoidal dendritic fields, often exceeding one millimeter in diameter, that are oriented orthogonally to incoming striatal axonal projections (Percheron *et al.*, 1984; Yelnik *et al.*, 1984; Yelnik, 2002). This geometry allows single pallidal neurons to sample afferent inputs arising from spatially distinct regions of the striatum, likely spanning multiple functional domains. Functional studies in monkeys are consistent with this anatomical organization, showing that individual pallidal neurons can respond to stimulation of different striatal territories and multiple cortical areas, providing evidence for convergence of information across both striatal and cortical sources (Flaherty & Graybiel, 1993; Yoshida *et al.*, 1993; Kimura *et al.*, 1996). Although SNr neurons do not display strictly discoidal dendrites, their dendritic arborizations are similarly extensive, supporting integration of inputs from numerous striatal neurons (François *et al.*, 1987).

1.3.1.4 Convergent cortico-subthalamic input

Although smaller in size and number of cells compared to the striatum, quantitative morphological studies have shown that the dendritic arborization of monkey STN neurons is larger and spread broader than MSNs, demonstrating a higher degree of convergence (Yelnik & Percheron, 1979). Anterograde labeling in the cortex showed that many rat cortical axons in the region of injection were projecting to the STN and single cortical axons were innervating a large extent of the nucleus, demonstrating a high percentage of shared cortical information (Bevan *et al.*, 1995). In addition, cortico-subthalamic projections arise from widespread cortical territories, particularly within frontal regions, supporting the notion that individual STN neurons integrate information from multiple cortical areas. The relatively high synaptic weight of cortico-subthalamic connections further enables rapid and effective transmission of cortical signals to downstream BG nuclei (Kita & Kita, 2012; Coudé *et al.*, 2018). Together, these features indicate that the STN acts as a major site of cortical information convergence within the BG.

1.3.1.5 Divergent subthalamic output

In contrast to its convergent cortical input, the output of the STN is strongly divergent. Single STN neurons project extensively to multiple downstream targets, including GPe, GPi and SNr, forming large numbers of synaptic contacts within each structure (Koshimizu *et al.*, 2013). As a result, the excitatory influence of the STN can be broadcasted broadly across BG output nuclei. Despite constituting a minority of pallidal afferents, subthalamic inputs account for a substantial proportion of excitatory synapses onto pallidal neurons, highlighting their capacity to exert a powerful and distributed modulatory effect (Yelnik, 2002). This divergent organization positions the STN as a critical structure for rapidly influencing global BG output.

1.3.2 Segregation in the basal ganglia

The second major view of information processing along the BG main axis emphasizes the segregation of information into parallel functional circuits. Originally, BG were believed to have a pure motor or sensorimotor role. Nowadays, it is widely accepted that the BG are topographically organized into at least three main functionally segregated parallel circuits (Figure 1-5): the sensorimotor circuit (motor and oculo-motor circuits), the associative circuit (dorsolateral prefrontal and lateral orbitofrontal circuits) and the limbic circuit which circulate from specific areas of the cortex down to restricted regions of the BG and thalamus and return to their cortical sources (Alexander *et al.*, 1986; Yin & Knowlton, 2006; Obeso *et al.*, 2008; Krack *et al.*, 2010; Redgrave *et al.*, 2010). This topographic and functional organization of the BG network especially arises from the large diversity of the cortical projections received by the striatum and is preserved at the different stages (input, central and output) of the network (Parent & Hazrati, 1995a, 1995b).

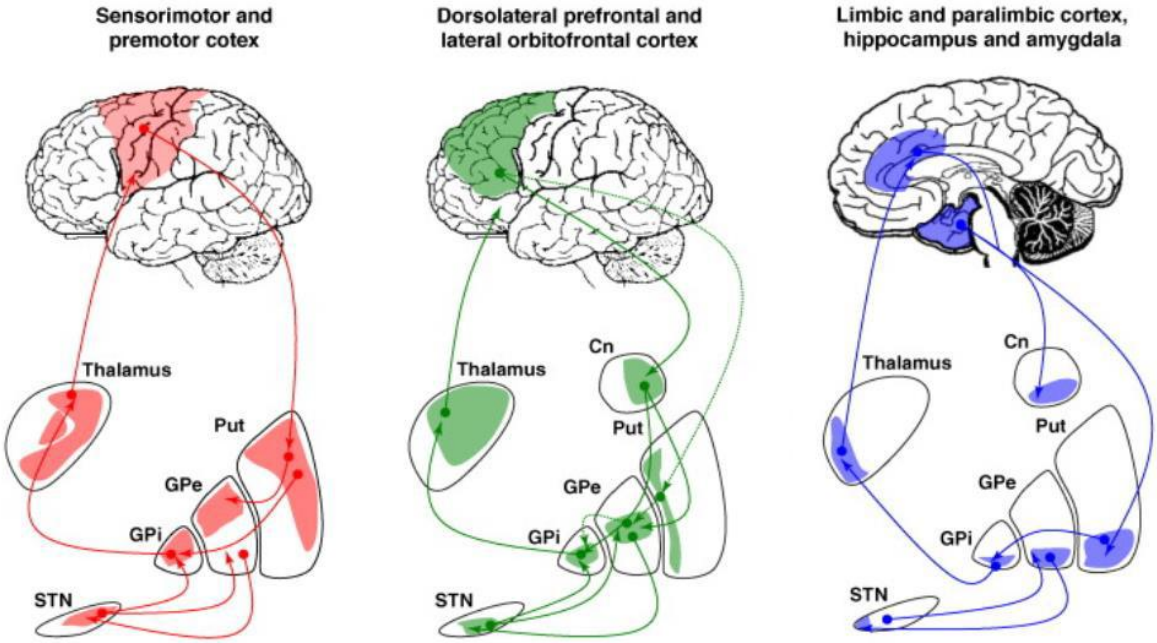

Figure 1-5. Parallel anatomofunctional circuits of the basal ganglia.

The figure illustrates the three main functionally segregated cortico-basal ganglia-thalamo-cortical loops: the sensorimotor circuit (left), the associative circuit (middle), and the limbic circuit (right). Each circuit originates from distinct cortical areas, projects to specific and topographically organized regions of the striatum (Put, putamen; Cn, caudate nucleus), and is relayed through corresponding territories of the globus pallidus (GPe, external globus pallidus; GPi, internal globus pallidus), subthalamic nucleus (STN), and thalamus before returning to its cortical source. Taken from (Krack et al., 2010).

1.3.2.1 Sensorimotor circuit

Tracing studies of the cortico-striatal projections have shown that the sensorimotor cortex, including the primary motor cortex (M1), the supplementary motor area (SMA), the premotor cortex, the somatosensory cortex and the arcuate premotor cortex, projects densely and topographically to the putamen posterior to the anterior commissure in primates (Künzle, 1975, 1977, 1978). Within this motor territory, projections are organized mediolaterally, with SMA inputs terminating more medially and M1 inputs more laterally, while the dorsomedial putamen is largely spared. In contrast, the frontal eye fields project preferentially to the central CD (Künzle & Akert, 1977). As described above, the putamen also receives dense dopaminergic innervation from the SNc. The motor putamen is further subdivided into three somatotopically organized regions arranged from dorsolateral to ventromedial putamen, corresponding to representations of the leg, arm, and face, respectively (Crutcher & DeLong, 1984; Alexander & DeLong, 1985a, 1985b; Alexander *et al.*, 1986; Nambu, 2011). Microstimulation studies have shown that neurons related to lower limb movements are distributed along the anteroposterior axis of the dorsolateral putamen, whereas neurons related to upper limb movements occupy an intermediate position and neurons related to orofacial movements are located ventromedially (Alexander & DeLong, 1985a, 1985b; Nambu, Kaneda, *et al.*, 2002). In contrast, microstimulation of the medial putamen did not elicit movement, suggesting that the medial to lateral somatotopy

is conserved along the BG and that these territories are independent. Moreover, it has been found that within somatotopic areas, clusters of neurons were specific of single body parts representations related to their fine movements (Alexander & DeLong, 1985b). This somatotopic organization is preserved in striatal efferent projections. Indeed, the striatal neurons receiving inputs from M1 innervate the ventral two thirds of the posterior GPe and GPi, whereas striatal neurons receiving inputs from the SMA project more anteriorly and dorsally within these nuclei (Smith & Parent, 1986; Parent, 1990; Yoshida *et al.*, 1993). Moreover, leg, arm, and face representations project to corresponding dorsolateral-to-ventromedial territories of both the GPe and GPi, as well as to the dorsal one-third of the SNr (Nauta & Mehler, 1966; Parent *et al.*, 1984; DeLong *et al.*, 1985; Smith & Parent, 1986; Yoshida *et al.*, 1993). Within the dorsal SNr, the orofacial territory (continuous with that of the GPi) is further subdivided into a ventral SMA-related territory and a more dorsal M1-related territory, whereas the anteromedial SNr contains the oculomotor territory (Hikosaka & Wurtz, 1983). BG output is then conveyed to the thalamus in a topographically organized manner. The GPi projects primarily to the pars oralis of the ventrolateral nucleus and to the ventroanterior nucleus, whereas the orofacial territory of the SNr projects to the medial subdivision of the ventrolateral nucleus and to the magnocellular subdivision of the ventroanterior nucleus. These thalamic regions project back to motor cortical areas, including the SMA, premotor cortex, and M1, thereby closing the sensorimotor loop (Schell & Strick, 1984).

The STN also contains a distinct motor territory located dorsally and organized somatotopically. Within this region, the lateral STN receives projections predominantly from M1, whereas the medial STN receives inputs from the SMA, premotor, and cingulate motor cortices (Monakow *et al.*, 1978; Carpenter *et al.*, 1981; Nambu *et al.*, 1996). Ventral to the motor territory lies the oculomotor region (Matsumura *et al.*, 1992). Somatotopic representations within the STN are arranged such that, in the dorsolateral STN, hindlimb, forelimb, and orofacial representations are organized from medial to lateral, whereas this organization is reversed in the dorsomedial STN (Nambu *et al.*, 1996). STN output is also topographically organized. The dorsomedial STN projects to the anteroventral regions of the GPe and GPi as well as to the SNr, the dorsolateral STN projects to posterodorsolateral regions of both GPe and GPi, and the central STN projects to the central GPe (Carpenter *et al.*, 1981; Smith *et al.*, 1994). In addition to its topographically organized output, the STN is embedded in a reciprocal and spatially ordered loop with the GPe. Tracing studies have shown that the anterior STN receives projections from the anterior GPe, whereas the lateral STN is preferentially innervated by the central GPe, further reinforcing the topographic organization of the subthalamo-pallidal network (Carpenter *et al.*, 1981).

1.3.2.2 Associative circuit

The dorsolateral prefrontal cortex (dlPFC), lateral orbitofrontal cortex (lOFC), parietal, temporal, and occipital cortices project to the anteromedial putamen and to the CD along the entire anteroposterior axis, defining the associative striatal territory. Within this territory, projections are organized topographically, with parietal inputs terminating most laterally, dorsolateral

prefrontal inputs more dorsolaterally, and orbitofrontal inputs more ventromedially (Goldman & Nauta, 1977; Yeterian & Van Hoesen, 1978; Selemon & Goldman-Rakic, 1985). As described above, the associative striatum also receives dense dopaminergic innervation from the SNc. Associative striatal neurons project primarily to the anterior segment of the GPe, the dorsal one third of the posterior GPe and GPi, and the anteromedial two thirds of the SNr (Smith & Parent, 1986). In parallel, the ventrolateral STN, which receives massive inputs from prefrontal cortical areas, projects to the associative territory of the GPi located in its dorsal and anteromedial regions (Monakow *et al.*, 1978; Parent, 1990). The dorsomedial GPi projects to the parvocellular subdivision of the ventral anterior thalamic nucleus, which in turn projects to frontal cortical areas including the prefrontal cortex (PFC) (Kim *et al.*, 1976; Kievit & Kuypers, 1977; Middleton & Strick, 1994). In parallel, the anterolateral SNr projects to the parvocellular subdivision of the mediodorsal thalamic nucleus, which sends dense projections to the dlPFC (Ilinsky *et al.*, 1985). In addition, associative regions of the ventral anterior thalamic nuclei project directly back to prefrontal cortical areas, thereby closing the associative CBG-thalamo-cortical loop (Kievit & Kuypers, 1977; Middleton & Strick, 1994).

1.3.2.3 Limbic circuit

Limbic and paralimbic cortical areas, including the anterior cingulate cortex (ACC) and medial orbitofrontal cortex (mOFC), as well as subcortical limbic structures such as the amygdala and hippocampus, project to the VS (Selemon & Goldman-Rakic, 1985; Haber *et al.*, 1990). The VS comprises the NAc, the olfactory tubercle, and ventral portions of the CD and ventromedial putamen, and constitutes the limbic striatal territory. As described above, this region receives dense dopaminergic innervation primarily from the VTA. Limbic striatal neurons project predominantly to the VP, as well as to the most anterior portion of the GPe and the most ventromedial region of the GPi. In addition, they project more diffusely to the substantia nigra including the anterodorsal SNr, with prominent projections to the SNc and only sparse projections to the VTA (Haber *et al.*, 1990; Parent, 1990). In parallel, the ventromedial tip of the STN constitutes the limbic subthalamic territory and participates in limbic BG processing (Parent, 1990). BG output from the limbic circuit is conveyed primarily through the mediodorsal nucleus of the thalamus. This limbic thalamic territory projects back to the ACC and mOFC, thereby closing the limbic CBG-thalamo-cortical loop (Haber *et al.*, 1990; Parent, 1990).

1.3.2.4 Summary

To summarize, there is a gradient of projections of the limbic, associative and sensorimotor cortices with the limbic territory being occupying the most anterior and ventromedial regions of the striatum and of the pallidum whereas the sensorimotor territory is located in the most posterior and dorsolateral regions of the striatum and pallidum and the associative territory laying in between the two as illustrated in Figure 1-6. To simplify, the BG can be divided into a dorsal, sensory-motor-associative circuit and a ventral, limbic circuit.

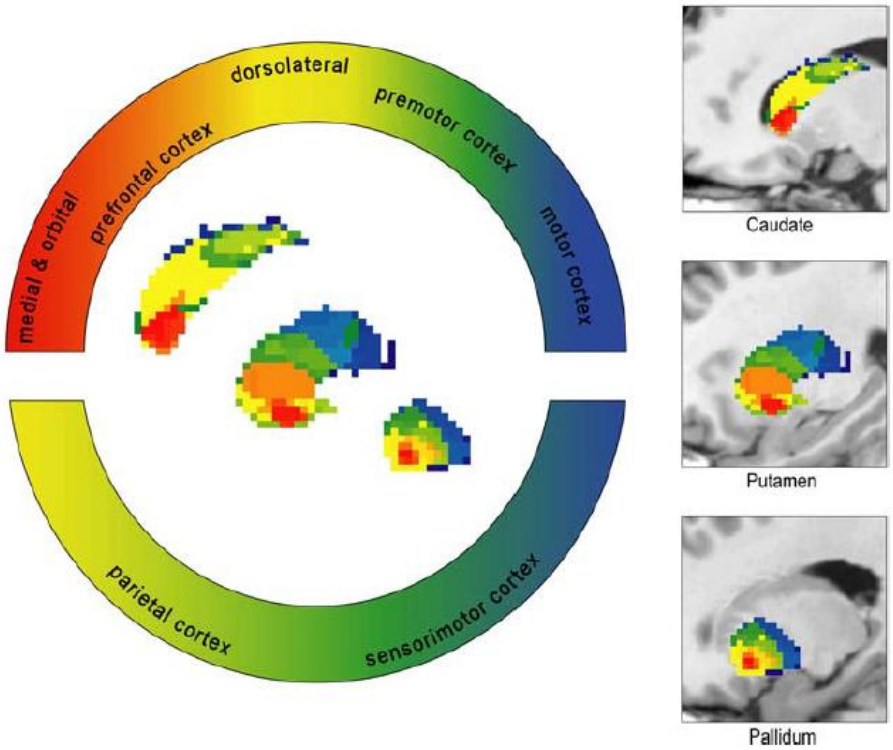

Figure 1-6. The gradient of projections of the limbic, associative and sensorimotor circuits.
The figure illustrates the continuous gradient of limbic, associative, and sensorimotor cortical inputs within the striatum (caudate nucleus and putamen) and pallidum in humans. Limbic inputs (red) are found in ventromedial and anterior regions, associative inputs (yellow) are located in intermediate territories, and sensorimotor inputs (green to blue) occupy dorsolateral and posterior regions. Taken from (Draganski et al., 2008).

1.3.3 Convergence and divergence within and between the segregated basal ganglia

Within each segregated BG circuit, anatomical and physiological studies have shown that there is convergence of cortical information at multiple stages. Indeed, as described above, the M1 territory extends to the dorsomedial putamen while the SMA territory extends to the ventrolateral with a convergence body representation of both M1 and SMA regions in the medio-lateral central zone that occupies one-quarter of each territory (Nambu, Kaneda, *et al.*, 2002). Double anterograde labeling studies have further shown that, within the arm representation of the putamen, terminals from different sensorimotor cortical areas overlap within the same striatal regions rather than occupying separate domains, indicating convergence of motor-related information at the striatal level (Alexander *et al.*, 1986; Flaherty & Graybiel, 1993; Inase *et al.*, 1996). This overlap was confirmed by microstimulation of M1 or SMA which showed activation of putaminal neurons in the central zones (Nambu, Kaneda, *et al.*, 2002). In addition, there is also convergence at the STN level, in which the SMA and M1 project in a reversed way with a partial convergence within the nucleus (Nambu *et al.*, 1996). Similarly in the associative circuit, some striatal neurons in the anterior head of the CD showed convergence of prefrontal and parietal axon terminals (Selemon & Goldman-Rakic, 1985). Some overlapping information were also found among different circuits such as between the associative and the

limbic circuits which showed separate but also converging territories in the anterior DS enabling modulation between circuits (Haber *et al.*, 2006).

At the same time, divergence of information is present within each circuit. In the sensorimotor system, single cortical representations of specific body parts are distributed across multiple sites within the putamen before reconverging onto downstream pallidal neurons, illustrating how divergent cortical inputs can be integrated at later stages of BG processing (Flaherty & Graybiel, 1994).

1.4 Electrophysiological properties

The BG nuclei are composed of various neurons with different electrophysiological properties. Information within the BG is conveyed through excitatory, glutamate-mediated inputs and inhibitory, GABA-mediated inputs. Projection neurons act on their downstream targets to increase or decrease their FR depending on the balance of these inputs. As described above DANs modulate differentially their downstream striatal targets depending on the type of receptor they express. Interneurons have a local inhibitory (GABA mediated) or modulatory (acetylcholine mediated) action. Described below are the spontaneous activity in terms of FR and pattern and evoked activity elicited by sensory and behavioral events of each neuronal type in the main axis of the BG and its modulator structures as described in the actor-critic model discussed above. Unless otherwise stated, the findings summarized here are from NHP studies.

1.4.1 Main axis

The main axis of the BG is composed of projection neurons from the input (striatum and STN), central (GPe) and output structures (GPi/SNr). The STN is the only excitatory structure in the BG whereas the remaining structures are inhibitory.

1.4.1.1 Basal ganglia input structures

1.4.1.1.1 Striatal medium spiny neurons

Spontaneous activity: MSNs, which constitute 85-95% of striatal neurons, are GABAergic projection neurons with a very low spontaneous FR in awake primates (see Figure 1-7a), typically around 0.5-2 spikes/s (Kimura *et al.*, 1990; Apicella, Ljungberg, *et al.*, 1991). Their spontaneous activity is largely uncorrelated across the population, indicating overall independent baseline firing.

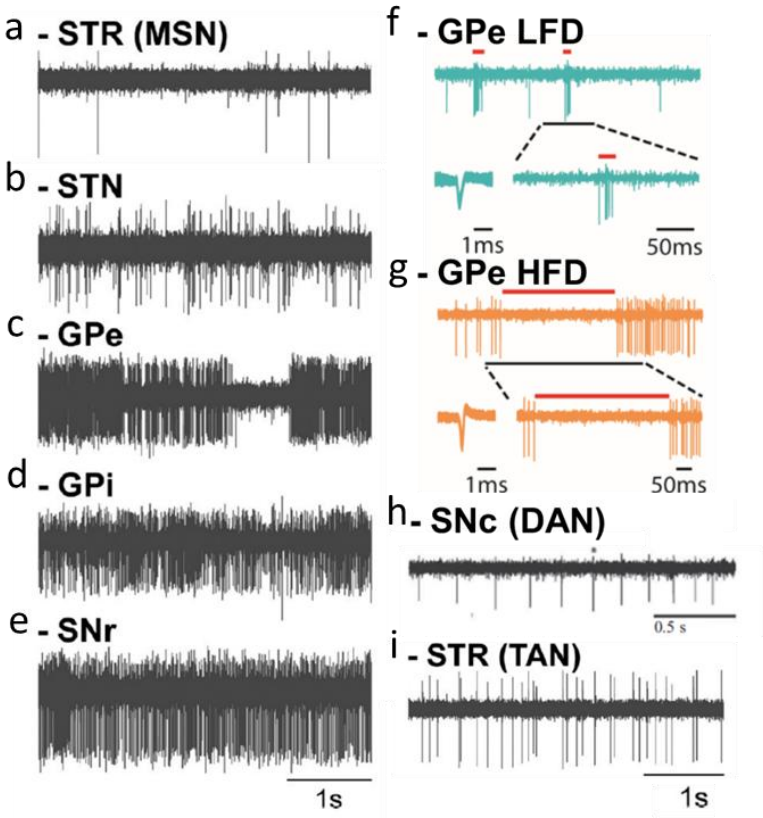

Figure 1-7. Example of spontaneous spiking activity of different basal ganglia neurons.
Left panel shows examples of neurons within the actor main axis with striatal MSNs (a), STN (b), GPe (c), GPi (d) and SNr (e) neurons. Top right panel shows examples of a low-frequency discharge (LFD) neuron (f) with bursts of activity and a high-frequency discharge (HFD) neuron (g) with a pause found in the GPe. Bottom right panel shows examples of critic neuromodulatory neurons with dopaminergic neurons (DANs, h) and striatal cholinergic neurons (TANs, i) from the SNc. Adapted from (Haber et al., 2012; Deffains et al., 2016; Katabi et al., 2023).

Event-related modulation: MSNs exhibit mainly transient increases in FR in response to behaviorally relevant events, including movement initiation, sensory cue presentation, reward anticipation and outcome delivery (Kimura *et al.*, 1984, 1990; Hikosaka *et al.*, 1989; Apicella, Ljungberg, *et al.*, 1991; Turner & DeLong, 2000; Samejima *et al.*, 2005). Because of these brief, event-locked responses, MSNs are also referred to as phasically active neurons.

Task-related response profile: Individual MSN responses are diverse and can be sharply phasic or more prolonged, with variable onset latencies relative to task events (Adler *et al.*, 2012; Adler, Finkes, *et al.*, 2013; Adler, Katabi, *et al.*, 2013). Notably, Adler and colleagues found that responding MSNs were clustered into 3 temporally differentiated but overlapping subsets: one group responded sharply and immediately after the cue presentation, another group with a delay in response which lasted until the extinction of the cue and an intermediate group (Adler *et al.*, 2012). Population-level analyses have shown that these heterogeneous response profiles produced a sustained modulation when averaged across neurons (Adler *et al.*, 2012; Adler, Finkes, *et al.*, 2013; Deffains *et al.*, 2016).

Population structure: During task events, transient correlations can emerge among subsets of MSNs with similar event-locked response timing, while the overall striatal population remains largely decorrelated (Adler *et al.*, 2012; Adler, Katabi, *et al.*, 2013). Notably, in the putamen, MSN-MSN pairs exhibit a pronounced bias toward positive signal correlations, indicating greater similarity in their average tuning profiles, as well as positive noise correlations, reflecting structured trial-to-trial population coupling, compared with MSN pairs in the CD or VS (Adler, Finkes, *et al.*, 2013). This organization reflects overall temporally structured but sparse coordination, with correlated activity restricted to neurons sharing similar temporal response profiles, rather than global striatal synchrony.

Functional interpretation: Together, the low baseline FR, heterogeneous event-related responses, and largely decorrelated population activity of MSNs support a role in high-dimensional encoding of task state and action-related information, consistent with an actor-like function in RL models.

1.4.1.1.2 Subthalamic neurons

Spontaneous activity: STN neurons exhibit relatively high spontaneous FR in awake primates, averaging around 20-30 spikes/s (Figure 1-7b), and frequently discharge in doublets or triplets bursts (Georgopoulos *et al.*, 1983; DeLong *et al.*, 1985). Baseline activity across STN neurons is largely uncorrelated, indicating independent firing under resting conditions (Wichmann *et al.*, 1994).

Event-related modulation: STN neurons are modulated by a wide range of task-related events, including sensory cues, movement initiation and execution, and motivational variables (Georgopoulos *et al.*, 1983; DeLong *et al.*, 1985; Wichmann *et al.*, 1994; Nambu *et al.*, 1996; Deffains *et al.*, 2016). Consistent with the encoding of motivational variables, in behaving primates, STN activity is modulated by reward-predicting cues, reward expectation, reward delivery, and outcome omission, often in conjunction with movement-related signals (Darbaky *et al.*, 2005; Espinosa-Parrilla *et al.*, 2013; Deffains *et al.*, 2016). More recent work has further demonstrated modulation of STN neurons by effort requirements and reward value, as well as by reward identity, particularly within ventromedial regions of the nucleus (Espinosa-Parrilla *et al.*, 2015; Nougaret *et al.*, 2022).

Task-related response profile: STN responses are typically phasic, with rapid increases in firing that precede or accompany behavioral events. Response timing varies across neurons, and both excitatory and inhibitory modulations can be observed depending on task demands and anatomical location within the nucleus (Georgopoulos *et al.*, 1983; DeLong *et al.*, 1985; Wichmann *et al.*, 1994; Nambu *et al.*, 1996).

Population structure: Despite robust task-related modulation at the single-neuron level, population activity in the STN remains largely decorrelated, both at rest and during task execution (Wichmann *et al.*, 1994). This decorrelation suggests that STN neurons contribute independently to BG processing rather than acting as a synchronized population.

Functional interpretation: The combination of high FR, rapid phasic modulation, and decorrelated population activity supports a role for the STN as part of the BG main axis involved in fast, high-dimensional control of action selection and inhibition, consistent with an actor-like computational function.

1.4.1.2 Basal ganglia central structure

Spontaneous activity: In primates, GPe neurons fire at relatively high rates and can be divided into two electrophysiological populations (see Figure 1-7c,f,g): HFD neurons and LFD neurons (DeLong, 1971; Georgopoulos *et al.*, 1983; Katabi *et al.*, 2023). The HFD neurons represent approximately 85% of total GPe and fire at high rates (55 spikes/s on average) with characteristic spontaneous pauses (Figure 1-7f). Indeed, the vast majority (95% of HFD neurons) show frequent interruptions in firing. The average pause duration is 620ms with a mean frequency of 13 pauses/min and were distributed randomly in time (Elias *et al.*, 2007). The LFD neurons account for the remaining 15% of total GPe, firing at lower rates (10 spikes/s on average) and showing short burst of activity (5 to 30 spikes per burst) with occasional long periods of single spike activity (Figure 1-7g) (DeLong, 1971; Georgopoulos *et al.*, 1983; Katabi *et al.*, 2023). Early electrophysiological recordings in humans and in rodents also observed these two types of neurons (Hutchison *et al.*, 1994; Benhamou *et al.*, 2012). More recent studies identified two types of GPe neurons as described above: the arkypallidal neurons and the prototypic neurons (Mallet *et al.*, 2012; Abdi *et al.*, 2015). Prototypic neurons project to the STN and output structures and resemble primate HFD neurons in their higher FR while arkypallidal neurons project back to the striatum and resemble primate LFD neurons in their lower and burstier FR (Katabi *et al.*, 2023). Still, despite their similarities in discharge rate and pattern, there is no evidence that the NHP GPe LFD and HFD neurons are homologous to the rodent arkypallidal and prototypic neurons, respectively. Cross-correlation analysis showed that spontaneous activity of the HFD neurons is decorrelated, demonstrating that GPe cells fire independently under healthy conditions (Nini *et al.*, 1995; Raz *et al.*, 2000). Consistent with this, Katabi and colleagues confirmed that HFD-HFD pairs exhibited decorrelated spontaneous activity, whereas LFD-LFD pairs were correlated (Katabi *et al.*, 2023). Similar heterogeneity in spontaneous discharge has been reported in the VP, where neurons exhibit either medium-to-high FR with pauses or low FR with bursty activity, albeit with a lower average FR than GPe neurons (Mitchell *et al.*, 1987).

Event-related modulation: GPe neurons show both increases and decreases in FR in response to task events such as movement initiation, sensory cues, reward-predicting stimuli and outcome delivery (Georgopoulos *et al.*, 1983; Kimura *et al.*, 1984; Joshua, Adler, Rosin, *et al.*, 2009; Adler *et al.*, 2012; Deffains *et al.*, 2016; Nougaret & Ravel, 2018). VP neurons on the other hand did not display modulatory activity in response to movements but did in response to reward predictive cues and to rewards (Mitchell *et al.*, 1987; Kaplan *et al.*, 2020).

Task-related response profile: Task-related responses in GPe neurons can be transient or sustained and may be excitatory or inhibitory (Adler *et al.*, 2012). Notably, Adler and colleagues found that cue-responding GPe neurons were clustered into two subsets: one group displayed a

sharp transient increase in FR whereas the second showed an immediate phasic decrease, most of the time followed in both groups by a prolonged component overlapping in time, resulting in an averaged sustained population activity (Adler *et al.*, 2012). At the population level, both increases and decreases occur with similar frequency, as shown by the symmetric distribution of correlation values pattern (Joshua, Adler, Prut, *et al.*, 2009). In the VP, two subsets were also identified: a persistently activated population correlated with monkey's behavior and a transiently activated population correlated with the rate of learning and RL model's prediction error (Kaplan *et al.*, 2020).

Population structure: Cross-correlation analyses indicate HFD neurons remain uncorrelated during task events, whereas LFD neuron pairs show correlated firing (Nini *et al.*, 1995; Raz *et al.*, 2000; Katabi *et al.*, 2023). Importantly, HFD neurons preferentially encode cue valence, exhibiting stronger and more selective responses to rewarding than to aversive cues, whereas LFD neurons are less selective and respond to a wide range of task events, including rewarding and aversive outcomes as well as omissions, suggesting a more general role in signaling behaviorally relevant events consistent with a salience signal (Joshua, Adler, Rosin, *et al.*, 2009). Similarly to the GPe, neurons in the VP that displayed sustained task-related activity showed little pairwise correlation, despite their firing remaining correlated with the monkey's behavior. In contrast, VP neurons with transient, phasic responses exhibited correlated activity and synchronized firing (Kaplan *et al.*, 2020).

Functional interpretation: The coexistence of heterogeneous response profiles, largely independent firing, and differentiated encoding of task variables supports the view that the GPe/VP sustained activity participate in high-dimensional integration and transformation of information within the BG main axis, consistent with an actor-like computational role.

1.4.1.3 Basal ganglia output structures

Spontaneous activity: Neurons in the GPi and SNr fire continuously at high rates in awake primates (Figure 1-7,e), typically around 70-90 spikes/s, without long silent periods (DeLong, 1971; Georgopoulos *et al.*, 1983). Unlike GPe which can be divided in two populations, GPi and SNr neurons are quite homogeneous in their spontaneous firing properties. Although firing is continuous, it is irregular and displays frequent brief fluctuations (DeLong, 1971; Georgopoulos *et al.*, 1983). Cross-correlation analyses have shown that baseline activity across neurons is largely uncorrelated, indicating independent firing of individual GPi and SNr neurons under healthy conditions (Nini *et al.*, 1995; Raz *et al.*, 2000; Nevet *et al.*, 2004).

Event-related modulation: GPi and SNr neurons are modulated by behavioral events such as movement initiation, sensory cue presentation, reward-predicting stimuli and outcome delivery (Georgopoulos *et al.*, 1983; Kimura *et al.*, 1984; Joshua, Adler, Rosin, *et al.*, 2009; Deffains *et al.*, 2016). Population responses to rewarding events are larger than responses to aversive or neutral events especially for the GPi, although individual neurons respond with either increases or decreases in FR (Joshua, Adler, Rosin, *et al.*, 2009). Moreover, SNr response latency to all predictive cues was shorter compared to pallidal neurons.

Task-related response profile: Task-related responses consist of transient increases or decreases in FR occurring in close temporal relation to task events. While individual GPi and SNr neurons exhibit diverse and largely phasic response profiles, population-level activity can appear temporally extended due to the overlap of heterogeneous single-neuron responses distributed across the task epoch (Joshua, Adler, Rosin, *et al.*, 2009; Deffains *et al.*, 2016).

Population structure: Despite strong task-related modulation, GPi and SNr neurons remain largely decorrelated at the population level, with approximately equal proportions of neurons showing increases and decreases in firing during task events and symmetric response correlation patterns (Joshua, Adler, Prut, *et al.*, 2009; Joshua, Adler, Rosin, *et al.*, 2009). This independence is consistent with earlier cross-correlation analyses demonstrating minimal synchrony among output neurons (Nini *et al.*, 1995; Raz *et al.*, 2000; Nevet *et al.*, 2004).

Functional interpretation: The high tonic FR, heterogeneous response profiles, and largely independent population activity of GPi and SNr neurons support their role as output components of the actor, transforming high-dimensional striatal and subthalamic signals into precise inhibitory control over downstream targets.

1.4.2 Modulator

As described in the actor-critic model of the BG, modulatory activity of the main axis mainly comes from midbrain DANs and from striatal cholinergic interneurons.

1.4.2.1 Midbrain dopaminergic neurons

Spontaneous activity: Midbrain DANs fire at low tonic rates, typically between 1 and 8 spikes/s in awake primates (see Figure 1-7h). Under baseline conditions, their activity is relatively sparse and only weakly correlated across neurons, indicating largely independent spontaneous firing (Morris *et al.*, 2004; Joshua, Adler, Prut, *et al.*, 2009).

Event-related modulation: DANs exhibit transient modulations of FR in response to primary rewards, reward-predictive cues, and violations of reward expectation (Schultz *et al.*, 1993, 1997). Rewarding events and reward-predicting stimuli typically elicit brief phasic increases in firing, whereas negative prediction errors, such as reward omission, are reflected by transient pauses. Dopaminergic responses to aversive events are more variable and generally weaker than responses to reward, indicating an asymmetry in motivational encoding (Schultz *et al.*, 1993; Morris *et al.*, 2004; Joshua, Adler, Prut, *et al.*, 2009).

Task-related response profile: With learning, responses shift from reward delivery to predictive cues, consistent with prediction error signaling. Importantly, dopaminergic responses are temporally coincident with the stereotyped pause-rebound responses of striatal cholinergic interneurons, although the two populations encode distinct aspects of task structure (Morris *et al.*, 2004; Joshua *et al.*, 2008).

Population structure: In contrast to BG projection neurons, DANs display highly homogeneous response profiles across the population, with similar polarity and timing across neurons. Correlation analyses reveal a strong bias toward positive correlations during task events, indicating coordinated population signaling (Joshua, Adler, Prut, *et al.*, 2009).

Functional interpretation: The low-dimensional, homogeneous, and correlated nature of dopaminergic signaling is consistent with a critic-like function, providing a global teaching signal that conveys prediction errors to guide learning in BG circuits (Schultz *et al.*, 1997; Schultz, 1998).

1.4.2.2 Striatal tonically active neurons (presumed cholinergic interneurons)

Spontaneous activity: Striatal TANs fire tonically at low-to-moderate rates in awake primates (approximately 2-7 spikes/s, see Figure 1-7i) and exhibit correlated spontaneous activity (Kimura *et al.*, 1990; Apicella, Scarnati, *et al.*, 1991; Aosaki *et al.*, 1994).

Event-related modulation: TANs display highly stereotyped, phasic responses to behaviorally and motivationally relevant events, including primary rewards and stimuli that have acquired motivational significance through learning (Kimura *et al.*, 1984; Aosaki *et al.*, 1994; Apicella *et al.*, 1997). TAN responses are reliably elicited by both rewarding and aversive events, particularly when these events occur unexpectedly or violate established temporal predictions (Apicella *et al.*, 1997; Ravel *et al.*, 1999; Apicella, 2002, 2007; Joshua *et al.*, 2008; Nougaret & Ravel, 2015). These responses are classically characterized by a pronounced pause in their tonic firing lasting ~200-300 ms, often preceded by a brief excitation and followed by a rebound increase in activity.

Task-related response profile: TAN responses are largely insensitive to the specific motor parameters of actions and to the sensory features of cues, as they can be elicited in both instrumental and passive contexts, including situations in which stimuli are presented without any requirement for action or response (Kimura *et al.*, 1984; Apicella, Scarnati, *et al.*, 1991). Nevertheless, a subset of TANs exhibits context-dependent directional or spatial selectivity to instruction or trigger cues, indicating that visuospatial information relevant for action selection can modulate TAN activity (Kimura, 1986, 1992; Shimo & Hikosaka, 2001). Overall, TAN responses primarily reflect behavioral context and, in particular, the temporal predictability of events (Apicella *et al.*, 1997). TAN phasic modulations are enhanced when the timing of outcomes is uncertain or irregular, and reduced when events are temporally predictable. In contrast to DANs, TAN responses at outcome omission do not encode signed RPEs but instead reflect violations of expected timing, with robust modulation observed at the end of trials when expected outcomes fail to occur (Apicella, 2002, 2007; Morris *et al.*, 2004; Joshua *et al.*, 2008).

Population structure: At the population level, TAN responses are highly homogeneous across neurons and tightly synchronized in time, producing a single dominant, transient response pattern aligned to behaviorally relevant events. Correlation analyses reveal positively skewed signal and noise correlation distributions among TANs, indicating that neurons share similar event-related response profiles and exhibit coordinated trial-to-trial variability, consistent with strong, event-locked temporal coordination across the TAN population (Joshua, Adler, Prut, *et*

al., 2009; Adler *et al.*, 2012; Adler, Finkes, *et al.*, 2013; Adler, Katabi, *et al.*, 2013). This coordinated activity is particularly pronounced in the putamen, where TAN-TAN noise correlations are stronger than in other striatal territories (Adler, Finkes, *et al.*, 2013).

Functional interpretation: The correlated, homogeneous, and context-sensitive nature of TAN signaling about motivationally relevant events supports a modulatory, critic-like role, complementing dopaminergic prediction-error signals by regulating plasticity and contextual gating of learning in the striatum (Deffains & Bergman, 2015).

1.4.3 Summary

In summary, projection neurons of the BG main axis exhibit heterogeneous, largely decorrelated activity modulated by diverse task events, consistent with high-dimensional encoding and actor-like computations involved in state-action representation and selection. In contrast, neuromodulatory systems such as dopaminergic and cholinergic neurons display homogeneous, correlated population responses to evaluative events, consistent with critic-like teaching signals in actor-critic RL models.

Chapter 2 Neurobiology of decision-making

2.1 Conceptual framework for decision-making

Decision-making (DM) is a higher-order brain process consisting in choosing between at least two different alternatives. DM has been studied in various fields as part of the study of human behavior in an attempt to understand and predict it. These fields include psychology, economics and sociology resulting in multiple theories of DM (Glimcher *et al.*, 2009). Early economic theories relied on simple principles such as revealed preference theories which predicted preferences from observed choices and moved later to mathematical models formalizing preferences such as the expected utility theory. Psychological research demonstrated that choices were not rational leading to the development of new theories taking into account biases and heuristics such as the Prospect Theory. Advances in the field of neuroscience have brought to light how the brain integrates sensory, emotional and motivational information to guide decisions and helped characterize the neural basis of healthy and pathological DM.

In experimental and theoretical neuroscience, perceptual and value-based DM can be viewed as two fundamental classes of decision processes distinguished by the type of evidence they operate on. Choices during perceptual DM rely on accumulation of sensory evidence and decision threshold (Bogacz, 2007; Gold & Shadlen, 2007; Heekeren *et al.*, 2008; Shadlen & Kiani, 2013) whereas value-based DM relies on the evaluation and comparison of expected outcomes (Rangel *et al.*, 2008; Kable & Glimcher, 2009). These processes are not mutually exclusive (Cisek, 2012; Summerfield & Tsetsos, 2012; Cisek & Pastor-Bernier, 2014) and can both be implemented across a range of conditions that are independent of the decision signal per se (i.e., sensory evidence vs EV), including decisions based on learned or instructed rules, varying degrees of uncertainty or risk, and model-based or model-free computational strategies (Daw *et al.*, 2005; Ernst & Paulus, 2005; Lee *et al.*, 2014; Niv, 2019). In this manuscript, the focus is restricted to value-based DM, which directly involves the computation, representation, and updating of value signals that guide behavior. These properties make value-based DM particularly relevant for understanding the neural mechanisms underlying RL and the role of the BG in adaptive behavior.

2.1.1 Definition of value-based decision-making

Value-based DM refers to the selection of actions based on the evaluation of their expected outcomes. Conceptually, value-based DM can be divided both temporally and functionally into distinct steps as illustrated in Figure 2-1 (Ernst & Paulus, 2005). The first step is the assessment and the formation of preferences among possible options, also called valuation or estimation, in which a value is attributed to each available option. The second step consists in selecting and executing a behavioral response or an action. It requires initiation, performance and completion of action which requires a fine planning in terms of sequencing and timing but also inhibition of competing actions. The third is outcome evaluation or the processing of the consequences of the experience which consists in comparing what was expected to what was actually obtained.

Depending on the outcome, a new value can be attributed to the different options which leads to learning. Because the context of the decision can influence preferences, some authors include this assessment as an additional step in the DM process, called the representation of the decision problem (Rangel *et al.*, 2008). This representation corresponds to the way the decision-maker encodes the relevant features of the situation. The context includes internal factors such as the decision-maker's level of hunger when facing appetitive rewards or their level of fatigue, as well as emotions, which will be discussed briefly below. It also includes external factors such as perceived threat, characteristics of the decision itself (e.g., uncertainty, ambiguity, or risk), and social influence (Ernst & Paulus, 2005; Allain, 2013).

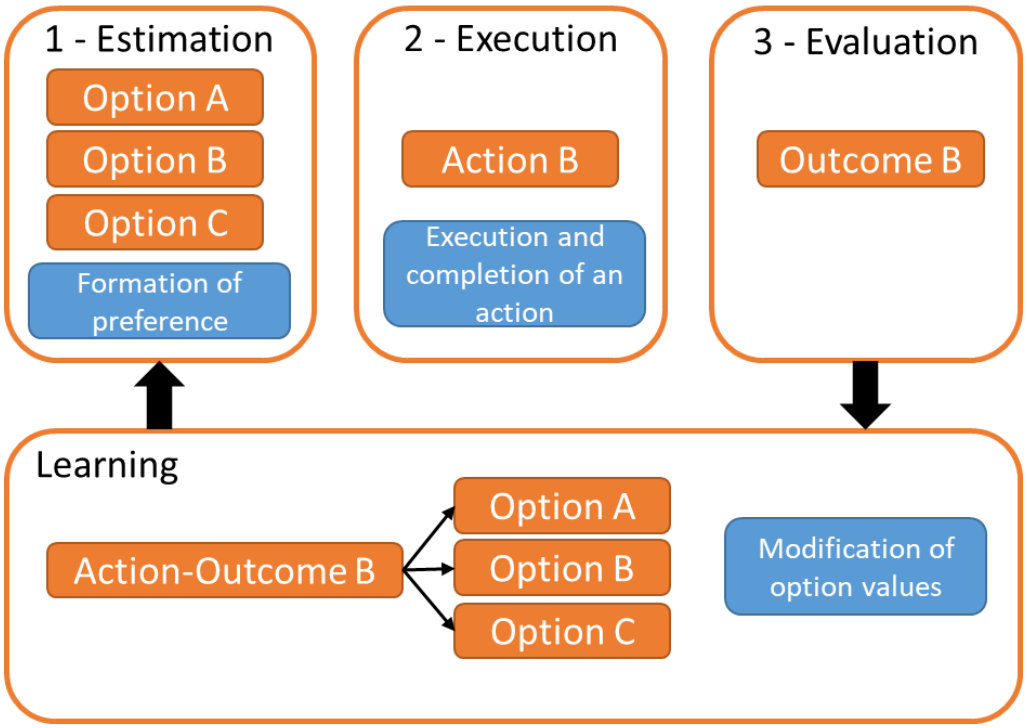

Figure 2-1. Functional and temporal division of goal-directed value-based decision-making process.
The decision-making process is divided into three main stages: (1) valuation or estimation, during which values are assigned to available options and preferences are formed; (2) action selection and execution, leading to the implementation of a chosen behavior; and (3) outcome evaluation, in which the obtained outcome is compared to the expected one. Outcome evaluation drives learning through the updating of option values based on action-outcome associations, thereby influencing subsequent decisions. Adapted from (Ernst & Paulus, 2005).

Value-based choice behavior can be implemented through at least three different valuation systems leading to the execution of the most appropriate action: Pavlovian, habitual and goal-directed systems (Rangel *et al.*, 2008). The goal-directed system corresponds to an outcome-based valuation which assigns values to options or actions based on the desirability of their expected outcomes. It assumes that the agent knows or predicts that actions have specific consequences and is therefore model-based. In contrast, the habitual system corresponds to an action-based valuation in which stimuli trigger learned stimulus-response associations that have been acquired though repeated past action-outcome pairings and relies on stored values. It is

therefore model-free. The Pavlovian system assigns value directly to stimuli which trigger innate or evolutionarily appropriate behaviors such as salivation when seeing food or hearing a bell associated with delivery of food. Although it is also model-free, it relies on stimulus-response associations and results in automatic specific responses rather than selected actions. Accordingly, in goal-directed systems, a single stimulus can lead to multiple possible actions among which one is selected based on the expected outcome whereas in habitual and Pavlovian systems, a single stimulus triggers a single automatic response.

Thus, goal-directed systems rely on flexible evaluation of action-outcome contingencies while Pavlovian and habitual systems rely on more automatic, respectively innate or learned associations. Habitual and Pavlovian systems differ from goal-directed systems by their resistance to outcome devaluation. Importantly, behavioral and computational studies have shown that even when tasks are designed to dissociate systems, behavior often reflects a mixture of model-based and model-free control (Daw *et al.*, 2005). In the present manuscript, we focus on goal-directed value-based DM because this form of DM most directly engages neural circuits underlying value representation, RL, and action selection, particularly within CBG networks.

2.1.2 Goal-directed value-based decision-making strategy

The aim of goal-directed value-based DM is to obtain and maximize desirable outcomes or rewards (in terms of pleasure, emotion and/or need) and to avoid or minimize undesirable ones. Goal-directed value-based DM refers to an outcome-oriented and learning-driven process relying on flexible evaluation of action-outcome contingencies and is driven by the EV which refers to the expected physical property (e.g., magnitude or quantity) of an outcome and is defined as the product of the probability of the outcome and the outcome in terms of magnitude or quantity.

Therefore, choosing the option with the highest EV maximizes rewards over time. Importantly these value estimates are not static but are continuously updated through experience using computational approach such as RL (Sutton & Barto, 1998). RL theory states that values are learned through iterative updating based on experience (i.e., by trial-and-error). Indeed, each time an agent experiences the outcome of its choice, the difference between the EV and the obtained outcome is computed and this RPE (also called temporal difference error) signal is used to update the value assigned to the option or action, leading to a reinforced behavior or its adjustment.

Overall, several kind of value-related signals are computed and used during value-based DM and RL. These include: (1) state value which corresponds to the expected cumulative future reward associated with being in a given state or context, independent of the action performed; (2) offer value which refers to the value associated with each offer or option, independent of the action required to obtain it (e.g., juice A has a higher value than juice B); (3) action value which corresponds to the value of the expected reward associated with a specific action (e.g., moving right is associated with the preferred juice A while moving left is associated with less preferred juice B); (4) chosen and non-chosen value which correspond to the value of the selected and unselected option or action, respectively; and (5) reward or outcome value which corresponds

to the value of the reward obtained and is used to compute the RPE (Samejima *et al.*, 2005; Padoa-Schioppa & Assad, 2006; Pasquereau *et al.*, 2007; Lau & Glimcher, 2008). In addition, value-based decisions can involve derived value-related signals including: (6) maximum value, which corresponds to the highest value among the available options or actions; and (7) value contrast, which corresponds to the difference in value between options or actions and supports comparative evaluation and difficulty during choice. It is noteworthy that many value-related signals coexist and are likely to covary during value-based DM, making it difficult to isolate the neural encoding of individual value variable. Therefore overcoming this collinearity is a central challenge when studying valuation and requires careful experimental and analytical strategies (Klein-Flügge *et al.*, 2011; Padoa-Schioppa, 2013; Elber-Dorozko & Loewenstein, 2018).

Moreover, the existence of multiple value-related signals does not imply that DM is driven exclusively by outcome value. Indeed, RL predicts that agents select the action that is associated with the highest learned value (e.g., the optimal action) for maximizing expected reward. However, this optimal action from a RL framework can be more costly (energetically or financially for example) than another one which would lead to a less valued outcome but sufficient enough to be chosen over the most valued or desired one. Decision-makers estimate the value associated with the action required through cost-benefit computation (Rangel & Hare, 2010). Costs are therefore also computed as a decision parameter during deliberation. Costs can be diverse depending on the context of the decision, including physical effort, cognitive effort (particularly when many alternatives are available) financial cost, or temporal delay to outcome delivery, which will be discussed in more detail below. Therefore, because cost matters, the EV influences not only choice behavior but also action vigor (Shadmehr & Ahmed, 2021). Vigor encompasses multiple aspects of movement, including velocity, reaction time (RT), and movement time (MT). When studying movements during DM, scientists found that humans and animals tended to move faster and with shorter RTs toward options that they value more. For instance, in studies involving humans and monkeys performing saccadic tasks toward visual targets associated with different reward magnitudes and probabilities (money or appetitive rewards, respectively), Milstein and Dorris showed that saccadic RTs were inversely correlated with the EV of the options (Milstein & Dorris, 2007, 2011). These findings suggest that movement vigor reflects not only motor execution but also the underlying motivational value of the selected option. Accordingly, vigor is closely related to motivational drive, which is commonly assessed through behavioral parameters such as response latency, duration, magnitude, frequency or probability of responding, and persistence over time (Berridge, 2004; Niv *et al.*, 2007; Shadmehr *et al.*, 2019; Shadmehr & Ahmed, 2021). Thus, vigor is a behavioral correlate of motivation and is often used as behavioral and measurable proxy for motivation. However, vigor is not a mere readout of motivation and is also influenced by additional task- and outcome-related factors. In particular, outcome valence (i.e., the attractiveness or aversiveness of an outcome) can modulate vigor when associated with high motivational stakes, independently of reward magnitude. In a task designed to dissociate motivational anticipation from outcome properties, Roesch and Olson showed that monkeys responded more rapidly both when approaching larger rewards and when avoiding larger penalties, and exhibited fewer fixation breaks compared to conditions involving

smaller rewards or penalties (Roesch & Olson, 2004). Further highlighting this complexity, Griffiths and Beierholm showed that although higher average punishment rates lead to slower action execution, immediate punishment was transiently associated with faster responses (Griffiths & Beierholm, 2017). Additionally, movement vigor can also be influenced by an urgency signal that depends on the context of the decision. Urgency reflects a time-dependent pressure to commit to a choice, increasing more rapidly in contexts where acting quickly maximizes reward rate. When urgency is high, decisions are made earlier and movements are more vigorous (Thura *et al.*, 2014; Thura, 2020). Conversely, when urgency is lower, decisions are delayed and movements are less vigorous, reflecting a strategy that favors prolonged evidence accumulation before commitment. Another key parameter that can influence vigor is the salience of the options which reflects the motivation and attentional significance of the outcome or in other words the "wanting" as stated in the incentive salience hypothesis (Berridge *et al.*, 1989; Robinson & Berridge, 1993).

As stated above, most theories formalize goal-directed value-based DM in terms of cost-benefit computations and address emotions as inputs to valuation or as mere consequences of decisions rather than as independent processes guiding deliberation (Rangel *et al.*, 2008; Rangel & Hare, 2010). In contrast, the somatic marker theory proposes that emotion-related bodily signals, acquired through prior experience, bias DM by marking options with positive or negative value during deliberation (Bechara *et al.*, 2000). In addition, affect, which is defined as the longer-lasting component of emotional states, can influence DM. For example, positive affect has been shown to alter the weighting of information by reducing the influence of probability of the outcome and increasing sensitivity to its magnitude, particularly in the loss domain (Nygren *et al.*, 1996).

2.1.3 Subjective valuation and deviations from normative expected value

Although EV defines a normative strategy for optimal value-based DM, observed behaviors frequently deviates from EV maximization leading to irrational behaviors. One of the earliest demonstrations of such deviations is the Allais paradox. In this experiment, participants chose between two options with identical EVs: a deterministic option guaranteeing a certain outcome and a probabilistic option offering a higher reward with some uncertainty. Despite equal EVs, participants consistently preferred the deterministic option, revealing an aversion to uncertainty (Allais, 1953). Moreover, it has been long known that the relationship between the amount of reward and the value is not linear but rather concave (Bernoulli, 1954). Similarly, probabilities are not perceived linearly, leading to systematic distortions in probability weighting (Gonzalez & Wu, 1999; Stauffer *et al.*, 2015). As a result, there is a subjective weighting of magnitude and probability on the EV function.

The Prospect Theory developed by Kahneman and Tversky provides a descriptive framework for DM under risk and uncertainty by explicitly incorporating these subjective distortions (Kahneman & Tversky, 1979). In this framework, outcomes are evaluated relative to a reference point and categorized as gains or losses. The value function is concave in the gain domain, indicating risk

aversion for higher magnitudes of gains, and convex in the loss domain, reflecting risk-seeking behavior for increasing losses as shown in Figure 2-2. Moreover, the value function in the loss domain has a steeper rate than in the gain domain indicating a higher sensitivity to losses. This higher sensitivity is a bias commonly referred to as loss aversion. Thus, outcome valence which determines the desirability or undesirability of the available options critically shapes the subjective valuation.

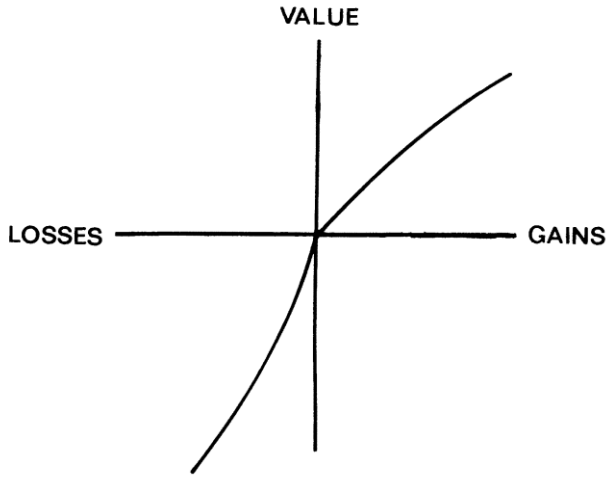

Figure 2-2. Value function in the loss and gain domains as proposed by the Prospect Theory.
The value function is defined relative to a reference point that separates gains from losses. It is concave in the gain domain, reflecting risk aversion, and convex in the loss domain, reflecting risk-seeking behavior. The steeper slope in the loss domain illustrates loss aversion, whereby losses are weighted more strongly than equivalent gains (Kahneman & Tversky, 1979).

Prospect Theory also takes into account the distortion of the probabilities as illustrated in Figure 2-3 by the nonlinear probability distortion function w(p) in both gain and loss domains. Indeed, objective probabilities are not weighted linearly and decision-makers display overweighting of low probabilities and underweighting of high probabilities behaviors as indicated by the inversed S-shape of the weighting function. This distortion is accentuated in the gain domain. Although other mathematical formulations of the weighting function exist depending on the experimental settings of the studies, they all converge on the conclusion that subjective probability weighting deviates systematically from rational choice predictions (Prelec, 1998).

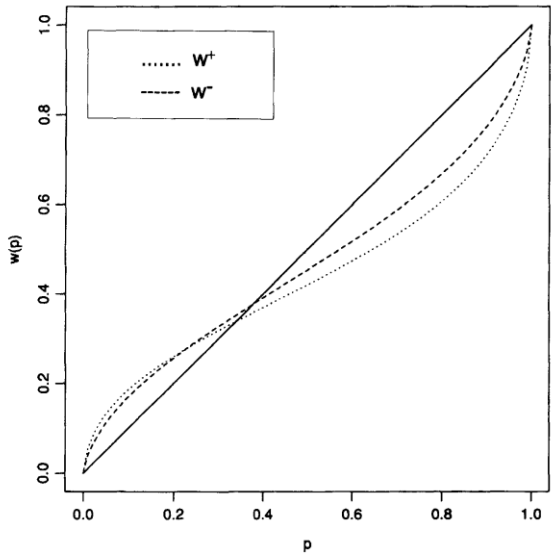

Figure 2-3. Probability weighting function as proposed by the Prospect Theory.

The nonlinear weighting function w(p) describes how objective probabilities are subjectively transformed in decision-making under risk. The inverse S-shaped curve reflects overweighting of low probabilities and underweighting of high probabilities. The functions w^+ and w^- correspond to probability weighting in the gain and loss domains, respectively (Tversky & Kahneman, 1992).

Together, these nonlinearities in reward magnitude and probability contribute to the concept of utility, first formalized by von Neumann and Morgenstern (von Neumann *et al.*, 1944), which reflects the subjective value assigned to outcomes. However, beyond distortions related to risk and probability, subjective value is also influenced by temporal factors. Indeed, an immediate reward is usually preferred over a delayed one. The temporal discounting function states that a lower value is assigned to delayed rewards whereas an immediate reward has a higher value (Frederick *et al.*, 2002). Thus, the relationship between value and time is not linear but rather convex. Two models of time discounting have been proposed, one exponential and one hyperbolic as illustrated in Figure 2-4.

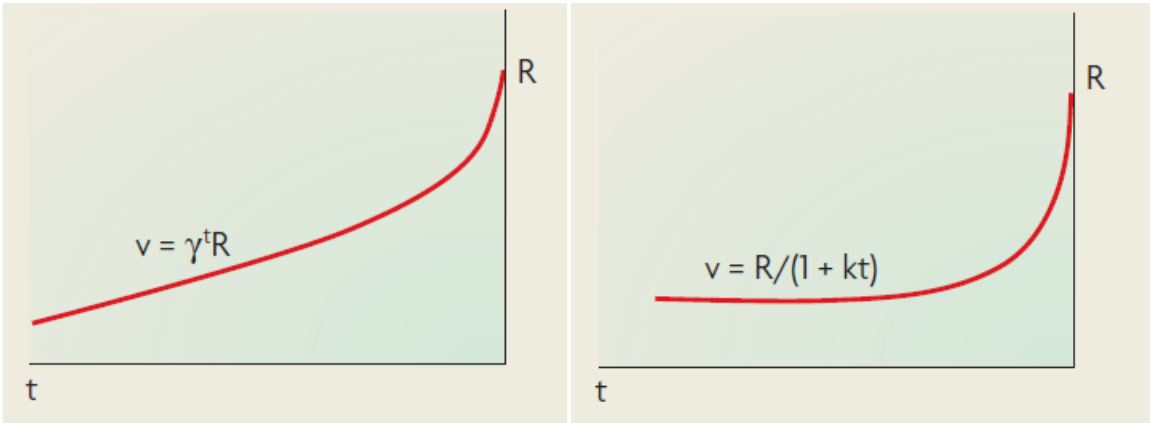

Figure 2-4. Models of time discounting functions.

The figure illustrates two models describing how the subjective value (v) of a reward (R) decreases as a function of delay (t). In the exponential model (left), value declines at a constant rate over time while in the hyperbolic model (right), value declines more steeply at short delays and more gradually at longer delays. Adapted from (Rangel et al., 2008).

Finally, subjective value is context-dependent and can be influenced by the available alternatives. In a choice task involving two juice types, A and B, Padoa-Schioppa and Assad showed that monkeys' preference for a given amount of juice A depended on the amount of juice B offered as an alternative. Although monkeys preferred juice A when both options were offered in equal quantities, increasing the amount of juice B progressively shifted choice toward B, indicating that the subjective value of juice A was defined relative to the available alternative rather than in absolute terms (Padoa-Schioppa & Assad, 2006).

2.2 The different substrates of value-based decision-making

As described above, value based-DM engages multiple cognitive and affective processes, including attention, reasoning, working memory and emotion as well as motor processes when action execution is required. It relies on the coordinated activity of a distributed network of cortical and subcortical brain regions innervated by midbrain DANs. The contribution of specific brain structures to the computation of distinct components of value-based DM has been investigated using various experimental approaches, including neuroimaging (primarily by functional magnetic resonance imaging (fMRI) which relies on blood-oxygen-level dependent (BOLD) signal), lesion studies, pharmacological manipulations and electrophysiological recordings, and in different species notably humans, monkeys and rodents. To avoid ambiguity, the species will be specified for each study in the following sections where relevant.

2.2.1 Cortical structures

The PFC which corresponds to the most anterior part of the frontal lobes, is highly involved in value-based DM and learning, as well as in higher-order cognitive processes such as goal-directed planning, working memory, attention and cognitive control. In contrast, posterior frontal regions including premotor and primary motor cortices are primarily involved in action selection, motor planning and action execution, while the sensory processing is largely supported by parietal, temporal and occipital cortical areas (Ungerleider & Haxby, 1994; Rizzolatti & Luppino, 2001; Borgognon *et al.*, 2025). Although these cortical regions are important for driving motor action and sensory processing during value-based DM involving visual or auditory stimuli and requiring motor output (Pastor-Bernier *et al.*, 2012; Summerfield & Tsetsos, 2012; Derosiere *et al.*, 2025), this paragraph will be mainly focused on the role of the PFC. The PFC can be broadly divided in lateral, medial and orbital regions. Because of their role in valuation processes described below, the ventromedial PFC (vmPFC) and OFC will be grouped together.

2.2.1.1 The ventromedial / orbitofrontal cortex

The OFC is commonly subdivided into lateral and medial portions, with the lOFC encompassing areas such as area 13 and lateral portions of area 11, and the mOFC including area 14 and medial

portions of area 11 (Ongür & Price, 2000; Haber & Knutson, 2010). The vmPFC broadly encompasses the mOFC, the ventromedial portion of Brodmann area 10 (frontopolar cortex), and ventral/anterior regions of the ACC, including the subgenual ACC (area 25) and the ventral portions of areas 24 and 32 (Ongür & Price, 2000; Haber & Knutson, 2010). Because some studies differentiate mOFC and lOFC in the context of valuation processes, sometimes grouping mOFC within vmPFC and sometimes treating OFC as a separate entity (particularly in NHP studies), this section refers to the OFC broadly while specifying mOFC and lOFC contributions when relevant.

A substantial body of fMRI research demonstrates that vmPFC and OFC encode multiple forms of value signals during both choice and outcome processing. These include EV, reward magnitude, reward probability, subjective value (e.g., preference and delay discounting), value signals defined relative to competing alternatives, and valence-specific outcome responses. In a seminal study, Knutson and colleagues used a probabilistic monetary incentive delay task and showed that activity within medial and orbital prefrontal regions correlated with EV (Knutson *et al.*, 2005). In another fMRI study, Tom and colleagues scanned human participants deciding whether to accept or reject gambles in which they had an equal chance of gaining or losing money (Tom *et al.*, 2007). They found that the activity in the vmPFC increased with potential gains and decreased with potential losses. Specifically, the decrease in activity in the loss domain was steeper than in the gain domain, providing neural evidence for loss aversion. This pattern is consistent with neural encoding of subjective value on a common scale integrating both positive and negative outcomes. Plassmann and colleagues investigated how much hungry human subjects were willing to pay for various snacks, reflecting how much participants valued the option proposed, and scanned their brain during the process. They found that during both free-bid and forced-bid trials, the willingness to pay was positively correlated with the activity in the mOFC, thus indicating that this region encodes subjective value of options independently of whether participants actively generated the bid (Plassmann *et al.*, 2007). Consistent with an integrative value representation role, Kable and Glimcher scanned subjects while they were choosing between an immediate smaller reward and a larger delayed one with the value of the larger reward varying in amount and in delay time and showed that the activity in the medial PFC (which largely corresponds to the vmPFC in this study) tracked the subjective time-discounted value of the delayed rewards, with a decrease in activity as delays increased (Kable & Glimcher, 2007). These findings support that vmPFC / OFC serve as a core valuation system. Extending this framework, Boorman and colleagues demonstrated that the vmPFC encodes the relative value of the chosen action during DM. Rather than reflecting the EV of the selected option alone, vmPFC activity correlated with the difference between the chosen and unchosen EVs (chosen - unchosen EV). This pattern indicates that vmPFC does not merely represent isolated option values but instead performs a comparative computation between competing alternatives. Activity increased with higher chosen value and decreased with higher unchosen value as illustrated in Figure 2-5, reflecting the value advantage of the selected action over its alternative (Boorman *et al.*, 2009). Therefore these results show that the vmPFC implements value comparison in addition to valuation. Outcome-related value (i.e., actual obtained reward or punishment) signals have also been observed in vmPFC and lOFC in an fMRI study where

participants repeatedly chose between two targets associated with different probabilistic gain and loss contingencies, which were periodically reversed (O'Doherty *et al.*, 2001). The authors reported a medial-lateral dissociation within OFC during outcome processing with mOFC showing greater activation following reward than punishment, and activity in this region scaled positively with reward magnitude. In contrast, lOFC was more strongly activated by punishment and its activity correlated with punishment magnitude. Although additional reward-related activation was observed in medial prefrontal regions along the ventromedial wall, the parametric magnitude effects were most clearly demonstrated within OFC. Together, these findings suggest that OFC may exhibit valence-specific coding during outcome processing, complementing the integrative and comparative valuation signals observed in vmPFC during DM.

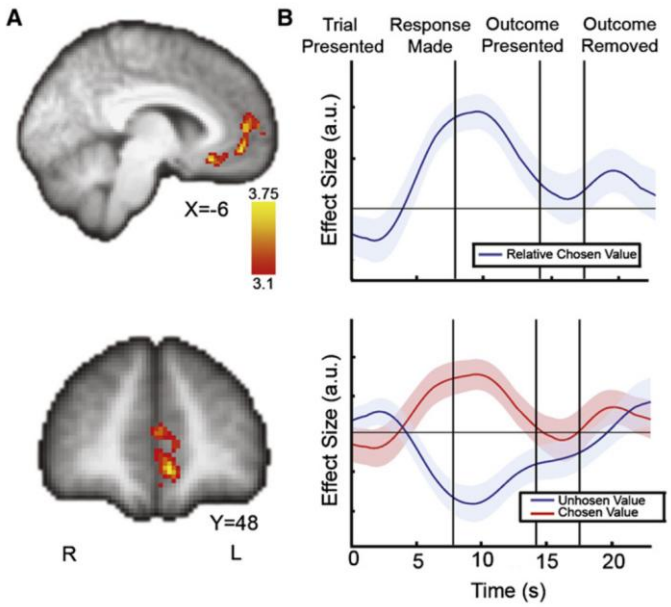

Figure 2-5. Ventromedial prefrontal cortex encodes the relative chosen value.
A: Sagittal and coronal views showing ventromedial prefrontal cortex (vmPFC) activity correlated with the difference between chosen and unchosen expected values (chosen - unchosen EV). B: Time course of regression estimates aligned to task events. Top: vmPFC activity tracks the relative chosen value. Bottom: decomposition of the signal reveals a positive correlation with chosen value (red) and a negative correlation with unchosen value (blue). Taken from (Boorman et al., 2009).

Lesion of the vmPFC has long been known to be associated with impaired value-based DM in humans while sparing general cognitive functions such as memory, attention, and language (Bechara *et al.*, 1996, 1998). Consistent with these findings, impaired value-based DM has also been observed in monkeys following OFC lesions. Lesioned monkeys failed to adjust their object choices after reinforcer devaluation (i.e., when the associated food was devalued through selective satiation) and showed deficits in contingency reversal learning when a previously rewarded object became non-rewarded (Izquierdo *et al.*, 2004). Importantly, these impairments occurred despite intact basic food preferences and satiety mechanisms, suggesting a disruption in using updated outcome value to guide behavior. Building on this, Rudebeck and Murray

examined the effects of selective lesions within OFC subregions in monkeys choosing between two appetitive reward-associated stimuli after devaluating one of them (Rudebeck & Murray, 2011). They reported that lOFC-lesioned monkeys chose less often the non-devaluated alternative than controls, indicating a failure to appropriately update stimulus-reward associations which was not observed in mOFC-lesioned monkeys. A complementary dissociation was demonstrated by Noonan and colleagues, who compared the effects of selective mOFC and lOFC lesions in a three-armed bandit task (Noonan *et al.*, 2010). In a first experiment using varying reward schedules, in which reward probabilities changed continuously during the session, lOFC-lesioned monkeys selected the optimal option less frequently than controls, reflecting impaired selective credit assignment. Specifically, rewards were not properly attributed to the stimulus that caused them, leading to inaccurate value updating. In contrast, mOFC lesions did not disrupt value learning. In a second experiment using fixed reward schedules, which minimized learning demands and isolated value comparison, mOFC-lesioned monkeys were impaired when the value difference between the best and second-best options was small, indicating a deficit in value comparison. Together, these findings support a functional dissociation in which lOFC contributes to value learning and updating, whereas mOFC is critical for comparing option values during DM.

Electrophysiological studies in NHP have confirmed that OFC encodes multiple forms of value signals during both choice and outcome processing. Indeed, Tremblay and Schultz demonstrated that OFC neurons fired in response to reward-predicting cues, during the expectation period preceding reward, and at the time of reward delivery (Tremblay & Schultz, 1999). These neurons discriminated between stimuli predicting different rewards, consistent with subjective value encoding. Importantly, the activity of some neurons (particularly within the most posteromedial recorded sites) reflected the animals' relative reward preferences. Specifically, when reward A was preferred over B, neuronal firing was greater (or lower, depending on the neuron) for A than B; however, when reward B was paired with C and became the preferred option, the same neurons now showed greater (or lower) firing for B. This context-dependent pattern indicates that OFC neurons encode the relative motivational value of available options. Building on this, population decoding work by Wallis and colleagues demonstrated that OFC implements value comparison through rapid, alternating neural states representing the chosen and unchosen value options (Rich & Wallis, 2016; Balewski *et al.*, 2022, 2023). In a subsequent study, Tremblay and Schultz recorded from OFC neurons (primarly lOFC and lateral portion of mOFC) while monkeys learned new stimulus-outcome associations (Tremblay & Schultz, 2000). They found that many neurons altered their responses to reward-predicting cues and during the reward expectation period as learning progressed, whereas responses to reward delivery remained largely stable. These findings suggest a role for OFC in flexibly updating values of available options during learning. Focusing specifically on outcome processing, Kennerley and Wallis examined how OFC neurons (primarily within lOFC) encoded experienced outcomes in blocks manipulating reward probability, magnitude, or required effort (Kennerley & Wallis, 2009). They found that in probability blocks, OFC neurons predominantly signaled whether reward was delivered or omitted. In magnitude blocks, a subset of OFC neurons encoded the size of the obtained reward in a graded manner. Although some neurons encoded outcome information across multiple

decision variables, many were selective for a single variable, indicating a distributed but partially overlapping representation of outcome value within OFC. Together, these findings support a role for the OFC in outcome-based valuation. Extending this view, Tsujimoto and colleagues showed that OFC neurons (primarily within lOFC) encoded the identity of the chosen response selectively near feedback time in a task requiring monkeys to monitor whether they repeated or switched their previous action (Tsujimoto *et al.*, 2009). This response-related signal was independent of reward outcome. This suggests that lOFC contributes to monitoring completed actions at evaluation time, a function that may support the updating of stimulus-reward associations and adaptive behavioral adjustments when outcome values change. Different kind of value encoding neurons have been reported in the monkey OFC, including offer value neurons which modulate their activity with the amount of one type of reward (juice) but not the other one, chosen value neurons which code the value of the chosen reward independently of its type and taste neurons which responded in a binary way to the identity of the chosen reward (Padoa-Schioppa & Assad, 2006; Padoa-Schioppa, 2013; Raghuraman & Padoa-Schioppa, 2014; Padoa-Schioppa & Conen, 2017; Ballesta *et al.*, 2020). The Figure 2-6 illustrates the different neurons found by the authors.

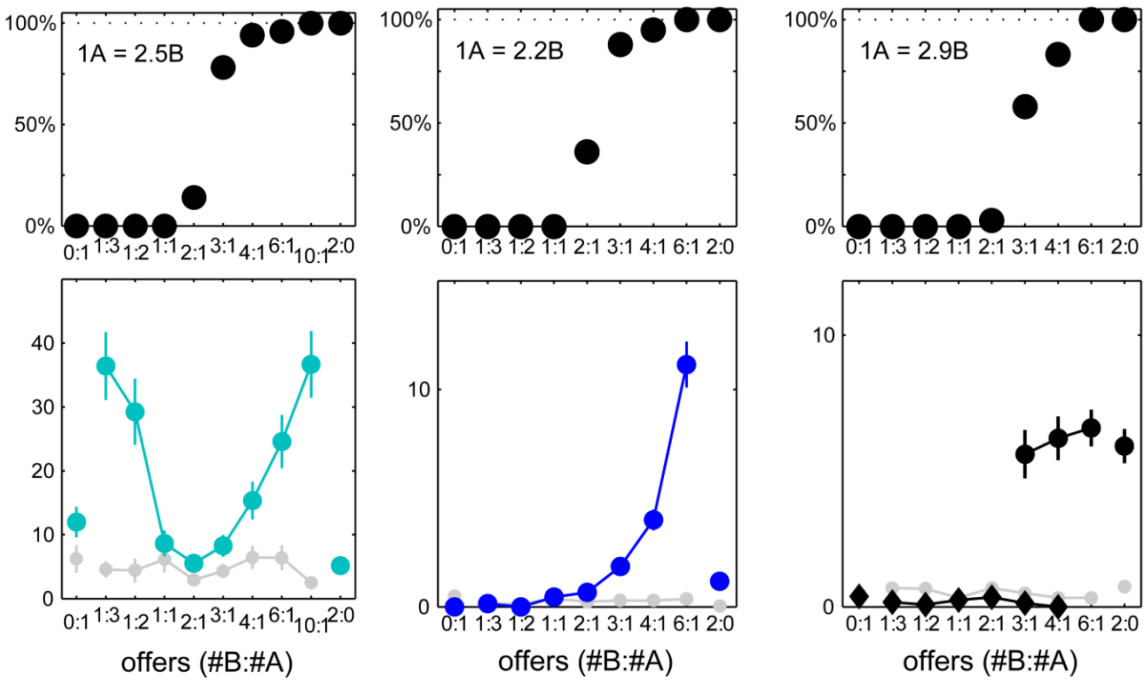

Figure 2-6. Examples of chosen value, offer value and taste neurons within the orbitofrontal cortex.
Top panels show the frequency of choice (y axis) as a function of the offer ratio between juices A and B (x axis). Bottom panels illustrate the activity of three different neurons types recorded in the orbitofrontal cortex. Left: a chosen value neuron, whose activity increases with the value of the chosen option, independently of reward identity. Middle: an offer value neuron, selectively encoding the value of one offered reward (juice B) but not the other. Right: a taste neuron, showing a binary response related to the identity of the consumed reward (e.g., juice A vs B), independent of its value. Taken from (Padoa-Schioppa & Assad, 2006).

Although anatomical boundaries were not always explicitly compared across studies, the overall pattern is consistent with a medial-lateral functional gradient, with more medial OFC regions

prominently involved in representing and comparing option values, and more lateral OFC regions contributing to credit assignment and the updating of stimulus-reward associations to guide behavioral adaptation. Importantly, these findings showing that vmPFC / OFC encode the value of different options, the value of obtained outcomes, and the relative value of competing actions across many tasks therefore suggest that these regions represent value on a common scale. This idea has led to the proposal that values are represented in the valuation network in a common neural currency enabling comparison between totally different options such as drinking a hot chocolate and eating a banana (Chib *et al.*, 2009; Levy & Glimcher, 2012).

2.2.1.2 The dorsomedial prefrontal cortex

The dorsomedial PFC (dmPFC) encompasses medial frontal regions including the dorsal ACC (dACC, dorsal portions of area 24 and 32). Similarly to the OFC, the dACC has been shown to contribute to value-based DM. To guide behavior, the dACC integrates several value components, assigns value to actions, computes cost-benefit trade-offs, and monitors choice difficulty or conflict as well as performance (outcome evaluation) in order to update action values.

In an fMRI study, Knutson and colleagues used a probabilistic monetary incentive delay task and showed that activity within the ACC (including its dorsal portion) correlated with EV, reflecting the integration of probability, magnitude and valence (Knutson *et al.*, 2005), confirming integration of value signals. Consistent with a role in monitoring decision conflict, dACC activity increases when individuals face difficult decisions involving options of similar desirability. For example, Pochon and colleagues scanned male participants who were asked to choose which of two female faces would be judged more attractive by other men (Pochon *et al.*, 2008). They showed that activity in the dACC increased with the level of decision conflict during these choices. This finding extends the classical conflict-monitoring role of the dACC, previously demonstrated in cognitive control tasks such as the Stroop task and the flanker task, in which the dACC detects competition between incompatible responses and signals the need for increased cognitive control (Botvinick *et al.*, 1999; Kerns *et al.*, 2004). Additionally, the dACC has been strongly linked to performance monitoring. Indeed, an fMRI study led by Holroyd and colleagues showed that during a trial-and-error learning task involving monetary gains and losses, the dACC was activated by both erroneous responses and error feedback signal, indicating that this region is sensitive to both internal and external error signals (Holroyd *et al.*, 2004). Consistent with this idea, other studies have shown that the dACC encodes both errors and rewards. For example, Walton and colleagues reported increased activation in the dACC following both positive or negative feedbacks, suggesting a role in monitoring the result of an action, regardless of whether the outcome is good or bad (i.e., regardless of its valence) (Walton *et al.*, 2004).

Kennerley and colleagues, later confirmed by Rudebeck and colleagues, showed that monkeys with lesions of the anterior cingulate sulcus, a region overlapping with the dACC, exhibited impaired value-based DM due to deficits in action-reward learning (Kennerley *et al.*, 2006; Rudebeck *et al.*, 2008). Specifically, lesioned animals failed to use reinforcement history

effectively to guide their choice and showed impairments in updating action values following reversals of action-outcome contingencies.

Electrophysiological studies confirmed that neurons in the dACC encode multiple decision variables during choice. In monkeys performing decisions in blocks manipulating reward probability, reward magnitude, or required effort, Kennerley and colleagues showed that dACC neurons encoded each of these variables and that many neurons were active across multiple blocks, indicating that they encoded more than one decision variable (Kennerley *et al.*, 2009). Compared with neurons in the OFC or in the dlPFC, dACC neurons more frequently multiplexed several variables simultaneously, suggesting that this region integrates costs and benefits relevant for action selection. In addition to integrating decision variables, dACC activity has been shown to contribute to the preparation of the chosen action. Population recordings revealed a ramping increase in dACC activity during deliberation that becomes direction-selective and precedes action execution (Balewski *et al.*, 2023). The slope of this ramp is influenced by the stability of value representations in OFC, linking value encoding to action commitment. Consistent with the role of dACC in guiding behavior through action-reward associations, Kennerley and Wallis also examined neuronal responses to outcomes and found that a substantial proportion of dACC neurons encoded outcome-related variables such as reward delivery and reward magnitude (Kennerley & Wallis, 2009). These outcome signals often emerged earlier in dACC than in OFC or dlPFC, and many neurons encoded multiple decision variables, suggesting an integrated representation of outcome value. Further evidence for outcome monitoring comes from studies examining performance feedback. Ito and colleagues found that a population of dACC neurons fired only after erroneous saccades corresponding to trials in which monkeys failed to withhold a saccade after a stop signal (Ito *et al.*, 2003). In addition, some neurons responded when an expected reward was omitted, indicating that the dACC evaluates action outcomes. Similar findings were reported by Matsumoto and colleagues in a task in which monkeys learned action-outcome contingencies by selecting between left and right lever presses (Matsumoto *et al.*, 2007). They showed that distinct populations of dACC neurons responded preferentially to positive or negative feedback, and that the magnitude of these responses decreased as learning progressed. As in Ito and colleagues, some neurons also responded to reward omission, further supporting a role of dACC in outcome evaluation. As previously suggested, the dACC is thought to guide decisions through the formation of associations between rewards and actions. Consistent with this role, Hayden and Platt showed that during a task in which monkeys directed saccades toward cues associated with different reward probabilities, dACC neurons sensitive to the reward were also sensitive to the direction of the saccade, indicating that dACC integrates reward information with action signals (Hayden & Platt, 2010). Together, these findings support a role for the dACC in evaluating the consequences of actions and integrating multiple decision variables to guide value-based DM.

Overall, the dACC is thought to evaluate the need for cognitive control (i.e., behavioral adjustment) based on signals such as conflict, errors or effort. It contributes to monitoring and updating action values, although it is generally not considered to directly implement control processes. Instead, it is proposed to signal the need for enhanced control to regions such as the

lateral prefrontal cortex (lPFC), which are more directly involved in implementing control. Consistent with this view, Kerns and colleagues showed that dACC activity related to conflict monitoring predicted subsequent increases in lateral prefrontal activity, supporting a role for the dACC in signaling the need for cognitive control (Kerns *et al.*, 2004).

2.2.1.3 The lateral prefrontal cortex

The lPFC encompasses the lateral frontopolar cortex (lateral portion of area 10), the dlPFC (areas 46 and 9) and the ventrolateral PFC (vlPFC; areas 47/12, 45 and 44) (Badre, 2008; Mackey & Petrides, 2010). Although anatomically lying on the lateral side of the OFC, the area 47/12 is functionally grouped with the vlPFC, particularly its dorsal portion in NHP studies. The lPFC plays a central role in the top-down control of behavior, supporting executive processes such as the representation and updating of task rules, working memory, and the planning and organization of goal-directed actions (Shallice, 1982; Petrides, 1985, 1991; Funahashi *et al.*, 1989, 1993; Goldman-Rakic, 1995; Baker *et al.*, 1996; Cohen *et al.*, 1997; White & Wise, 1999; Stuss *et al.*, 2000; Miller & Cohen, 2001; Monchi *et al.*, 2001; Curtis & Lee, 2010). Through these mechanisms, the lPFC provides a cognitive framework that enables the integration of value information and its translation into action selection. Although evidence suggests functional differentiation within the lPFC along rostro-caudal and dorsoventral axes, such as hierarchical organization of control and abstraction, a detailed discussion of these subdivisions is beyond the scope of this section and has been reviewed elsewhere (Badre, 2008). Therefore, in the present section the lPFC is considered as a unified functional system, while specific subregions will be mentioned when relevant.

The lPFC also contributes directly to decision processes by integrating value information and translating it into action selection. Neuroimaging studies have shown that the lPFC represents value-related information during DM. For example, activity in dlPFC has been shown to vary with reward magnitude and valence during anticipation of potential outcomes (Knutson *et al.*, 2005). Similarly, dlPFC activity has been shown to correlate with participants' willingness to pay when freely bidding for food items, but not during forced bids, suggesting that this region contributes to translating subjective value into action selection (Plassmann *et al.*, 2007). Electrophysiological studies in NHP provide further insight into the neuronal mechanisms underlying these processes. Although less prevalent than in the OFC or ACC, individual lPFC neurons have been shown to encode multiple decision variables, including reward magnitude, probability, and effort costs, during both choice and outcome evaluation (Kennerley *et al.*, 2009; Kennerley & Wallis, 2009). These findings suggest that value-related signals in the lPFC contribute both to the selection of actions and to the evaluation of their consequences. Importantly, neurons in the lPFC can link value information to specific actions. In a visuo-motor stimulus-reward association learning task, Wallis and Miller showed that neurons in the dlPFC encoded reward magnitude, frequently in combination with information about stimulus identity and the direction of the upcoming saccade (Figure 2-7) (Wallis & Miller, 2003). In addition, a subset of dlPFC neurons exhibited spatially selective activity that was independent of stimulus identity or reward value, further supporting

a role for this region in linking value representations to action planning. Finally, the lPFC also contributes to adaptive decision making by tracking information about previous choices and outcomes. Neuronal activity in the dlPFC has been shown to reflect signals related to choices and rewards from previous trials, suggesting that this region participates in updating decision strategies based on recent experience (Seo *et al.*, 2007). Together, these findings indicate that the lPFC plays a key role in integrating value signals with action representations and in guiding adaptive DM.

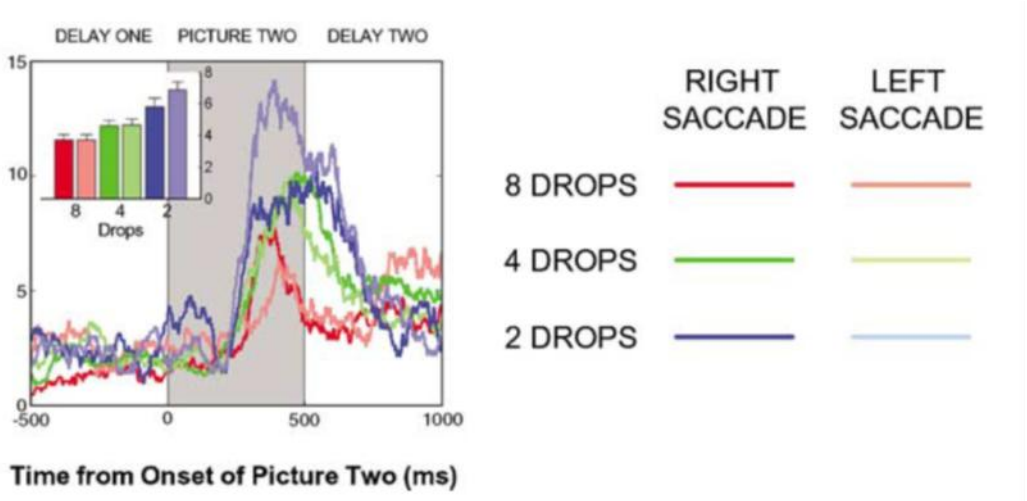

Figure 2-7. Example of an action value neuron in the dorsolateral prefrontal cortex.
Neuronal activity is shown as a function of time following stimulus presentation for different reward magnitudes (2, 4, and 8 drops of juice) and saccade directions (left vs right). The neuron's activity is modulated by both reward magnitude and the direction of the upcoming saccade. In this example, firing rates decrease as reward magnitude increases, and this modulation differs depending on the selected action, illustrating the encoding of action value signals. Taken from (Wallis & Miller, 2003).

2.2.2 Basal ganglia

Although cortical regions including vmPFC, OFC, ACC, and lPFC play key roles in value representation, outcome evaluation, and executive control, the implementation of value-based DM relies on subcortical circuits and most notably the BG, which integrate cortical signals to guide behavior. As described in the previous chapter, the BG integrates inputs from virtually the entire cortex though distinct segregated but partially overlapping functional circuits in which the dorsal and the most ventral BG areas preferentially transfer motor/cognitive and limbic information, respectively, from state-encoding thalamo-cortical fields to brain motor centers. This topographic and functional organization of the BG network especially arises from the large diversity of the cortical projections received by the striatum and is preserved at the different stages (input, central and output) of the network (Parent & Hazrati, 1995a, 1995b). For simplicity, these circuits can be broadly divided into dorsal and ventral circuits (Redgrave *et al.*, 2010).

2.2.2.1 Dorsal circuit

The DS comprises partially distinct territories that contribute to different modes of behavioral control. The DMS (CD, in primates) is primarily involved in goal-directed action-outcome control, whereas the DLS (putamen in primates) contributes more strongly to habitual stimulus-response control (Divac *et al.*, 1967; Yin & Knowlton, 2006; Tanaka *et al.*, 2008; Corbit, 2018). A large body of work, including imaging, lesion, pharmacological, and electrophysiological studies, have shown that behavioral control gradually shifts from DMS-dependent goal-directed mechanisms toward DLS-dependent habitual mechanisms with practice and automatization (Miyachi *et al.*, 2002; Lehéricy *et al.*, 2005; Tricomi *et al.*, 2009; Corbit, 2018). Importantly, several studies suggest that DMS and DLS can also be active in parallel during learning, with varying levels of engagement (Yin *et al.*, 2009; Thorn *et al.*, 2010; Kupferschmidt *et al.*, 2017; Bergstrom *et al.*, 2018) and may interact competitively, such that disruption of DMS function can facilitate the emergence of habitual control mediated by the DLS (Turner *et al.*, 2022). Although this goal-directed versus habitual framework is extremely useful for understanding dorsal striatal function, the present work focuses specifically on value-based, goal-directed DM. Therefore, the following sections primarily emphasize the role of the CD/DMS, and functionally related BG nuclei, in encoding action-outcome relationships and value signals relevant for value-based action selection and DM.

Consistent with this role, CD neurons encode different value-related signals which are linked to action, such as action value, chosen value and prediction error signals enabling adjustment of behavior. Indeed, Knutson and colleagues observed an increase in BOLD activity in the medial CD that scaled with the magnitude of anticipated monetary outcomes in a monetary incentive delay task, in which outcome delivery depended on the execution of an instrumental response (Knutson *et al.*, 2001). In this task, participants pressed a button after a variable delay to obtain rewards, avoid punishments, or receive no outcome, as signaled by visual cues. This anticipatory CD activity was similarly present for both rewards and punishments, consistent with a role in encoding the motivational value of actions rather than outcome valence. In contrast, no modulation of CD activity was reported when trained participants were passively presented with previously learned conditioned cues predicting either a pleasant, an unpleasant or a neutral primary reinforcer, consistent with a role in encoding value signals specifically when actions are required to obtain outcomes (O'Doherty *et al.*, 2002). Moreover the CD preferentially encodes RPE signals (defined as the difference between the EV of an outcome and the value actually received) during instrumental rather than Pavlovian learning. Indeed, in an fMRI study, O'Doherty and colleagues compared instrumental and Pavlovian conditioning tasks in which participants either actively selected between stimuli associated with different probabilities of delivering a pleasant juice reward or a neutral solution, or passively observed the computer's selection (O'Doherty *et al.*, 2004). The authors demonstrated that the CD exhibited significant BOLD activity during instrumental but not Pavlovian conditioning as participants learned the action-outcome contingencies. Using a RL model, the authors further showed that CD activity correlated with RPE signals. This indicates that the CD encoded prediction errors specifically during action-outcome learning, but not during stimulus-outcome learning in which outcomes

were delivered independently of action. This confirms the role of the CD in encoding value signals that guide actions.

At the neuronal level, the CD has been shown to encode the value of specific actions before choice. Indeed, Samejima and colleagues recorded the activity of neurons in the CD and putamen of monkeys while they were freely choosing between turning a handle to the right or to the left (Samejima *et al.*, 2005). Following each action, a green light indicated delivery of a large reward and a red light indicated a small reward. Reward probabilities were fixed within a block but changed across blocks, such that the value of choosing the left or right turn could vary from block to block, requiring monkeys to track and update these action values. The authors found that approximately one third of task-related MSNs in the striatum encoded the values of the available actions during the delay period preceding movement, representing action values prior and independent of the final choice. In their study, Lau and Glimcher selectively looked at the activity of the CD during an oculomotor choice task in which monkeys repeatedly chose between two actions (i.e., left and right saccades) whose reward values varied across blocks (Lau & Glimcher, 2008). Each side delivered rewards according to an independent probabilistic schedule, and the relative reward magnitudes associated with the two actions changed unpredictably across blocks, requiring the monkey to continuously estimate and track the value of each action. The authors confirmed that a significant number of MSNs in the CD encoded action values prior to choice (i.e., action value neurons). They further showed that a distinct subset of neurons encoded the direction of the movement after the cue (i.e., action only neurons) while other encoded the value of the chosen action after the saccadic movement (i.e., chosen value neurons), consistent with a role in evaluating outcomes and updating action values to guide future action selection. The different types of information and their temporal encoding are presented in Figure 2-8. Together, these findings support the presence of action values encoding neurons in the DS. Nevertheless, the existence of "pure" action-value signals in the striatum remains debated. A major reason is that many value-related variables (see section entitled "Goal-directed value-based decision-making strategy", page 43-45), coexist and strongly covary during value-based DM, making it difficult to isolate the neural encoding of a given value variable (Padoa-Schioppa, 2013; Elber-Dorozko & Loewenstein, 2018; Shin *et al.*, 2021). Consequently, several other rodent and NHP studies have attempted to identify which decision variables are encoded in the CD and putamen by fitting multiple linear regression (MLR) models including different combinations of value-related predictors (Kim *et al.*, 2009; Ito & Doya, 2015; Shin *et al.*, 2021; Balewski *et al.*, 2022). Although these approaches have revealed neurons encoding action value, chosen value, choice-related variables, and other decision variables (e.g., state value, policy, reward), the variable attributed to neuronal encoding and its strength often depends on the predictors included in the model and the temporal window analyzed, leading to variability across studies.

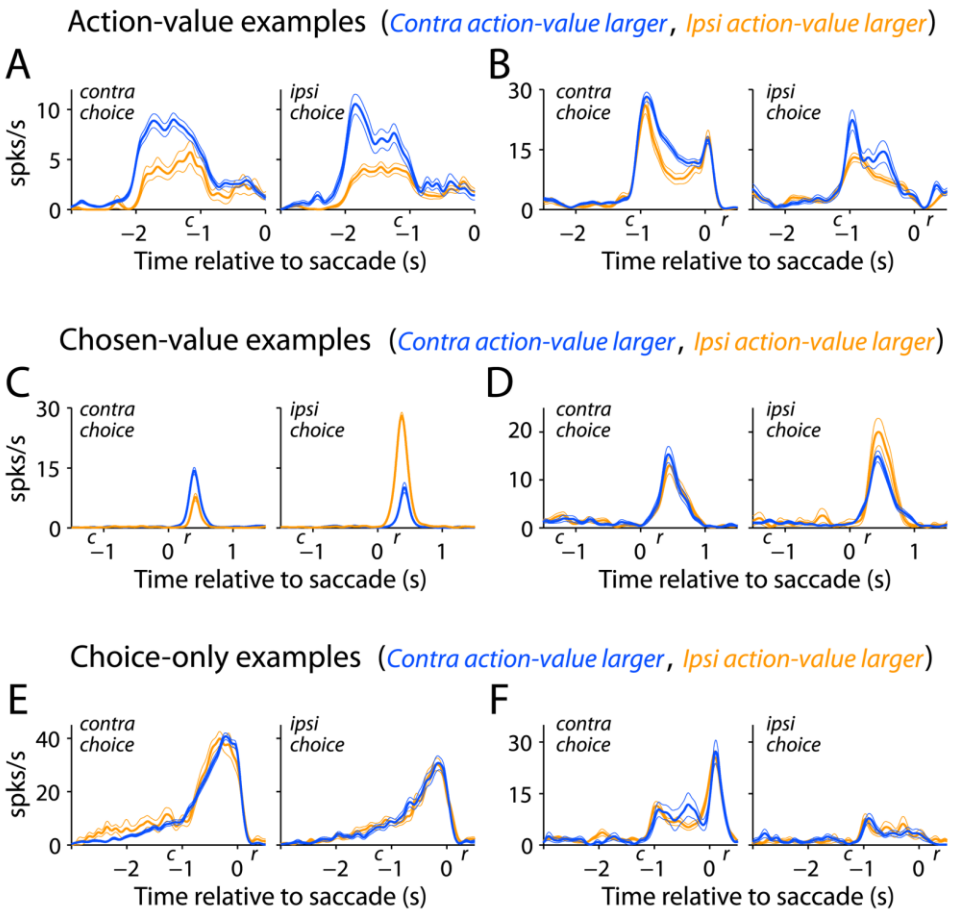

Figure 2-8. Example neurons encoding action value, chosen-value and choice information in the caudate nucleus.

Spike density functions are aligned to saccade completion (time 0); c, represents the cue onset and r, the reward onset. A and B shows examples of action value neurons encoding the value of a specific available action (contralateral action for both A and B neurons), independently of the action ultimately selected. C and D represent two types of chosen-value neurons: one encoding the value of the chosen action irrespective of action identity (C), and another encoding the value of the chosen action selectively when a particular action is chosen (D). These neurons exhibit post-choice activity reflecting outcome evaluation rather than action selection. E and F illustrate examples of choice neurons which encode the selected movement independently of action value. Taken from (Lau & Glimcher, 2008).

In contrast to the extensive research conducted in the DS, other BG nuclei have been comparatively less investigated. Still, Arkadir and colleagues recorded neuronal activity in the GPe while monkeys performed a probabilistic visuomotor task in which visual cues predicted reward probability and instructed movement direction (Arkadir *et al.*, 2004). A large fraction of pallidal neurons encoded reward probability, movement direction, or both parameters either simultaneously or across the course of the trial, with the largest proportion encoding both variables. Notably, some neurons encoded reward probability early in the trial and later switched to encoding movement-related information. When two cues were presented simultaneously, GPe neurons selectively encoded the value of the chosen direction (i.e., the chosen value which usually corresponded to the higher-value option as monkeys tended to choose optimally), consistent with a role for the GPe in biasing behavior toward more valuable actions. Similarly, Pasquereau and colleagues recorded the neuronal activity in the dorsal motor striatum

(putamen) and in the GPi, a major output structure of the BG, while monkeys performed a probabilistic DM task requiring movement (Pasquereau *et al.*, 2007). In both structures, a significant proportion of neurons encoded movement direction, reward probability, or both simultaneously during the preparatory period preceding movement initiation, consistent with action value representations. During the movement-related epoch, the proportion of neurons encoding the chosen value increased in the GPi compared to the putamen, in addition to movement direction, suggesting a progressive biasing of BG output toward the selected high-value action as information flows downstream. Extending these findings, subsequent studies showed that value-related modulation is distributed across the pallidal-nigral network. In a probabilistic classical conditioning task in monkeys, in which cues were predicting appetitive, neutral, or aversive outcomes, Joshua and colleagues showed that neurons in the GPe and GPi responded more strongly, more frequently, and with better probability discrimination to appetitive events than to aversive or neutral outcomes. In contrast, SNr neurons exhibited more balanced responses across incentive conditions, indicating that pallidal activity is biased toward encoding appetitive value (Joshua, Adler, Rosin, *et al.*, 2009). More recent electrophysiological recordings in monkeys engaged in a similar classical conditioning task demonstrated that GPe neurons are functionally heterogeneous. Specifically, HFD neurons, which are thought to correspond to prototypical neurons described in rodent, preferentially encode cue valence, whereas LFD neurons, which are considered rodent homologs of arkypallidal neurons, more strongly encode cue salience (Katabi *et al.*, 2023). Consistent with this organization, rodent recordings further showed that prototypical (PV+) GPe neurons exhibit more robust and sustained encoding of cue-predicted reward value than arkypallidal neurons (Farries *et al.*, 2023). Together, these findings therefore indicate that value representations in the GPe are organized in a cell-type specific manner.

Remarkably, the STN also carries motivational and value-related information. Electrophysiological recordings in rodents have shown that STN neuronal activity is modulated by reward-predictive cues as well as reward delivery, indicating that it participates in reinforcement-related processing (Lardeux *et al.*, 2009). In this task, rats were required to hold and release a lever in response to a light cue whose location predicted either a low- or high-value reward. Interestingly, when the high-value reward was replaced with water, rats showed increased MTs to retrieve the outcome, accompanied by a reduction in STN neurons responding to the previously high-value reward. This finding indicates that STN activity is sensitive to changes in reward value and may contribute to the influence of motivational signals on action execution. Neuronal recordings in monkeys showed that during an instrumental task, many STN neurons encoded both movement-related and outcome-related signals, suggesting that the STN integrates motivational information with motor output (Espinosa-Parrilla *et al.*, 2013). These findings support the idea that the STN participates in the motivational control of behavior, linking action execution with expected outcomes. Extending these findings, the same group later showed that STN activity rarely distinguished between different rewards when no choice was required (Espinosa-Parrilla *et al.*, 2015). In contrast, when animals choose between actions

leading to different rewards, a large proportion of neurons differentiated reward outcomes, mainly after action completion. These findings suggest that the STN contributes to evaluating the outcomes of chosen actions.

Nevertheless, the STN is best known for its role in the regulation of response inhibition and decision conflict. Consistent with its position within the hyperdirect pathway, the STN is thought to exert a transient inhibitory influence during high-conflict situations, and increased STN activity has been associated with reduced impulsivity. In an fMRI conditional stop-signal task, participants responded to the direction of arrows by pressing the corresponding key, but were instructed to inhibit their response only when the stop signal occurred for a designated arrow direction ("critical" trials), while continuing to respond when the stop signal occurred for the other direction ("noncritical" trials) (Aron *et al.*, 2007). The presence of a salient stop signal on noncritical trials created response conflict, which led to slower response times. This conflict-induced slowing was accompanied by coactivation of the preSMA and the STN. During successful stopping on critical trials, this network also recruited downstream BG structures, including the globus pallidus. STN activation during conflict-induced slowing is consistent with a braking mechanism that temporarily suppresses motor output, as proposed by Frank's "Hold your horses" model (Frank, 2006; Frank *et al.*, 2007). Consistent with this framework, evidence from STN lesion studies in rats performing attentional choice tasks demonstrates profound impairments in response control (Baunez & Robbins, 1997). In the five-choice serial RT task, rats were required to respond, after a fixed delay, to a briefly illuminated spatial location in order to obtain a reward. Although STN-lesioned rats exhibited prolonged response latencies, they also showed marked increases in premature responding and spatial errors, indicating a failure to appropriately inhibit competing responses and to regulate action selection under conditions requiring controlled responding. Beyond its role in response inhibition and conflict monitoring, the STN also influences activity across the BG network. Indeed, the STN has been shown to drive moment-to-moment modulation of activity in downstream BG structures (Deffains *et al.*, 2016). By recording neuronal activity in the STN and downstream nuclei (GPe, GPi, and SNr) in monkeys performing an immediate or delayed conditioning task with appetitive, neutral, or aversive cues, the authors demonstrated that fluctuations in STN activity were correlated with corresponding modulations in downstream BG activity across different task epochs, as revealed by cross-correlation analyses.

Overall, although dorsal BG circuit is primarily considered a cognitive/sensorimotor circuit, it also integrates value-related signals that contribute to guiding action selection, decision control, and the adaptive modulation of behavior. These value signals likely interact with motor and executive representations to bias the selection and execution of actions according to their expected outcomes.

2.2.2.2 Ventral circuit

During value-based DM, the VS, including the NAc, plays a central role in integrating predictive, motivational and evaluative signals that guide behavior, consistent with recent circuit-level frameworks highlighting NAc contributions in linking value and valence representations to motivated action (Vieitas-Gaspar *et al.*, 2025). Mechanistically, the idea that limbic circuits influence motor behavior was originally proposed by Mogenson and colleagues, who described the NAc as a functional interface between motivation and action (Mogenson *et al.*, 1980). Subsequent anatomical work by Haber and colleagues refined this view and proposed that information flows between limbic, associative, and motor BG circuits through an ascending striato-nigro-striatal spiral (Haber *et al.*, 2000). In this organization, the VS influences midbrain DANs, which then project to progressively more dorsal striatal regions, allowing motivational signals from limbic circuits to gradually shape cognitive and motor processing.

Consistent with a role in the valuation system, early fMRI studies have shown that the VS activity increases during the anticipation of rewarding outcomes in both Pavlovian and instrumental contexts. Specifically, VS BOLD responses are enhanced during passive anticipation of pleasant liquid rewards and scaled with anticipated monetary gains but not losses during an instrumental task (Knutson *et al.*, 2001; O'Doherty *et al.*, 2002). These findings were later extended using a probabilistic variant of the monetary incentive delay task, in which VS activity was linearly correlated with EV (defined as valence × magnitude × probability of the outcome) (Knutson *et al.*, 2005). Decomposition analyses revealed that this activity was primarily driven by reward valence and magnitude, suggesting that the VS primarily reflects the affective value component of expected rewards. Additional fMRI studies showed that the VS encodes the subjective value of outcomes. For example, in an intertemporal choice task in which participants chose between an immediate reward and a larger delayed option varying in magnitude and delay, VS activity increased with reward magnitude and decreased with delay, consistent with the encoding of discounted subjective value (Kable & Glimcher, 2007). Consistent with a role in value representation independently of action, O'Doherty and colleagues directly compared instrumental and Pavlovian conditioning by having participants either actively choose between two options or passively observe outcomes selected by the computer (O'Doherty *et al.*, 2004). In both conditions, visual stimuli predicted high or low probabilities of receiving either a pleasant juice reward or a neutral solution. Using a RL model, they showed that VS activity correlated with RPE signals (i.e., the difference between expected and obtained value) in both the instrumental and Pavlovian tasks. This finding is consistent with a role for the VS in encoding prediction errors about the value of the current state, independently of whether an action is required.

Complementary electrophysiological studies in rodents further show that the VS preferentially represents task-state information and the EV associated with that state at cue onset (Ito & Doya, 2015), thus providing the EV signals that can serve as the basis for prediction-error computations about the value of the current situation. Additional single-unit recordings in NHP also show that the VS encodes multiple reward-related signals, including neuronal responses to reward-predictive cue and reward delivery. Indeed, in a go/no-go task, Schultz and colleagues identified neurons displaying sustained activation during the interval between a trigger light signaling

possible movement and the subsequent reward delivery in both go and no-go correctly performed trials (Schultz *et al.*, 1992). Many of these neurons showed anticipatory activity that was stronger for juice than water rewards, indicating that their activity is sensitive to reward value and motivational significance. In addition, other neurons exhibited phasic responses at the time of reward delivery. These expectation-related signals were demonstrated to be modified during learning when monkeys learned stimulus-response-reward contingencies through trial-and-error in a delayed go/no-go task (Tremblay *et al.*, 1998). Tremblay and colleagues confirmed that many neurons in the anterior striatum, including the VS, encode reward expectation, and further demonstrated that this activity, initially generalized or inappropriate, became progressively refined as learning proceeded. This adaptation reflected the updating of the animal's subjective reward expectations, indicating that the anterior striatum (including the VS) represents and dynamically updates reward expectations during learning. Additionally, Cromwell and Schultz demonstrated that reward-expectation signals in the anterior striatum, including VS, scale with reward magnitude, consistent with value encoding (Cromwell & Schultz, 2003). Further evidence for value-related signals in the VS comes from electrophysiological recordings in the rodent NAc in response to rewarding and aversive taste stimuli. Roitman and colleagues found that most NAc neurons were selective for either the rewarding or the aversive stimulus, consistent with encoding of stimulus valence (Roitman *et al.*, 2005). Notably, neurons responding to the aversive taste displayed excitatory activity, whereas those responding to the rewarding taste showed inhibitory activity. These neural responses were correlated with oromotor behaviors reflecting rejection (e.g., gaping) or ingestion (e.g., licking), linking hedonic evaluation of stimuli to corresponding motor output.

Beyond its role in value representation, the VS has also been implicated in motivational control. In the monetary incentive delay task, Knutson and colleagues showed that participants expecting a larger reward exhibited increased VS activation and faster RTs, consistent with a role for the VS activity in motivation and response preparation for rewards (Knutson *et al.*, 2001). In line with this view, neurons recorded in the VS during a value-based DM task encoded both the expected reward value and the direction of the upcoming action, but only when the action was subsequently executed. This activity was also correlated with response speed, supporting the idea that the VS links motivational value to motor output during DM (Roesch *et al.*, 2009). The involvement of the VS in motivational control has been causally demonstrated by lesion studies. As explained above, goal-directed behavior is sensitive to outcome devaluation and contingency degradation (see section entitled "Goal-directed value-based decision-making strategy", pages 43-45). Lesions of the NAc core in rats abolished sensitivity to outcome devaluation without impairing action-outcome contingency learning in a two-lever task with distinct rewards, indicating a role in incentive motivation based on the current value of outcomes (Corbit *et al.*, 2001). In contrast, lesions of the NAc shell disrupted Pavlovian-instrumental transfer, as lesioned rats failed to show the expected increase in instrumental responding during presentation of a reward-predictive cue, demonstrating a role in cue-driven motivational influences on behavior. Moreover, rats presenting selective DA depletion in the NAc, shifted their behavior away from high-effort, high-value reward toward low-effort, low-value food (Cousins & Salamone, 1994). In

this task, rats could either press a lever on a fixed ratio 5 schedule to obtain high-value food pellets or approach and consume low-value lab chow. After DA depletion, rats significantly decreased their engagement with lever pressing when both options were available as compared to control rats, demonstrating a role for ventral striatal DA and for the VS in effort-related motivation. Extending these findings to primates, monkeys with ventral striatal lesions showed reduced adjustment of performance across RL environments, particularly for gain-associated cues, despite preserved stimulus-outcome learning, consistent with a role of the VS in motivational engagement (Taswell *et al.*, 2023).

The VP, a major downstream output structure of the VS, has also been shown to encode the expected reward value and motivational signals that regulate motor action. Electrophysiological recordings in NHP performing a saccade task with cues predicting different reward magnitudes showed that many VP neurons modulated their activity according to the expected reward value (Tachibana & Hikosaka, 2012). Behaviorally, larger expected rewards produced faster and more vigorous saccades. Following contingency reversals, both saccade vigor and VP neuronal responses rapidly adjusted to reflect the updated reward values, indicating that VP activity tracks updated reward expectations and contributes to translating EV into motivational control of action. Consistent with this, bilateral reversible VP inactivation abolished this reward-dependent modulation of saccade vigor, supporting a causal role for the VP in motivational regulation of action. In line with this interpretation, Lederman and colleagues showed that cue-evoked activity in VP neurons precedes reward-seeking movements and correlates with parameters of movement vigor, such as approach speed and path efficiency, as well as the animal's proximity to the reward target at cue onset, but not with specific movement features such as direction, supporting a role for the VP in invigorating motivated actions (Lederman *et al.*, 2021).

Consistent with a role in motivation, the VP has been shown to encode incentive motivational signals. Using a serial Pavlovian conditioning task in rats, Tindell and colleagues found that VP neurons fired most strongly to cues temporally closest to reward delivery (Tindell *et al.*, 2005). In this task, rats learned that an initial auditory cue predicted the later occurrence of reward, followed after a delay by a second auditory cue that immediately preceded reward delivery. Although many VP neurons responded to both auditory cues as well as to reward delivery, the strongest phasic firing was elicited by the cue signaling imminent reward. Moreover, amphetamine activation selectively enhanced cue-evoked responses despite unchanged cue-reward contingencies and did not primarily alter responses at reward delivery. These findings indicate that the VP reflects incentive motivational signal, or the "wanting" of the reward (i.e., how much the cue motivates behavior), rather than reward prediction or consumption. Extending these findings, causal manipulations further support this role, as chemogenetic inhibition of VP GABAergic neurons reduces the pursuit of high-value rewards and biases DM toward safer, lower-value options without affecting reward discrimination or consumption (Farrell *et al.*, 2021). In addition to incentive "wanting," the VP has also been implicated in encoding hedonic "liking" signals. Specifically, in sodium-depleted rats, VP neurons doubled the

magnitude of their firing in response to an otherwise aversive salty taste, which became pleasant under depletion (Tindell *et al.*, 2006). The encoding of incentive "wanting" and hedonic "liking" signals are illustrated in Figure 2-9.

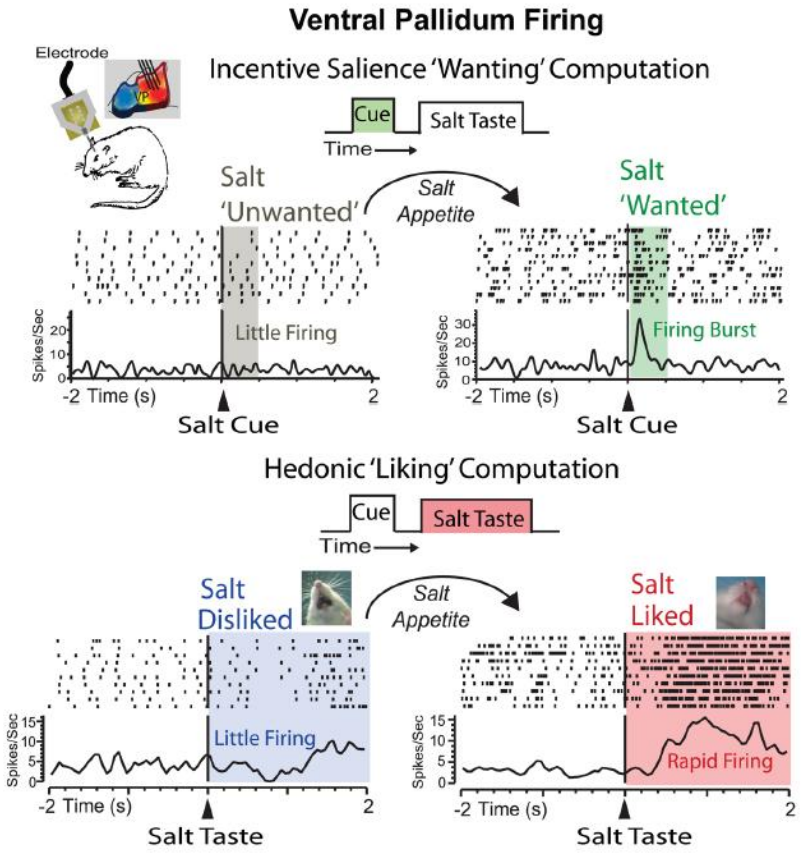

Figure 2-9. Ventral pallidal neurons encode incentive salience motivational signal ("wanting") and hedonic value ("linking") of rewards.

Top: ventral pallidum (VP) neuronal activity related to incentive salience. In sodium-depleted rats, cues predicting a salty reward elicit increased firing, reflecting enhanced motivational value ("wanting") of the expected outcome. Bottom: VP neuronal activity related to hedonic evaluation. When sodium-depleted rats consume a salty solution that has become palatable, VP neurons show increased firing in response to the taste itself, reflecting enhanced hedonic value ("liking"). Taken from (Smith et al., 2009).

Altogether, these findings indicate that both the VS and the VP encode motivational information related to how strongly reward-predictive cues energize behavior and support a role for the ventral striatopallidal circuit in transforming reward-related and motivational signals into behavioral action. Consistent with this view, Ottenheimer and colleagues compared neuronal activity in the NAc and VP of rats performing a behavioral task in which an auditory cue signaled the availability of one of the two appetitive rewards, with sucrose identified as the preferred outcome (Ottenheimer *et al.*, 2018). Reward-specific neurons were observed in both regions, but they were more prevalent and exhibited earlier modulation in the VP (Figure 2-10). Decoding analysis revealed that reward identity could be decoded more accurately from VP activity than from NAc activity. Moreover, VP neurons were strongly modulated by recent reward history,

consistent with a relative reward value signal which was more prominent in the VP compared with the NAc. Interestingly, subsequent work from the same group showed that a subset of VP neurons encodes RPE signals, with these signals expressed more robustly in the VP than in the NAc (Ottenheimer, Bari, *et al.*, 2020). Single-unit recordings in the VP of monkeys engaged in a classical conditioning task with cues predicting appetitive, neutral or aversive outcome in a deterministic or probabilistic manner also revealed a subset of neurons exhibiting transient synchronized responses to task events that were consistent with RPE encoding (Kaplan *et al.*, 2020). Together, these results challenge a strictly serial model in which reward value is first computed in the NAc and then passively relayed to the VP. They suggest instead that the VP can independently contribute to value-updating computations within the ventral BG circuitry. In addition to its role in value updating, VP reward-related activity tracks trial-by-trial variations in task engagement, and optogenetic manipulation of VP neurons during reward delivery bidirectionally alters subsequent reward-seeking behavior, demonstrating a causal role of the VP in reward-guided actions (Ottenheimer, Bari, *et al.*, 2020). Consistently, VP neuronal activity also tracks dynamic changes in reward value driven by physiological state, such as satiety, and manipulation of VP activity biases subsequent reward choices, indicating that VP value signals integrate both updating-related information and internal motivational state to guide behavior (Ottenheimer, Wang, *et al.*, 2020).

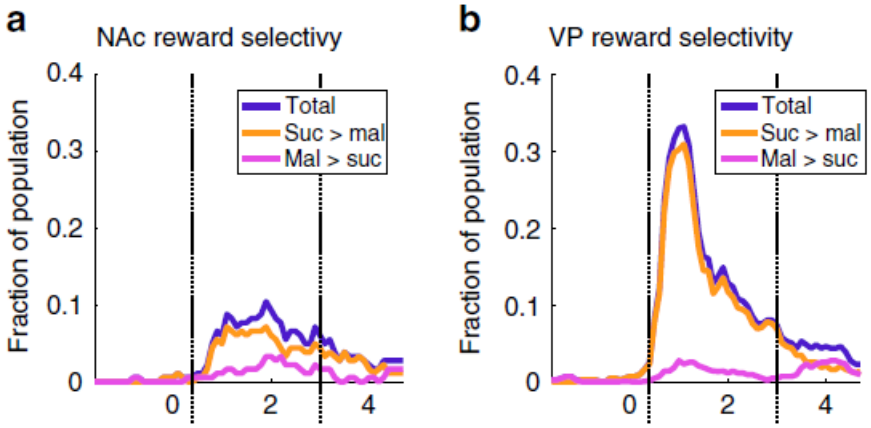

Figure 2-10. Nucleus accumbens and ventral pallidal reward-specific neuronal activity in response to reward delivery.

(a) Fraction of nucleus accumbens (NAc) neurons modulating their activity in response to reward delivery over time. (b) Corresponding population response in the ventral pallidum (VP). Solid lines indicate the total fraction of responsive neurons, while colored lines distinguish neurons selective for sucrose (preferred reward) or maltodextrin. Reward-selective responses are observed in both regions but are more prevalent and occur earlier in the VP compared to the NAc, indicating a stronger and faster encoding of reward value in the VP. Taken from (Ottenheimer et al., 2018).

In comparison with the extensive research devoted to the ventral striatopallidal circuit, considerably less attention has been paid to the contribution of other ventral BG nuclei, such as the limbic territories of the STN and SNr. Anatomical studies have demonstrated that ventromedial regions of the STN receive inputs from prefrontal and limbic cortical areas and participate in motivational and executive control circuits (Haynes & Haber, 2013). Neuronal

recordings in monkeys showed that STN neurons responded to reward-predicting cues, reward expectation and reward delivery, even when rewards were delivered passively or unexpectedly (Espinosa-Parrilla *et al.*, 2013). These findings suggest that limbic territories of the STN contribute to the encoding of motivational value signals that may influence value-based DM. Consistent with a role of the ventromedial STN in executive control, electrophysiological recordings in NHP have shown that a subset of STN neurons exhibited short-latency activity changes during the cancellation of a movement triggered in response to a Go signal (i.e., reactive stopping) during a Go/NoGo-coutermanding task (Pasquereau & Turner, 2017). These switch-stop related neurons were localized in the most anterior ventromedial STN, supporting a role for this region in inhibitory control. Moreover, Yasuda and Hikosaka showed that neurons in the SNr (including in anterior limbic SNr) encode reward value associated with visual objects, with high-value objects producing stronger inhibitory responses than low-value objects (Yasuda & Hikosaka, 2015). This value-dependent modulation is thought to contribute to biases in gaze orienting toward more valuable stimuli. Together, these findings suggest that ventromedial STN and anterior SNr regions form additional components of the limbic BG circuit that most likely complement ventral striatal and pallidal functions.

2.2.2.3 Dopaminergic influence on value-based decision-making

DANs of the midbrain, primarily located in the VTA and SNc, play a central modulatory role in BG circuits by encoding RPE signals that act as teaching signals to update value representations and guide adaptive behavior. Several lines of evidence indicate that phasic dopamine activity adjusts processing along the BG main axis by modulating the efficacy of cortico-striatal transmission (Reynolds *et al.*, 2001; Shen *et al.*, 2008). Other neuromodulatory systems also contribute to this regulation, including striatal cholinergic interneurons (Deffains & Bergman, 2015). Single-unit recordings in NHP performing associative learning tasks have demonstrated these properties of dopaminergic signaling. Indeed, Schultz and colleagues showed that an unexpected reward lead to the increase of the DANs activity, signaling a positive RPE as this reward was not anticipated (i.e., outcome is better than expected) (Schultz *et al.*, 1997). After learning, when the stimulus became predictive of the reward, the increase in FR was shifted to the time of the stimulus, signaling the expectation of the reward, and the phasic increase of activity was no longer observable at the time of delivery. However, when the reward was omitted, DANs decreased their FR at the time of the expected reward, signaling that the expectations were not met and that the value of the predictive stimulus should be updated, consistent with a negative RPE (i.e., outcome is worse than expected). These modulatory signals are illustrated in Figure 2-11.

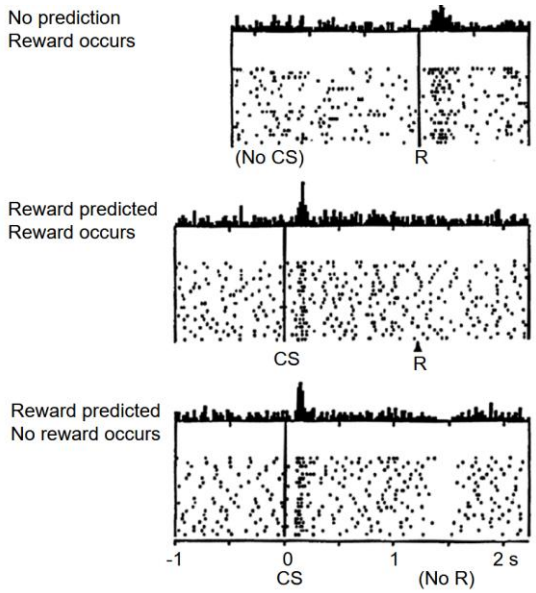

Figure 2-11. Reward prediction error signaling by dopaminergic neurons.

Top: An unexpected reward (R) elicits a phasic increase in dopaminergic activity, corresponding to a positive reward prediction error (RPE). Middle: After learning, the phasic response shifts from the time of reward delivery to the conditioned stimulus (CS) that predicts the reward, reflecting reward expectation. No additional response is observed at reward delivery when it is fully predicted. Bottom: When a predicted reward is omitted, a decrease in dopaminergic activity occurs at the expected time of reward, corresponding to a negative RPE. Taken from (Schultz *et al.*, 1997)*.*

The theory that midbrain DANs encode signed RPEs is now widely accepted, and numerous studies since 1997 have supported this framework. In particular, DANs have been shown to encode information about expected reward magnitude and probability, key variables for computing RPE signals (Fiorillo *et al.*, 2003; Tobler *et al.*, 2005). More recently, evidence suggests that DANs encode subjective value by integrating nonlinear transformations of reward magnitude and probability (Ferrari-Toniolo *et al.*, 2025).

Interestingly, early studies reported that some DANs display small excitatory responses to stimuli that do not predict reward (Tobler *et al.*, 2003), despite the general RPE pattern of increased activity for reward-predicting cues and decreased activity for reward omission or aversive events (Tobler *et al.*, 2003; Ungless *et al.*, 2004; Matsumoto & Hikosaka, 2009). Although these responses were not interpreted as attentional signals, they suggest that DANs may initially respond to stimulus occurrence before its value is fully evaluated. Subsequent work further showed that a subset of DANs respond with excitation to both rewarding and aversive predictive cues, a pattern interpreted as signaling motivational salience (Matsumoto & Hikosaka, 2009). Building on these observations, Schultz and colleagues proposed that dopaminergic responses consist of two temporal components (Figure 2-12) (Schultz, 2016; Stauffer *et al.*, 2016). The first is a rapid, short-latency activation that detects salient environmental events regardless of their eventual value, acting as a detection signal for potentially important stimuli. The second component develops shortly afterward and reflects reward value by encoding an RPE signal, increasing for outcomes better than expected and decreasing for outcomes worse than expected.

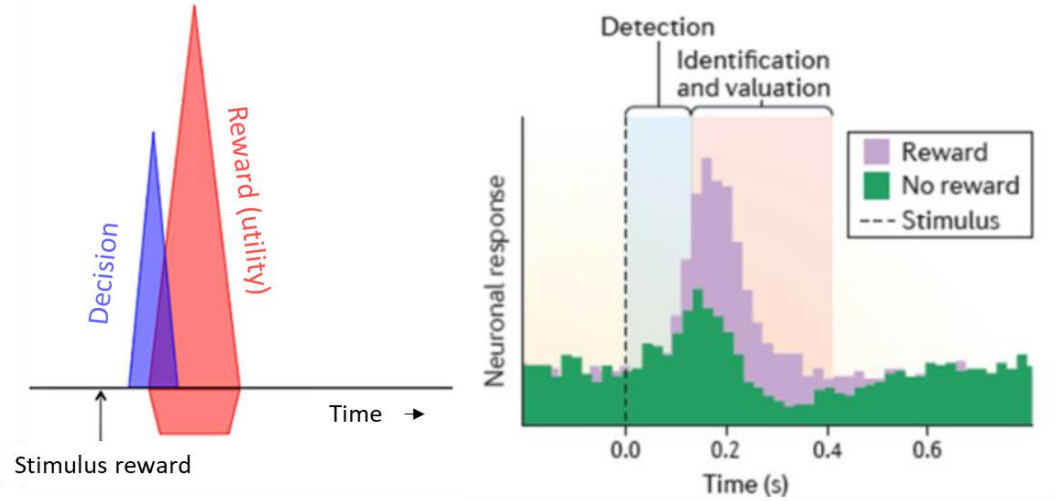

Figure 2-12. Dopaminergic response to stimulus is divided into two components.

Dopaminergic responses to stimuli can be decomposed into two temporal components. An initial, short-latency response reflects rapid detection of salient environmental events, independent of their reward value. This is followed by a later component that encodes reward value through a reward prediction error (RPE) signal, increasing for better-than-expected outcomes and decreasing for worse-than-expected outcomes. The left panel illustrates this conceptual framework, whereas the right panel shows neuronal responses, with an early detection signal present for both rewarding and non-rewarding stimuli and a later component that differentiates between rewarded and non-rewarded outcomes. Taken from (Schultz, 2016; Stauffer et al., 2016).

While salience broadly refers to the attentional or behavioral significance of a stimulus regardless of its valence, another form of salience was proposed by Berridge and colleagues, called the incentive salience (Berridge *et al.*, 1989; Robinson & Berridge, 1993). Incentive salience refers to the motivational attractiveness of reward-predictive stimuli and the "wanting" of the anticipated reward. In this framework, DA signaling is thought to confer motivational value to reward-predictive cues and promote approach behavior. Consistent with this view, injection of DA antagonist in the core of the NAc of rats lead to a reduced approach behavior toward reward-predictive conditioned stimuli without affecting the cue-reward associations and goal-directed conditioned responses (Saunders & Robinson, 2012).

Together, these findings indicate that dopaminergic signaling is multifaceted, conveying RPE, value-related and salience signals that collectively shape learning, motivation, and value-based DM. Accordingly, disruptions of dopaminergic transmission, such as the degeneration of midbrain DANs observed in PD, are expected to profoundly impair these processes and contribute to DM deficits.

Chapter 3 Parkinson's disease and value-based decision-making dysfunction

Diverse BG pathologies have been associated with impairments in DM. These BG-related disorders include psychiatric conditions such as obsessive-compulsive disorders, in which hyperactivity within limbic and associative CBG circuits has been linked to maladaptive DM under uncertainty (for a review of cognitive impairments in obsessive-compulsive disorders, see (Benzina *et al.*, 2016)). Neurological disorders, and more specifically neurodegenerative diseases, have also been associated with DM impairments. For example, Huntington's disease, is characterized by the progressive and irreversible loss of SPNs, which severely disrupts BG function and leads to impaired DM (for a review, see (Morris *et al.*, 2022)). In Huntington's disease, dysfunction of the valuation system leads to impaired cost-benefit assessment, resulting in apathetic and impulsive behaviors.

Another neurodegenerative disorder involving BG dysfunction is PD. PD is commonly characterized by motor deficits including impaired movement initiation (akinesia), slowness and reduced amplitude of movements (bradykinesia), abnormal postures, rigidity and resting tremor, as originally described by James Parkinson in 1817 in *An Essay on the Shaking Palsy* (Parkinson, 1817). These symptoms are attributed to the progressive degeneration of midbrain DANs, particularly in the SNc, likely due to the abnormal accumulation and aggregation of the protein α-synuclein within these neurons (Emborg, 2007). This degeneration causes severe DA depletion across several brain regions, including the striatum, with the DS typically more severely affected during the early stages of the disease (Hornykiewicz, 1975; Spillantini *et al.*, 1997; Emborg, 2007). Beyond its motor symptoms, PD has also been associated with impairments in DM (Brand *et al.*, 2004; Herz *et al.*, 2018). Importantly, α-synuclein pathology is not restricted to the dorsal regions and can involve limbic and paralimbic structures early in the disease process, even when midbrain dopaminergic loss remains relatively limited (Braak *et al.*, 2003). This dissociation between the progression of dopaminergic degeneration and the broader distribution of protein pathology may explain why cognitive and motivational alterations can appear early in some patients despite the predominance of motor symptoms arising from dorsal BG circuit dysfunction (Ziemssen & Reichmann, 2007). PD therefore provides a valuable framework for examining how differential alterations of dorsal and ventral BG circuits contribute to distinct components of value-based DM. Accordingly, the following sections examine how impairments of dorsal circuit disrupts action selection and action value learning, and how alterations of the ventral circuit affect reward valuation and motivational decision processes.

3.1 Dorsal circuit : impaired action selection and action-value learning

Because dopaminergic degeneration in PD initially predominates within nigrostriatal projections targeting dorsal striatal territories, many of the behavioral alterations observed in patients can be interpreted as consequences of dysfunction within dorsal CBG circuits. In line with this view, DA depletion affects multiple components of action control, including the invigoration of actions,

RL from outcomes, the flexible updating of action policies, and the regulation of decision thresholds during conflict. Together, these findings indicate that Parkinsonian impairments in DM largely reflect disruption of dorsal BG mechanisms involved in the selection, learning, and control of goal-directed actions.

3.1.1 Dopamine depletion disrupts action selection, initiation and motor flexibility

The loss of midbrain DANs in PD causes striatal DA depletion that leads to a cascade of physiological changes along the BG network, affecting neuronal FRs, patterns and synchronization (Wichmann & DeLong, 2003; Hammond *et al.*, 2007; Galvan *et al.*, 2015; Nambu *et al.*, 2015; Deffains *et al.*, 2018; McGregor & Nelson, 2019). According to the classical model of BG function, DA loss reduces excitation of D1-MSNs, weakening inhibition of BG output nuclei, while enhancing the inhibitory influence of D2-MSNs on the GPe, disinhibiting the BG output nuclei (Albin *et al.*, 1989; Alexander & Crutcher, 1990; Bergman *et al.*, 1990; Gerfen *et al.*, 1990). This imbalance results in increased inhibitory output from the BG to the thalamus, disrupting the thalamocortical drive required for normal action selection, initiation, and execution. Concurrently, the loss of dopaminergic inhibition of striatal cholinergic interneurons leads to increased acetylcholine tone, which amplifies the activity of the D2 indirect pathway and contributes to the suppression of motor responses. These changes have been observed across the BG network in both parkinsonian animal models (rodent and NHP) and patients. In particular, electrophysiological recordings in monkeys intoxicated with the dopaminergic neurotoxin 1-methyl-4-phenyl-1,2,3,6-tetrahydropyridine (MPTP) revealed decreased FRs in the GPe and increased FRs in the GPi/SNr and STN (Miller & DeLong, 1987; Filion & Tremblay, 1991; Wichmann & DeLong, 2003). The MPTP-treated monkey is considered as the gold-standard experimental model of PD because it reproduces key features of the disease, including degeneration of the nigrostriatal dopaminergic pathway and the emergence of both motor and non-motor symptoms, as well as α-synuclein aggregation (Emborg, 2007, 2017; Deffains *et al.*, 2021). Similar FR patterns have been reported in PD patients (Hutchison *et al.*, 1994, 1998; Benazzouz *et al.*, 2002). Beyond changes in FRs, PD is also characterized by the emergence of abnormal synchronized oscillatory activity throughout the BG network in both animal models and patients (Figure 3-1) (Hutchison *et al.*, 1994, 1998; Benazzouz *et al.*, 2002; Deffains *et al.*, 2016, 2018). It is commonly assumed that low-frequency oscillations (4-7 Hz) are associated with tremor, whereas exaggerated beta-band oscillations (~8-35 Hz) are linked to bradykinesia and akinesia (Brown, 2003; Neumann *et al.*, 2023). The association between oscillatory activity and parkinsonian motor symptoms is supported by the effects of DA replacement therapy (DRT) and deep brain stimulation (DBS), particularly when targeting the STN. Both interventions have been shown to reduce pathological beta oscillatory activity while improving motor impairments in patients with PD and in animal models (Heimer *et al.*, 2002; Kühn *et al.*, 2004, 2008; Meissner *et al.*, 2005). Under physiological conditions, beta oscillatory activity is known to play an important functional role in maintaining the current motor state, or "status quo" (Engel & Fries, 2010; Brittain & Brown, 2014). Supporting this hypothesis, enhanced cortical beta synchrony in healthy individuals has been associated with posture maintenance and suppression of new motor

programs (Gilbertson *et al.*, 2005). Moreover, beta oscillatory activity has been observed in the CBG-thalamo-cortical network of healthy monkeys during post-performance or hold periods, when behavioral state changes are unlikely (Courtemanche *et al.*, 2003; Feingold *et al.*, 2015). Accordingly, the exaggerated beta oscillatory activity observed in PD is thought to reflect an abnormally stable network state that impairs movement initiation and reduces behavioral flexibility, thereby contributing to akinesia and bradykinesia (Engel & Fries, 2010; Brittain & Brown, 2014).

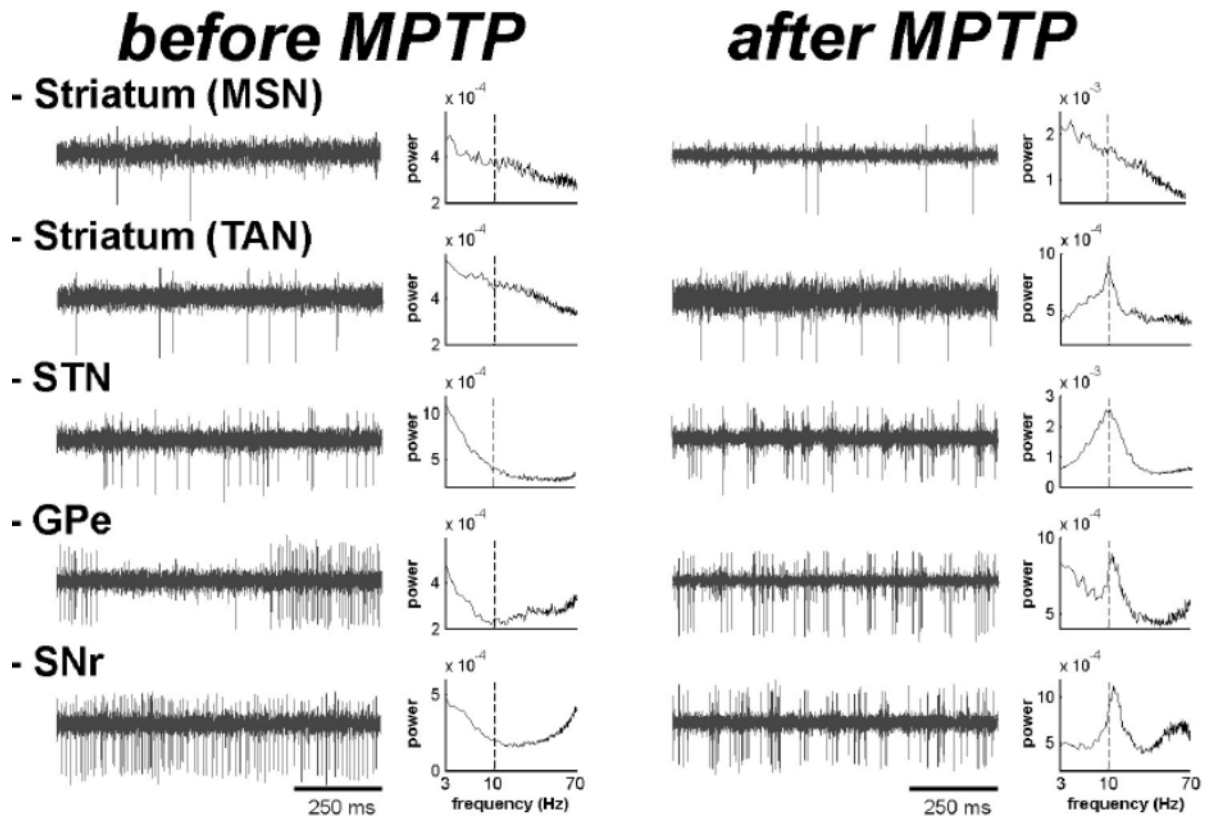

Figure 3-1. Abnormal oscillatory spiking activity across the monkey basal ganglia network following MPTP treatment.

Representative traces of single-unit activity (SUA) recorded from striatal medium spiny neurons (MSNs), tonically active neurons (TANs), subthalamic nucleus (STN), external globus pallidus (GPe), and substantia nigra pars reticulata (SNr) are shown before (left) and after (right) MPTP treatment. Corresponding power spectral densities of nearby multi-unit activity (MUA) are displayed alongside each trace. After MPTP treatment, neuronal activity exhibits increased oscillatory synchronization, with a prominent peak in the low beta range (8–15 Hz), centered around ~10 Hz, across multiple basal ganglia structures. Taken from (Deffains et al., 2016).

3.1.2 Dopamine regulates the vigor of selected actions

In addition to impairments in action initiation and motor flexibility, bradykinesia may also reflect reduced engagement in executing the chosen action. While motivational signals partly arise from ventral circuits, their translation into the vigor with which actions are executed depends critically on dopaminergic modulation of dorsal motor loops. Consistent with this idea, although

bradykinesia is traditionally viewed as a motor deficit, evidence from Mazzoni and colleagues suggests that it reflects altered valuation of movement vigor within the nigrostriatal motor loop, rather than impaired motor execution per se (Mazzoni *et al.*, 2007). In their study, participants moved a cursor from a start circle to a target in a single self-initiated movement while satisfying imposed peak-velocity constraints of varying difficulty. Task difficulty was manipulated by changing both target distance and required speed, and participants were required to produce 20 valid trials per condition. Among the PD participants, half were receiving DRT. By comparing early PD patients with healthy controls, the authors showed that, PD patients were able to generate fast and accurate movements when explicitly instructed, indicating preserved motor execution abilities. However, as task difficulty and energetic demands increased, PD patients were less likely to select movements with sufficient speed (vigorous movements) to meet the required peak-velocity threshold, resulting in a greater number of trials rejected for being too slow (below threshold trials) and more attempts needed to reach criterion. This increased sensitivity to movement energetic cost, observed despite heterogeneity in treatment status, led the authors to propose a role for DA in signaling implicit "motor motivation," regulating the willingness to expend energy to move quickly.

Extending this concept, Le Bouc and colleagues further dissociated the motor and motivational contributions of DA to effortful behavior using two complementary tasks: an incentive force task and a binary choice task (Le Bouc *et al.*, 2016). In the incentive force task, participants exerted force on a handgrip to obtain monetary rewards proportional to the produced force, whereas in the binary choice task they selected between options combining different levels of reward and effort before generating the required force. PD patients were tested ON and OFF dopaminergic medication and compared with healthy controls. During the force production in both tasks, the authors measured not only the peak force generated by participants but also the rate of force change ("yank"), which reflects the speed at which movements are produced. PD patients tested OFF medication generated force with slower contraction dynamics, even when achieving similar force levels. This deficit appeared as a downward shift in the normal relationship between force and yank, indicating that equivalent motor outputs were produced more slowly, consistent with bradykinesia. Computational modeling further showed that this effect was best explained by a reduction in a motor activation rate parameter, which determines how efficiently motor commands are translated into movement dynamics. Importantly, dopaminergic medication selectively increased this parameter, and its change predicted improvements in clinical motor symptoms, including bradykinesia. These findings indicate that DA depletion impairs the invigoration of executed movements by altering the computation of movement vigor.

In addition, Shiner and colleagues demonstrated that DA depletion affects movement invigoration in a valence-specific manner (Shiner, Seymour, Symmonds, *et al.*, 2012). In their study, PD patients tested OFF dopaminergic medication and healthy controls performed a movement task requiring two sequential button presses executed as quickly as possible following a cue signaling the opportunity to obtain a monetary reward or avoid a painful electric shock. The interval between the two button presses was used as an index of MT and thus movement vigor. The authors showed that although PD patients were overall slower than controls, they

moved significantly faster in the aversive (shock-avoidance) condition than in the appetitive (monetary reward) condition. Compared with controls, patients exhibited prolonged MTs primarily in reward contexts. These results suggest that DA depletion disrupts the normal modulation of movement vigor by action outcomes rather than producing a uniform motor slowing.

3.1.3 Dopamine depletion biases reinforcement learning

Consistent with the reduced impact of reward signals on action vigor, DA depletion also biases RL mechanisms toward negative outcomes. Indeed, PD patients exhibit selective impairments in associative learning during DM tasks, as demonstrated by Frank and colleagues (Frank *et al.*, 2004). In this study, healthy older adults and non-demented PD patients OFF medication performed a probabilistic DM task in which they repeatedly chose between pairs of stimuli associated with different probabilities of positive ("correct") or negative ("incorrect") feedback. Although the task did not involve explicit punishment, negative feedback signaled that the chosen option was less likely to yield reward, allowing participants to learn which stimuli should be avoided. The authors showed that PD patients OFF dopaminergic medication learned more effectively to avoid options associated with negative feedback than to select those associated with positive outcomes compared with healthy controls, indicating a bias toward learning driven by negative feedback. This pattern can be explained by the effects of DA depletion on RL mechanisms. Indeed, in computational models of BG learning, phasic increases in DA encode positive RPEs that reinforce recently selected actions via the direct ("Go") pathway, whereas decreases in DA promote learning to suppress actions through the indirect ("NoGo") pathway. In PD, reduced dopaminergic signaling diminishes the impact of positive prediction errors while biasing striatal processing toward indirect pathway dominance, resulting in relatively enhanced learning from negative outcomes. Consistent with this framework, DRT reverses this bias. Indeed, PD patients ON medication were shown to exhibit impaired learning from negative feedback but improved learning from positive outcomes, reflecting reduced influence of indirect ("NoGo") pathway-mediated learning (Frank *et al.*, 2004). Converging neuroimaging evidence further supports selective dysfunction of the dorsal associative striatum. In an fMRI study, Schonberg and colleagues compared striatal activity in PD patients ON dopaminergic medication and healthy controls during a probabilistic monetary DM task (Schonberg *et al.*, 2010). Although behavioral performance was comparable between groups, PD patients exhibited significantly reduced prediction-error related activity in the DS, whereas prediction-error signals in the VS were preserved. This dissociation mirrors the known pattern of dopaminergic degeneration in PD, which preferentially affects the nigrostriatal pathway innervating the DS.

Importantly, because those dorsal striatal territories impairments are also involved in stimulus-response learning, the gradual transfer of behavioral control from goal-directed to habits is disrupted in PD (Redgrave *et al.*, 2010). As a result, patients may rely more heavily on cognitively controlled goal-directed processes for routine actions, increasing the computational demands of action selection during everyday behavior.

3.1.4 Dysfunction of the subthalamic nucleus alters decision thresholds and impulsivity

As part of the dorsal CBG circuit, dysfunction of the STN alters decision-threshold regulation, thereby affecting how competing options are evaluated and when value-based choices are committed, particularly under conditions of conflict or uncertainty. By inducing response conflict, task-set switching paradigms engage competing action representations that require dynamic regulation of the speed-accuracy trade-off during action selection. Because the STN exerts a global inhibitory influence on BG output via the hyperdirect pathway, its activation is hypothesized to adjust decision thresholds, thereby delaying responses under conflict (Frank, 2006; Frank *et al.*, 2007).

Beyond the role of the STN in reactive inhibition during conflict, recent electrophysiological recordings in PD patients indicate that STN activity is also associated with proactive inhibitory control during uncertain decision contexts, reflecting cognitive control mechanisms engaged in anticipation of action inhibition (Damiani *et al.*, 2025). Using a Go/NoGo task designed to dissociate proactive from reactive inhibition by manipulating response uncertainty, Damiani and colleagues showed that low-frequency STN activity (2-7 Hz) increased during proactive slowing under uncertainty, whereas beta-band activity (12-30 Hz) was associated with motor inhibition and slower responding. Importantly, these neural signatures of proactive control (i.e., low-frequency STN activity (2-7 Hz)) were largely independent of dopaminergic medication, suggesting that STN-mediated regulation of proactive control and response timing reflects disease-related circuit dysfunction rather than DA depletion alone.

Further support for the role of the STN in response inhibition comes from studies examining the effects of STN DBS on conflict-driven DM. Frank and colleagues compared non-demented patients tested ON and OFF DBS with healthy participants during a probabilistic DM task (Frank *et al.*, 2007). In this task, participants chose between stimulus pairs associated with different reward probabilities (80/20, 70/30, and 60/40). When faced with high-conflict combinations, such as win-win or lose-lose pairs with similar reinforcement values (e.g., 80% vs 70%) both healthy participants and PD patients tested OFF DBS showed increased RTs under high-conflict conditions relative to low-conflict choices. In contrast, when DBS was ON, PD patients failed to exhibit conflict-related slowing and instead showed reduced RTs during high-conflict decisions, leading to more impulsive and suboptimal choices, as reflected by faster responses on error trials. More recent work suggests that these effects do not reflect a continuous disruption of a global inhibitory “braking” mechanism, but rather interference with temporally specific processes that set decision thresholds. Using temporally patterned STN stimulation, Herz and colleagues showed that DBS affected behavior only when applied within a brief window early during deliberation (Herz *et al.*, 2018). This indicates that the STN does not continuously inhibit motor output but instead contributes to the early regulation of response caution, a process that is disrupted in PD and leads to impaired, and often excessive, adjustments of decision thresholds.

3.2 Ventral circuit: impaired valuation and motivational decision processes

3.2.1 Early limbic pathology and ventral circuit dysfunction

Although the ventral (limbic) striatum is relatively preserved from DA depletion during early stages of PD, Braak and colleagues demonstrated that limbic regions are already affected by α-synuclein pathology at the time motor symptoms emerge (Braak *et al.*, 2003). Based on postmortem analyses of brains from patients at different disease stages, the authors showed that α-synuclein pathology is already present in limbic structures such as the amygdala, transentorhinal cortex, and hippocampal formation at the onset of motor symptoms, and subsequently spreads to additional limbic and paralimbic areas including the ACC and insular cortex. Consistent with this broader distribution of pathology, studies in the MPTP-treated NHP model of PD have also reported α-synuclein accumulation beyond the nigrostriatal motor system, extending to limbic and cortical regions such as the hippocampus and temporal cortex (Deffains *et al.*, 2021). Because the model can rapidly reproduce degeneration of the nigrostriatal pathway, it is often used to study late-stage motor symptoms. However, the broader anatomical distribution of α-synuclein pathology indicates that it also captures key features of PD beyond the motor domain and supports its relevance for investigating early non-motor pathophysiological mechanisms, particularly those involving limbic circuits that partly underlie DM processes. Evidence for early mesolimbic dysfunction in PD also comes from neuroimaging studies. Using PET with a high-affinity DA transporter ligand in unmedicated early-stage PD patients, Ouchi and colleagues reported reduced dopaminergic innervation not only in the DS, where it correlated with motor severity, but also in limbic regions such as the amygdala and OFC (Ouchi *et al.*, 1999). Although the VS itself was not directly assessed, these findings suggest early alterations within the mesolimbic and mesocortical dopaminergic systems. Given that the VS receives major afferent inputs from limbic regions including the OFC and amygdala, dysfunction in these structures is likely to influence ventral BG processing at the circuit level.

Further support for early limbic circuit dysfunction comes from functional imaging studies of value-based DM. Thiel and colleagues investigated CBG loop activity in early-stage PD patients tested OFF medication while performing the Iowa Gambling Task, a paradigm that engages both associative and limbic circuits (Thiel *et al.*, 2003). This task requires participants to repeatedly choose between card decks associated with different reward-penalty contingencies and to progressively learn which options yield higher long-term EV. Using PET imaging, the authors showed that, despite preserved behavioral performance, PD patients exhibited reduced activation of the limbic CBG circuit during task execution, whereas activity within the associative loop was relatively preserved. Consistent with early limbic system dysfunction, Kobayakawa and colleagues also reported impaired emotional feedback processing in PD patients during the Iowa Gambling Task (Kobayakawa *et al.*, 2008). Using skin conductance responses as an index of autonomic emotional reactivity, the authors showed that early-stage PD patients failed to exhibit the typical increase in anticipatory and outcome-related responses when selecting disadvantageous decks and displayed overall reduced emotional reactivity (i.e., lower skin conductance responses) compared with control participants. Together, these findings indicate

that limbic circuit dysfunction emerges early in PD and contributes to altered value-based DM, reflecting intrinsic disease-related network alterations rather than acute effects of DRT.

3.2.2 Apathy and motivational symptoms linked to the ventral circuit

PD is associated with a wide range of neuropsychiatric symptoms that affect the majority of patients within a few years after diagnosis. Among these, apathy, commonly defined as a loss of motivation, is one of the most frequent and severe manifestations. In a population-based study, Aarsland and colleagues reported that apathy displayed the highest severity scores among neuropsychiatric symptoms when present, highlighting its clinical relevance in PD (Aarsland *et al.*, 1999). At the network level, Baggio and colleagues conducted a resting-state fMRI connectivity study and showed that apathy in treated PD patients was associated with reduced connectivity within the limbic CBG loop, compared with non-apathetic patients and healthy controls (Baggio *et al.*, 2015). Reduced connectivity were notably found between the limbic striatum and vmPFC but also between limbic striatum and the rest of the striatum. Importantly, these findings were obtained in patients receiving dopaminergic treatment, suggesting that apathy reflects persistent dysfunction of the limbic CBG network that is only partially compensated by DRT. Further insight into the neurochemical basis of apathy was provided by Thobois and colleagues, who examined PD patients developing apathy following STN DBS and a marked reduction in dopaminergic medication (Thobois *et al.*, 2010). Using PET imaging with the D2/D3 receptor ligand [^{11}C]-raclopride, the authors showed that apathetic patients exhibited higher raclopride binding across a distributed set of limbic and paralimbic regions, including the OFC, ACC, and VS, compared with non-apathetic patients. Dopaminergic dysfunction was more pronounced in cortical regions than in the VS, indicating reduced baseline DA tone within cortical valuation systems (see section “The different substrates of decision-making / Cortical structures”, pages 48-56). Following pharmacological stimulation of DA release with methylphenidate, raclopride binding remained relatively elevated in these structures in apathetic patients, reflecting a reduced capacity for DA release. Together, these findings support a role for dopaminergic dysfunction within limbic circuits in the emergence of apathy in PD.

Importantly, apathy obviously reflects a broader motivational syndrome that can affect multiple cognitive processes beyond DM and therefore should not be considered a deficit in value-based DM per se. Nevertheless it may indirectly influence decision-related behavior by reducing motivation, task engagement and the willingness to exert effort to obtain potential rewards or benefits.

3.2.3 Effort-based decision-making and motivational control

Converging evidence indicates that dysfunction of the ventral CBG circuit in PD critically impairs effort-based DM and motivated behavior. As described earlier (see section “The different substrates of decision-making / Basal ganglia / Ventral circuit”, pages 62-67), selective DA depletion in the rat NAc was examined using an effort-based choice task in which animals could either press a lever under a fixed-ratio schedule to obtain preferred food pellets (high-

effort/high-value option) or freely consume standard lab chow (low-effort/low-value option) (Cousins & Salamone, 1994). The authors showed that DA depletion lead to a reduced engagement in high-effort, high-value option in favor of low-effort, low-value alternatives. Consistent with an altered cost-benefit valuation, PD patients displayed a reduced willingness to exert effort for low rewards compared with healthy controls, even in the absence of clinically defined apathy and regardless of dopaminergic medication status (Chong *et al.*, 2015). By estimating the effort indifference point corresponding to the level of effort at which participants accepted the offer on 50% of trials, the authors showed that both ON and OFF medication PD patients exhibited lower indifference points than controls for low reward magnitudes. In contrast, while effort indifference points for high rewards were comparable between controls and PD patients OFF medication, PD patients ON medication selectively increased their willingness to exert effort for high rewards, shifting indifference points upward following DRT.

3.2.4 Dopamine, reward sensitivity and action invigoration

DA depletion in PD has been shown to alter cost-benefit valuation by reducing sensitivity to reward, rather than by increasing the perceived effort costs. Le Bouc and colleagues combined an incentive force task with a binary choice task paradigm to dissociate the contribution of reward valuation from effort cost processing (Le Bouc *et al.*, 2016). In the incentive force task, participants produced force on a handgrip to obtain a monetary reward proportional to the exerted force, while reward magnitude varied across trials. This paradigm allowed the authors to examine whether increasing reward magnitude energizes effort production, independently of explicit cost-benefit choices. In the binary choice task, participants repeatedly chose between options combining different levels of reward and effort before exerting the required force, allowing assessment of how individuals trade reward benefits against effort costs when making effort-based decisions. Across both tasks, PD patients tested OFF dopaminergic medication showed a reduced increase in effort as reward magnitude increased and were less likely to select high-effort/high-reward options compared with healthy controls and with patients tested ON dopaminergic treatment. Computational modeling demonstrated that these behavioral changes were best explained by a reduction in reward sensitivity, rather than by an increase in perceived effort cost. Importantly, this motivational parameter predicted the severity of apathy symptoms, indicating that DA depletion diminishes the motivational impact of expected rewards and reduces the effort individuals are willing to invest in goal-directed actions.

Le Heron and colleagues showed that DA depletion alone does not fully account for motivational deficits in PD (Le Heron *et al.*, 2018). By comparing apathetic and non-apathetic patients performing an effort-based DM task ON and OFF dopaminergic medication, the authors demonstrated that DA increased willingness to engage in high-effort/high-reward actions regardless of apathy status, as reflected by increased acceptance of such offers in both groups. However, apathetic patients both ON and OFF medication, consistently exhibited reduced sensitivity to reward, leading to lower acceptance rates particularly for low-reward offers even when effort costs were minimal. Importantly, although dopaminergic treatment increased the

force output during action execution in both groups, the apathy status did not affect movement vigor. These findings indicate that, although DA depletion can reduce reward-driven motivation, apathy reflects an additional impairment in motivational valuation (particularly for low value options) that is not fully restored by DRT. Further evidence for impaired reward valuation in apathy comes from a neuroimaging study by Lawrence and colleagues showing that apathetic PD patients exhibit reduced neural responses to monetary reward in the vmPFC, amygdala, striatum, and midbrain compared with non-apathetic patients, indicating dysfunction of limbic reward-valuation circuits (Lawrence *et al.*, 2011). Consistent with this interpretation and as discussed earlier, apathy has also been associated with reduced resting-state functional connectivity within limbic CBG networks in treated PD patients (Baggio *et al.*, 2015). All together, these results show that DA acts as a gain modulator of subjective reward value, thereby increasing the amount of effort individuals are willing to invest and invigorating action execution. These effects become most apparent under high effort demands, whereas apathy reflects a more fundamental impairment of reward valuation that leads to disengagement even when effort costs are minimal. At the circuit level, these processes rely on partially dissociable BG circuits, with ventral circuits primarily supporting reward-driven motivation and effort allocation, and dorsal motor circuits contributing more strongly to the invigoration of movement, that is, the speed and force with which movements are executed once an action has been selected. Overall, dysfunction in both systems may therefore largely contribute to value-based DM alterations in PD.

Part 2 Problematic and objectives

Problematic

Value-based DM relies on the transformation of value-related information into appropriate actions through coordinated activity within the CBG network. This computation depends on partially dissociable CBG circuits organized along a dorsoventral axis. Ventral BG circuits primarily support reward-driven motivation and effort allocation, whereas dorsal BG circuits contribute more strongly to action selection, initiation, and movement invigoration. As highlighted in the literature reviewed above, the CBG network participates in multiple stages of DM through this dorsoventral functional organization, and dysfunction at these different stages leads to impaired value-based DM. Nevertheless, how value and action representations are organized and integrated across these circuits during choice remains poorly understood and does not fully capture the anatomical, connectivity, and physiological complexity of the CBG network.

Importantly, value-based DM involves multiple decision variables that coexist and often covary during choice. Reported value-related neural signals therefore cannot be unambiguously interpreted, and conclusions regarding which variable is encoded strongly depend on the decision variables included in the analysis. As a result, the precise nature of value representations within CBG circuits and their integration with action signals during choice remains unresolved. Overcoming this limitation represents a central challenge for understanding the neuronal substrate of value-based DM along the CBG circuits.

This issue becomes even more critical in pathological conditions such as PD. Beyond motor symptoms, DA depletion disrupts value-based DM by differentially affecting ventral and dorsal CBG circuits. Ventral circuit dysfunction reduces reward valuation and motivational drive, diminishing willingness to exert effort, whereas dorsal circuit impairment disrupts action selection, movement vigor, RL, cognitive flexibility, and decision-threshold regulation. However, the variability and task-dependence of these impairments indicate that the circuit-level mechanisms underlying value-based DM deficits in PD remain unclear. Although electrophysiological studies in parkinsonian animal models have extensively characterized DA depletion-induced alterations in FRs, patterns, synchronization, and network dynamics within CBG circuits, little is known about how DA loss affects the neuronal encoding of decision variables such as value, action, or engagement during value-based DM. Direct circuit-level electrophysiological evidence linking DA depletion to disrupted value-action representations, as well as reduced neural responsiveness (i.e., reduced neural gain) and disengagement-related activity states, remains limited. Addressing this gap is essential for understanding the neural computations underlying DM in both healthy and pathological states.

Objectives

The overall objective of this project was to elucidate the neuronal computations underlying value-based DM across the dorsoventral functional organization of the CBG network in both healthy and parkinsonian states.

More specifically, we aimed at:

(1) Characterizing the spatiotemporal encoding of value- and action-related signals across dorsal and ventral BG territories during DM:

This aim sought to determine where and when value and action signals are represented along the dorsoventral axis of the BG, and how these representations relate to behavioral performance and engagement during choice.

(2) Defining the computational organization of value-action representations within BG circuits:

Beyond identifying where signals are encoded, this aim addressed how value and action information are weighted and integrated (i.e., computational organization) within BG circuits. Specifically, we sought to dissociate value-dominant, action-dominant, and integrative (i.e., their interaction) representations in order to clarify how value-related information is transformed into action selection along the dorsoventral axis.

(3) Determining how DA depletion reshapes this computational organization and neural engagement states in the parkinsonian state:

This aim examined how DA loss alters value-action representations across BG circuits. In parallel, we assessed whether DA depletion is associated with reductions in neural responsiveness (i.e., neural gain) and disengagement-related activity states, and how these alterations relate to DM impairments.

Together, these three complementary objectives were designed to provide a comprehensive characterization of value-action computations across the dorsoventral BG network in healthy conditions and to determine how DA depletion reorganizes these computations. Overall, we aimed to bridge the gap between circuit-level physiology and the DM impairments observed in PD.

Part 3 Experimental approach

To address these objectives, we used a multidisciplinary approach in NHPs, combining behavior (value-based DM task), electrophysiology (large-scale neuronal recordings), pharmacological lesioning (MPTP intoxication), and multivariate neural population analyses, including MLR, principal component analysis (PCA), neural trajectory analysis, and linear discriminant analysis (LDA) decoding. The methods are described in detail in the following study by Simic et al. (in preparation). Here, only a brief overview of the experimental and analytical procedures is provided.

Non-human primates

Two female rhesus monkeys (Macaca mulatta), Havane (Monkey H) and Chouros (Monkey C), weighing approximately 5-6 kg, were included in this study. Animals were pair-housed with a conspecific under standard housing conditions (12 h light/dark cycle, ~60% humidity, ~22 °C).

Behavior

Animals performed a value-based DM task in which they selected between two visual targets associated with different reward magnitudes and probabilities. The task included both potential gains and losses relative to a fixed reference point, allowing assessment of valuation and choice under different decision contexts. Behavioral performance was assessed using RT, MT, success rate and omission rate.

Electrophysiology

Large-scale multisite electrophysiological recordings were performed in several BG subregions, including the CD, NAc, GPe, and VP, while animals performed the task. Neural activity was analyzed in direct relation to behavioral measures of choice, engagement, and performance. Recordings were obtained longitudinally in the same animals across healthy and parkinsonian states.

Parkinsonian lesion model

A parkinsonian syndrome was progressively induced by repeated low-dose administration of the MPTP neurotoxin. This longitudinal within-subject design allowed each animal to serve as its own control, thereby reducing inter-individual variability and enabling a causal evaluation of DA-dependent changes in neuronal computations. Post-mortem tyrosine hydroxylase immunohistochemistry was used to verify the extent of DA depletion after completion of recordings.

Multivariate neuronal population analyses

Neural data were analyzed using complementary approaches at both the single-unit and population levels.

MLR was used to quantify the encoding of value-, action-, and interaction-related signals at the single-neuron level. To overcome the collinearity inherent to multi-option tasks, we adopted a minimal yet informative encoding framework centered on the value of the best available option as a proxy for state value, capturing the dominant valuation component shared across correlated value variables. By reducing the model to this core valuation signal, we avoided unstable parameter estimation and arbitrary allocation of shared variance among correlated predictors. Importantly, because both the value and spatial position of the best available option are defined prior to commitment, this framework enabled the isolation of pre-choice evaluative signals independently of the animal's final choice. This value regressor was combined with a action variable corresponding to the position of the best available option and with an interaction term between value and position to quantify their respective and joint contributions across dorsal and ventral BG circuits. Neural encoding was quantified using generalized linear modeling, with standardized regression coefficients (β) and partial R^2 used to assess the strength, and unique variance explained by each predictor. This approach allowed us to dissociate value-dominant, action-dominant, and integrative value-action representations at the single-neuron level while ensuring robustness to collinearity.

At the population level, PCA, neuronal population trajectory analyses, and LDA decoding were used to examine low-dimensional structure, collective dynamics, and discriminability of population activity associated with the value and spatial position of the best available option, consistent with our adopted framework.

- PCA to identify low-dimensional structure and dominant population axes underlying value-action representations.
- Neuronal trajectory analysis to characterize the temporal evolution of population activity during the decision process.
- LDA decoding to assess the discriminability of value and action information at the population level.

Together, these approaches provided a quantitative description of how value and action signals are represented, weighted, and dynamically organized across striatal and pallidal circuits, as well as across the broader BG network.

Finally, using this framework, we examined how DA depletion alters value-related, action-related, and integrative representations in the BG, and whether these changes are associated with reductions in neural responsiveness (i.e., neural gain) and with disengagement-related activity states.

Part 4 Experimental study

Dopamine Depletion Dissociates Engagement from the Dorsoventral Organization of Value- and Action-Related Signals in the Basal Ganglia

Milesa Simic[1], Nathalie Biendon[1], Sandra Dovero[1], Hugues Orignac[1], Tho-Haï Nguyen[1], Thomas Boraud[1] & Marc Deffains[1,*]

[1] Bordeaux University, CNRS, IMN, UMR 5293, F-33000 Bordeaux, France

* Correspondence: marc.deffains@u-bordeaux.fr

Abstract

Value-based decision-making (DM) relies on transforming value into action through coordinated activity of dorsal and ventral basal ganglia (BG) circuits, yet their respective contributions in health and parkinsonism remain unclear. Here, we performed multisite electrophysiological recordings in non-human primates performing a probabilistic DM task involving gains and losses, before and after induction of a parkinsonian state. Ventral regions encoded value nonlinearly, with maximal sensitivity at the loss-gain transition, whereas dorsal regions preferentially represented action-related signals. Dopaminergic depletion increased omissions and slowed responses, while selectively reducing value encoding in the nucleus accumbens despite preserved choice accuracy. These changes were accompanied by a shift toward low-gain neural states associated with disengagement. Together, our findings indicate that dopamine depletion may biases the network toward a state that is less likely to generate action, rather than abolishing value representation.

Introduction

Value-based decision-making (DM) is a higher-order brain function that enables organisms to select actions by evaluating the potential rewards and costs of available options. It relies on several core computations, including the valuation of available options, the transformation of value information into actions (action selection and execution), the evaluation of action outcomes, and the updating of option values (Ernst & Paulus, 2005; Rangel *et al.*, 2008). These processes are supported by the coordinated activity of distributed cortical and subcortical circuits innervated by midbrain dopaminergic neurons (Schultz *et al.*, 1997; Reynolds *et al.*, 2001; Joel *et al.*, 2002; Shen *et al.*, 2008). Within this network, the basal ganglia (BG) play a central role through partially dissociable circuits organized along a dorsoventral axis.

Indeed, at least two partially overlapping functional circuits exist within the cortico-BG (CBG) network, in which dorsal and ventral regions integrate motor/cognitive and limbic information, respectively (Alexander *et al.*, 1986; Yin & Knowlton, 2006; Krack *et al.*, 2010; Redgrave *et al.*, 2010). This topographical and functional organization of the BG network arises in particular from the great diversity of cortical projections (both motor and non-motor), converging onto the striatum and is preserved at the different levels of the network (input, central, and output levels) (Parent & Hazrati, 1995a, 1995b). Accordingly, the dorsal CBG circuit is primarily involved in action selection, whereas the ventral circuit is more closely associated with valuation,

motivation, and outcome evaluation (Graybiel *et al.*, 1994; Mink, 1996; Balleine *et al.*, 2007; Kim *et al.*, 2009; Haber & Knutson, 2010; Ito & Doya, 2015; Rich & Wallis, 2016; Shin *et al.*, 2021; Balewski *et al.*, 2022, 2023). Moreover, several electrophysiological studies in both rodents and non-human primates (NHPs) have reported that BG neurons encode a range of decision-related variables - including action value, chosen value, state value, policy, reward expectation, and engagement signals - identified using multiple linear regression (MLR) models with different combinations of predictors (Samejima *et al.*, 2005; Pasquereau *et al.*, 2007; Lau & Glimcher, 2008; Kim *et al.*, 2009; Ito & Doya, 2015; Shin *et al.*, 2021; Balewski *et al.*, 2023). However, many of these decision variables are inherently collinear and often covary during choice, making it difficult to isolate neural representations of any single value-related variable (Klein-Flügge *et al.*, 2011; Padoa-Schioppa, 2013; Elber-Dorozko & Loewenstein, 2018; Shin *et al.*, 2021). Consequently, value-related neural signals cannot be unambiguously interpreted, and conclusions regarding which variable is encoded strongly depend on the specific set of predictors included in the analysis. As a result, the precise nature of value representations in the dorsal and ventral CBG circuits, and how decision variables are organized and integrated across these distinct territories during the choice process remains incompletely understood.

This issue becomes even more critical in pathological conditions such as Parkinson's disease (PD). Beyond motor symptoms, dopamine (DA) depletion disrupts value-based DM by differentially affecting ventral and dorsal CBG circuits. Dorsal circuit impairment disrupts notably action selection, movement vigor (Mazzoni *et al.*, 2007; Shiner, Seymour, Symmonds, *et al.*, 2012; Le Bouc *et al.*, 2016) and reinforcement learning (Frank *et al.*, 2004; Schonberg *et al.*, 2010). In contrast, dysfunction within ventral CBG circuits compromises reward valuation and motivational drive, reducing willingness to exert effort for reward (Cousins & Salamone, 1994; Lawrence *et al.*, 2011; Chong *et al.*, 2015; Le Bouc *et al.*, 2016) and contributing to motivational deficits such as apathy, which has been associated with reduced reward sensitivity during effort-based DM (Le Heron *et al.*, 2018). Together, alterations in value-to-action implementation and motivational valuation contribute to value-based DM deficits in PD (Brand *et al.*, 2004; Herz *et al.*, 2018) with their expression depending on task demands and dopaminergic state (Ryterska *et al.*, 2013; Kjær *et al.*, 2018). Electrophysiological studies in animal models of PD and PD patients have extensively characterized DA depletion-induced alterations in firing rates (FRs), patterns, synchronization, and network dynamics within CBG circuits (Miller & DeLong, 1987; Filion & Tremblay, 1991; Hutchison *et al.*, 1994, 1998; Benazzouz *et al.*, 2002; Brown, 2003; Wichmann & DeLong, 2003; Hammond *et al.*, 2007; Deffains *et al.*, 2016, 2018), that contribute to the emergence of synchronized oscillatory activity along the CBG network. These exaggerated synchronous neural oscillations are known to disturb information flow through the CBG network and significantly reduce the coding capacity of the CBG neurons (Bar-Gad *et al.*, 2003; Gatev *et al.*, 2006; Mallet *et al.*, 2008). However, how DA loss affects the neuronal encoding of decision variables during value-based DM remains largely unknown. Direct circuit-level electrophysiological evidence linking DA depletion to disrupted value-action representations, as well as reduced neural responsiveness (i.e., reduced neural gain) and disengagement-related activity states, remains limited. Addressing this gap is essential for understanding the neural computations underlying DM in both healthy and pathological states.

Here, we first characterized the spatiotemporal encoding and computational organization of value and action representations along the dorsoventral BG axis and related these signals to behavioral performance and engagement. We then tested how DA depletion reshapes these representations in a parkinsonian state and alters neural responsiveness (i.e., neural gain) and disengagement-related activity states, and whether these changes are associated with DM impairments. To this end, we performed multi-site, multi-electrode recordings in the caudate nucleus (CD), nucleus accumbens (NAc), external globus pallidus (GPe), and ventral pallidum (VP) while monkeys performed a value-based DM task involving both gains and losses (Figure 4-1a,b), enabling neural activity to be directly linked to behavioral measures of choice and engagement. A parkinsonian syndrome was induced through progressive 1-methyl-4-phenyl-1,2,3,6-tetrahydropyridine (MPTP) intoxication, and recordings were obtained longitudinally in the same animals before and after DA depletion, enabling within-subject comparisons.

Results

Neuronal database

Data were collected from two monkeys performing a DM task (Nioche *et al.*, 2019), in which animals made an arm-reaching movement toward one of two visual cues displayed on a touchscreen to select the option with higher expected value (EV; Figure 4-1a,b). Neuronal activity was obtained in both healthy and pathological parkinsonian states from the CD, NAc, GPe and VP. Because the ventral portions of the anterior CD and GPe receive massive limbic inputs (Haber *et al.*, 2006; Haber & Knutson, 2010), recording sites within these structures were further subdivided into dorsal (dCD, dGPe) and ventral (vCD, vGPe) regions. Ventral regions were defined as the most ventral third of the dorsoventral extent of each structure.

The NHP striatum is composed predominantly of striatal projection neurons (SPNs; ~85-95%) (Graveland & Difiglia, 1985; Yelnik *et al.*, 1991; Del Rey *et al.*, 2022), and thus the vast majority of recorded striatal units in CD were SPNs. Neuronal heterogeneity has been described in the NHP GPe (DeLong, 1971; Nougaret & Ravel, 2018; Katabi *et al.*, 2023), but it remains unclear whether it also exists in the NHP VP. Therefore, neuronal subtypes were not distinguished in either structure. All recorded units were sorted offline and assessed for FR stability, isolation quality, recording duration and sufficient task trials (see methods). A total number of 1341 neurons were recorded in the CD and the NAc (1172 in the healthy state and 169 in the parkinsonian state), including 881 in the dCD (823/58), 153 in the vCD (149/4) and 307 in the NAc (200/107). In the pallidum, 866 neurons were recorded (549 in the healthy state and 317 in the parkinsonian state), including 387 in the dGPe (305/82), 198 in the vGPe (119/79) and 281 in the VP (125/156). Neuronal recording sites in the healthy state are shown separately for each animal in Figure 4-2a, and neuronal database details are given in Table 1.

Table 1. Recording database summary across structures and disease stages.

		dCD	**vCD**	**NAc**	**dGPe**	**vGPe**	**VP**
N	H	823	149	200	305	119	125
	E	29	4	78	58	43	88
	L	29	-	29	24	36	68
SNR	H	6.36 ± 1.54	6.69 ± 4.07	6.05 ± 1.57	4.19 ± 1.21	4.30 ± 1.56	4.72 ± 1.47
	E	5.73 ± 1.42	7.55 ± 1.34	5.86 ± 1.05	4.38 ± 1.38	4.02 ± 0.89	4.18 ± 1.18
	L	6.03 ± 1.41	-	6.06 ± 1.05	4.14 ± 1.01	5.03 ± 1.71	4.60 ± 2.30
RPV ratio	H	$6.0\times10^{-3} \pm 1.0\times10^{-2}$	$6.6\times10^{-3} \pm 1.2\times10^{-2}$	$6.7\times10^{-3} \pm 1.3\times10^{-2}$	$1.9\times10^{-2} \pm 1.4\times10^{-2}$	$2.0\times10^{-2} \pm 1.5\times10^{-2}$	$1.6\times10^{-2} \pm 1.5\times10^{-2}$
	E	$7.2\times10^{-3} \pm 1.2\times10^{-2}$	$1.9\times10^{-3} \pm 3.7\times10^{-3}$	$3.3\times10^{-3} \pm 5.2\times10^{-3}$	$1.5\times10^{-2} \pm 1.3\times10^{-2}$	$2.1\times10^{-2} \pm 1.2\times10^{-2}$	$2.1\times10^{-2} \pm 1.4\times10^{-2}$
	L	$3.5\times10^{-3} \pm 8.3\times10^{-3}$	-	$7.5\times10^{-3} \pm 1.2\times10^{-2}$	$1.7\times10^{-2} \pm 1.5\times10^{-2}$	$1.7\times10^{-2} \pm 1.4\times10^{-2}$	$1.8\times10^{-2} \pm 1.4\times10^{-2}$
Duration	H	36 ± 9	38 ± 9	39 ± 10	39 ± 10	39 ± 8	41 ± 9
	E	35 ± 9	26 ± 9	38 ± 10	41 ± 8	33 ± 6	43 ± 9
	L	41 ± 12	-	38 ± 13	39 ± 12	36 ± 11	41 ± 11

N indicates the number of isolated neurons. SNR represents the signal-to-noise ratio; RPV, the refractory period violation ratio. The recording duration is given in minutes. H, indicates information for the healthy condition; E and L, represent the early and late stages of the disease, respectively. Values are shown as mean ± SD.

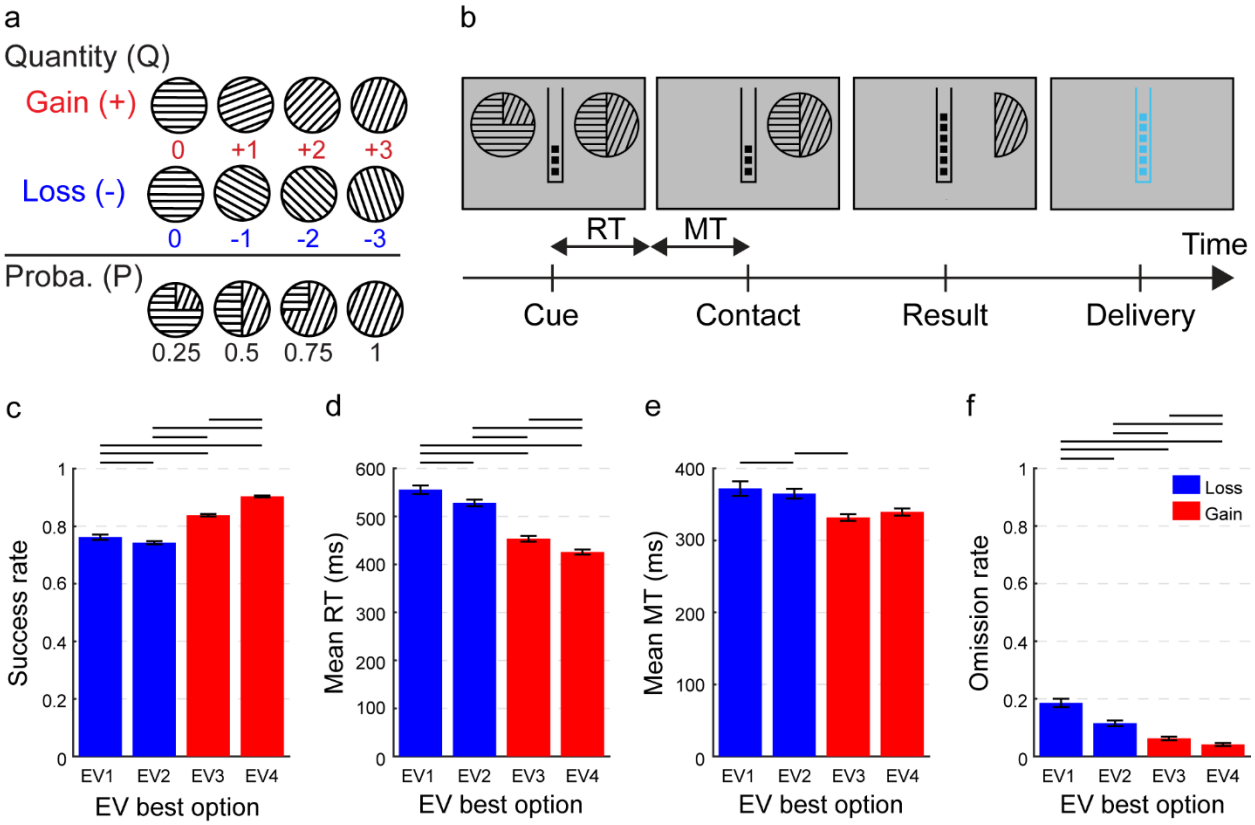

Figure 4-1. Task design and behavioral performance.

a, *Representation of outcomes and probabilities. Top: outcome magnitude (Quantity, Q) for gains and losses is encoded by the orientation of the lines within each slice. Bottom: outcome probability (Proba., P) is encoded by the arc length (relative size) of each slice.* ***b,*** *Trial structure. Monkeys initiated each trial by holding a joystick and were then presented with two lotteries (Cue) on the left and right sides of the screen. They indicated their choice by touching one target (Contact), leading to the disappearance of the non-chosen one. After the choice, they returned to the joystick and held it until the outcome associated with the chosen target was determined probabilistically (Result) and displayed using a token gauge that was incremented (gain) or decremented (loss). The number of tokens obtained was converted into applesauce reward at the end of the trial (Delivery). Reaction time (RT) was defined as the interval between cue onset and joystick release and movement time (MT) as the interval between joystick release and contact with the screen* ***c,*** *Success rate (mean ± SEM) represents the proportion of correct trials in which the animal selected the option with the highest expected value (EV), averaged across sessions and monkeys.* ***d,*** *RT (mean ± SEM).* ***e,*** *MT (mean ± SEM).* ***f,*** *Omission rate (mean ± SEM) represents the proportion of trials in which the animal failed to initiate or complete its choice within the allotted time.* ***c-f,*** *Behavioral performance is shown as a function of the EV of the best option, grouped into four categories: EV1 (low), EV2 (mid-low), EV3 (mid-high), and EV4 (high). Data were pooled across monkeys. In all panels, blue denotes trials in which the best option was a loss, and red denotes trials in which it was a gain. Bars indicate statistically significant differences.*

Behavioral results

EVs were grouped into four categories (EV1-EV4) to ensure sufficient trials per condition and approximately even spacing across the EV range: low (EV1), medium-low (EV2), medium-high (EV3), and high (EV4). Analyses used the EV category of the higher-EV lottery in each trial (see methods). Behavioral metrics were analyzed across 300 healthy recording sessions, comprising 79 352 trials pooled from both monkeys. Overall, monkeys performed the task accurately, selecting the higher-EV option in the majority of trials (~74-90%, depending on the EV category). Success rates differed significantly across EV categories (Kruskal-Wallis test, $p < 0.001$, Figure 4-

1c). All pairwise comparisons revealed significant differences between all EV categories (Holm-corrected, all $p < 0.05$), with the largest contrast observed between EV2 and EV3 at the loss-gain transition. Reaction times (RTs) also differed significantly across EV categories (Kruskal-Wallis test, $p < 0.001$, Figure 4-1d) and decreased monotonically as EV increased, thus indicating faster responses for higher EVs. All pairwise comparisons were significant (Holm-corrected, all $p < 0.05$), with the largest difference again observed between EV2 and EV3. In contrast, movement times (MTs) were still significantly influenced by EV category (Kruskal-Wallis test, $p < 0.001$, Figure 4-1e), but the modulation was less systematic, with a significant contrast remaining between EV2 and EV3 (Holm-corrected, $p < 0.05$). Finally, omission rates did not exceed 20% across EV categories and showed a pattern similar to RTs (Kruskal-Wallis test, $p < 0.01$, Figure 4-1f). Taken together, these results indicate that monkeys' behavior was strongly modulated by EV. Higher EVs were associated with increased success rates, faster responses, fewer omissions, notably reflecting greater task engagement and behavioral vigor. The largest behavioral changes occurred between EV2 and EV3, at the transition from loss to gain, suggesting a non-linear influence of EV that may reflect an additional contribution of outcome valence.

Value and action encoding during DM

Variance inflation factor (VIF) analysis revealed collinearity among value-derived predictors based on the same two offer values (e.g., EV Left, EV Right, EV Sum, EV Ch, EV Unch, EV Max, and EV Diff; see methods; Figure 4-2b), and indicated that some variables capture distinct task dimensions (e.g., EV Diff reflects choice difficulty rather than value magnitude). Because monkeys reliably selected the higher-EV option, the EV of the best option (EV Max) provides a direct and behaviorally meaningful proxy that captures the dominant value signal on each trial. Indeed, EV Max encompasses information otherwise captured by the value of the chosen option (EV Ch; VIF = 20.48) and the overall state value (EV Sum; VIF = 5.65), while avoiding redundancy among predictors. Combined with the position of the best option, EV Max also enables assessment of action value encoding through their interaction in the MLR model (Figure 4-2c), effectively capturing value signals associated with each action (Left vs Right). The impact of each regressor on neuronal FR was assessed across consecutive time bins using the corresponding absolute β coefficients and partial R^2, allowing us to track value-related, action-related, and action value-related activity over time (see methods). Population heatmaps (neurons × time) of absolute β coefficients and partial R^2 revealed time-locked modulation of neuronal firing related to value, action and their interaction (action value) following cue and release onset in both striatal (dCD, vCD and NAc) and pallidal (dGPe, vGPe and VP) subregions (Figure 4-2d-g). When pooling striatal and pallidal structures separately, the temporal distribution of significant and maximal β coefficients and partial R^2 values revealed that value encoding emerged earlier in the trial, preceding both action and action value encoding in the striatal regions and only action in the pallidal regions (Kruskal-Wallis test; β coefficients: $p < 0.05$ in striatum and GPe; partial R^2 values: $p < 0.01$ in striatum and $p < 0.05$ in GPe ; Figure 4-2h,i).

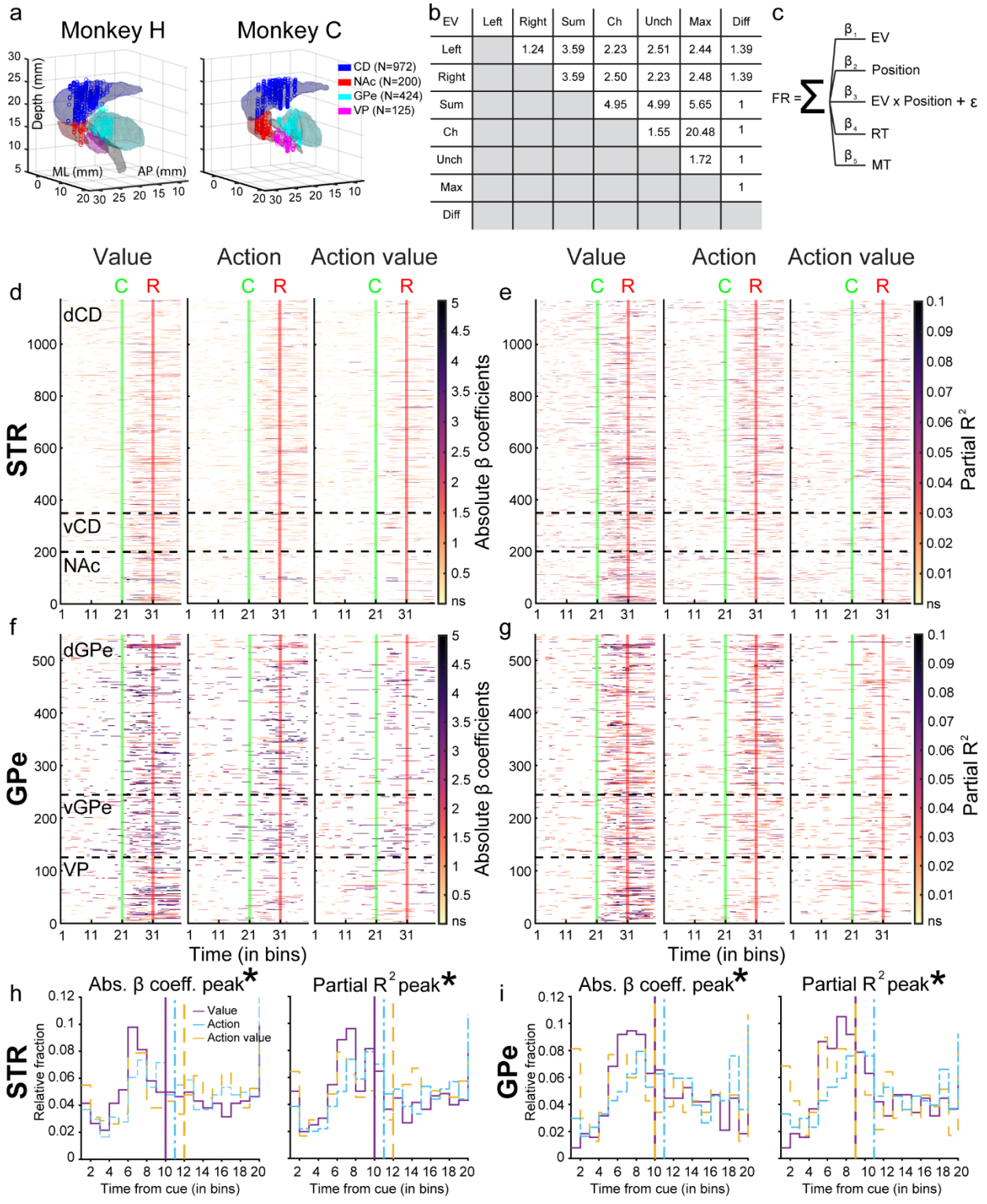

Figure 4-2. Time-resolved encoding of value and action during decision-making.

a, *Three-dimensional spatial distribution of the recording sites in the caudate nucleus (CD; blue, N = 972 neurons), nucleus accumbens (NAc; red, N = 200), external globus pallidus (GPe; cyan, N = 424) and ventral pallidum (VP; magenta, N = 125), plotted as a function of the depth, the anteroposterior position relative to ear bars and mediolateral position relative to the midline for monkey H (left) and monkey C (right).* ***b,*** *Variance inflation factors (VIFs) assessing collinearity between predictors in the regression model. Left and Right denote the EVs of the left and right options; Ch and Unch denote the EVs of the chosen and unchosen options; Sum corresponds to the sum of both options; Max to the higher EV of the two options; and Diff to the difference between left and right options.* ***c,*** *Schematic of the multiple linear regression model used to analyze the contributions of decision variables on individual*

firing rates. Predictors included EV as a continuous variable of the value of the best option (1-4), position as a binary variable for the position of the best option (0, Left; 1, Right), EV x Position (the interaction term) and reaction time (RT) and movement time (MT) as additional continuous covariates. ***d-g,*** *Time-resolved neuronal encoding in striatum (d,e) and pallidum (f,g).* ***d,f,*** *Heatmaps of absolute β coefficients for value (left), action (middle) and action value activity (right).* ***e,g,*** *Heatmaps of partial R^2 for the same activity categories. Each row corresponds to one neuron and each column to one time bin. Green and red vertical lines indicate cue onset (C) and joystick release (R), respectively.* ***h,i,*** *Relative fraction of value (purple), action (blue), and action-value (yellow) neurons as a function of the time bin corresponding to the maximal absolute β coefficient (left) and maximal partial R^2 (right), relative to cue onset. Data are pooled across CD/NAc (h) and GPe/VP (i). For each neuron, the time of peak encoding was defined as the bin in which the absolute β coefficient or partial R^2 reached its maximum value. Histograms are normalized to represent the relative fraction of neurons per time bin. Vertical lines indicate the median peak bin for each neuronal type. Asterisks denote statistically significant differences in peak timing across neuronal types.*

We next examined coding properties within each structure and compared them separately across striatal and pallidal subregions. To do so, we first focused on striatal subregions (dCD, vCD, and NAc) and analyzed the fraction of neurons significantly modulated by the EV of the best option, its spatial position, and their interaction during the decision time (DT, from cue onset to screen contact - i.e., RT+MT period). Value-encoding neurons were more frequent in the NAc followed by the vCD and the dCD (61%, 51% and 49%, respectively; permutation-based χ^2 test, Holm-corrected, $p < 0.05$, Cramér's $V^2 = 0.008$; Figure 4-3a). Value encoding also persisted longer in the ventral striatum (VS) covering 30 ± 15% of the DT in the NAc and 30 ± 10% in the vCD, compared to 20 ± 10% in the dCD (permutation-based Kruskal-Wallis test, Holm-corrected, $p < 0.001$, $\eta^2 = 0.034$; Figure 4-3b). While the strength of value encoding (absolute β coefficients) did not differ across regions (Figure 4-3c), the variance explained by value (partial R^2) differed significantly and was slightly higher in the NAc than in the dCD and vCD (0.039 ± 0.015, 0.032 ± 0.010, and 0.031 ± 0.011, respectively; permutation-based Kruskal-Wallis test, Holm-corrected, $p < 0.01$, $\eta^2 = 0.016$; Figure 4-3d). In contrast, action encoding showed a distinct dorsal bias. Indeed, action-encoding neurons were more prevalent in the dCD compared to the vCD and NAc (48%, 42% and 42%, respectively; Figure 4-3a), although this increase did not reach significance. Moreover, action encoding persisted significantly longer in the dCD than in the vCD and NAc (20 ± 10%, 15 ± 5% and 10 ± 5%, respectively; permutation-based Kruskal-Wallis test, Holm-corrected, $p < 0.001$, $\eta^2 = 0.04$; Figure 4-3b). While no differences in absolute β coefficients were observed between sub-regions (Figure 4-3c), the variance explained by the position of the best option differed significantly and appeared to be greater in the dCD than in the vCD, but not in the NAc (0.029 ± 0.008, 0.026 ± 0.005 and 0.030 ± 0.008, respectively; permutation-based Kruskal-Wallis test, Holm-corrected, $p < 0.05$, $\eta^2 = 0.01$; Figure 4-3d). Action value neurons were also more frequently observed in the dCD and vCD than in the NAc (38%, 35% and 28%, respectively; permutation-based χ^2 test, Holm-corrected, $p < 0.05$, Cramér's $V^2 = 0.007$; Figure 4-3a). However, no regional differences were observed in encoding duration, encoding strength, or variance explained for this coding type.

In the pallidum, value-encoding activity was highly prevalent across subregions with no significant differences in the fraction of responsive neurons (VP: 73%; vGPe: 71%; dGPe: 67%, Figure 4-3e) or in encoding duration (VP: 35 ± 25%; vGPe: 30 ± 20%, dGPe: 30 ± 15%; Figure 4-3f). Although the strength of value encoding (absolute β coefficients) differed significantly across

pallidal subregions (permutation-based Kruskal-Wallis test, Holm-corrected, $p < 0.001$, $\eta^2 = 0.039$; Figure 4-3g), with lower values in the VP (VP: 2.71 ± 1.34; vGPe: 3.71 ± 1.10; dGPe: 3.73 ± 1.42), the variance explained by value (partial R^2) also showed a significant regional effect (permutation-based Kruskal-Wallis test, Holm-Bonferroni corrected, $p < 0.05$, $\eta^2 = 0.017$; Figure 4-3h), with higher values observed in ventral pallidal regions (VP: 0.050 ± 0.025; vGPe: 0.039 ± 0.016; dGPe: 0.037 ± 0.013), still indicating a relative ventral bias in value-related signals. In contrast, action-encoding was more strongly represented in the more dorsal pallidal regions. The proportion of action-encoding neurons was significantly different across regions with higher fractions in dGPe and vGPe compared to VP (60%, 59% and 40%, respectively; permutation-based χ^2 test, Holm-corrected, $p < 0.01$, Cramér's $V^2 = 0.028$, Figure 4-3e). Moreover, despite similar encoding durations (Figure 4-3f), action encoding in the dGPe and vGPe was characterized by both larger encoding strength (dGPe: 3.46 ± 1.26; vGPe: 3.57 ± 0.90; VP: 2.18 ± 0.67; permutation-based Kruskal-Wallis test, Holm-corrected, $p < 0.001$, $\eta^2 = 0.013$, Figure 4-3g) and greater variance explained (dGPe: 0.031 ± 0.010; vGPe: 0.030 ± 0.007; VP: 0.025 ± 0.005; permutation-based Kruskal-Wallis test, Holm-corrected $p < 0.001$, $\eta^2 = 0.066$, Figure 4-3h). Action value neurons did not differ across pallidal subregions in prevalence, encoding duration, or variance explained (Figure 4-3e-f,h). However, their encoding strength were significantly modulated with larger absolute β coefficients in the dGPe and vGPe compared to the VP (2.99 ± 1.01, 3.01 ± 0.76 and 1.78 ± 0.95, respectively; permutation-based Kruskal-Wallis test, Holm-corrected; $p < 0.001$, $\eta^2 = 0.095$; Figure 4-3g). Taken together, these results indicate that information related to both the EV and the spatial position of the best option is broadly distributed across the recorded neuronal populations, rather than confined to specific subregions. However, value encoding showed a strong ventral bias in the striatum and a more limited ventral effect in the pallidum, whereas action encoding exhibited a dorsal bias in both structures. Action value signals were less structured, with modest regional differences and generally lower encoding in ventral regions.

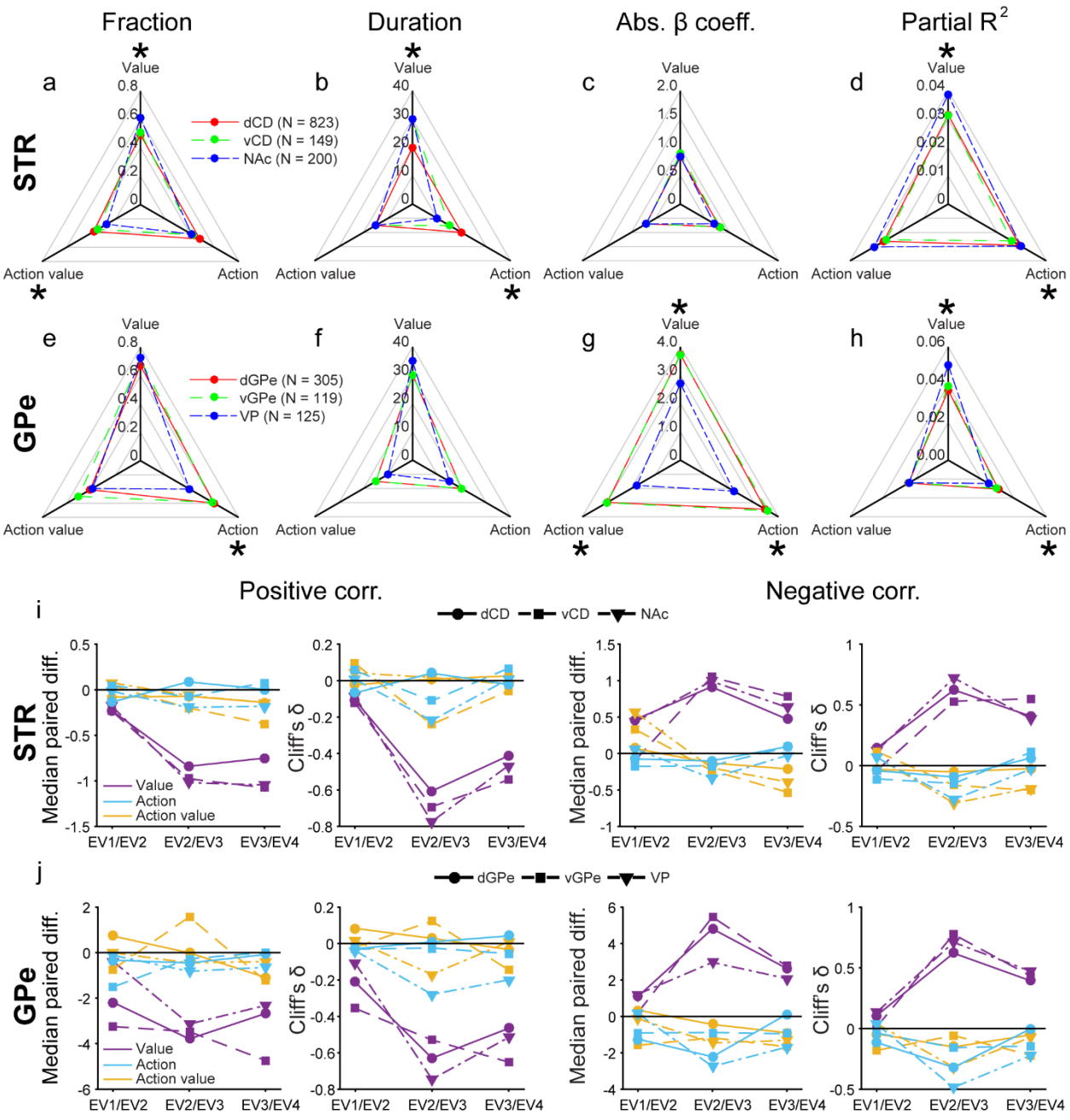

Figure 4-3. Single-neuron encoding of value-related information during decision time.

a-h, *Regression results in the healthy state in the striatum (a-d; dCD: red, N = 823; vCD: green, N = 149; NAc: blue, N = 200) and pallidum (e-h; dGPe: red, N = 305; vGPe: green, N = 119; VP: blue, N = 125).* ***a,e,*** *Fraction of neurons significantly modulated by value, action or action value (median).* ***b,f,*** *Encoding duration (median).* ***c,g,*** *Absolute beta coefficients (median).* ***d,h,*** *Partial R^2 (median). Neurons were classified as value, action, or action-value based on significant effects of EV, position, or their interaction (EV × position), respectively. Neurons showing both EV and position main effects (without interaction) were included in both value and action categories. For each neuron, absolute β coefficients and partial R^2 were averaged across significant bins, and encoding duration was defined as the percentage of significant bins. All analyses were restricted to the decision time (from cue onset to screen contact; RT and MT). Asterisks indicate statistically significant differences across subpopulations* ***i,j,*** *Summary of tuning curve analyses in the striatum (i) and pallidum (j), derived from Supplementary Figures 2 and 3. For each neuron, firing rates were averaged across time bins with significant encoding during the decision period, separately for each EV category, and normalized across EV levels by mean subtraction. Circles denote dCD/dGPe, squares vCD/vGPe, and inverted triangles NAc/VP. Neurons are grouped as positively (left half) or negatively (right half) correlating with EV. Left panels show median paired differences between successive EV levels (EV1/EV2, EV2/EV3, EV3/EV4); right panels*

show corresponding Cliff's δ values (effect size quantifying the tendency for values in one condition to be greater or smaller than those in another) for each neuronal type (value: purple; action: blue; action value: yellow).

Non-linear encoding of value during DM

To further characterize how EV is encoded during DM, we examined whether neuronal responses varied linearly across EV levels by analyzing tuning profiles separately according to the spatial position of the better option (Left versus Right), for each neuronal type. For each neuron, FRs were first averaged across time bins showing a significant effect of EV, position, or their interaction during the DT), separately for each EV × position condition, and normalized across conditions by mean subtraction. Neuronal activity was thus summarized across four EV categories in striatal (Supplementary Figure 1) and pallidal (Supplementary Figure 2) subregions. For value neurons, we identified positively and negatively correlated profiles based on whether FRs increased or decreased, respectively, as a function of EV. For action neurons, positively correlated profiles showed higher normalized FRs for leftward compared to rightward choices, irrespective of EV, whereas negatively correlated profiles showed the opposite preference. For action value neurons, positively correlated profiles were characterized by increasing FRs for leftward choices and decreasing FRs for rightward choices as a function of EV, with the reverse pattern observed for negatively correlated profiles. Direct comparison of value-related activity across the four EV levels revealed that FR modulation was not uniformly distributed across EV categories. Instead, responses exhibited a steeper change between mid-low and mid-high EVs (EV2 vs EV3) than between low and mid-low (EV1 vs EV2) or mid-high and high (EV3 vs EV4) as reflected by median paired difference comparisons. Indeed, for positively correlated value neurons, the largest median paired difference consistently occurred at the EV2-EV3 transition across regions (Figure 4-3i,j). This effect was observed in the dCD (−0.84 vs −0.23 and −0.75 for EV1/EV2 and EV3/EV4, respectively), as well as in pallidal regions, including the dGPe (−3.79 vs −2.18 and −2.68) and the VP (−3.14 vs−0.38 and −2.32). Similarly, negatively correlated value neurons showed their largest median paired differences at EV2/EV3 across all subregions (Figure 4-3i,j), including the dCD (0.99 vs 0.43 and 0.63), vCD (1.05 vs−0.09 and 0.78), NAc (0.99 vs 0.43 and 0.63), dGPe (4.81 vs 1.09 and 2.63), vGPe (5.45 vs 0.21 and 2.75) and VP (2.96 vs 1.21 and 2.08). To assess the consistency of these shifts across neurons, effect sizes were quantified using Cliff's δ (i.e., a measure of the tendency for values in one condition to be greater or smaller than those in another, Figure 4-3i,j). Cliff's δ values were largest for the EV2-EV3 transition across regions, indicating that this transition was the most consistently represented across neurons. This pattern was observed in the dCD (−0.61 and 0.62 for positively and negatively correlated neurons, respectively), vCD (−0.69 and 0.53), NAc (−0.77 and 0.72), dGPe (−0.63 and 0.62), and VP (−0.74 and 0.71), as well as in the vGPe for negatively correlated neurons (0.77). Notably, even in regions where the EV3/EV4 comparison yielded a numerically larger median paired difference (e.g., vCD and NAc), the EV2-EV3 transition exhibited larger Cliff's δ values (vCD: −0.69 vs −0.54; NAc: −0.77 vs −0.47), indicating that this transition was more consistently represented across neurons. Importantly, the transition from EV2 to EV3 corresponds to the shift from losses to gains, with mid-low EVs (EV2) associated with losses and mid-high EVs (EV3) associated with gains. Thus, neuronal sensitivity was greatest around the loss-gain transition. In contrast, this non-linear

transition was less pronounced and less consistently observed in action and action value neurons. For these neuronal types, median paired differences and Cliff's δ values were generally closer to zero, indicating comparable modulation across EV transitions and reduced sensitivity to the loss-gain transition (Figure 4-3i,j). Together, these findings demonstrate that EV encoding during DM is characterized by a non-linear tuning profile, with enhanced EV-related modulation at the transition from losses to gains. This pattern mirrors the behavioral results, in which the largest changes occurred between EV2 and EV3, suggesting a non-linear influence of EV. Notably, this effect at the loss-gain transition was particularly evident in value-encoding neurons, suggesting that their activity may reflects sensitivity to outcome valence.

Population dynamics of value and action during DM

While the previous analyses focused on value-related encoding at the single-neuron level, we next examined its representation across neuronal populations within each structure. To address this question, we analyzed population dynamics using principal component analysis (PCA) applied to trial-averaged neural activity to capture collective activity patterns across neurons and their temporal evolution. For each neuron, trials were grouped according to either the EV category of the best option (EV1-EV4) or its spatial position (Left or Right), and FRs were averaged within each condition. These trial-averaged responses were then combined across neurons to form the population activity used for PCA (see methods). PCA was then performed separately for each structure and condition (EV category and spatial position), and the first three principal components (PCs), were used to visualize low-dimensional neural trajectories over the course of the trial in subspaces capturing the dominant variance of each neuronal population under each condition (Figure 4-4a-f).

Across structures, population trajectories exhibited clear temporal structure aligned to task events, reflecting the evolution of neural activity during the DM process. Importantly, trajectories corresponding to different EV categories were structured during the DT, with EV1 and EV4 occupying extreme positions in the low-dimensional PCA space, indicating that population activity carried information about the value of the best option. However, the geometry of these trajectories differed markedly along the dorsal-ventral axis. In ventral regions, particularly the NAc and VP, trajectories corresponding to EV2 and EV3 showed clear segregation (Figure 4-4e,f). In contrast, EV-related differentiation was weaker in dorsal regions, with vCD and vGPe showing an intermediate profile.

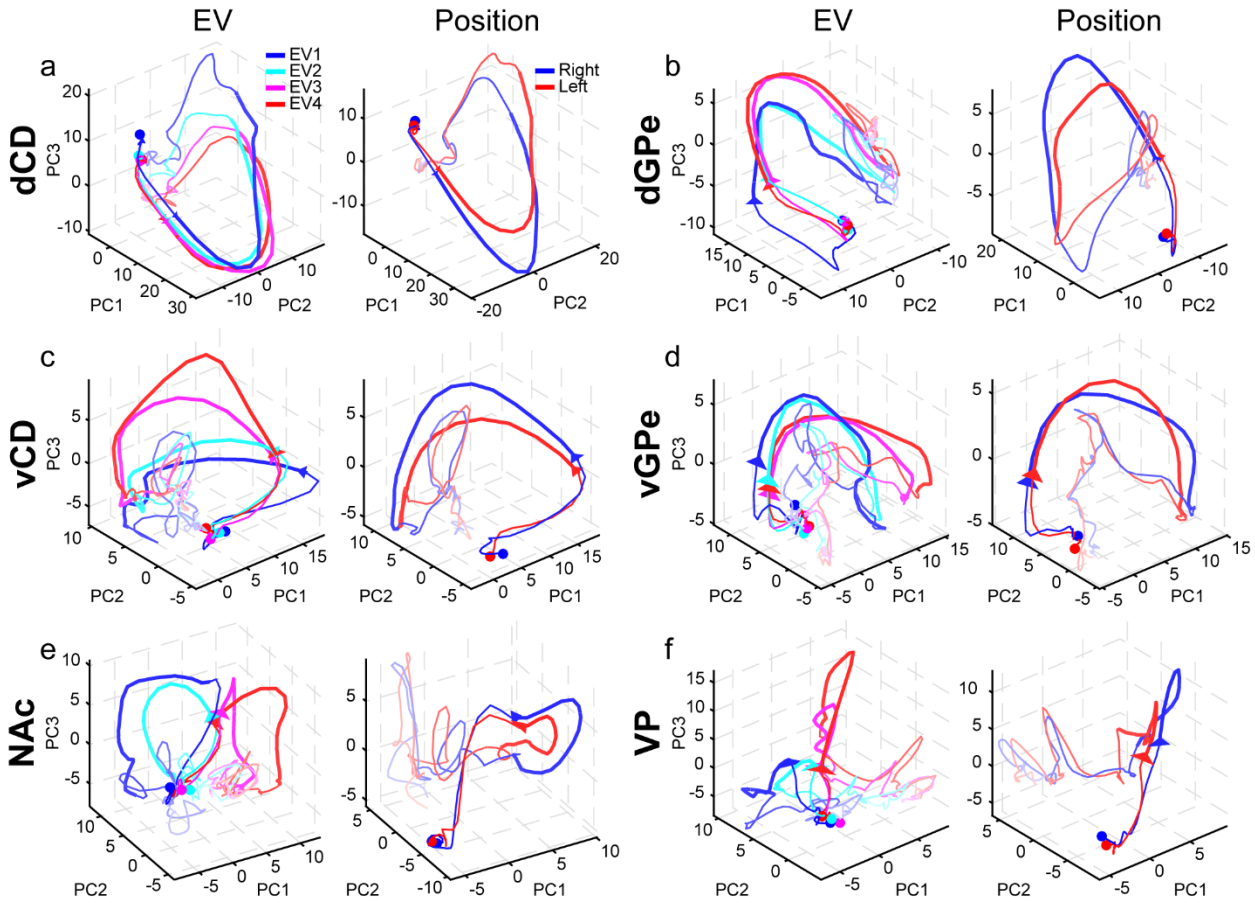

Figure 4-4. Neuronal population trajectories during decision making.

a-f, *Neuronal trajectories computed from trial-averaged population activity in PCA space (PC1-3), constructed separately for EV (left panels: EV1, blue; EV2, cyan; EV3, magenta, EV4, red) and position (right panels: Right, blue; Left; red) in the dCD (a), vCD (c), NAc (e), dGPe (b), vGPe (d) and VP (f). Dots indicate trial onset, triangles indicate cue presentation and trajectory direction and thicker lines mark decision time.*

These differences in geometry were reflected in the alignment of EV-related signals with the PCs. In these regions, EV-related variance was already captured by the first PC (PC1), which explained 11.64% of the total variance in the NAc and 17.27% in the VP. The segregation between EV2 and EV3 was especially pronounced along this component and further distributed across additional PCs (Supplementary Figure 3c,f). In contrast, in dorsal regions EV information emerged only in lower-variance components. In the dCD, EV-related segregation became apparent in PC3 (5.41% variance) and more prominently in PC4 (5.01%), while in the dGPe it was primarily visible in PC4 (6.30%) (Supplementary Figure 3a,d). The vCD and vGPe exhibited an intermediate profile, with EV-related differentiation observable starting in PC1 but less pronounced than in the NAc or VP (Supplementary Figure 3b,e). These findings indicate that EV information is both more strongly represented and more prominently aligned with dominant population axes in ventral regions, whereas in dorsal regions it is embedded in lower-variance dimensions. To quantify trajectory separation and divergence, we computed integrated Euclidean distances between adjacent EV trajectories in reduced PCA space (see methods). The largest significant differences were for EV2-EV3 in the NAc and VP (permutation-based test, Holm-corrected $p < 0.001$ for both structures;

Figure 4-5), thus indicating this transition exhibits the most robust trajectory separation and divergence in these BG structures.

We next examined trajectories associated with the spatial position of the best option and showed an opposing dorsal-ventral organization. In the dCD and dGPe, left and right trajectories were clearly segregated early in the trial (Figure 4-4a,b). This organization was already captured by PC1, which explained 14.92% of the variance in the dCD and 19.72% in the dGPe (Supplementary Figure 4-4a,d). In the more ventral regions (vCD, NAc, vGPe, VP), spatial segregation was less pronounced (Supplementary Figure 4-4b,c,e,f). Indeed, distance analyses confirmed this geometry, with the largest significant spatial trajectory separation and divergence in dCD and dGPe (permutation-based test, Holm-corrected $p < 0.001$ for both structures; Figure 4-5).

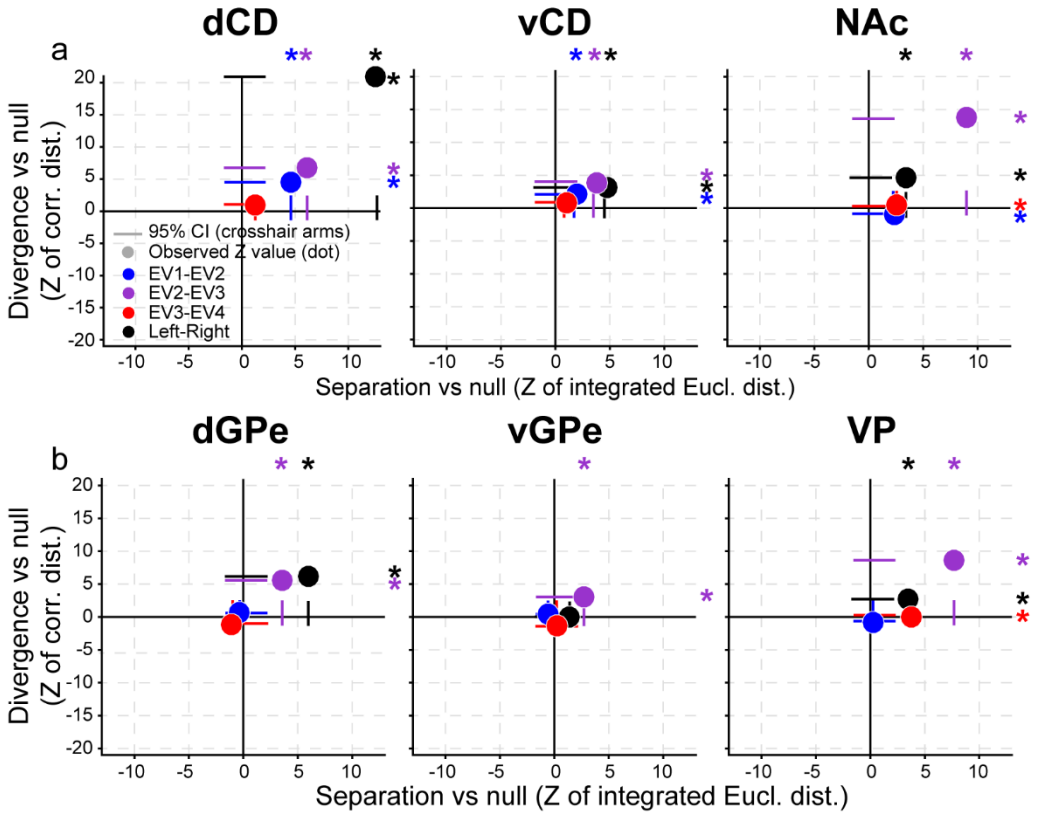

Figure 4-5. Geometric comparison of neuronal trajectories.

Geometric maps of pairwise trajectory comparisons in the striatum (a) and pallidum (b). Colored markers indicate EV contrasts (EV1-EV2, blue; EV2-EV3, purple; EV3-EV4, red) and spatial position contrast (Left-Right, black). Each point represents the standardized integrated Euclidean distance (separation, x-axis) and correlated distance (divergence, y-axis) derived from their permutation null distributions. Bars represent the 95% central interval of the permutation null distribution, expressed in standardized units. Colored asterisks mark statistically significant deviations from the null distribution for separation (horizontal) and divergence (vertical).

PCA was performed separately for each structure and condition, comparisons of trajectory metrics across structures and conditions therefore reflect deviations within condition-specific subspaces rather than absolute differences in a common neural space. Direct comparison revealed that spatial separation and divergence were strongest in dorsal regions, particularly dCD and dGPe, whereas EV-related separation and divergence dominated in ventral regions, especially NAc and VP with the largest effects observed for the EV2-EV3 transition.

Together, these results demonstrate that value-related and spatial information are reflected not only in single-neuron activity but also in the coordinated dynamics of neural populations, revealing a structured dorsal-ventral gradient in DM-related information representation within the BG. While encoding at the single-neuron level was sparse and heterogeneous, population-level analyses revealed robust and structured representations of both EV and spatial information, indicating that these signals are distributed across neuronal populations. Moreover, the distinct geometry of trajectories associated with EV and spatial position indicates that these variables are represented by distinct patterns of population activity over time. Consistent with this, ventral regions preferentially encode EV information along dominant population axes, with robust EV2-EV3 separation and divergence reflecting loss-gain transition, whereas dorsal regions more strongly represent spatial (action-related) information.

Population decoding of value and action

To further characterize the temporal evolution of information at the population level, we used linear discriminant analysis (LDA) to decode the EV and the spatial position of the best option from neural population activity. In contrast to the trial-averaged population activity used for population dynamics, decoding was performed on pseudo-population activity constructed separately for each structure and each condition (EV category or spatial position) by randomly subsampling trials for each neuron and concatenating them across neurons (see methods). Decoding was performed over time using the first three PC scores for each trial (Figure 4-6a,c) and decoding accuracy for EV and spatial position was evaluated separately for striatal and pallidal regions during the DT. Chance performance corresponded to 25% for EV decoding (four categories) and 50% for spatial position decoding (Left vs Right). In the striatum, EV decoding was highest in the NAc with accuracies comprised between 52-75% depending of the EV category (Figure 4-6b). Decoding performance was also above chance in the vCD (33-44%) and dCD (34-59%). A similar dorsal-ventral pattern was observed in the pallidum: EV decoding was strongest in the VP (48-62%), compared to the vGPe (28-59%) and dGPe (33-53%), all exceeding chance level (Figure 4-6d). In contrast, decoding of the spatial position of the best option showed an opposite organization along the dorsal-ventral axis. In the striatum, spatial decoding accuracy was highest in the dCD (79-85%), and reduced in the vCD (60-69%) and NAc (61-64%) (Figure 4-6b). A comparable pattern was observed in the pallidum, where spatial decoding reached 79-80% in the dGPe but declined to 62-63% in the vGPe and 58-59% in the VP (Figure 4-6d). This decoding profile is consistent with the dorsal-ventral dissociation between value and action representations observed in the population dynamics and demonstrates that these distributed population signals are sufficiently robust to support reliable single-trial decoding, enabling prediction of both EV and action (spatial position).

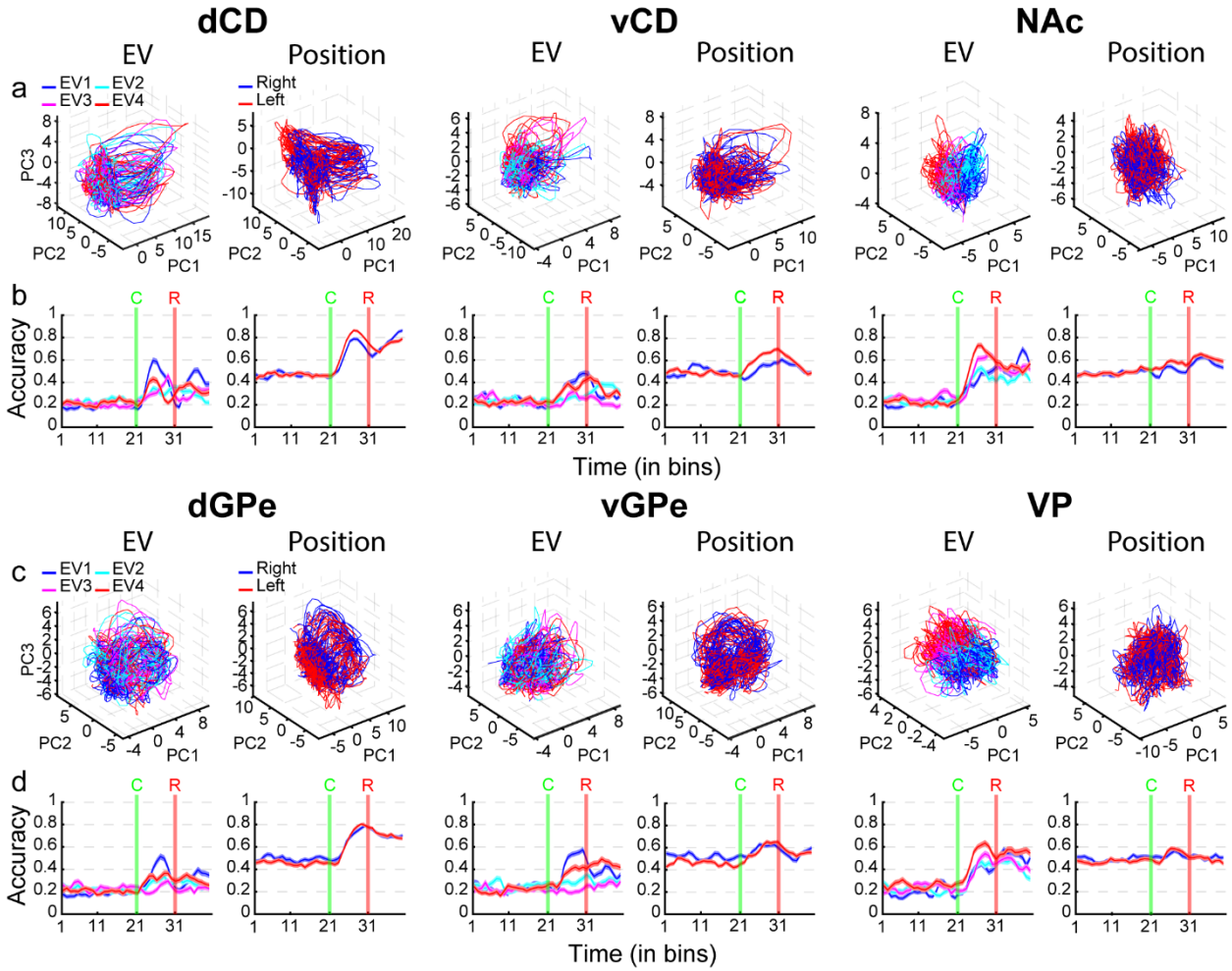

Figure 4-6. Decoding of value and position from population activity.

Population activity was used to decode EV and spatial position using pseudo-populations constructed by trial subsampling and concatenation across neurons. In each region, left panels show EV decoding (EV1, blue; EV2, cyan; EV3, magenta; EV4, red), and right panels show position decoding (Right, blue; Left, red). ***a,b,*** *Striatum (dCD, left; vCD, middle; NAc, right).* ***c,d,*** *Pallidum (dGPe, left; vGPe, middle; VP, right).* ***a,c,*** *Neuronal trajectories in PCA space (PC1-3) used for decoding. Each line represents the neuronal trajectory of a single trial (12 trials per EV category and 24 trials per position).* ***b,d,*** *Decoding accuracy as a function of time. Green and red vertical lines indicate cue onset (C) and joystick release (R), respectively. Chance performance corresponds to 25% for EV decoding (four categories) and 50% for spatial position decoding (left vs right).*

Dissociation between preserved value-based choice and impaired engagement following parkinsonism

Following MPTP intoxication, tyrosine hydroxylase (TH)-positive neurons were markedly reduced in the ventral tier of the substantia nigra pars compacta (SNc), while relatively preserved in the ventral tegmental area (VTA) (Figure 4-7a, top panels). TH staining was largely absent in the dorsal striatum (CD and Put) but relatively preserved in the VS (NAc) (Figure 4-7a, middle panels). TH-positive staining in pallidal regions (GPe and VP) was weak even in the healthy state (Figure 4-7c, bottom panels), indicating that these regions receive comparatively sparse dopaminergic innervation from midbrain dopaminergic neurons relative to the striatum which is the primary site of dopaminergic depletion in parkinsonism.

To assess the consequences of DA depletion on behavior, we analyzed behavioral data during the early stage of the disease and during the late stage, when motor symptoms (including bradykinesia/akinesia, rigidity, abnormal flexed posture and low-frequency tremor) were more pronounced (Figure 4-7b-d). Analyses were performed across 56 sessions (13,410 trials) in the early stage and across 74 sessions (11,059 trials) in the late stage. At the behavioral level, DM abilities remained largely preserved following the induction of parkinsonism. Monkeys continued to select the option with the higher EV in the majority of trials (Figure 4-7e). Success rates increased monotonically with EV, with a more pronounced contrast at the transition between loss and gain conditions (Figure 4-7e). Still, disease stage was associated with a reduction in success rates, particularly during the late stages. A significant effect of disease stage was observed for low and high EV categories (EV1 and EV4) (Kruskal-Wallis test, Holm-corrected $p < 0.05$; Figure 4-7e). In contrast to the relatively modest impact on DM performance per se (i.e., the propensity to choose the best option), disease stage had a systematic effect on task engagement measures. RT, MT, and omission rates were significantly affected across most EV categories (Kruskal-Wallis test, Holm-corrected $p < 0.001$; Figure 4-7f-h). Specifically, RT, MT and omission rates increased across EV conditions as the disease progressed. Moreover, although the monotonic decrease in omission rates with increasing EV was preserved across disease stages, the monotonic relationship between RT and EV, observed in the healthy and early stages, was disrupted and no longer present at the late stage. Together, these results indicate that following parkinsonism induction, monkeys exhibit a marked reduction in task engagement, accompanied by impaired behavioral vigor and a progressive loss of EV-dependent response initiation, despite largely preserved choice accuracy.

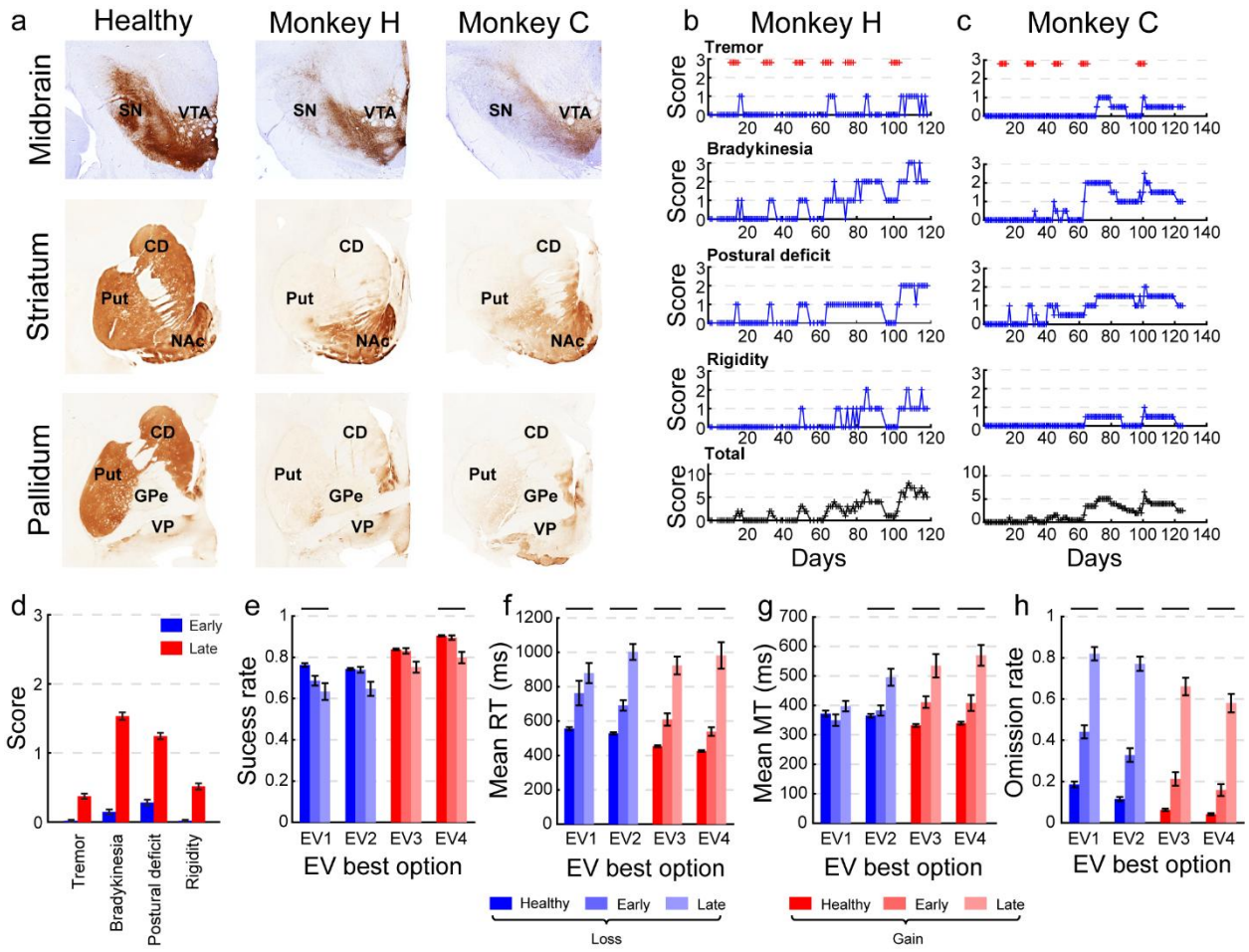

Figure 4-7. Dopamine depletion, parkinsonism assessment and behavioral performance after MPTP treatment.

a, *Photomicrographs of tyrosine hydroxylase (TH) immunostaining illustrating dopaminergic neuron loss in the ventral tier of the substantia nigra pars compacta (SNc) following MPTP treatment. Images from MPTP-treated monkeys (H and C; middle and right panels) are compared with a healthy control (left panels). Top, middle, and bottom rows correspond to midbrain, rostral striatal, and pallidal levels, respectively. CD, caudate nucleus; GPe, external globus pallidus; NAc, nucleus accumbens; Put, putamen; SN, substantia nigra; VP, ventral pallidum; VTA, ventral tegmental area.* ***b,c****, Clinical assessment scores across days for monkey H (b) and monkey C (c), including tremor, bradykinesia, postural deficit, rigidity and total score. Red crosses indicate days of MPTP injection. The level of parkinsonism was assessed by using a primate parkinsonism scale that rates each motor parkinsonian symptom (bradykinesia, rigidity, posture and tremor) from 0 (normal) to 3 (severe). Hence, the minimum score is 0 and the maximum is 12.* ***d,*** *Clinical scores (mean ± SEM) for each symptom, computed separately for early and late disease stages and pooled across monkeys. The early stage (blue) corresponds to the period before the fourth series of MPTP injections, and the late stage (red) to the period after.* ***e,*** *Success rate (mean ± SEM), defined as the proportion of correct trials in which the animal selected the option with the highest EV, averaged across sessions and monkeys.* ***f,*** *Reaction time (RT; mean ± SEM).* ***g,*** *Movement time (MT; mean ± SEM).* ***h,*** *Omission rate (mean ± SEM), defined as the proportion of trials in which the animal failed to initiate or complete its choice within the allotted time.* ***e,h,*** *Same conventions as in Figure 4-1c-f, except that color intensity reflects disease progression (lighter shades indicate late stage).*

Parkinsonism-related changes in neuronal encoding across striatal and pallidal regions

To assess how parkinsonism alters neural encoding during DM, we applied the same MLR analysis as in the healthy condition, comparing encoding metrics across disease stages (healthy, early PD, late PD) within each subregion. To account for differences in neuron and trial courts across stages, analyses were repeated using a downsampling procedure matched to the smallest dataset (late PD; see methods). Robustness of significant effects was evaluated based on the stability of effect sizes (median and IQR) and the consistency of directional effects across resampling iterations.

In the striatum, significant effects were limited to fractions. In dCD, disease stage significantly modulated the fraction of neurons encoding action (48%, 38%, and 17% for healthy, early PD, and late PD stages, respectively; permutation-based χ^2 test, Holm-corrected $p < 0.01$, Cramér's $V^2 = 0.01$, Figure 4-8a and Table 2) and action value (38%, 38%, and 10% for healthy, early PD, and late PD stages, respectively; permutation-based χ^2 test, Holm-corrected $p < 0.05$, Cramér's $V^2 = 0.01$, Figure 4-8a and Table 2). For action, there was a tendency for higher fractions in the healthy condition compared to both early and late PD, with weaker separation between early and late stages, whereas action value did not show a consistent ordering across stages. However, these effects were very small and not robust, with effect sizes close to zero, strong sampling sensitivity, and inconsistent directionality across subsamples, indicating that these differences are not reliably preserved under resampling (Table 2).

In contrast, the most pronounced striatal effect was observed in the NAc for value encoding, where disease stage significantly modulated the fraction of neurons encoding value (61%, 64%, and 28% for healthy, early PD, and late PD stages, respectively; permutation-based χ^2 test, Holm-corrected $p < 0.01$, Cramér's $V^2 = 0.04$, Figure 4-8e and Table 2). Although small, this effect showed a clear directional pattern (late < early and late < healthy, with no difference between healthy and early), indicating a selective late-stage reduction in value encoding. Median effect sizes were stable across resampling with small IQRs shifted away from zero, supporting a relatively robust effect compared to the other striatal effects (Table 2).

In the pallidum, disease-stage effects were more widespread and involved both absolute β coefficient and partial R^2, as well as fraction in vGPe. In dGPe, disease stage significantly modulated value, action and action value encoding as reflected in absolute β coefficient and/or partial R^2 (permutation-based Kruskal-Wallis test, Holm-corrected $p < 0.05$, $\eta^2 = 0.03$-0.05, Figure 4-8k,l and Table 3). However, these effects did not follow a consistent decrease with disease progression and instead often showed increases in the late stage. Robustness analyses further indicated that these effects were highly sampling-sensitive as shown by median effect sizes close to zero, small IQRs centered near zero, and/or inconsistent directionality across subsamples (Table 3).

In vGPe, disease stage significantly modulated the fraction of neurons encoding value (71%, 53%, and 56% for healthy, early PD, and late PD stages, respectively; permutation-based χ^2 test, Holm-corrected $p < 0.05$, Cramér's $V^2 = 0.03$, Figure 4-8m and Table 3), action (59%, 40%, and 22%; permutation-based χ^2 test, Holm-corrected $p < 0.001$, Cramér's $V^2 = 0.08$, Figure 4-8m and Table 3), and action value (50%, 23%, and 33%; permutation-based χ^2 test, Holm-corrected $p < 0.05$, Cramér's $V^2 = 0.05$, Figure 4-8m and Table 3). In addition, disease stage also significantly

modulated regression-based metrics in vGPe. Partial R^2 increased with disease for value encoding (permutation-based Kruskal-Wallis test, Holm-corrected $p < 0.05$, $\eta^2 = 0.05$, Figure 4-8p and Table 3), as well as for action and action value encoding (permutation-based Kruskal-Wallis test, Holm-corrected $p < 0.001$, $\eta^2 = 0.22$-0.24, Figure 4-8p and Table 3). Thus, vGPe exhibited significant disease-stage effects across both fraction-based and regression-based (partial R^2) metrics. However, only fractions showed a coherent and interpretable pattern, with a late-stage reduction in value (healthy > early PD and healthy > late PD) and action (healthy > late PD and early PD > late PD), while action value showed no clear pattern. In contrast, partial R^2 results were not robust, with median effect sizes close to zero, small IQRs centered near zero, and/or inconsistent directionality across subsamples (Table 3). Still, value-related partial R^2 showed an opposite directional pattern (healthy > early ≈ late), suggesting that value encoding among the remaining neurons may be relatively preserved or even increased despite a reduction in the proportion of encoding neurons.

In VP, disease stage significantly modulated value, action and action value encoding as reflected in absolute β coefficient and/or partial R^2 (permutation-based Kruskal-Wallis test, Holm-corrected $p < 0.01$, $\eta^2 = 0.04$-23, Figure 4-8s,t and Table 3). However, robustness analyses showed that median effect sizes were consistently close to zero with IQRs overlapping zero, even for the largest effects, and directionality was inconsistent across disease stages, indicating a lack of stable structure (Table 3).

Taken together, across striatal and pallidal regions, coherent disease-stage effects were restricted to the fraction of encoding neurons, with fewer neurons encoding value in the NAc and a broader reduction across value and action in vGPe at the late stage. For value encoding, both subregions showed a consistent directional pattern (late < healthy), indicating a shared late-stage reduction in value-related signals. Notably, effect sizes - including median estimates across resampling - were similarly stable in both regions, indicating comparable robustness of the value-related effect. However, the structure of this effect differed between them. In the NAc, the effect showed a clearer stage-dependent organization, with additional evidence for late < early, supporting a well-defined late-stage alteration. In contrast, in vGPe, although the reduction in value-related fraction was comparable in magnitude and consistently observed relative to the healthy condition, stage disease differentiation was less complete, with weaker separation between early and late stages. Thus, while value encoding is reduced at the late stage in both regions, the effect is more clearly structured in the NAc, whereas in vGPe it reflects a broader but less precisely organized pattern of reduction across encoding variables, including value encoding.

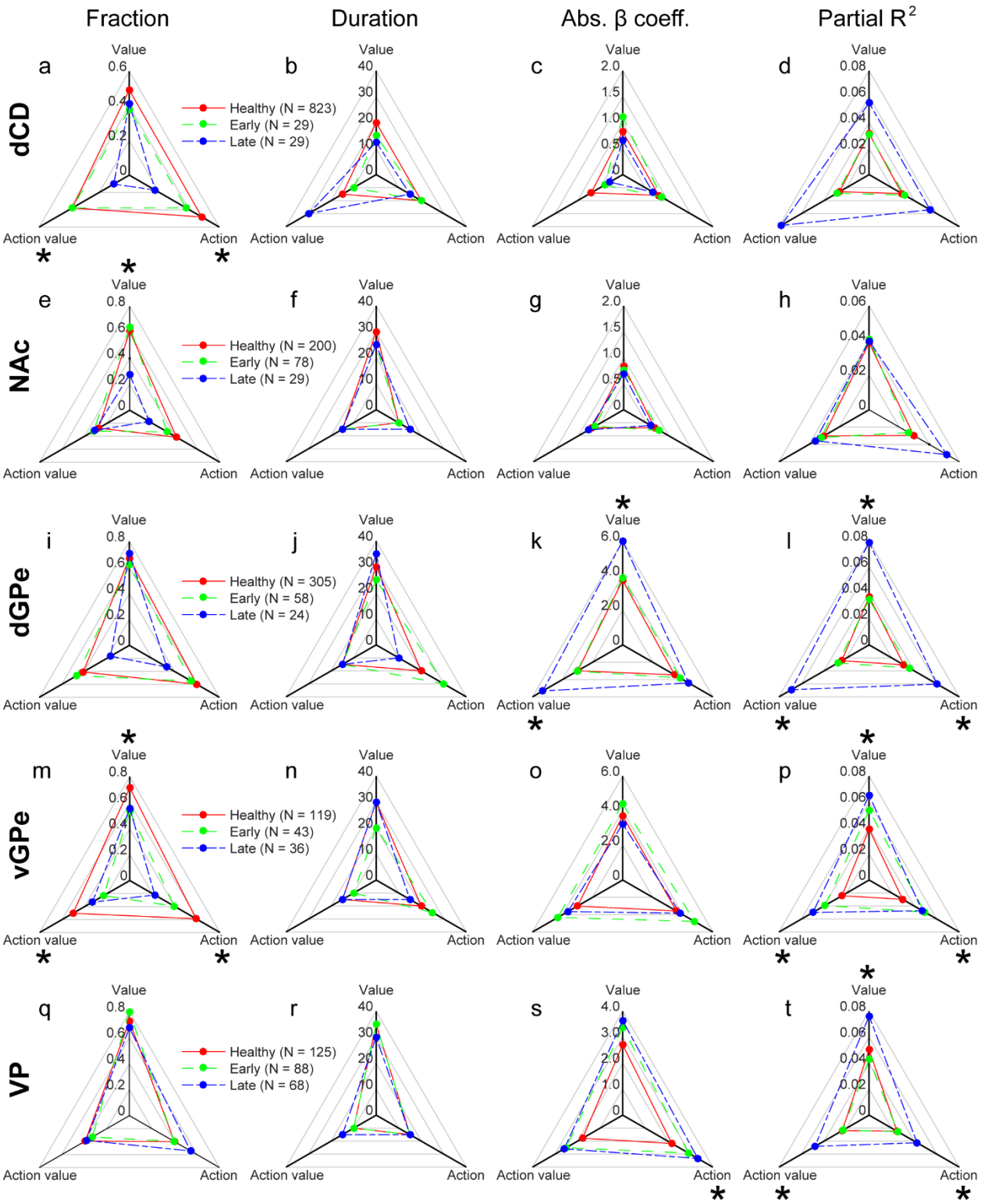

Figure 4-8. Single-neuron encoding of value-related information during decision time after dopamine depletion and induction of parkinsonism.

a-t, *Regression results across disease stages in dCD (a-d; healthy: red, N = 823; early PD: green, N = 29; late PD: blue, N = 29), NAc (e-h; healthy: red, N = 200; early PD: green, N = 78; late PD: blue, N = 29), dGPe (i-l; healthy: red, N = 305; early PD: green, N = 58; late PD: blue, N = 24), vGPe (m-p; healthy: red, N = 119; early PD: green, N = 43; late PD: blue, N = 36), and VP (q-t; healthy: red, N = 125; early PD: green, N = 88; late PD: blue, N = 68).* ***a,e,i,m,q,*** *Fraction of neurons significantly modulated by value, action, or action value (median).* ***b,f,j,n,r,*** *Encoding duration (median).*

c,g,k,o,s, *Absolute β coefficients (median).* ***d,h,l,p,t,*** *Partial R^2 (median). Same conventions as in Figure 4-3, except that asterisks indicate statistically significant differences across disease stages.*

Table 2. Robustness of encoding metric magnitude and direction under downsampling in the striatum across disease states.

Subregion	Encoding variable	Fraction (V^2)	Duration (η^2)	β (η^2)	Partial R^2 (η^2)
dCD	Value	**0**	**0**	**0**	**0.01**
		0.02 [0.01–0.04]	0 [0–0.06]	0.01 [0–0.07]	0 [0–0.05]
		(68/58/28)	(59/46/23)	(77/87/65)	(67/61/36)
	Action	**0.01**	**0**	**0**	**0.01**
		0.03 [0.01–0.05]	0 [0–0.04]	0.06 [0–0.16]	0 [0–0.07]
		(75/87/60)	(35/54/51)	(70/88/78)	(66/77/64)
	Action value	**0.01**	**0.01**	**0.01**	**0.01**
		0.02 [0.01–0.03]	0 [0–0.03]	0.01 [0–0.11]	0 [0–0.03]
		(56/47/41)	(37/39/34)	(76/87/66)	(54/46/42)
NAc	Value	**0.04**	**0**	**0**	**0**
		0.04 [0.02–0.07]	0 [0–0.06]	0 [0–0.07]	0 [0–0.04]
		(52/94/92)	(55/73/60)	(65/81/78)	(66/76/62)
	Action	**0.02**	**0**	**0**	**0.03**
		0.01 [0.01–0.03]	0 [0–0.05]	0 [0–0.06]	0 [0–0.05]
		(56/54/33)	(35/31/36)	(54/74/63)	(51/68/70)
	Action value	**0**	**0**	**0**	**0.03**
		0.02 [0.01–0.03]	0 [0–0.08]	0 [0–0]	0 [0–0.06]
		(54/59/40)	(37/19/29)	(56/45/45)	(52/37/38)
		(54/59/40)	(37/19/29)	(56/45/45)	(52/37/38)

The first value in each cell (**bold**) indicates the effect size computed from the full dataset. The second line reports the median and interquartile range (IQR) across 100 random downsampling iterations with matched neuron counts and trial numbers. The third line shows the percentage of iterations satisfying the expected ordering (healthy > early PD / healthy > late PD / early PD > late PD). Effect sizes were computed using Cramér's V^2 for fractions of significant neurons and η^2 for encoding duration, standardized β coefficients, and partial R^2. Cramér's V^2 quantifies the strength of association between categorical variables, whereas η^2 represents the proportion of variance explained by the variable of interest. Effect sizes were interpreted using conventional thresholds (small ≈ 0.01, medium ≈ 0.06, large ≥ 0.14) following Cohen (Cohen, 1988). Red indicates significant effects detected on the full dataset.

Table 3. Robustness of encoding metric magnitude and direction under downsampling in the pallidum across disease states.

Subregion	Encoding variable	Fraction (V^2)	Duration (η^2)	β (η^2)	Partial R^2 (η^2)
dGPe	Value	**0**	**0**	**0.05**	**0.05**
		0.03 [0.01–0.05]	0.04 [0–0.10]	0.08 [0.03–0.20]	0 [0–0.04]
		(46/18/19)	(58/14/9)	(62/7/3)	(57/36/27)
	Action	**0.02**	**0.03**	**0**	**0.03**
		0.03 [0.01–0.06]	0 [0–0.03]	0 [0–0.02]	0 [0–0.05]
		(24/66/80)	(46/54/51)	(60/43/32)	(46/73/77)
	Action value	**0.02**	**0**	**0.04**	**0.04**
		0.03 [0.01–0.04]	0 [0–0.06]	0 [0–0.08]	0 [0–0.05]
		(39/56/59)	(49/43/45)	(62/23/16)	(52/58/56)
vGPe	Value	**0.03**	**0.02**	**0**	**0.05**
		0.02 [0.01–0.03]	0 [0–0.04]	0.05 [0.02–0.10]	0.01 [0–0.06]
		(81/73/40)	(71/56/22)	(87/100/84)	(88/82/45)
	Action	**0.08**	**0.02**	**0.04**	**0.22**
		0.02 [0.01–0.04]	0 [0–0.03]	0 [0–0.03]	0 [0–0.03]
		(51/86/76)	(34/42/46)	(52/81/82)	(63/68/64)
	Action value	**0.05**	**0**	**0.01**	**0.24**
		0.01 [0.01–0.02]	0 [0–0.01]	0 [0–0.02]	0 [0–0.02]
		(59/57/43)	(40/35/30)	(48/79/71)	(63/50/38)
VP	Value	**0.01**	**0**	**0.02**	**0.04**
		0 [0–0.01]	0 [0–0.01]	0.02 [0–0.03]	0 [0–0.02]
		(42/53/64)	(52/28/13)	(4/32/94)	(69/32/22)
	Action	**0.02**	**0**	**0.10**	**0.22**
		0.01 [0–0.02]	0 [0–0.02]	0.02 [0–0.04]	0 [0–0.01]
		(49/20/15)	(27/22/20)	(9/38/88)	(53/41/34)
	Action value	**0**	**0**	**0.04**	**0.23**
		0.01 [0–0.01]	0 [0–0.02]	0.04 [0.01–0.07]	0 [0–0]
		(45/47/42)	(29/30/30)	(7/55/100)	(60/50/45)

Same conventions as in Table 2.

Impact of dopamine depletion on neural gain and disengagement-related activity states.

For each unit, gain was defined as the absolute change in activity relative to baseline (see methods) and was computed separately for performed (touched; T) and omitted (not-touched; N) trials within each structure, disease stage, and task epoch (RT and MT). The number of units ranged from N = 29-823 (touched) and N = 2-123 (not-touched). Gain during not-touched trials was consistently reduced relative to touched trials, indicating preserved trial outcome selectivity in neuronal gain (Figure 4-9a).

In dCD, differences between touched and not-touched trials depended on stage and epoch. During RT, reductions were 84.0% and 73.9% in the healthy and late PD stages, respectively (permutation-based Kruskal-Wallis tests, Holm-corrected $p < 0.01$ to 0.001, $\eta^2 = 0.07$ and 0.16),

whereas the early PD stage was not significant. During MT, a significant reduction was observed only in the healthy stage (77.9%, permutation-based Kruskal-Wallis test, Holm-corrected $p < 0.001$, $\eta^2 = 0.06$). In NAc, differences were smaller overall. A significant effect was observed only in the healthy stage during MT (49.3%, permutation-based Kruskal-Wallis test, Holm-corrected $p < 0.01$, $\eta^2 = 0.04$), whereas all other stages were not significant. In dGPe, differences were large and consistently significant across all stages and epochs. During RT, reductions were 69.2%, 92.7%, and 65.7% in the healthy, early PD, and late PD stages, respectively (all permutation-based Kruskal-Wallis tests, Holm-corrected $p < 0.001$; $\eta^2 = 0.07$, 0.22, and 0.33). During MT, reductions were 79.3%, 91.5%, and 85.9%, respectively (all permutation-based Kruskal-Wallis tests, Holm-corrected $p < 0.001$; $\eta^2 = 0.09$, 0.28, and 0.27), indicating robust preservation of trial outcome selectivity. In vGPe and VP, differences were substantial and followed a similar pattern, with significant effects emerging only in PD stages. During RT, reductions were 53.9% and 72.1% in vGPe, and 72.4% and 87.9% in VP, in the early PD and late PD stages, respectively (permutation-based Kruskal-Wallis tests, Holm-corrected $p < 0.01$ to 0.001; $\eta^2 = 0.08$-0.30). In the healthy stage, a significant effect was observed only in VP (82,1%, permutation-based Kruskal-Wallis test, Holm-corrected $p < 0.05$ $\eta^2 = 0.03$). During MT, reductions were 85.0% and 84.9% in vGPe, and 80.8% and 91.3% in VP, in the early PD and late PD stages, respectively (all permutation-based Kruskal-Wallis tests, Holm-corrected $p < 0.001$; $\eta^2 = 0.16$-0.33), whereas the healthy stage was not significant in either structure.

Importantly, although the magnitude and statistical significance of these effects varied across structures and disease stages, touched trials consistently exhibited higher gain than not-touched trials. Thus, neuronal gain continues to differentiate successful from unsuccessful trials across disease progression, even in conditions where this contrast does not reach statistical significance. This indicates that DA depletion does not abolish the neural distinction between trial outcomes, and that the absence of disease effects should not be interpreted as a loss of outcome selectivity.

To assess whether neural trial outcome selectivity changed across disease stages, we examined the distribution of ΔGain(T-N) contributions (see methods). This analysis directly tests whether the strength of neural differentiation between touched and not-touched trials (trial outcome selectivity) varies with disease state (Figure 4-9b). Significant stage effects were observed in dCD and VP in both RT and MT (permutation-based Kruskal-Wallis tests, Holm-corrected $p < 0.001$; $\eta^2 = 0.03$ for dCD, and $p < 0.05$; $\eta^2 = 0.02$ for VP in both epochs). Additional stage-dependent effects were observed depending on the structure and the epoch, including in NAc during MT (permutation-based Kruskal-Wallis test, Holm-corrected $p < 0.05$; $\eta^2 = 0.02$), in dGPe during MT (permutation-based Kruskal-Wallis test, Holm-corrected $p < 0.001$; $\eta^2 = 0.03$), and in vGPe during RT (permutation-based Kruskal-Wallis test, Holm-corrected $p < 0.001$; $\eta^2 = 0.12$). These effects were not consistently observed across structures and epochs, were small to moderate in magnitude ($\eta^2 = 0.02$-0.12), and did not reflect a systematic decrease in ΔGain(T-N) contributions with disease progression (i.e., neural trial outcome selectivity is not systematically reduced as disease progresses). Instead, values remained broadly stable across disease stages, indicating that the strength of neural differentiation between trial outcomes was not uniformly altered by DA depletion. Moreover, even when no significant stage effect was detected, ΔGain(T-N)

contributions remained positive, reflecting preserved differentiation between touched and not-touched trials.

Finally, to assess whether neural gain and omission rate co-varied across global behavioral states, we examined relationships between ΔGain(T-N) contributions and omission rates across disease stages (Figure 4-9c). At the stage level, where median ΔGain(T-N) contributions and omission rates were computed separately for each disease stage and compared across stages, relationships were heterogeneous and non-systematic. In RT, slopes were weakly negative (dCD: -0.024; NAc: -0.022; dGPe: -0.286; vGPe: -2.70), except for VP (+1.16). In MT, slopes were predominantly positive (NAc: +0.21; dGPe: +6.99; vGPe: +0.33; VP: +1.15), with only dCD remaining negative (-0.33). Similar results were obtained when omission rates were recomputed using only sessions with recorded neurons (Supplementary Figure 5c), indicating that these findings were robust to differences in how omission rate was estimated. Although omission rate increased from healthy to late PD stages, ΔGain(T-N) did not show a consistent monotonic change across disease stages (Figure 4-9c), explaining the absence of a consistent relationship at the stage level.

In contrast, pooled unit-level analyses, in which data from all disease stages were combined at the single-unit level, revealed negative relationships between ΔGain(T-N) contributions and omission rates (Supplementary Figure 5a). In RT, all structures showed significant negative slopes (dCD: -1.52; NAc: -1.68; dGPe: -5.43; vGPe: -4.36; VP: -1.56; permutation-based tests, Holm-corrected $p < 0.01$ to 0.001; Supplementary Figure 5b). In MT, the effect was weaker and reached significance only in dCD and vGPe (-1.24 and -2.49; permutation-based tests, Holm-corrected $p < 0.05$ to 0.001), although all remaining structures also showed negative slopes that did not reach significance. Because omission rate increased from healthy to late PD, and the healthy stage was characterized by lower omission rates and a greater number of units with high ΔGain(T-N) values, these pooled relationships likely reflect differences between disease stages (i.e., distinct ranges of omission rate and ΔGain contribution) rather than reflecting a consistent pattern across stages (i.e., a uniform increase or decrease across healthy, early, and late PD). Indeed, linear regression analyses performed at the unit level within each structure, epoch, and disease stage revealed heterogeneous relationships, with slopes varying in both direction and magnitude depending on the structure, stage, and epoch (data not shown). This heterogeneity also explains the bidirectional relationships observed at the population level between omission rate and ΔGain(T–N) contributions.

Together, these findings reveal two complementary mechanisms underlying task disengagement. First, trial outcome selectivity, captured by ΔGain(T-N) contribution, did not exhibit a consistent and robust monotonic change across disease stages and remained positive across all conditions, indicating preserved neural differentiation between touched (correct) and not-touched (omission) trials. Second, omission rates increased markedly across disease stages. Because omissions are associated with lower gain, this shift led the network to spend more time in a low-gain regime. As a result, overall neural engagement decreased even in the absence of systematic changes in ΔGain(T-N) contribution. These findings reveal a dissociation between engagement and selectivity: DA depletion shifts the network toward a disengaged, low-gain regime, increasing the prevalence of omission-related states while largely preserving trial outcome selectivity.

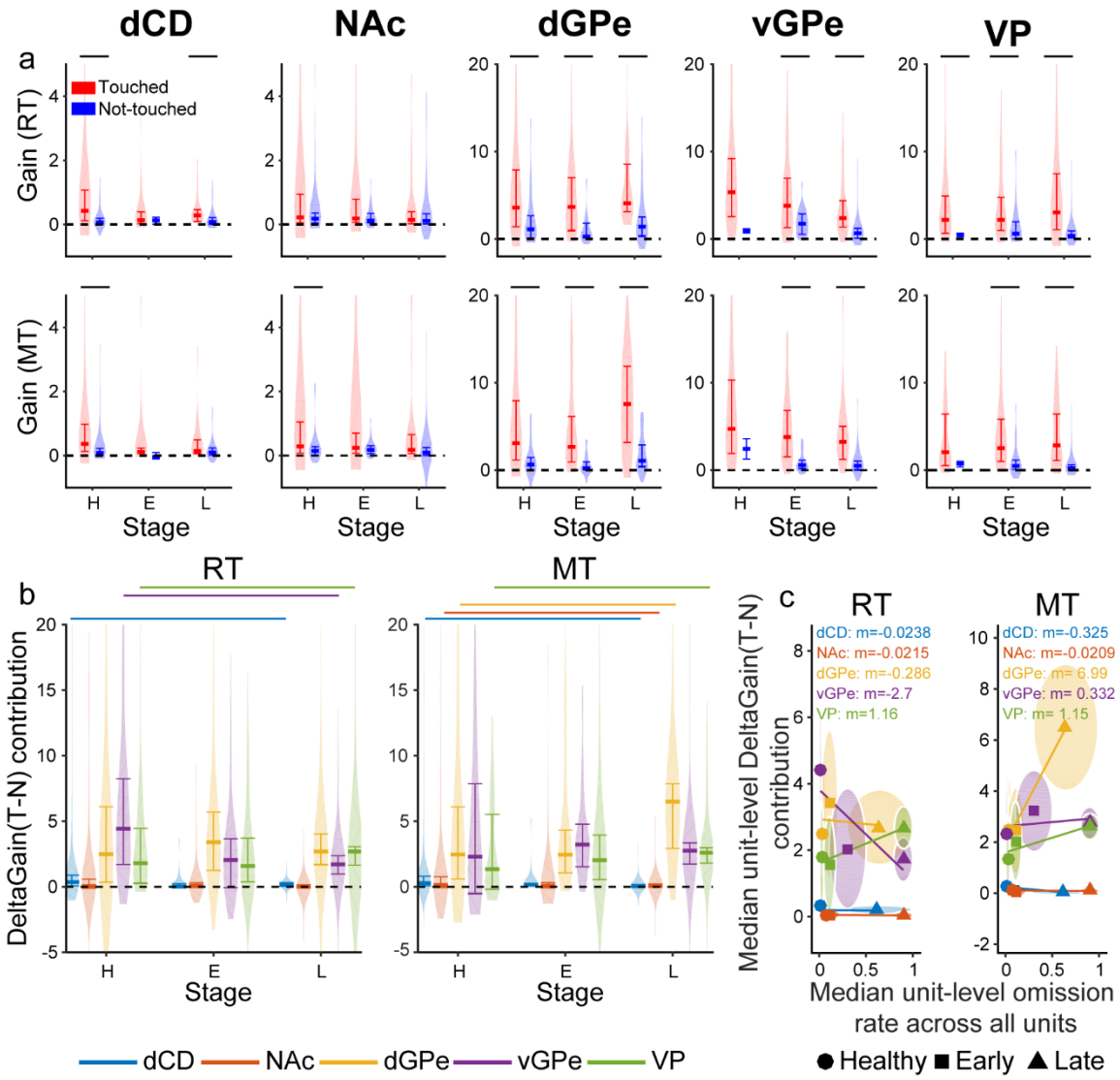

Figure 4-9. Neuronal gain and task engagement across disease stages and structures.

***a**, Distributions of neuronal gain during touched (correct, red) and not-touched (omission, blue) trials are shown for each structure (dCD, NAc, dGPe, vGPe and VP) during RT (Top) and MT (Bottom) epochs. Gain was computed for each unit as the absolute change in activity relative to baseline. Within each disease stage - healthy (H), early MPTP (E) and late MPTP (L) -, groups are displayed side by side. Shaded violin-like profiles represent distribution density. Central lines indicate the median and interquartile range (IQR). The dashed horizontal line denotes zero gain. Bars indicate statistically significant differences. **b,** Distributions of ΔGain(T-N) contribution (T, touched; N, not-touched) are shown across disease stages for each structure and epoch. Gain values for touched (gT) and not-touched (gN) units were summarized by their medians (mT and mN, respectively), and individual contributions were computed relative to the median of the opposite trial type (touched: gT−mN; ; not-touched: mT−gN). Shaded violin-like profiles represent distribution density. Central lines indicate the median and IQR. The dashed horizontal line denotes zero. Bars indicate statistically significant differences. **c,** Relationship between omission rate and ΔGain(T-N) contribution across structures. Median omission rate computed across all sessions (and not only the sessions with recorded neurons) is plotted against median ΔGain(T-N) contribution for each structure and epoch (RT and MT) across disease stages. Each marker represents one stage (healthy, circle; early MPTP, square; late MPTP, triangle), with colors indicating structures (dCD, blue; NAc, red; dGPe, yellow; vGPe, purple; VP, green). Ellipses are centered on the median and extend by the MAD along each axis. Solid lines indicate linear fits across stage-specific points, with slope values shown in each panel.*

Discussion

The present study investigated how value, action value and action representations are functionally organized along the dorsoventral axis of key BG structures during healthy value-based DM and how they are reorganized after DA depletion as observed in PD. Our results show that value-related signals are preferentially encoded in ventral regions, with dynamics reflecting the set of available options. These signals differentiate more strongly between gains and losses than between values within the same domain, although differences within domains (gains or losses) remain detectable. In contrast, dorsal regions preferentially encode the action to be performed, with neuronal activity segregating according to the spatial positions available for choice. Importantly, we find that action value neurons do not constitute the dominant population in either circuit and are present in similar proportions across dorsal and ventral pathways, suggesting a more distributed and heterogeneous coding scheme than classical models emphasizing action value representations in BG. Additionally, we show that following DA depletion, the fraction of neurons encoding value decreases selectively in the VS (NAc) and to a lesser extent in the vGPe, while no comparable reduction is observed in the VP, despite relatively preserved DM accuracy. This modest decrease in the vGPe is accompanied by an increase in partial R^2, indicating a greater contribution of value to neural activity in the remaining value-encoding neurons. We also show that engaged and disengaged neuronal states remain dissociable across structures regardless of disease stage. However, as the disease progresses, a low-gain neuronal state resembling omission-related activity becomes more frequent and is associated with reduced behavioral engagement. Notably, when monkeys remain engaged in the task, the value signals and decision variables preserved in pallidal regions appear sufficient to support near-optimal choice.

Representation of decision variables along the dorsoventral axis of the BG

Our dorsoventral encoding analysis aligns with previous studies suggesting a functional dissociation between ventral and dorsal BG circuits, with ventral regions contributing primarily to valuation and dorsal regions contributing to action selection and implementation (Graybiel *et al.*, 1994; Mink, 1996; Balleine *et al.*, 2007; Kim *et al.*, 2009; Haber & Knutson, 2010; Ito & Doya, 2015; Rich & Wallis, 2016; Shin *et al.*, 2021; Balewski *et al.*, 2022, 2023). However, comparisons across studies remain challenging because different tasks and modeling approaches rely on different combinations of predictors. Many of these predictors covary, making it difficult to isolate neuronal representations of specific decision variables and leading to conclusions that depend strongly on the predictor set used. Moreover, the design of the task varies across studies, making results difficult to compare. Different task structures can emphasize different decision variables, and if these variables covary or are not properly accounted for, they may lead to misleading interpretations. For example, VS BOLD signal in human that was initially interpreted as encoding RPEs was later shown to reflect task-relevant timing information when reward timing was manipulated experimentally (Klein-Flügge *et al.*, 2011). More generally, because DM involves multiple interrelated variables (e.g., offer value, chosen value, and state value etc.), neural activity may appear to encode different signals depending on the predictors included in the model and how the task is structured (Padoa-Schioppa, 2011, 2013), consistent with evidence for

distributed and heterogeneous representations of decision variables in the striatum (Kim *et al.*, 2009; Ito & Doya, 2015; Shin *et al.*, 2021). Similarly, studies using block-based designs where action values are temporally correlated, such as Samejima and colleagues (Samejima *et al.*, 2005), may detect apparent action value signals that partly reflect the representation of other decision variables or temporal correlations rather than genuine value coding (Elber-Dorozko & Loewenstein, 2018). In contrast, our task design minimized such correlations by presenting randomized lottery pairs, with the best option appearing equally often on the left or right and reward probabilities and magnitudes varying independently across trials. This design ensures that key decision variables are largely free from temporal correlations. Furthermore, we incorporated an integrative representation of action and value signals through an interaction term, allowing us to examine how value-related information is transformed into action selection while reducing collinearity among predictors. Our results indicate that action value signals are represented in similar proportions along the dorsoventral axis, suggesting that their role may be less dominant than previously proposed. This observation is consistent with recent work suggesting that some earlier studies may have overestimated the prevalence of action value neurons due to methodological confounds (Elber-Dorozko & Loewenstein, 2018; Shin *et al.*, 2021). Finally, we used the EV of the higher-value option (EV Max) as a proxy for value in our analyses. This choice reduces collinearity among value-related predictors that the brain might use during DM. In principle, the brain computes the EVs of the available options (e.g., EV Left and EV Right) and compares them to guide choice, which is reflected in the chosen value. The decision context can also be represented by the sum of the option values, corresponding to a form of state value. Because the higher-value option alternates equally between spatial positions in our task, EV Max captures information contained in EV Left, EV Right, and their combination while avoiding redundancy across predictors. Including EV Max in our interaction-based analysis therefore helps ensure that neurons classified as encoding action value are less likely to reflect correlated variables such as state value or policy signals.

Non-linear value encoding and gain-loss asymmetry

Beyond the dorsoventral organization of value- and action-related signals in BG circuits, explicitly incorporating both gain and loss outcomes within the same task reveals that value encoding is not linear but depends on the context of the choice. In particular, careful examination of the tuning curves of value-, action- and action value-encoding neurons revealed a steeper encoding of value around the gain-loss transition than within either the gain or loss. Consistent with this pattern the dynamics of neuronal population trajectories showed greater segregation and divergence at the gain-loss boundary (see also section entitled “Distributed representation of decision variables in population dynamic”). Behavior similarly exhibited an asymmetry in gain-loss integration, with stronger effects at the loss-gain transition, consistent with the Prospect Theory. This framework actually proposes that decision-makers evaluate outcomes relative to a reference point and weight gains and losses asymmetrically depending on the decision context (Kahneman & Tversky, 1979). Rather than behaving as perfectly rational agents maximizing expected utility, individuals tend to evaluate outcomes differently across gain and loss domains. Beyond previous behavioral demonstrations of asymmetric processing of gain and loss lotteries

in monkeys using the same paradigm (Nioche *et al.*, 2019), our results extend these observations to the neuronal level. Specifically, we show that neurons within BG structures, including the NAc and the VP, encode value differently across gain and loss domains, with a larger change in activity at the transition between gains and losses. This differential encoding suggests that ventral BG circuits represent not only EV but also the valence of outcomes, highlighting a contextual representation of decision variables within these circuits. Similar asymmetries between gains and losses have been reported previously in neural studies of DM. For example, activity in the VS and prefrontal cortex has been shown to reflect behavioral loss aversion during risky DM (Tom *et al.*, 2007). In addition, previous work has demonstrated that the striatum encodes both gains and losses, with different patterns of neural activity within overlapping and interacting circuits (Seymour *et al.*, 2007). However, other studies have suggested that the VS primarily represents gain-related EV, whereas loss-related prediction signals may involve additional structures such as the amygdala (Knutson *et al.*, 2005; Yacubian *et al.*, 2006). Importantly, these apparent discrepancies across studies may partly reflect differences in task structure. Many previous paradigms relied on mixed gain-loss gambles or gain vs no gain and loss vs no loss contrasts, which may limit the ability to dissociate gain and loss representations (Knutson *et al.*, 2005; Yacubian *et al.*, 2006). In contrast, our task included gain-only lotteries, loss-only lotteries, and mixed gain-loss lotteries within the same session. This design allowed us to dissociate value and valence effects more clearly and demonstrates that value encoding is enhanced at the loss–gain transition, suggesting that neuronal activity may encode value together with information related to outcome valence. Task structure may also influence the reference point used by subjects when evaluating outcomes. In many monetary incentive tasks, cumulative rewards are displayed across the session, potentially shifting the reference point over time and influencing subsequent decisions. Consistent with this idea, previous work has shown that activity in the VS reflects reference-dependent value computations, whereas dorsal striatum is less sensitive to such reference effects and is more closely associated with action-related processing (De Martino *et al.*, 2009). In our paradigm, rewards were delivered after each trial with a fixed reference point across trials, thereby reducing the influence of previous trials on subsequent decisions. This design also ensured that individual trials were largely independent, although gradual satiation across the session could potentially influence reward encoding. However, this effect is unlikely to account for our results, as monkeys showed similar levels of engagement and comparable RTs when sessions were divided into early and late halves (data not shown).

Distributed representation of decision variables in population dynamic

Population dynamics analysis allows neural activity within a given structure to be represented in a high-dimensional space defined by the activity of all recorded neurons and reduced to a lower-dimensional representation capturing the dominant patterns of population activity. In this framework, decision variables are not encoded by individual neurons but emerge from patterns of activity across the population (Shenoy *et al.*, 2013; Ebitz & Hayden, 2021). This approach is particularly important because individual neurons often exhibit mixed selectivity, responding to multiple decision variables simultaneously (Rigotti *et al.*, 2013; Fusi *et al.*, 2016). As a result, assigning a single functional label to individual neurons may be misleading and fails to capture

how information is represented at the population level during value-based DM. By performing population analyses on condition-averaged activity separately for EV and spatial position, we isolated how neural populations within each structure differentiate value and action variables, respectively. This approach reveals that both value and action representations are distributed across neurons, through shared patterns of activity rather than neuron-specific tuning. Moreover, it highlights that ventral BG regions, including the NAc and VP, do not simply encode the values of individual options but appear to represent the broader context of the decision (gain vs loss) which was not as structure-specific at the single-unit level. Such contextual (valence) representations may play an important role in guiding decision strategies, for example by influencing whether it is worth engaging in a given choice based on a cost-benefit evaluation. This interpretation is consistent with the idea that ventral BG circuits contribute to motivational and state-related aspects of DM rather than directly specifying actions (Haber & Knutson, 2010; Ito & Doya, 2015; Shin *et al.*, 2021). However, because value and action were analyzed separately, the present approach does not directly address how value information is transformed into action selection. Future analyses examining population dynamics with value and spatial variables jointly included would be necessary to characterize this transformation. Performing such analyses within individual structures would clarify the contribution of each region to this process, while analyses across structures could reveal how value-to-action transformations are distributed within the BG network. Still, although the observed population-level structure supports distributed coding, it does not exclude the possibility that specific subpopulations contribute preferentially to particular computations under different task conditions or behavioral states. This view is supported by studies showing that neurons within the CBG form coactive assemblies comprising individual neurons with diverse coding properties (Yuste, 2015; Härmson *et al.*, 2025).

Value encoding and choice accuracy are not abolished after dopaminergic depletion

Previous studies have suggested that DM impairments in PD may arise from dysfunction within fronto-striatal circuits, including limbic BG loops, as well as deficits in feedback processing and executive control, which together impair the ability to appropriately use value information to guide behavior (Thiel *et al.*, 2003; Brand *et al.*, 2004). However, whether these deficits reflect a primary impairment in value encoding itself remains unclear. Our results indicate that DA depletion does not abolish value-related information across BG circuits. Although the fraction of value-encoding neurons was selectively reduced in the NAc, and to a lesser extent in the vGPe, value encoding remained detectable in downstream ventral pallidal structures including the VP and in dorsal regions. Importantly, success rates were relatively preserved when monkeys engaged in the task, indicating that value information remained sufficiently available to support near-optimal choice. Thus, the parkinsonian deficit in our task is better characterized as a partial degradation of ventral value representations rather than a complete impairment of value encoding or comparison. This is consistent with previous work suggesting that dopaminergic dysfunction primarily affects the expression or utilization of learned value representations rather than value learning per se (Shiner, Seymour, Wunderlich, *et al.*, 2012; Smittenaar *et al.*, 2012). Consistent with this view, converging evidence indicates that value-related signals in VP are robust and not only originate from NAc. In rodents, VP neurons encode relative reward value

earlier and more prominently than NAc neurons (Ottenheimer *et al.*, 2018). Moreover, a subset of VP neurons encodes RPE signals more robustly than those observed in the NAc, and these signals predict subsequent changes in task engagement and causally influence reward-seeking behavior (Ottenheimer, Bari, *et al.*, 2020). Together, these findings challenge a strictly serial model in which value is computed in the NAc and passively relayed to the VP, and instead suggest that the VP can contribute independently to value computation within ventral BG circuits. In this framework, the persistence of value signals in the VP may help explain why animals can still choose appropriately when they remain engaged despite a selective reduction of NAc value coding.

Motivational invigoration and motor motivation

Our results indicate that DM impairments in the parkinsonian state was not a collapse of value-based choice accuracy, but a marked reduction in task engagement, reflected by increased RTs, MT, and omissions, especially for low-EV options. Although monkeys remained able to perform the task after MPTP treatment, and omission rates continued to reflect EVs, with more omissions for low-EV trials, EV-dependent modulation of RTs progressively diminished, along with a loss of gain-loss asymmetry. The fact that omissions remained sensitive to EV, and were most frequent for low-value options, indicates that disengagement was linked to the motivational significance of the available options rather than to a purely motor inability to respond. This pattern is consistent with evidence that PD alters reward sensitivity and cost-benefit evaluation, reducing the impact of incentive value on behavior rather than abolishing value representation (Le Bouc et al., 2016). Together, these findings suggest that dopamine depletion weakens the recruitment and behavioral impact of ventral value signals, particularly those related to incentive motivation, while preserving sufficient value information to support accurate choice when action is initiated. At the neural level, engaged and disengaged trials remained dissociable across disease stages, as shown by persistent differences in neural gain between touched and omitted trials. Here, neural gain refers to changes in neuronal responsiveness or response amplitude without altering selectivity (Salinas & Thier, 2000; Salinas & Sejnowski, 2001), indicating that these states differ primarily in the strength of task-related activity rather than in the type of information encoded. However, our results indicates that the balance between these states appears altered with DA depletion.

The system occupies more often a low-gain, omission-like state, and this shift correlates with increased disengagement. This suggests that the DA depletion in parkinsonian state does not abolish the neural capacity to engage, but biases the network toward a state that is less likely to generate action. Accordingly, the deficit may reflect a reduced probability of entering or sustaining an engaged state rather than a total loss of task-related coding. This interpretation is consistent with theoretical and experimental works proposing that DA regulates the willingness to expend effort and the vigor of movements (Niv *et al.*, 2007; Salamone *et al.*, 2016; Berke, 2018). In PD, bradykinesia has been interpreted not as a primary motor impairment leading to slow movements, but as an reduced willingness to move fast as vigorous movements are selected less often (Mazzoni *et al.*, 2007). In addition, movement speed in PD appears to be modulated by

motivational valence. Patients exhibit longer MTs overall, but this slowing is more pronounced in reward contexts than in aversive contexts, consistent with a diminished impact of reward-related signals on behavior (Shiner, Seymour, Symmonds, *et al.*, 2012). In line with this, our results show that MTs are particularly increased for higher-value rewards (gains), whereas low-value conditions (losses) are less affected, suggesting a selective impairment in reward-driven motor motivation.

From a mechanistic perspective, one possible interpretation is that weakened ventral value signals are less effectively propagated to circuits involved in action initiation and invigoration. In this framework, reduced value encoding in the NAc may limit the transmission of incentive motivational signals within BG networks. According to the striato-nigro-striatal ascending spiral organization described by Haber and colleagues, ventral striatal regions can influence more dorsal circuits involved in action selection and motor output (Haber *et al.*, 2000). A disruption of this ventral-to-dorsal transfer of information following dopaminergic depletion could therefore impair the recruitment of action-related processes despite preserved value information elsewhere. This framework provides a potential mechanism linking the selective reduction of ventral value encoding to the observed deficits in engagement and movement vigor.

Taken together, these results are consistent with a role of the BG in driving task engagement during value-based DM by regulating the vigor with which actions are executed according to the decision context. Following DA depletion, the BG circuits may become less effective at promoting engagement and modulating vigor, leading to a bias toward low-gain states despite the persistence of value encoding within ventral circuits. In this sense, the parkinsonian deficit observed in our task may arise less from a failure to identify the best option than from a failure to be in an engaged state and respond with sufficient vigor.

Methods

Animals

This study was performed on two female rhesus monkeys (*Macaca mulatta*), Monkey H (born in 2012) and Monkey C (born in 2009), weighing ~ 5-6kg. The monkeys were housed in the animal facility of the Institute of Neurodegenerative Diseases (CNRS UMR 5293, Bordeaux, France - agreement number: E33063268) under standard conditions (12/12h light/dark cycle, ~ 60% humidity and ~ 22°C). All experimental procedures were performed in accordance with the Council Directive of 2010 (2010/63/EU) of the European Community and the National Institute of Health Guide for the Care and Use of Laboratory Animals. The protocol received agreement from the Ethical Committee for Animal Research CE50 and authorized by the French Ministry of Research and Education.

Behavioral task and analysis

Monkeys performed a two-alternative lottery DM task as previously described in (Nioche *et al.*, 2019). In each trial, monkeys selected between two probabilistic options associated with potential gains or losses of reward. Each option was represented by a pie chart indicating the EV of the lottery. A total of 96 lottery pairs were used, with one lottery having a higher EV than the

other within each pair. The EV of the lotteries ranged from 0 to 6 (16 discrete values), but did not include EV = 3, which served as the reference point separating gains from losses. Thus, lotteries with EV < 3 predicted an expected loss, whereas lotteries with EV > 3 predicted an expected gain. The position of the two lotteries was counterbalanced such that each option appeared equally often on the left and right sides and all lottery pairs were presented with equal frequency across trials. During the task, monkeys were seated in a primate chair equipped with a joystick positioned at waist level and facing a touchscreen. The sequence of major task events is illustrated in Figure 4-1b. Trials were initiated by grasping the joystick, followed by presentation of the two lottery cues (Cue). Monkeys selected one option by touching the corresponding cue on the touchscreen (Contact). After the choice, monkeys returned their hand to the joystick and held it until the outcome was revealed. The outcome of the selected lottery was then determined probabilistically (Result) and displayed using a token gauge that was incremented (gain) or decremented (loss). Finally, the number of tokens obtained was converted into applesauce reward at the end of the trial (Delivery). Trials were separated by a variable inter-trial interval. Failure to complete any trial step within the allotted time resulted in an error trial followed by a brief timeout. Monkeys were extensively trained on the task prior to electrophysiological recordings. Assessment of the monkeys' behavior was made by monitoring RTs, MTs, success rates, and omission rates. RT was defined as the interval between cue presentation onset and joystick release, whereas MT corresponded to the interval between joystick release and contact with the touchscreen. Success rate corresponds to the proportion of correct trials in which the animal selected the option with the highest EV and omission rate to the proportion of trials in which the animal failed to initiate or complete its choice within the allotted time, averaged across sessions and monkeys.

EVs were grouped into four categories (EV1 - EV4) to ensure sufficient trial numbers per condition while maintaining approximately evenly spaced mean EVs across the EV range: low ($0 \leq EV \leq 1.5$), medium-low ($1.5 < EV < 3$), medium-high ($3 < EV < 4.5$), and high ($4.5 \leq EV \leq 6$). For each trial, analyses were based on the EV category of the higher-EV lottery within the pair. The higher-EV option was determined from the original EV values prior to grouping, such that even when both lotteries in a pair belonged to the same category (e.g., EV1), one option could still be identified as having the higher EV. Because several value-related variables derived from the two options are inherently correlated, the higher EV reflects the EV of the best option which was used as a proxy for the overall value of the decision context while reducing multicollinearity (see MLR analysis).

Brain imaging

Anatomical magnetic resonance imaging (MRI) and computed tomography (CT) scans were performed prior to surgery. High-resolution T2-weighted MRI images were acquired on a 3T Siemens Prisma scanner (Siemens Healthineers, Erlangen, Germany) operated with syngo MR E11 software and using a 3D SPACE (Sampling Perfection with Application-optimized Contrasts using different flip angle Evolutions) sequence. Acquisition parameters were as follows: TR = 3200 ms, TE = 384 ms, flip angle = 120°, voxel size = 0.5 × 0.5 × 0.5 mm^3, matrix = 320 × 320, field of view = 160 × 160 mm^2, slice thickness = 0.5 mm, echo train length = 181, and 4 signal averages.

In addition, CT imaging of the monkey skull was performed using a Planmeca ProMax cone-beam CT scanner (Planmeca Oy, Helsinki, Finland) operated with Romexis 6.4.3.33 / 3.9.14.89 software at 90 kVp and 10 mA. The acquisition produced 534 axial slices with a slice thickness and isotropic voxel size of 0.15 mm. Images were reconstructed in Hounsfield units using the manufacturer's standard reconstruction algorithm. Preoperative MRI and CT scans were co-registered using 3D Slicer (www.slicer.org) to allow for accurate segmentation of the targeted BG nuclei and to stereotaxically estimate both the optimal placement of the recording chamber and the intended electrode trajectories. Additional CT scans were acquired and co-registered to the preoperative MRI on a monthly basis to monitor electrode positioning over time. These follow-up registrations allowed us to re-validate and, when necessary, re-evaluate the precise location of the electrodes within the targeted BG nuclei relative to the planned trajectories.

Surgery

Implantation of the titanium 32-channel, form-fitting titanium microdrive and recording chamber system (Gray Matter research, Bozeman, MT, USA) was performed in a two-stage delayed surgical procedure (Dotson *et al.*, 2017) on the contralateral side to the acting hand. Surgeries were performed under aseptic conditions using isoflurane and O2 deep anesthesia, following induction with ketamine (10mg/kg IM) and atropine (0.05mg/kg IM). The head of the animal was fixed in a stereotaxic frame (M2e-Unimécanique, Eaubonne, Val-d'Oise, France) and body temperature, heart rate, blood pressure and SpO2 were monitored throughout the entire surgical procedure. During the first surgery, the chamber was positioned above the targeted BG nuclei in the left hemisphere - the CD, NAc, GPe, and VP - and sealed around its perimeter with a thin bead of C&B Metabond quick adhesive cement (Parkell, Edgewood, NY, USA). It was then fixed to the skull using titanium bone screws and acrylic bone cement. The cranial bone was left intact, and a silicone gasket together with a short plug were mounted onto the chamber and covered with a protective cap. The animals were allowed a 3-4 weeks recovery period before the next stage. During the second surgery, a craniotomy was performed within the interior of the chamber while leaving the dura intact. The interior of the chamber was rinsed and the dura was punctured at the putative electrode entry points using a puncture grid kit to facilitate subsequent electrode penetration. The microdrive was then positioned in its predefined location within the chamber and secured using machine screws, after which it was covered with a protective aluminum cap. The animals were given an additional 3-4 weeks recovery period during which the electrodes were gradually lowered to the targeted BG nuclei. Once mounted, the microdrive remained in place for the duration of the experiment. The chamber also provided a distributed ground and reference via a ground wire connection to the PCB.

Parkinsonism induction and assessment

After completion of the neuronal recordings in the healthy state, animals underwent multiple courses of injections of MPTP (MPTP hydrochloride, Sigma, St Louis, MO, USA). Each course consisted of daily intramuscular injections of low doses of MPTP (0.125 to 0.25 mg/kg) for five consecutive days. The courses were spaced 1-2 weeks apart, and a total of 5-6 courses were administered to gradually induce a moderate parkinsonian state while preserving the animals'

ability to perform operant tasks (Slovin *et al.*, 1999). Neurophysiological recordings were conducted between the courses of MPTP injection following a mandatory 72-h biohazard isolation period during which recordings were not possible. Severity of the parkinsonian motor symptoms (bradykinesia, rigidity, posture and tremor) was assessed daily using a modified Benazzouz primate parkinsonism scale (Benazzouz *et al.*, 1995). Following completion of the neuronal recordings in the parkinsonian state, post-mortem TH immunohistochemistry was performed to assess the extent of DA depletion induced by MPTP treatment.

Data collection and physiological recording

Electrical signals were recorded from the 32 independently movable, glass-coated tungsten microelectrodes of the microdrive (impedance range at 1 kHz: 0.3-2.0 MΩ), which were slightly advanced through CD, NAc, GPe and VP after each daily recording session (5-7 sessions per week over a period of 10-12 months totalizing 227 days for Monkey H and 208 days for Monkey C) in healthy and parkinsonian states. The signals were amplified by 100, band-pass filtered between 1 and 5000 Hz (using a hardware two-pole Butterworth filter) and sampled at 20 kHz prior to digitization via a wireless recording system (WS-16, Multichannel Systems, Reutlingen, BW, Germany). The band-pass filtered signal (1-5000 Hz) contained both local field potential (LFP; 1-250 Hz), which is thought to reflect global synaptic input and dendritic processing, and multi-unit activity (MUA; 250-5000 Hz), which represents the efferent activity of local neuronal populations. LFPs and MUAs were further processed offline using digital band-pass filters. Single-unit activity (SUA) was extracted from the MUA by applying automated offline spike detection and sorting pipeline. Spikes were detected using a threshold-crossing method, waveform features were extracted using principal PCA, and units were identified using K-means clustering following classical spike-sorting approaches (Lewicki, 1998; Rey *et al.*, 2015). Finally, SUAs were subjected to offline quality analysis, including assessments of FR stability, signal-to-noise ratio (SNR), refractory period violation (RPV) ratio and recording duration to ensure quantitative and objective measures of spike isolation. SNR was defined as the ratio between the absolute amplitude of the spike waveform and an estimate of background noise, computed from the MAD of the MUA. The RPV ratio was defined as the proportion of inter-spike intervals ≤ 2 ms relative to the total number of inter-spike intervals. Units were included if they met the following criteria: SNR ≥ 3, RPV ≤ 0.05, and recording duration ≥ 15 min. To examine ventral subregions of the CD and GPe, the dorsoventral extent of each structure was defined as the difference between the most dorsal and most ventral recording depths at which neuronal activity was detected. This extent was divided into three equal segments, and neurons located in the most ventral third were classified as belonging to the ventral subregion.

Tyrosine hydroxylase immunohistochemistry

Following completion of the neuronal recordings in the parkinsonian state, monkeys were deeply anesthetized with an overdose of sodium pentobarbital (100 mg/kg i.v.). Exsanguination was performed by intracardiac perfusion with 1-2L of 0.9% NaCl containing 1% heparin. After confirmation of death, brains were removed, divided into two hemispheres and post-fixed for one week in 4% formaldehyde in 0.1 M phosphate-buffered saline (PBS) at 4 °C. Tissue was then

cryoprotected in 20% followed by 30% sucrose in PBS. Brains were frozen by fast immersion in isopentane at −55 °C, and serial 50 µm-thick cryostat-cut sections were collected from the CD to the posterior extent of the substantia nigra (coronal plane - antero-posterior axis, free floating sections in 0.2% sodium azide-PBS).

DA depletion was assessed by TH immunohistochemistry on striatal sections encompassing anterior, middle and posterior regions of the striatum (Bregma -00,45mm / -03,15mm / -06,30mm (Paxinos *et al.*, 2024)), as well as on substantia nigra sections from one hemisphere per animal. Free-floating sections were first thoroughly rinsed in PBS, and endogenous peroxidase activity was quenched using a peroxidase-blocking solution (Dako REAL, S2023) for 10 min. After PBS washes, non-specific binding was reduced by blocking antigenic sites for 30 minutes in PBS containing 2% bovine serum albumin (BSA), 0.3% Triton X-100, and 0.01% thimerosal. Sections were then incubated overnight at room temperature with a primary antibody against TH (monoclonal rabbit anti-TH, [EP1532Y], ab137869, Abcam) diluted 1:5000 in PBS containing 0.2% BSA, 0.3% Triton X-100, and 0.01% thimerosal. The following day, sections were rinsed in PBS and incubated for 30 min with a polymer-based horseradish peroxidase (HRP)-conjugated anti-rabbit secondary antibody (Dako EnVision+™ Kit, K4011). Following further PBS washes, TH staining was revealed with 3,3'-diaminobenzidine (DAB) (Dako DAB Kit, K3468) for 45 seconds, and the reaction was stopped with multiple PBS rinses. Sections were mounted onto gelatin-coated slides. Substantia nigra sections were additionally counterstained with Nissl stain. Finally, sections were dehydrated, cleared in xylene, and coverslipped with a permanent mounting medium.

Task period segmentation and neural data preprocessing

For each neuron, SUA was segmented for each correct trial into distinct task periods (grasping, RT, MT, return time, holding, outcome display, and reward delivery). Because several task periods had variable durations, spikes within each period were binned into a fixed number of bins, resulting in variable bin durations across trials. Each task period was divided into 10 bins, except for the outcome and reward delivery periods, which were longer and therefore divided into 30 bins. Baseline activity was defined as the last 500ms of the inter-trial interval preceding grasping, which was also divided into 10 bins. Spike counts within each bin were converted to FRs by dividing by the bin duration. FR time series were smoothed using a Gaussian kernel (σ = 1 bin) and baseline-subtracted relative to the mean baseline activity.

Multiple linear regression analysis

To assess potential multicollinearity among value-related predictors, we computed the VIF for EV-related variables used in the task: EV Left and EV Right (offer/option/action values), EV Ch and EV Unch (chosen and unchosen values), EV Sum (EV Left + EV Right; state value), EV Diff (EVleft - Evright; value contrast) and EV Max (higher value). Based on this analysis, the higher EV which reflect the EV of the best option was considered to capture the overall value of the decision context.

Only neurons recorded during at least 48 correct trials were included in the analysis. For each neuron and each time, an MLR (MATLAB fitglm function) model was used to quantify the influence of task variables on FR:

$$FR = \beta 0 + \beta 1 \times EV + \beta 2 \times Position + \beta 3 \times (EV \times Position) + \beta 4 \times RT + \beta 5 \times MT + \varepsilon$$

where EV is a continuous predictor representing the EV category of the best option (coded 1-4, as described above), Position is a binary variable indicating the spatial position of the best option (0 = left, 1 = right), EV × Position is the interaction term, RT and MT are continuous covariates and ε denotes the residual error. All regressors were z-scored to reduce collinearity, particularly for the interaction term, and to facilitate comparison of the β coefficients. To quantify the contribution of each predictor, partial correlations between FR and each regressor were computed while controlling for the other regressors in the model (MATLAB partialcorr function), and the corresponding partial R^2 values were calculated. Standardized β coefficients reflected the relative strength of FR modulation by each predictor, whereas partial R^2 quantified the unique variance in FR explained by that predictor. Together, these measures provided a comprehensive characterization of neural encoding.

Neuronal classification

Time bins showing a significant EV × Position interaction were classified as interaction bins and excluded from analyses of the main effects. Neuronal classification and coding characterization of neural encoding were restricted to the DT, defined as the interval from cue onset to screen contact (including RT and MT). Because classification relied on the presence of significant bins, a neuron could belong to multiple categories across different time bins within the DT. Neurons exhibiting at least one significant bin for the main effect of EV were classified as value neurons (indicating value encoding independent of spatial position). Neurons exhibiting at least one significant bin for the main effect of Position were classified as action neurons (indicating spatial encoding independent of value). Neurons exhibiting at least one significant bin for the EV × Position interaction were classified as action value neurons (indicating value encoding that depended on spatial position). Neurons exhibiting both EV and Position main effects (without interaction) were included in both the value and action categories. For each value, action, and action value neuron, the standardized β coefficient and partial R^2 were averaged across significant bins, and coding duration was defined as the percentage of significant bins. For the calculation of standardized β coefficients and partial R^2 during the decision period, using the median and the peak bin value across significant bins, rather than the mean, yielded similar results (data not shown).

Under healthy conditions, the fraction of significant neurons, regression coefficients (standardized β), partial R^2, and encoding duration during the DT were compared across striatal subregions (dCD, vCD, and NAc) and pallidal subregions (dGPe, vGPe, and VP). The same metrics were also compared across disease stages (healthy, early PD, and late PD) within each subregion (dCD, NAc, dGPe, vGPe, and VP). These analyses were performed separately for each encoded variable (value, action, and action value) using permutation-based tests. Because of the limited

number of recorded neurons in the vCD after MPTP treatment, this structure was excluded from comparison across disease stages.

To assess robustness to differences in neuron and trial sample sizes across disease stages, the full MLR analysis was repeated 100 times after random downsampling without replacement, with neuron counts matched to the smallest dataset (late PD) and 48 trials selected per disease stage. For each iteration, all encoding metrics were recomputed. Robustness was evaluated by examining the stability of effect size magnitude across iterations and the consistency of effect direction across pairwise contrasts.

Neural Trajectory Geometry and Dynamics

PCA was used to characterize population-level neural dynamics. Analyses were performed separately for each BG region (dCD, vCD, NAc, dGPe, vGPe and VP). For each neuron, trials were grouped either according to the EV category of the best option (EV1 - EV4) or according to the spatial position of the best option (Left or Right).

Binned and smoothed FR - computed using the fixed-bin approach described above but without baseline normalization - were averaged across trials within each group. Only neurons recorded in at least 48 trials and with activity available in all condition groups were included. For each group, a matrix of size 120 × N was constructed, where rows corresponded to time bins and columns to individual neurons (N). Group-specific matrices were then concatenated along the temporal dimension, yielding a 480 × N matrix for the EV analysis and a 240 × N matrix for the position analysis.

Prior to PCA, neuronal activity was z-scored across time for each neuron and PCA was performed on the z-scored data without additional centering (MATLAB pca function, with centering disabled). For each structure and condition (EV or Position), the first ten PCs were retained, and analyses focused on the top five PCs explaining the largest fraction of population variance. Neural population trajectories were visualized using the first three PCs, which capture the dominant dynamics of neural activity and define a condition-specific optimal low-dimensional subspace of population activity.

To quantify differences between neural population trajectories across conditions, we measured both their spatial separation and dynamic divergence within condition-specific optimal low-dimensional subspace during the DT. Spatial separation was quantified as the Euclidean distance between trajectories in the three-dimensional PCA subspace (PC1 - PC3) and summarized by the integrated Euclidean distance across the decision period. Dynamic divergence was quantified using correlation distance, defined as $d=1-r$, where r is the Pearson correlation between vectorized trajectories in the PC1-PC3 subspace across the decision period. Larger Euclidean distances indicate greater spatial separation between trajectories and larger correlation distances indicate greater divergence in the temporal evolution of population activity. Trajectory differences was assessed using permutation-based tests. Comparisons were performed between adjacent EV categories (EV1-EV2, EV2-EV3, EV3-EV4) and between spatial positions (Left vs Right). Condition-averaged population activity was then recomputed and projected onto the original PCs used for trajectory visualization and for computing the observed metrics, yielding surrogate trajectories in the same/fixed three-dimensional PCA subspace. Trajectory metrics

were subsequently computed from these trajectories to generate empirical null distributions. This ensured that trajectory comparisons and statistical inference were performed within a consistent neural geometry across conditions. To facilitate comparisons across conditions and brain structures, trajectory metrics were standardized (z-scored) relative to their permutation null distributions. The 95% central null interval was computed in metric units and expressed in standardized units for visualization. Because PCA was performed separately for each condition, standardized metrics reflect deviations from the corresponding null distributions within their optimal low-dimensional subspaces rather than absolute differences in a common neural state space.

Trial-Level Decoding of Value and Position

Analyses were conducted separately for each BG regions. Neuron inclusion was determined separately for decoding the EV and position of the best option. Neurons were required to have at least 12 trials in each EV category (EV1-EV4) for EV decoding, and at least 24 trials in each position (Left and Right) for position decoding. For each neuron, we randomly subsampled 12 trials per EV category or 24 trials per position and binned smoothed and non-normalized activity (120 bins per trial) were concatenated across trials and vectorized (yielding 12 × 120 = 1440 samples per EV category or 24 × 120 = 2880 samples per position). Vectorized activity was then concatenated across neurons to form a population matrix. Matrices from each EV category or position were subsequently concatenated and transposed to obtain a samples × neurons matrix (5760 × N for both EV and position analyses). Neural activity was z-scored across time for each neuron prior to PCA, and PCA was performed on the z-scored data without additional centering (MATLAB pca function, with centering disabled). Population activity was projected onto the first three PCs, and the resulting PC scores were segmented into 120-bin trajectories corresponding to individual trials and their associated EV categories or positions.

Decoding was performed independently at each time bin using an LDA classifier (MATLAB fitcdiscr function, pseudo-linear, Gamma = 0.8) trained on the three-dimensional PC representation of population activity. Decoder performance was evaluated using a repeated random subsampling cross-validation procedure. For EV decoding, classifiers were trained on 8 trials per category (32 total) and tested on 4 trials per category (16 total); for position decoding, classifiers were trained on 16 trials per position (32 total) and tested on 8 trials per position (16 total). Decoder performance was quantified using classification accuracy returned by the classifier. The procedure was repeated 100 times, with trials randomly subsampled from the available trials for each neuron and a new train-test partition generated at each iteration. Decoding metrics were averaged across iterations to obtain accuracy traces over time for each EV category or position.

Neural gain and omission-related analyses

Neural gain was defined as the magnitude of task event-induced modulation relative to baseline activity, independent of response sign. For each unit, peri-event activity (i.e., baseline-centered, binned, and smoothed FRs) was averaged across trials and rectified using the absolute operator to capture task-related response regardless of excitation or suppression. The mean absolute

baseline activity was subsequently subtracted from the rectified task event-induced (cue/bar release) response to establish a natural baseline, and gain was quantified as the mean modulation amplitude following cue/bar release presentation. Touched (performed) and not-touched (omission) trials were analyzed separately. During touched trials, RT and MT were defined from the animal's behavioral performance and normalized into 10 bins. For not-touched trials - where these epochs could not be defined - two fixed 500 ms windows were used and similarly divided into 10 bins to allow comparable measurements across trial types. Units were selected independently for each trial type (≥ 48 trials), resulting in generally unpaired populations contributing to touched and not-touched gain. Unit counts were therefore reported separately for touched and not-touched trials and individual neurons could contribute to both groups and were not mutually exclusive. Gain differences between touched and not-touched trials were first assessed by comparing the gain distributions of these unpaired unit populations for each structure, disease stage and epoch. To further quantify trial-type differences without requiring unit pairing, we then computed a ΔGain(T-N) contribution measure (where T denotes touched trials and N denotes not-touched trials). For each structure, disease stage and epoch, the median gain of touched units (mT) and not-touched units (mN) was computed independently. Individual unit contributions were defined relative to the median gain of the opposite trial type (touched units: GainT - mN; not-touched units: mT - GainN), yielding a distribution whose central tendency reflects the population-level difference in gain between touched and not-touched trials.

Relationships between ΔGain(T-N) contributions and omission rate were examined at two levels. At the population level, values were compared descriptively across disease stages to assess whether neural gain and omission rate co-varied across global behavioral states. At the single-unit level, relationship between individual ΔGain(T-N) contributions and omission rate were evaluated separately for each disease stage and for the pooled dataset across all stages. Omission rates at the population level were computed both across entire sessions and across sessions containing the recorded units, whereas at the single-unit level, omission rates were computed only from sessions containing the recorded units.

Software and statistics

Data from the two monkeys were pooled for analysis. Given the limited number of subjects (n = 2), statistical comparisons at the animal level were not performed, although the results were qualitatively similar across animals. Instead, analyses were conducted at the level of neurons or recording sessions, consistent with common practice in single-unit neurophysiology where inference relies on large numbers of observations obtained within subjects (Asaad & Sheth, 2024) and where pooling observations allows inference about the sampled neuronal population rather than a population of animals (Fries & Maris, 2022).

Behavioral comparisons across EV categories were performed using non-parametric Kruskal-Wallis tests. When a significant main effect was detected, post hoc pairwise comparisons were conducted using the Holm-Bonferroni correction to account for multiple comparisons.

For neural analyses, permutation-based tests was used with 10,000 permutations. Differences in the fraction of responsive neurons were assessed using permutation-based χ^2 tests, in which labels (BG subregion or disease stage) were randomly reassigned across observations to generate

empirical null distributions. Effect sizes were quantified using Cramér's V^2. Differences in continuous neural metrics (e.g., regression coefficients, partial R^2, encoding duration, and neural gain measures) were assessed using permutation-based non-parametric omnibus tests (Kruskal-Wallis type) by randomly permuting group labels across observations, with effect sizes reported as eta squared (η^2).

Trajectory differences were evaluated using permutation-based tests, in which condition labels (EV category or position) were randomly permuted and neural trajectories recomputed within the same PCA subspace to generate empirical null distributions. Observed trajectory metrics (Euclidean distance and correlation distance) were compared with these distributions using one-sided permutation tests.

Relationships between individual ΔGain(T–N) contributions and omission rate were assessed using simple linear regression. For each structure and epoch, permutation tests were used to evaluate the significance of the regression slope by randomly permuting omission rate values relative to ΔGain(T–N) contributions and recomputing the regression slope to generate a null distribution of slope estimates.

When multiple comparisons were performed, p-values were adjusted using the Holm-Bonferroni correction, and statistical significance was defined as $p \leq 0.05$. Data are presented as median ± MAD, unless specified otherwise.

Large language model (LLM) declaration

We used ChatGPT 5.0 to assist in improving the clarity and academic style of the English language in our already-written manuscript. The scientific content, analyses, and conclusions were entirely developed by the authors.

Supplementary Figures

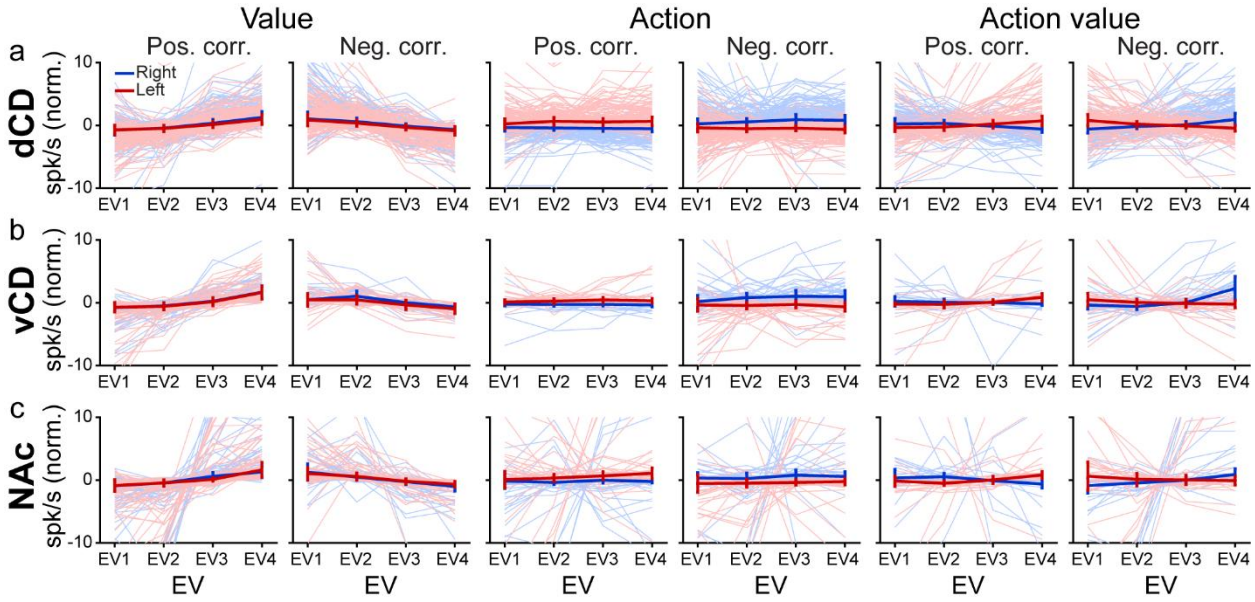

Supplementary Figure 1. Striatal tuning curves. a,c, Firing rates as a function of the expected value (EV) of the best option (EV1-EV4) in dCD (a), vCD (b), and NAc (c), shown separately depending on whether the best option was on the right (blue) or left (red). Panels are organized by neuronal type: value (left), action (middle), and action value (right). For each type, left subpanels show neurons positively correlated with EV and right subpanels show neurons negatively correlated with EV. For each neuron, firing rates were averaged across time bins with significant encoding during the decision period for each EV × position condition, and normalized across conditions by mean subtraction. Dark curves indicate the median ± MAD across units; light traces show individual unit activities.

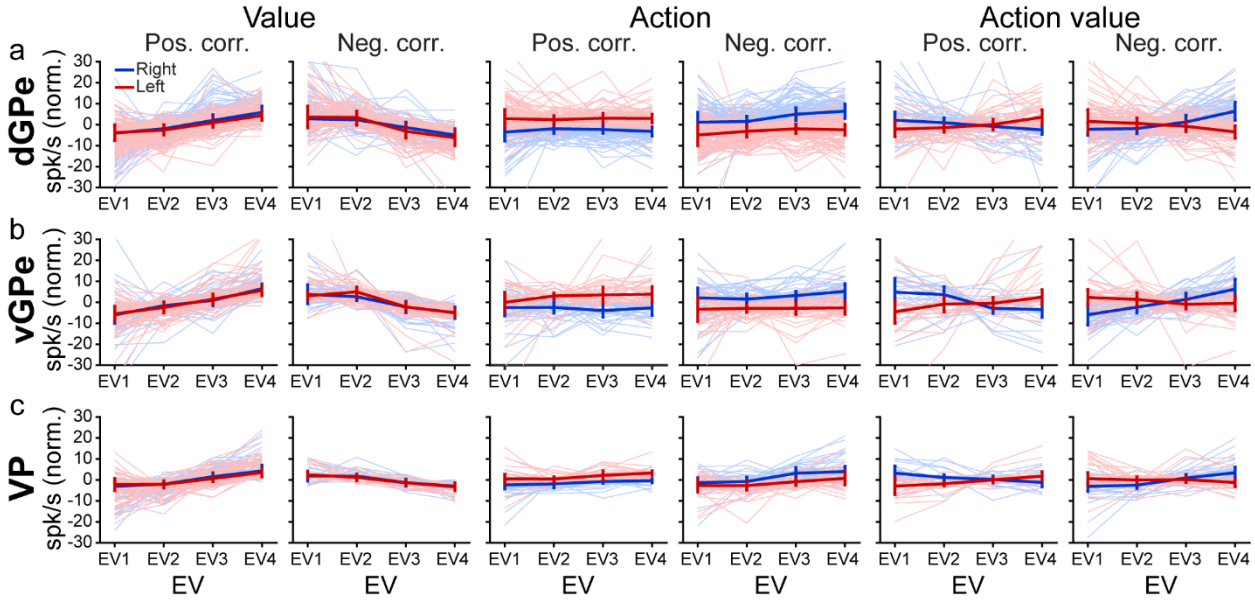

Supplementary Figure 2. Pallidal tuning curves. Same conventions as in Supplementary Figure 1, for dGPe (a), vGPe (b), and VP (c).

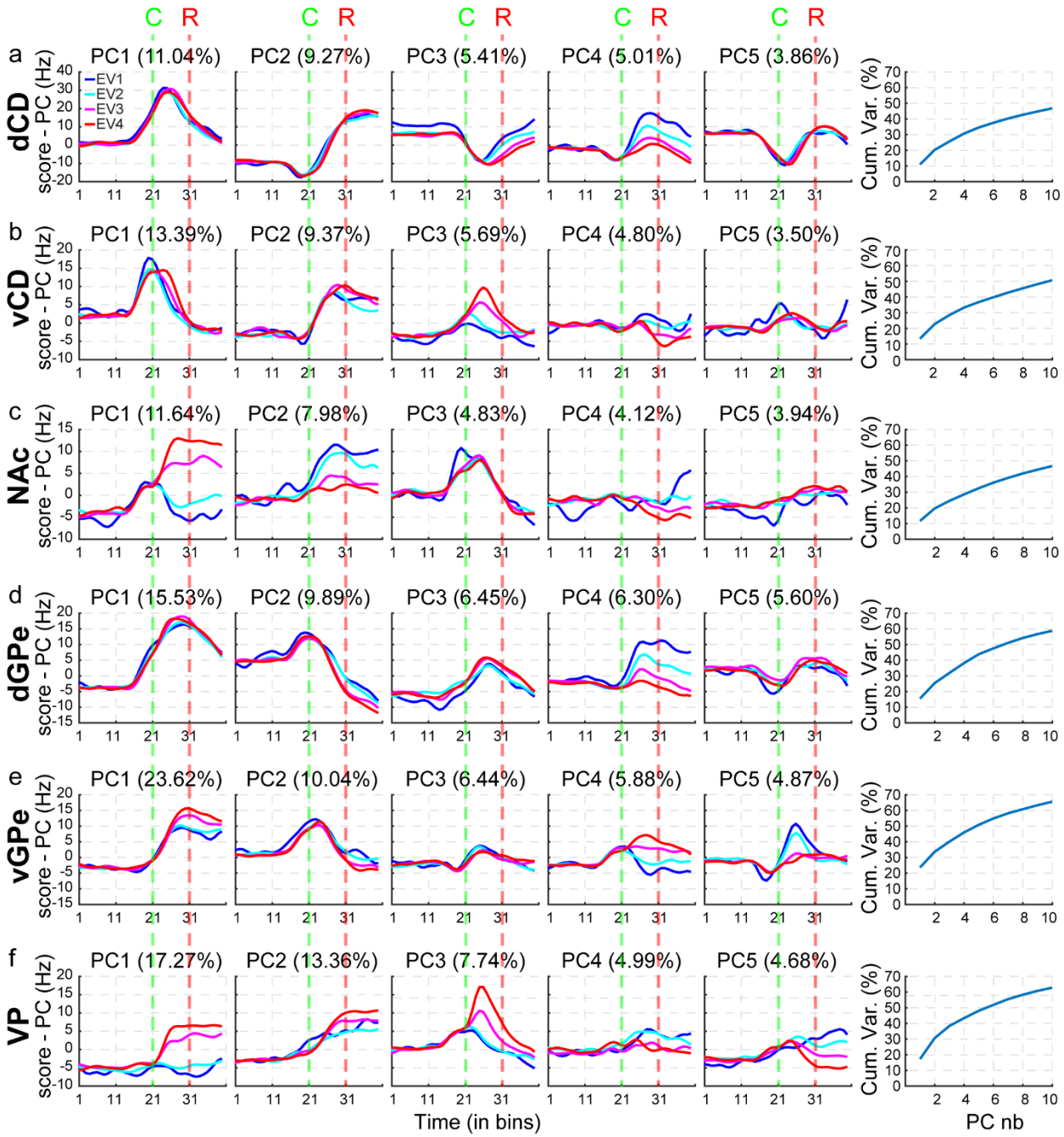

Supplementary Figure 3. Principal component analysis of value-related population activity. Principal component analysis (PCA) of trial-averaged population activity used to construct neuronal trajectories in Figure 4-4. **a-f**, Time courses of the scores for PC1-PC5 and cumulative percentage of variance explained by the first 10 PCs in dCD (a), vCD (b), NAc (c), dGPe (d), vGPe (e), and VP (f). Colors indicate EV levels: EV1 (blue), EV2 (cyan), EV3 (magenta), and EV4 (red). Green and red vertical dashed lines indicate cue onset (C) and joystick release (R), respectively.

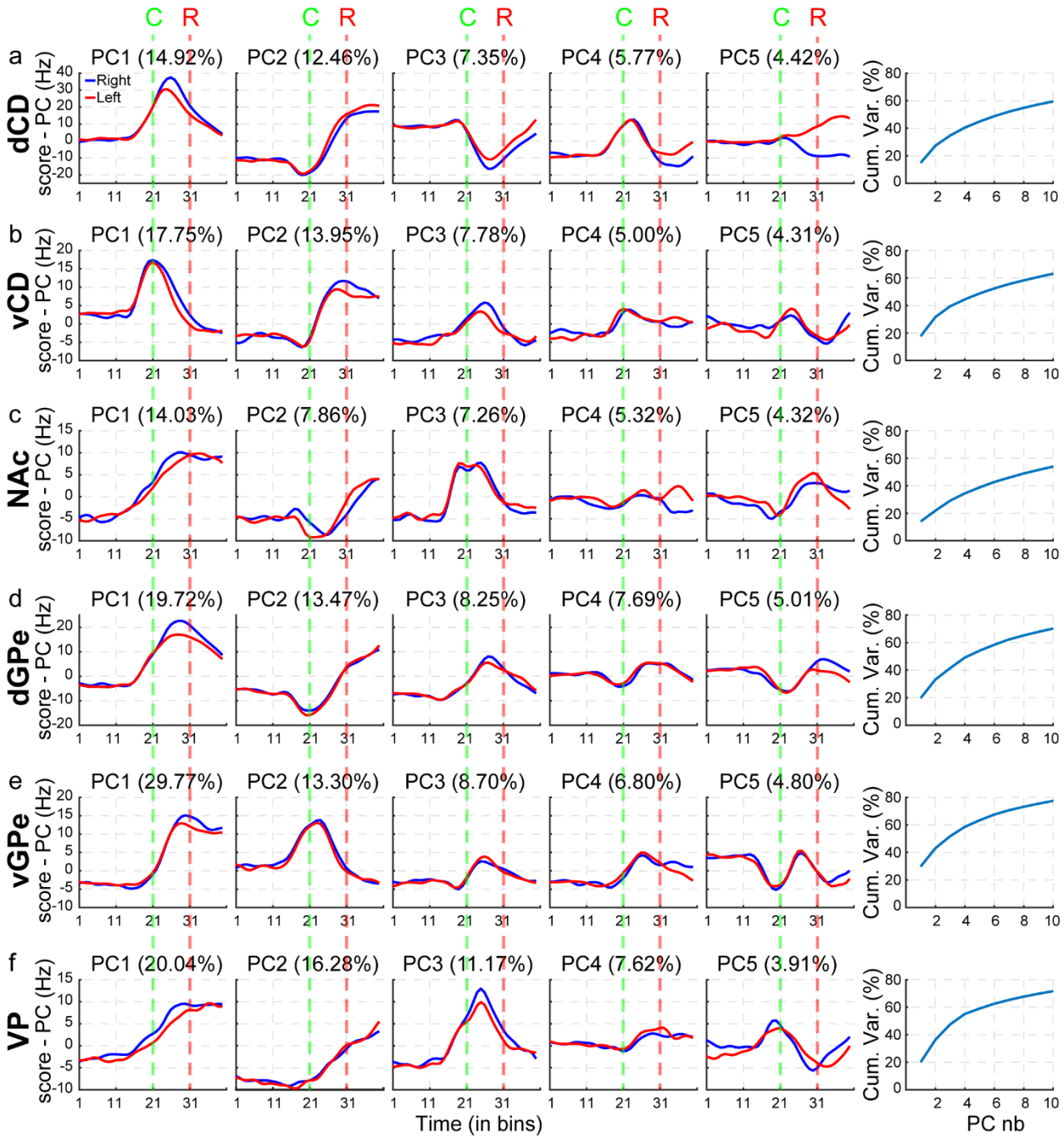

Supplementary Figure 4. Principal component analysis of position-related population activity. Same conventions as in Supplementary Figure 3, except that colors indicate spatial position: Right (blue) and Left (red).

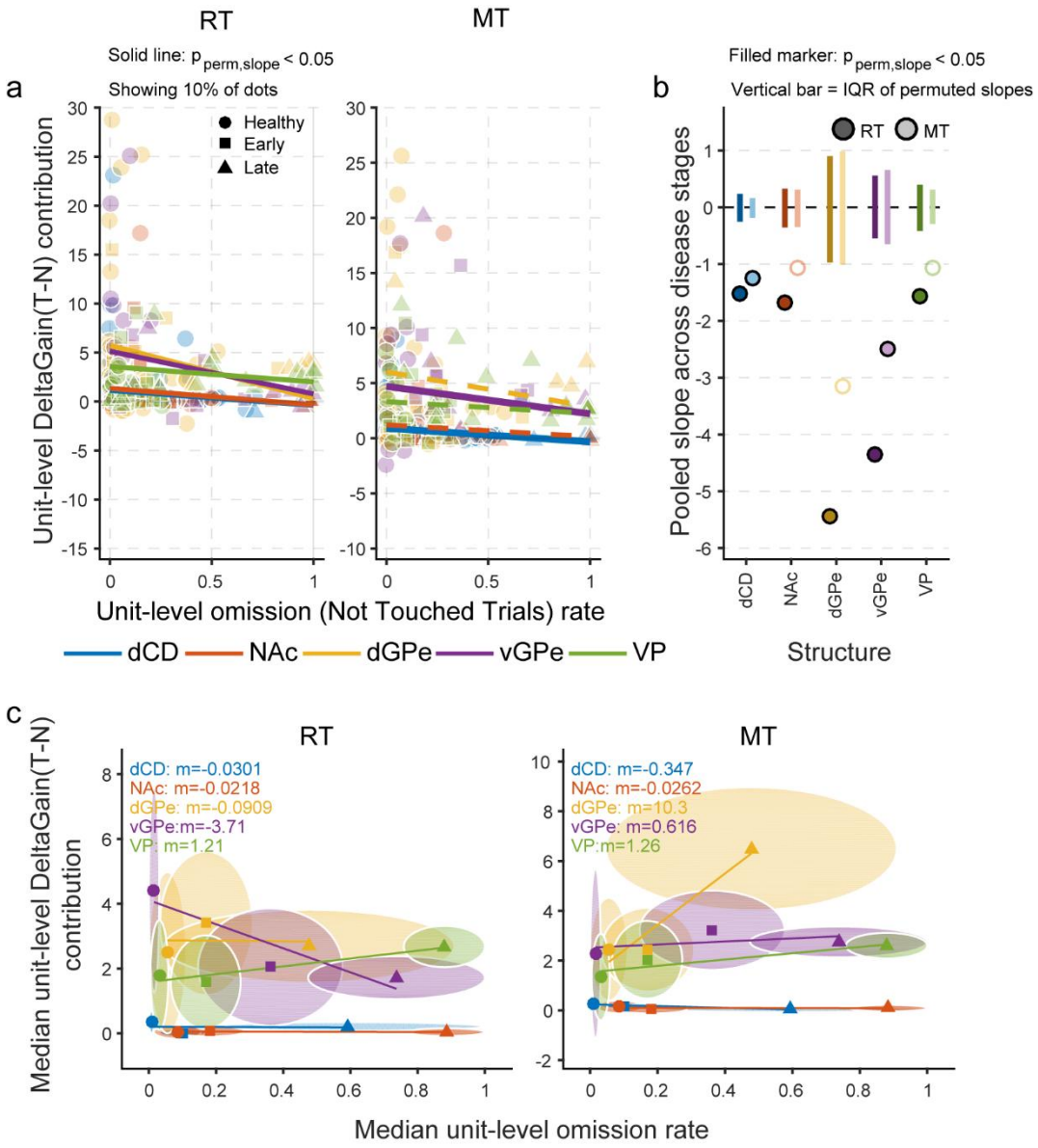

Supplementary Figure 5. Unit-level coupling between neuronal gain and task engagement across structures. a, Relationship between task engagement and ΔGain(T-N) contribution at the unit level during RT (left) and MT (right). Unit-specific omission rate (computed across trials for each recorded unit) was plotted against unit-level ΔGain(T-N) contribution, with data pooled across disease stages and each point representing paired values from the same unit. ΔGain(T-N) was computed relative to the median gain of the opposite trial type (touched: gT−mN; not-touched: mT−gN). Regression lines were fitted using the full pooled dataset for each structure, whereas only a random subset of points is shown for visualization. Marker shape denotes disease stage (Healthy, circle; early MPTP, square; late MPTP, triangle), and color denotes structure (dCD, NAc, dGPe, vGPe and VP). Solid lines indicate significant slopes and dashed lines indicate non-significant slopes. **b,** Summary of regression slopes across structures. For each structure, slopes from the RT and MT relationships (shown in a) are plotted separately. RT and MT are shown as darker and lighter shades of the same structure color. Vertical bars indicate the IQR of the permuted slope distribution, and the dashed horizontal line marks zero. Filled markers indicate significant slopes. **c,** Relationship between omission rate and ΔGain(T-N) contribution across structures. Same conventions as in Figure 4-9c, except that the median omission rate was computed from sessions containing the recorded units, rather than across all sessions.

Part 5 General conclusion

The present work aimed to characterize how value and action representations are organized and integrated across the dorsoventral BG network during value-based DM, and how this organization is reshaped following DA depletion. By combining electrophysiological recordings with behavioral analyses in the same animals before and after induction of a parkinsonian state, this study provides novel insights into the circuit-level computations underlying DM in both healthy and pathological conditions.

By explicitly dissociating value, action, and their interaction while minimizing collinearity between predictors, our results reveal a clear functional organization of decision variables along the dorsoventral axis of the BG. Ventral regions preferentially encode value-related information, with dynamics reflecting both the EV and valence of available options, whereas dorsal regions primarily represent action-related variables such as their spatial position. At the single-neuron level, value encoding is enhanced at the loss-gain transition in most structures, suggesting that value encoding is non-linear, depends on the context of the choice and could account for both EV and outcome valence. At the population level, neural trajectories show stronger separation between EVs at this transition, particularly in ventral BG regions, including NAc and VP. This indicates that valence-related modulation is especially prominent in ventral circuits and largely emerges in a distributed manner across neuronal populations. Together, these findings suggest that value representations in ventral BG circuit are shaped by both value and outcome valence, and may relate to the motivational significance of available options. Importantly, while selective neurons encoding value and action are present, population-level analyses indicate that these signals are not confined to specialized units but are also represented in distributed neural dynamics. Surprisingly, it appears that action value-related signals, represented in similar proportions along the dorsoventral axis, were less prominent than value or action signals, challenging classical models that emphasize action-value coding in BG circuits. Still, given their hypothesized role in guiding behavior toward higher-value actions and the distributed encoding of decision parameters, action value signals may be more effectively captured at the population level. Future work integrating value and action variables within a unified population dynamics framework will be essential to determine how these signals interact to guide behavior and reveal the degree of implication of each structure in the decision process over time. Extending these analyses across structures, including cortical areas such as OFC, ACC, dlPFC, and premotor cortex, as well as subcortical regions such as the STN and amygdala, will be critical to capture the full spatiotemporal dynamics of DM and assess the contribution of each structure in the process.

Most importantly, our results clarify how dopaminergic depletion reshapes these computations in the parkinsonian state. Contrary to the view that DA depletion notably impairs value-related signals, we show that value representations are not abolished but selectively reduced within the NAc, while remaining present in downstream structures such as the VP. Behaviorally, animals retain the ability to choose optimally when engaged, indicating that value information remains functionally available. These findings indicate that DM deficits in the parkinsonian state do not primarily result from an inability to represent or compare value. Instead, dopaminergic depletion

profoundly alters engagement, motivational invigoration, and motor motivation. This is evidenced by increased omission rates, prolonged RTs and MTs, and a loss of gain-loss asymmetry. At the neuronal level, these behavioral impairments are associated with a shift of the network toward a disengaged, low-gain regime, despite the persistence of distinct engaged and disengaged neural states. This suggests that DA depletion characterized in PD does not eliminate task-relevant representations, but may bias the system toward states that are less likely to generate action. In this framework, DM deficits may arise not from a failure to compute value, but from an impaired ability to recruit and translate value signals into motivated behavior. Additional population dynamics analyses following dopaminergic depletion will be essential to determine how the integration of decision variables is disrupted at the network level, and how action value representations emerge (or fail to emerge) within population activity. In addition, the origin and regulation of these low-gain states remain to be elucidated. The potential contribution of other neuromodulatory systems, such as serotonin, in regulating engagement and neural gain also represents an important avenue for future research.

Mechanistically, our findings support the idea that DA plays a critical role in enabling the propagation and effective use of ventral value signals within the BG network. In line with the striato-nigro-striatal ascending spiral organization, weakened value encoding in the VS may reduce the influence of motivational signals on dorsal circuits involved in action initiation and vigor. At the same time, our results also challenge a strictly serial model in which value is computed in the NAc and passively relayed to VP, and instead suggest that the VP can contribute independently to value computation within ventral BG circuits. However, how these computations are implemented with BG circuits remains to be determined. Future studies combining electrophysiology with pathway-specific manipulations (e.g., opto and/or chemogenetic stimulation or inactivation) will be necessary to test how activity in the VS influences dorsal BG circuits during DM and to identify the sources of value-related signals in the VP, which may arise independently of striatal and dopaminergic inputs.

Taken together, this work provides a unified framework in which value-based DM is implemented through distributed and interacting representations across the dorsoventral CBG network. Within this framework, dopamine depletion primarily affects motivation and task engagement through shifts in global neural states and the selective vulnerability of ventral striatal circuits, while pallidal populations may help sustain accurate decision performance by maintaining representations of task-relevant decision variables. By bridging circuit-level physiology with behavioral impairments within the same subjects, these findings offer new insights into the neuronal basis of DM in both healthy and pathological states. Importantly, they highlight motivational and engagement-related processes as key contributors to DM deficits in PD, suggesting that therapeutic approaches targeting these processes, beyond motor function alone, may improve patient outcomes. Future work should investigate whether low-gain neural states can serve as biomarkers of motivational deficits in PD and guide the optimization of dopaminergic and neuromodulatory treatments.

References

Aarsland, D., Larsen, J.P., Lim, N.G., Janvin, C., Karlsen, K., Tandberg, E., & Cummings, J.L. (1999) Range of neuropsychiatric disturbances in patients with Parkinson's disease. *Journal of Neurology, Neurosurgery & Psychiatry*, **67**, 492–496.

Abdi, A., Mallet, N., Mohamed, F.Y., Sharott, A., Dodson, P.D., Nakamura, K.C., Suri, S., Avery, S.V., Larvin, J.T., Garas, F.N., Garas, S.N., Vinciati, F., Morin, S., Bezard, E., Baufreton, J., & Magill, P.J. (2015) Prototypic and arkypallidal neurons in the dopamine-intact external globus pallidus. *The Journal of Neuroscience*, **35**, 6667–6688.

Adler, A., Finkes, I., Katabi, S., Prut, Y., & Bergman, H. (2013) Encoding by Synchronization in the Primate Striatum. *The Journal of Neuroscience*, **33**, 4854–4866.

Adler, A., Katabi, S., Finkes, I., Israel, Z., Prut, Y., & Bergman, H. (2012) Temporal convergence of dynamic cell assemblies in the striato-pallidal network. *The Journal of Neuroscience*, **32**, 2473–2484.

Adler, A., Katabi, S., Finkes, I., Prut, Y., & Bergman, H. (2013) Different correlation patterns of cholinergic and GABAergic interneurons with striatal projection neurons. *Frontiers in Systems Neuroscience*, **7**, 47.

Afsharpour, S. (1985) Topographical projections of the cerebral cortex to the subthalamic nucleus. *The Journal of Comparative Neurology*, **236**, 14–28.

Aizman, O., Brismar, H., Uhlén, P., Zettergren, E., Levey, A.I., Forssberg, H., Greengard, P., & Aperia, A. (2000) Anatomical and physiological evidence for D1 and D2 dopamine receptor colocalization in neostriatal neurons. *Nature Neuroscience*, **3**, 226–230.

Albin, R.L., Young, A.B., & Penney, J.B. (1989) The functional anatomy of basal ganglia disorders. *Trends in Neurosciences*, **12**, 366–375.

Alegre-Cortés, J., Sáez, M., Montanari, R., & Reig, R. (2021) Medium spiny neurons activity reveals the discrete segregation of mouse dorsal striatum. *eLife*, **10**, e60580.

Alexander, G.E. & Crutcher, M.D. (1990) Functional architecture of basal ganglia circuits: neural substrates of parallel processing. *Trends in Neurosciences*, **13**, 266–271.

Alexander, G.E. & DeLong, M.R. (1985a) Microstimulation of the primate neostriatum. I. Physiological properties of striatal microexcitable zones. *Journal of Neurophysiology*, **53**, 1401–1416.

Alexander, G.E. & DeLong, M.R. (1985b) Microstimulation of the primate neostriatum. II. Somatotopic organization of striatal microexcitable zones and their relation to neuronal response properties. *Journal of Neurophysiology*, **53**, 1417–1430.

Alexander, G.E., DeLong, M.R., & Strick, P.L. (1986) Parallel Organization of Functionally Segregated Circuits Linking Basal Ganglia and Cortex. *Annual Review Neuroscience*, **9**, 357–381.

Allain, P. (2013) La prise de décision : aspects théoriques, neuro-anatomie et évaluation: *Revue de neuropsychologie*, **5**, 69–81.

Allais, M. (1953) Le Comportement de l'Homme Rationnel devant le Risque: Critique des Postulats et Axiomes de l'Ecole Americaine. *Econometrica*, **21**, 503–546.

Andén, N.-E., Carlsson, A., Dahlström, A., Fuxe, K., Hillarp, N.A., & Larsson, K. (1964) Demonstration and mapping out of nigro-neostriatal dopamine neurons. *Life Sciences*, **3**, 523–530.

Andén, N.-E., Fuxe, K., Hamberoer, B., & Hökfelt, T. (1966) A Quantitative Study on the Nigro-Neostriatal Dopamine Neuron System in the Rat. *Acta Physiologica Scandinavica*, **67**, 306–312.

Aosaki, T., Graybiel, A.M., & Kimura, M. (1994) Effect of the Nigrostriatal Dopamine System on Acquired Neural Responses in the Striatum of Behaving Monkeys. *Science*, **265**, 412–415.

Apicella, P. (2002) Tonically active neurons in the primate striatum and their role in the processing of information about motivationally relevant events. *European Journal of Neuroscience*, **16**, 2017–2026.

Apicella, P. (2007) Leading tonically active neurons of the striatum from reward detection to context recognition. *Trends in Neurosciences*, **30**, 299–306.

Apicella, P., Legallet, E., & Trouche, E. (1997) Responses of tonically discharging neurons in the monkey striatum to primary rewards delivered during different behavioral states: *Experimental Brain Research*, **116**, 456–466.

Apicella, P., Ljungberg, T., Scarnati, E., & Schultz, W. (1991) Responses to reward in monkey dorsal and ventral striatum. *Experimental Brain Research*, **85**, 491–500.

Apicella, P., Scarnati, E., & Schultz, W. (1991) Tonically discharging neurons of monkey striatum respond to preparatory and rewarding stimuli. *Experimental Brain Research*, **84**, 673–675.

Arkadir, D., Morris, G., Vaadia, E., & Bergman, H. (2004) Independent coding of movement direction and reward prediction by single pallidal neurons. *The Journal of Neuroscience*, **24**, 10047–10056.

Arluison, M., Agid, Y., & Javoy, F. (1978) Dopaminergic nerve endings in the neostriatum of the rat--1. Identification by intracerebral injections of 5-hydroxydopamine. *Neuroscience*, **3**, 657–673.

Aron, A.R., Behrens, T.E., Smith, S., Frank, M.J., & Poldrack, R.A. (2007) Triangulating a cognitive control network using diffusion-weighted magnetic resonance imaging (MRI) and functional MRI. *The Journal of Neuroscience*, **27**, 3743–3752.

Asaad, W.F. & Sheth, S.A. (2024) What's the n? On sample size vs. subject number for brain-behavior neurophysiology and neuromodulation. *Neuron*, **112**, 2086–2090.

Badre, D. (2008) Cognitive control, hierarchy, and the rostro–caudal organization of the frontal lobes. *Trends in Cognitive Sciences*, **12**, 193–200.

Baggio, H.C., Segura, B., Garrido-Millan, J.L., Marti, M., Compta, Y., Valldeoriola, F., Tolosa, E., & Junque, C. (2015) Resting-state frontostriatal functional connectivity in Parkinson's disease–related apathy. *Movement Disorders*, **30**, 671–679.

Baker, S.C., Rogers, R.D., Owen, A.M., Frith, C.D., Dolan, R.J., Frackowiak, R.S.J., & Robbins, T.W. (1996) Neural systems engaged by planning: a PET study of the Tower of London task. *Neuropsychologia*, **34**, 515–526.

Balewski, Z.Z., Elston, T.W., Knudsen, E.B., & Wallis, J.D. (2023) Value dynamics affect choice preparation during decision-making. *Nature Neuroscience*, **26**, 1575–1583.

Balewski, Z.Z., Knudsen, E.B., & Wallis, J.D. (2022) Fast and slow contributions to decision-making in corticostriatal circuits. *Neuron*, **110**, 2170-2182.e4.

Balleine, B.W., Delgado, M.R., & Hikosaka, O. (2007) The role of the dorsal striatum in reward and decision-making. *The Journal of Neuroscience*, **27**, 8161–8165.

Balleine, B.W. & O'Doherty, J.P. (2010) Human and rodent homologies in action control: corticostriatal determinants of goal-directed and habitual action. *Neuropsychopharmacol*, **35**, 48–69.

Ballesta, S., Shi, W., Conen, K.E., & Padoa-Schioppa, C. (2020) Values encoded in orbitofrontal cortex are causally related to economic choices. *Nature*, **588**, 450–453.

Bar-Gad, I., Morris, G., & Bergman, H. (2003) Information processing, dimensionality reduction and reinforcement learning in the basal ganglia. *Progress in Neurobiology*, **71**, 439–473.

Baunez, C. & Robbins, T.W. (1997) Bilateral lesions of the subthalamic nucleus induce multiple deficits in an attentional task in rats. *European Journal of Neuroscience*, **9**, 2086–2099.

Bayer, H.M. & Glimcher, P.W. (2005) Midbrain Dopamine Neurons Encode a Quantitative Reward Prediction Error Signal. *Neuron*, **47**, 129–141.

Bechara, A., Damasio, H., & Damasio, A.R. (2000) Emotion, decision making and the orbitofrontal cortex. *Cerebral Cortex*, **10**, 295–307.

Bechara, A., Damasio, H., Tranel, D., & Anderson, S.W. (1998) Dissociation Of Working Memory from Decision Making within the Human Prefrontal Cortex. *J. Neurosci.*, **18**, 428–437.

Bechara, A., Tranel, D., Damasio, H., & Damasio, A.R. (1996) Failure to Respond Autonomically to Anticipated Future Outcomes Following Damage to Prefrontal Cortex. *Cereb Cortex*, **6**, 215–225.

Beckstead, R.M., Domesick, V.B., & Nauta, W.J.H. (1979) Efferent connections of the substantia nigre and ventral tegmental area in the rat. *Brain Research*, **175**, 191–217.

Benazzouz, A., Boraud, T., Dubédat, P., Boireau, A., Stutzmann, J.-M., & Gross, C. (1995) Riluzole prevents MPTP-induced parkinsonism in the rhesus monkey: a pilot study. *European Journal of Pharmacology*, **284**, 299–307.

Benazzouz, A., Breit, S., Koudsie, A., Pollak, P., Krack, P., & Benabid, A.-L. (2002) Intraoperative microrecordings of the subthalamic nucleus in Parkinson's disease. *Movement Disorders*, **17**, S145–S149.

Benhamou, L., Bronfeld, M., Bar-Gad, I., & Cohen, D. (2012) Globus Pallidus External Segment Neuron Classification in Freely Moving Rats: A Comparison to Primates. *PLOS One*, **7**, e45421.

Benzina, N., Mallet, L., Burguière, E., N'Diaye, K., & Pelissolo, A. (2016) Cognitive Dysfunction in Obsessive-Compulsive Disorder. *Current Psychiatry Reports*, **18**, 80.

Bergman, H., Wichmann, T., & DeLong, M.R. (1990) Reversal of Experimental Parkinsonism by Lesions of the Subthalamic Nucleus. *Science*, **249**, 1436–1438.

Bergstrom, H.C., Lipkin, A.M., Lieberman, A.G., Pinard, C.R., Gunduz-Cinar, O., Brockway, E.T., Taylor, W.W., Nonaka, M., Bukalo, O., Wills, T.A., Rubio, F.J., Li, X., Pickens, C.L., Winder, D.G., & Holmes, A. (2018) Dorsolateral Striatum Engagement Interferes with Early Discrimination Learning. *Cell Reports*, **23**, 2264–2272.

Berke, J.D. (2018) What does dopamine mean? *Nature Neuroscience*, **21**, 787–793.

Bernoulli, D. (1954) Exposition of a New Theory on the Measurement of Risk. *Econometrica*, **22**, 23–36.

Berridge, K.C. (2004) Motivation concepts in behavioral neuroscience. *Physiology & Behavior*, **81**, 179–209.

Berridge, K.C., Venier, I.L., & Robinson, T.E. (1989) Taste Reactivity Analysis of 6-Hydroxydopamine-Induced Aphagia: Implications for Arousal and Anhedonia Hypotheses of Dopamine Function. *Behavioral Neuroscience*, **103**, 36–45.

Bevan, M.D. (2016) The Subthalamic Nucleus. In *Handbook of Behavioral Neuroscience*. Elsevier, pp. 277–291.

Bevan, M.D., Booth, P.A.C., Eaton, S.A., & Bolam, J.P. (1998) Selective Innervation of Neostriatal Interneurons by a Subclass of Neuron in the Globus Pallidus of the Rat. *The Journal of Neuroscience*, **18**, 9438–9452.

Bevan, M.D., Francis, C.M., & Bolam, J.P. (1995) The glutamate-enriched cortical and thalamic input to neurons in the subthalamic nucleus of the rat: Convergence with GABA-positive terminals. *The Journal of Comparative Neurology*, **361**, 491–511.

Bogacz, R. (2007) Optimal decision-making theories: Linking neurobiology with behaviour. *Trends in Cognitive Sciences*, **11**, 118–125.

Bolam, J.P., Hanley, J.J., Booth, P.A.C., & Bevan, M.D. (2000) Synaptic organisation of the basal ganglia. *Journal of Anatomy*, **196**, 527–542.

Bolam, J.P. & Smith, Y. (1992) The striatum and the globus pallidus send convergent synaptic inputs onto single cells in the entopeduncular nucleus of the rat: a double anterograde labelling study combined with postembedding immunocytochemistry for GABA. *The Journal of Comparative Neurology*, **321**, 456–476.

Bonnavion, P., Varin, C., Fakhfouri, G., Martinez Olondo, P., De Groote, A., Cornil, A., Lorenzo Lopez, R., Pozuelo Fernandez, E., Isingrini, E., Rainer, Q., Xu, K., Tzavara, E., Vigneault, E., Dumas, S., De Kerchove d'Exaerde, A., & Giros, B. (2024) Striatal projection neurons coexpressing dopamine D1 and D2 receptors modulate the motor function of D1- and D2-SPNs. *Nature Neuroscience*, **27**, 1783–1793.

Boorman, E.D., Behrens, T.E.J., Woolrich, M.W., & Rushworth, M.F.S. (2009) How Green Is the Grass on the Other Side? Frontopolar Cortex and the Evidence in Favor of Alternative Courses of Action. *Neuron*, **62**, 733–743.

Borgognon, S., Macellari, N., Hickey, A.M., Perich, M.G., Javaheri, H., Ornelas-Kobayashi, R., Delacombaz, M., Hitz, C., Fallegger, F., Lacour, S.P., Bezard, E., Rouiller, E.M., Bloch, J., Milekovic, T., Seáñez, I., & Courtine, G. (2025) Regional specialization of movement encoding across the primate sensorimotor cortex. *Nature Communications*, **16**, 5729.

Botvinick, M., Nystrom, L.E., Fissell, K., Carter, C.S., & Cohen, J.D. (1999) Conflict monitoring versus selection- for-action in anterior cingulate cortex. *Nature*, **402**, 179–181.

Braak, H., Tredici, K.D., Rüb, U., De Vos, R.A.I., Jansen Steur, E.N.H., & Braak, E. (2003) Staging of brain pathology related to sporadic Parkinson's disease. *Neurobiology of Aging*, **24**, 197–211.

Brand, M., Labudda, K., Kalbe, E., Hilker, R., Emmans, D., Fuchs, G., Kessler, J., & Markowitsch, H.J. (2004) Decision-making impairments in patients with Parkinson's disease. *Behavioral Neurology*, **15**, 77–85.

Brittain, J.-S. & Brown, P. (2014) Oscillations and the basal ganglia: Motor control and beyond. *NeuroImage*, **85**, 637–647.

Brown, P. (2003) Oscillatory nature of human basal ganglia activity: Relationship to the pathophysiology of Parkinson's disease. *Movement Disorders*, **18**, 357–363.

Carpenter, M.B., Carleton, S.C., Keller, J.T., & Conte, P. (1981) Connections of the subthalamic nucleus in the monkey. *Brain Research*, **224**, 1–29.

Carpenter, M.B. & Strominger, N.L. (1967) Efferent fibers of the subthalamic nucleus in the monkey. A comparison of the efferent projections of the subthalamic nucleus, substantia nigra and globus pallidus. *The american journal of anatomy*, **121**, 41–72.

Carrillo-Reid, L., Tecuapetla, F., Tapia, D., Hernández-Cruz, A., Galarraga, E., Drucker-Colin, R., & Bargas, J. (2008) Encoding Network States by Striatal Cell Assemblies. *Journal of Neurophysiology*, **99**, 1435–1450.

Carter, D.A. & Fibiger, H.C. (1978) The projections of the entopeduncular nucleus and globus pallidus in rat as demonstrated by autoradiography and horseradish peroxidase histochemistry. *The Journal of Comparative Neurology*, **177**, 113–123.

Cepeda, C., Buchwald, N.A., & Levine, M.S. (1993) Neuromodulatory actions of dopamine in the neostriatum are dependent upon the excitatory amino acid receptor subtypes activated. *Proc. Natl. Acad. Sci. U.S.A.*, **90**, 9576–9580.

Chib, V.S., Rangel, A., Shimojo, S., & O'Doherty, J.P. (2009) Evidence for a Common Representation of Decision Values for Dissimilar Goods in Human Ventromedial Prefrontal Cortex. *The Journal of Neuroscience*, **29**, 12315–12320.

Chong, T.T.-J., Bonnelle, V., Manohar, S., Veromann, K.-R., Muhammed, K., Tofaris, G.K., Hu, M., & Husain, M. (2015) Dopamine enhances willingness to exert effort for reward in Parkinson's disease. *Cortex*, **69**, 40–46.

Cisek, P. (2012) Making decisions through a distributed consensus. *Current Opinion in Neurobiology*, **22**, 927–936.

Cisek, P. & Pastor-Bernier, A. (2014) On the challenges and mechanisms of embodied decisions. *Philos Trans R Soc Lond B Biol Sci*, **369**, 20130479.

Clavier, R.M., Atmadja, S., & Fibiger, H.C. (1976) Nigrothalamic projections in the rat as demonstrated by orthograde and retrograde tracing techniques. *Brain Research Bulletin*, **1**, 379–384.

Cohen, J. (1988) *Statistical Power Analysis for the Behavioral Sciences*, 2nd ed. edn. L. Erlbaum Associates, Hillsdale, N.J.

Cohen, J.D., Perlstein, W.M., Braver, T.S., Nystrom, L.E., Noll, D.C., Jonides, J., & Smith, E.E. (1997) Temporal dynamics of brain activation during a working memory task. *Nature*, **386**, 604–608.

Cohen, J.Y., Amoroso, M.W., & Uchida, N. (2015) Serotonergic neurons signal reward and punishment on multiple timescales. *eLife*, **4**, e06346.

Corbit, L.H. (2018) Understanding the balance between goal-directed and habitual behavioral control. *Current Opinion in Behavioral Sciences*, **20**, 161–168.

Corbit, L.H., Muir, J.L., & Balleine, B.W. (2001) The Role of the Nucleus Accumbens in Instrumental Conditioning: Evidence of a Functional Dissociation between Accumbens Core and Shell. *The Journal of Neuroscience*, **21**, 3251–3260.

Cospito, J.A. & Kultas-Ilinsky, K. (1981) Synaptic organization of motor corticostriatal projections in the rat. *Experimental Neurology*, **72**, 257–266.

Costa, K.M., Shimbo, A., Stalnaker, T., Raheja, N., Mirani, J., Sercander, C., & Schoenbaum, G. (2025) Striatal dopamine signals errors in prediction across different informational domains. *Science Advances*, **11**, eadq9684.

Coudé, D., Parent, A., & Parent, M. (2018) Single-axon tracing of the corticosubthalamic hyperdirect pathway in primates. *Brain Structure and Function*, **223**, 3959–3973.

Courtemanche, R., Fujii, N., & Graybiel, A.M. (2003) Synchronous, Focally Modulated beta-Band Oscillations Characterize Local Field Potential Activity in the Striatum of Awake Behaving Monkeys. *The Journal of Neuroscience*, **23**, 11741–11752.

Cousins, M.S. & Salamone, J.D. (1994) Nucleus accumbens dopamine depletions in rats affect relative response allocation in a novel cost/benefit procedure. *Pharmacology Biochemistry and Behavior*, **49**, 85–91.

Cromwell, H.C. & Schultz, W. (2003) Effects of Expectations for Different Reward Magnitudes on Neuronal Activity in Primate Striatum. *Journal of Neurophysiology*, **89**, 2823–2838.

Crutcher, M.D. & DeLong, M.R. (1984) Single cell studies of the primate putamen. I. Functional organization. *Experimental Brain Research*, **53**, 233–243.

Cui, G., Jun, S.B., Jin, X., Pham, M.D., Vogel, S.S., Lovinger, D.M., & Costa, R.M. (2013) Concurrent activation of striatal direct and indirect pathways during action initiation. *Nature*, **494**, 238–242.

Cui, Q., Pamukcu, A., Cherian, S., Chang, I.Y.M., Berceau, B.L., Xenias, H.S., Higgs, M.H., Rajamanickam, S., Chen, Y., Du, X., Zhang, Y., McMorrow, H., Abecassis, Z.A., Boca, S.M., Justice, N.J., Wilson, C.J., & Chan, C.S. (2021) Dissociable Roles of Pallidal Neuron Subtypes in Regulating Motor Patterns. *The Journal of Neuroscience*, **41**, 4036–4059.

Curtis, C.E. & Lee, D. (2010) Beyond working memory: the role of persistent activity in decision making. *Trends in Cognitive Sciences*, **14**, 216–222.

Czubayko, U. & Plenz, D. (2002) Fast synaptic transmission between striatal spiny projection neurons. *Proc. Natl. Acad. Sci. U.S.A.*, **99**, 15764–15769.

Damiani, L., Albares, M., Laviron, P., Le Douget, J., Boulinguez, P., Karachi, C., Welter, M., Munuera, J., & Lau, B. (2025) Subthalamic Activity Is Associated With Proactive Inhibition in Parkinson's Disease Patients. *European Journal of Neuroscience*, **61**, e70055.

Darbaky, Y., Baunez, C., Arecchi, P., Legallet, E., & Apicella, P. (2005) Reward-related neuronal activity in the subthalamic nucleus of the monkey. *Neuroreport*, **16**, 1241–1244.

Daw, N.D., Niv, Y., & Dayan, P. (2005) Uncertainty-based competition between prefrontal and dorsolateral striatal systems for behavioral control. *Nature Neuroscience*, **8**, 1704–1711.

De Martino, B., Kumaran, D., Holt, B., & Dolan, R.J. (2009) The Neurobiology of Reference-Dependent Value Computation. *The Journal of Neuroscience*, **29**, 3833–3842.

Deffains, M. & Bergman, H. (2015) Striatal cholinergic interneurons and cortico-striatal synaptic plasticity in health and disease. *Movement Disorders*, **30**, 1014–1025.

Deffains, M., Canron, M., Teil, M., Li, Q., Dehay, B., Bezard, E., & Fernagut, P. (2021) L-DOPA regulates α-synuclein accumulation in experimental parkinsonism. *Neuropathology Appl Neurobio*, **47**, 532–543.

Deffains, M., Iskhakova, L., Katabi, S., Haber, S.N., Israel, Z., & Bergman, H. (2016) Subthalamic, not striatal, activity correlates with basal ganglia downstream activity in normal and parkinsonian monkeys. *eLife*, **5**, e16443.

Deffains, M., Iskhakova, L., Katabi, S., Israel, Z., & Bergman, H. (2018) Longer β oscillatory episodes reliably identify pathological subthalamic activity in Parkinsonism. *Movement Disorders*, **33**, 1609–1618.

Del Rey, N.L., Trigo-Damas, I., Obeso, J.A., Cavada, C., & Blesa, J. (2022) Neuron types in the primate striatum: Stereological analysis of projection neurons and interneurons in control and parkinsonian monkeys. *Neuropathology and Applied Neurobiology*, **48**, e12812.

DeLong, M.R. (1971) Activity of pallidal neurons during movement. *Journal of Neurophysiology*, **34**, 414–427.

DeLong, M.R., Crutcher, M.D., & Georgopoulos, A.P. (1985) Primate globus pallidus and subthalamic nucleus: functional organization. *Journal of Neurophysiology*, **53**, 530–543.

Denny-Brown, D. (1946) *Diseases of the Basal Ganglia and Subthalamic Nuclei*. Oxford University Press.

Derosiere, G., Shokur, S., & Vassiliadis, P. (2025) Reward signals in the motor cortex: from biology to neurotechnology. *Nature Communications*, **16**, 1307.

Difiglia, M., Pasik, P., & Pasik, T. (1982) A Golgi and ultrastructural study of the monkey globus pallidus. *The Journal of Comparative Neurology*, **212**, 53–75.

Divac, I., Rosvold, H.E., & Szwarcbart, M.K. (1967) Behavioral effects of selective ablation of the caudate nucleus. *Journal of Comparative and Physiological Psychology*, **63**, 184–190.

Donoghue, J.P. & Herkenham, M. (1986) Neostriatal projections from individual cortical fields conform to histochemically distinct striatal compartments in the rat. *Brain Research*, **365**, 397–403.

Dotson, N.M., Hoffman, S.J., Goodell, B., & Gray, C.M. (2017) A Large-Scale Semi-Chronic Microdrive Recording System for Non-Human Primates. *Neuron*, **96**, 769-782.e2.

Draganski, B., Kherif, F., Klöppel, S., Cook, P.A., Alexander, D.C., Parker, G.J.M., Deichmann, R., Ashburner, J., & Frackowiak, R.S.J. (2008) Evidence for Segregated and Integrative Connectivity Patterns in the Human Basal Ganglia. *The Journal of Neuroscience*, **28**, 7143–7152.

Driscoll, M.E., Bollu, P.C., & Tadi, P. (2023) Neuroanatomy, Nucleus Caudate. In *StatPearls*. StatPearls Publishing, Treasure Island (FL).

Dunovan, K. & Verstynen, T. (2016) Believer-Skeptic Meets Actor-Critic: Rethinking the Role of Basal Ganglia Pathways during Decision-Making and Reinforcement Learning. *Frontiers in Neuroscience*, **10**, 106.

Ebitz, R.B. & Hayden, B.Y. (2021) The population doctrine in cognitive neuroscience. *Neuron*, **109**, 3055–3068.

Eblen, F. & Graybiel, A. (1995) Highly restricted origin of prefrontal cortical inputs to striosomes in the macaque monkey. *The Journal of Neuroscience*, **15**, 5999–6013.

Elber-Dorozko, L. & Loewenstein, Y. (2018) Striatal action-value neurons reconsidered. *eLife*, **7**, e34248.

Elias, S., Joshua, M., Goldberg, J.A., Heimer, G., Arkadir, D., Morris, G., & Bergman, H. (2007) Statistical Properties of Pauses of the High-Frequency Discharge Neurons in the External Segment of the Globus Pallidus. *The Journal of Neuroscience*, **27**, 2525–2538.

Emborg, M.E. (2007) Nonhuman Primate Models of Parkinson's Disease. *ILAR Journal*, **48**, 339–355.

Emborg, M.E. (2017) Nonhuman Primate Models of Neurodegenerative Disorders. *ILAR Journal*, **58**, 190–201.

Engel, A.K. & Fries, P. (2010) Beta-band oscillations — signalling the status quo? *Current Opinion in Neurobiology*, **20**, 156–165.

Ernst, M. & Paulus, M.P. (2005) Neurobiology of decision making: a selective review from a neurocognitive and clinical perspective. *Biological Psychiatry*, **58**, 597–604.

Espinosa-Parrilla, J., Baunez, C., & Apicella, P. (2013) Linking reward processing to behavioral output: motor and motivational integration in the primate subthalamic nucleus. *Frontiers in Computational Neuroscience*, **7**, 175.

Espinosa-Parrilla, J., Baunez, C., & Apicella, P. (2015) Modulation of neuronal activity by reward identity in the monkey subthalamic nucleus. *European Journal of Neuroscience*, **42**, 1705–1717.

Faget, L., Zell, V., Souter, E., McPherson, A., Ressler, R., Gutierrez-Reed, N., Yoo, J.H., Dulcis, D., & Hnasko, T.S. (2018) Opponent control of behavioral reinforcement by inhibitory and excitatory projections from the ventral pallidum. *Nature Communications*, **9**, 849.

Farrell, K., Lak, A., & Saleem, A.B. (2022) Midbrain dopamine neurons signal phasic and ramping reward prediction error during goal-directed navigation. *Cell Reports*, **41**, 111470.

Farrell, M.R., Esteban, J.S.D., Faget, L., Floresco, S.B., Hnasko, T.S., & Mahler, S.V. (2021) Ventral Pallidum GABA Neurons Mediate Motivation Underlying Risky Choice. *The Journal of Neuroscience*, **41**, 4500–4513.

Farries, M.A., Faust, T.W., Mohebi, A., & Berke, J.D. (2023) Selective encoding of reward predictions and prediction errors by globus pallidus subpopulations. *Current Biology*, **33**, 4124-4135.e5.

Féger, J., Bevan, M., & Crossman, A.R. (1994) The projections from the parafascicular thalamic nucleus to the subthalamic nucleus and the striatum arise from separate neuronal populations: A comparison with the corticostriatal and corticosubthalamic efferents in a retrograde fluorescent double-labelling study. *Neuroscience*, **60**, 125–132.

Féger, J. & Crossman, A.R. (1984) Identification of different subpopulations of neostriatal neurones projecting to globus pallidus or substantia nigra in the monkey: A retrograde fluorescence double-labelling study. *Neuroscience Letters*, **49**, 7–12.

Feingold, J., Gibson, D.J., DePasquale, B., & Graybiel, A.M. (2015) Bursts of beta oscillation differentiate postperformance activity in the striatum and motor cortex of monkeys performing movement tasks. *Proc. Natl. Acad. Sci. U.S.A.*, **112**, 13687–13692.

Ferrari-Toniolo, S., Seak, L.C.U., & Schultz, W. (2025) Coding of the basic components of subjective value in primate dopamine neurons: subjectively weighted reward amount and probability. *bioRxiv*,.

Filion, M. & Tremblay, L. (1991) Abnormal spontaneous activity of globus pallidus neurons in monkeys with MPTP-induced parkinsonism. *Brain Research*, **547**, 142–151.

Fiorillo, C.D., Tobler, P.N., & Schultz, W. (2003) Discrete Coding of Reward Probability and Uncertainty by Dopamine Neurons. *Science*, **299**, 1898–1902.

Fitzgerald, N.D. & Day, J.J. (2025) Neuronal heterogeneity in the ventral tegmental area: Distinct contributions to reward circuitry and motivated behavior. *Addiction Neuroscience*, **14**, 100191.

Flaherty, A.W. & Graybiel, A.M. (1993) Output architecture of the primate putamen. *The Journal of Neuroscience*, **13**, 3222–3237.

Flaherty, A.W. & Graybiel, A.M. (1994) Input-output organization of the sensorimotor striatum in the squirrel monkey. *The Journal of Neuroscience*, **14**, 599–610.

Fox, C.A. & Rafols, J.A. (1976) The striatal efferents in the globus pallidus and in the substantia nigra. *Res Publ Assoc Res Nerv Ment Dis*, **55**, 37–55.

François, C., Percheron, G., Yelnik, J., & Tande´, D. (1988) A topographic study of the course of nigral axons and of the distribution of pallidal axonal endings in the centre médian-parafascicular complex of macaques. *Brain Research*, **473**, 181–186.

François, C., Yelnik, J., & Percheron, G. (1987) Golgi study of the primate substantia nigra. II. Spatial organization of dendritic arborizations in relation to the cytoarchitectonic boundaries and to the striatonigral bundle. *Journal of Comparative Neurology*, **265**, 473–493.

Frank, M.J. (2006) Hold your horses: A dynamic computational role for the subthalamic nucleus in decision making. *Neural Networks*, **19**, 1120–1136.

Frank, M.J., Samanta, J., Moustafa, A.A., & Sherman, S.J. (2007) Hold your horses: impulsivity, deep brain stimulation, and medication in parkinsonism. *Science*, **318**, 1309–1312.

Frank, M.J., Seeberger, L.C., & O'Reilly, R.C. (2004) By Carrot or by Stick: Cognitive Reinforcement Learning in Parkinsonism. *Science*, **306**, 1940–1943.

Frederick, S., Loewenstein, G., & O'Donoghue (2002) Time Discounting and Time Preference: A Critical Review. *Journal of Economic Literature*, **40**, 351–401.

Frey, S., Pandya, D.N., Chakravarty, M.M., Bailey, L., Petrides, M., & Collins, D.L. (2011) An MRI based average macaque monkey stereotaxic atlas and space (MNI monkey space). *NeuroImage*, **55**, 1435–1442.

Fries, P. & Maris, E. (2022) What to Do If *N* Is Two? *Journal of Cognitive Neuroscience*, **34**, 1114–1118.

Fujimoto, K. & Kita, H. (1993) Response characteristics of subthalamic neurons to the stimulation of the sensorimotor cortex in the rat. *Brain Research*, **609**, 185–192.

Funahashi, S., Bruce, C., & Goldman-Rakic, P. (1993) Dorsolateral prefrontal lesions and oculomotor delayed-response performance: evidence for mnemonic "scotomas." *The Journal of Neuroscience*, **13**, 1479–1497.

Funahashi, S., Bruce, C.J., & Goldman-Rakic, P.S. (1989) Mnemonic coding of visual space in the monkey's dorsolateral prefrontal cortex. *Journal of Neurophysiology*, **61**, 331–349.

Fusi, S., Miller, E.K., & Rigotti, M. (2016) Why neurons mix: high dimensionality for higher cognition. *Current Opinion in Neurobiology*, **37**, 66–74.

Gaertner, Z., Azcorra, M., Dombeck, D.A., & Awatramani, R. (2022) Molecular heterogeneity in the substantia nigra: A roadmap for understanding PD motor pathophysiology. *Neurobiology of Disease*, **175**, 105925.

Galvan, A., Devergnas, A., & Wichmann, T. (2015) Alterations in neuronal activity in basal ganglia-thalamocortical circuits in the parkinsonian state. *Frontiers in Neuroanatomy*, **9**, 5.

Gatev, P., Darbin, O., & Wichmann, T. (2006) Oscillations in the basal ganglia under normal conditions and in movement disorders. *Movement Disorders*, **21**, 1566–1577.

Georgopoulos, A.P., DeLong, M.R., & Crutcher, M.D. (1983) Relations between parameters of step-tracking movements and single cell discharge in the globus pallidus and subthalamic nucleus of the behaving monkey. *The Journal of Neuroscience*, **3**, 1586–1598.

Gerfen, C.R. (1984) The neostriatal mosaic: compartmentalization of corticostriatal input and striatonigral output systems. *Nature*, **311**, 461–464.

Gerfen, C.R. (1985) The neostriatal mosaic. I. compartmental organization of projections from the striatum to the substantia nigra in the rat. *The Journal of Comparative Neurology*, **236**, 454–476.

Gerfen, C.R., Baimbridge, K.G., & Thibault, J. (1987) The neostriatal mosaic: III. Biochemical and developmental dissociation of patch-matrix mesostriatal systems. *The Journal of Neuroscience*, **7**, 3935–3944.

Gerfen, C.R., Engber, T.M., Mahan, L.C., Susel, Z., Chase, T.N., Monsma, F.J., & Sibley, D.R. (1990) D_1 and D_2 Dopamine Receptor-regulated Gene Expression of Striatonigral and Striatopallidal Neurons. *Science*, **250**, 1429–1432.

Ghandili, M. & Munakomi, S. (2023) Neuroanatomy, Putamen. In *StatPearls*. StatPearls Publishing, Treasure Island (FL).

Gilbertson, T., Lalo, E., Doyle, L., Di Lazzaro, V., Cioni, B., & Brown, P. (2005) Existing Motor State Is Favored at the Expense of New Movement during 13-35 Hz Oscillatory Synchrony in the Human Corticospinal System. *The Journal of Neuroscience*, **25**, 7771–7779.

Giménez-Amaya, J.M. & Graybiel, A.M. (1990) Compartmental origins of the striatopallidal projection in the primate. *Neuroscience*, **34**, 111–126.

Giménez-Amaya, J.M., McFarland, N.R., De Las Heras, S., & Haber, S.N. (1995) Organization of thalamic projections to the ventral striatum in the primate. *Journal of Comparative Neurology*, **354**, 127–149.

Glimcher, P.W., Camerer, C., Fehr, E., & Poldrack, R.A. (2009) Introduction: A Brief History of Neuroeconomics. In *Neuroeconomics*. Elsevier, pp. xvii–xxviii.

Gold, J.I. & Shadlen, M.N. (2007) The Neural Basis of Decision Making. *Annual Review of Neuroscience*, **30**, 535–574.

Goldberg, J.A. & Bergman, H. (2011) Computational physiology of the neural networks of the primate globus pallidus: function and dysfunction. *Neuroscience*, **198**, 171–192.

Goldman, P.S. & Nauta, W.J.H. (1977) An intricately patterned prefronto-caudate projection in the rhesus monkey. *The Journal of Comparative Neurology*, **171**, 369–385.

Goldman-Rakic, P.S. (1995) Cellular basis of working memory. *Neuron*, **14**, 477–485.

Gonon, F. (1997) Prolonged and Extrasynaptic Excitatory Action of Dopamine Mediated by D1 Receptors in the Rat Striatum *In Vivo*. *The Journal of Neuroscience*, **17**, 5972–5978.

Gonzalez, R. & Wu, G. (1999) On the Shape of the Probability Weighting Function. *Cognitive Psychology*, **38**, 129–166.

Graveland, G.A. & Difiglia, M. (1985) The frequency and distribution of medium-sized neurons with indented nuclei in the primate and rodent neostriatum. *Brain Research*, **327**, 307–311.

Graybiel, A.M. (1990) Neurotransmitters and neuromodulators in the basal ganglia. *Trends in Neurosciences*, **13**, 244–254.

Graybiel, A.M., Aosaki, T., Flaherty, A.W., & Kimura, M. (1994) The Basal Ganglia and Adaptive Motor Control. *Science*, **265**, 1826–1831.

Graybiel, A.M., Baughman, R.W., & Eckenstein, F. (1986) Cholinergic neuropil of the striatum observes striosomal boundaries. *Nature*, **323**, 625–627.

Graybiel, A.M. & Matsushima, A. (2023) Striosomes and Matrisomes: Scaffolds for Dynamic Coupling of Volition and Action. *Annual Review of Neuroscience*, **46**, 359–380.

Graybiel, A.M. & Ragsdale, C.W. (1978) Histochemically distinct compartments in the striatum of human, monkeys, and cat demonstrated by acetylthiocholinesterase staining. *Proc. Natl. Acad. Sci. U.S.A.*, **75**, 5723–5726.

Graybiel, A.M., Ragsdale, C.W., Yoneoka, E.S., & Elde, R.P. (1981) An immunohistochemical study of enkephalins and other neuropeptides in the striatum of the cat with evidence that the opiate peptides are arranged to form mosaic patterns in register with the striosomal compartments visible by acetylcholinesterase staining. *Neuroscience*, **6**, 377–397.

Griffiths, B. & Beierholm, U.R. (2017) Opposing effects of reward and punishment on human vigor. *Scientific Reports*, **7**, 42287.

Groenewegen, H.J., Wright, C.I., Beijer, A.V., & Voorn, P. (1999) Convergence and Segregation of Ventral Striatal Inputs and Outputs. *Annals of the New York Academy of Sciences*, **877**, 49–63.

Gurney, K.N., Humphries, M.D., & Redgrave, P. (2015) A New Framework for Cortico-Striatal Plasticity: Behavioural Theory Meets In Vitro Data at the Reinforcement-Action Interface. *PLOS Biology*, **13**, e1002034.

Haber, S.N., Adler, A., & Bergman, H. (2012) The Basal Ganglia. In *The Human Nervous System*. Elsevier, pp. 678–738.

Haber, S.N., Fudge, J.L., & McFarland, N.R. (2000) Striatonigrostriatal Pathways in Primates Form an Ascending Spiral from the Shell to the Dorsolateral Striatum. *The Journal of Neuroscience*, **20**, 2369–2382.

Haber, S.N., Kim, K.-S., Mailly, P., & Calzavara, R. (2006) Reward-Related Cortical Inputs Define a Large Striatal Region in Primates That Interface with Associative Cortical Connections, Providing a Substrate for Incentive-Based Learning. *The Journal of Neuroscience*, **26**, 8368–8376.

Haber, S.N. & Knutson, B. (2010) The Reward Circuit: Linking Primate Anatomy and Human Imaging. *Neuropsychopharmacol*, **35**, 4–26.

Haber, S.N., Lynd, E., Klein, C., & Groenewegen, H.J. (1990) Topographic organization of the ventral striatal efferent projections in the rhesus monkey: An anterograde tracing study. *Journal of Comparative Neurology*, **293**, 282–298.

Haber, S.N. & Nauta, W.J.H. (1983) Ramifications of the globus pallidus in the rat as indicated by patterns of immunohistochemistry. *Neuroscience*, **9**, 245–260.

Hammond, C., Bergman, H., & Brown, P. (2007) Pathological synchronization in Parkinson's disease: networks, models and treatments. *Trends in Neurosciences*, **30**, 357–364.

Hardman, C.D., Henderson, J.M., Finkelstein, D.I., Horne, M.K., Paxinos, G., & Halliday, G.M. (2002) Comparison of the basal ganglia in rats, marmosets, macaques, baboons, and humans: Volume and neuronal number for the output, internal relay, and striatal modulating nuclei. *Journal of Comparative Neurology*, **445**, 238–255.

Harman, P.J. & Carpenter, M.B. (1950) Volumetric comparisons of the basal ganglia of various primates including man. *Journal of Comparative Neurology*, **93**, 125–137.

Härmson, O., Grennan, I., Perry, B., Toth, R., McNamara, C.G., Denison, T., Cagnan, H., Manohar, S.G., Walton, M.E., & Sharott, A. (2025) Multi-level encoding of reward, effort, and choice across the frontal cortex and basal ganglia during cost-benefit decision-making. *Cell Reports*, **44**, 115209.

Hayden, B.Y. & Platt, M.L. (2010) Neurons in Anterior Cingulate Cortex Multiplex Information about Reward and Action. *J. Neurosci.*, **30**, 3339–3346.

Haynes, W.I.A. & Haber, S.N. (2013) The Organization of Prefrontal-Subthalamic Inputs in Primates Provides an Anatomical Substrate for Both Functional Specificity and Integration: Implications for Basal Ganglia Models and Deep Brain Stimulation. *J. Neurosci.*, **33**, 4804–4814.

Hazrati, L.N., Parent, A., Mitchell, S., & Haber, S.N. (1990) Evidence for interconnections between the two segments of the globus pallidus in primates: a PHA-L anterograde tracing study. *Brain Research*, **533**, 171–175.

Heekeren, H.R., Marrett, S., & Ungerleider, L.G. (2008) The neural systems that mediate human perceptual decision making. *Nature Reviews Neuroscience*, **9**, 467–479.

Heimer, G., Bar-Gad, I., Goldberg, J.A., & Bergman, H. (2002) Dopamine Replacement Therapy Reverses Abnormal Synchronization of Pallidal Neurons in the 1-Methyl-4-Phenyl-1,2,3,6-Tetrahydropyridine Primate Model of Parkinsonism. *The Journal of Neuroscience*, **22**, 7850–7855.

Herkenham, M. & Pert, C.B. (1981) Mosaic distribution of opiate receptors, parafascicular projections and acetylcholinesterase in rat striatum. *Nature*, **291**, 415–418.

Herz, D.M., Little, S., Pedrosa, D.J., Tinkhauser, G., Cheeran, B., Foltynie, T., Bogacz, R., & Brown, P. (2018) Mechanisms Underlying Decision-Making as Revealed by Deep-Brain Stimulation in Patients with Parkinson's Disease. *Current Biology*, **28**, 1169-1178.e6.

Hikosaka, O., Sakamoto, M., & Usui, S. (1989) Functional properties of monkey caudate neurons. III. Activities related to expectation of target and reward. *Journal of Neurophysiology*, **61**, 814–832.

Hikosaka, O. & Wurtz, R.H. (1983) Visual and oculomotor functions of monkey substantia nigra pars reticulata. I. Relation of visual and auditory responses to saccades. *Journal of Neurophysiology*, **49**, 1230–1253.

Hollerman, J.R. & Schultz, W. (1998) Dopamine neurons report an error in the temporal prediction of reward during learning. *Nature Neuroscience*, **1**, 304–309.

Holroyd, C.B., Nieuwenhuis, S., Yeung, N., Nystrom, L., Mars, R.B., Coles, M.G.H., & Cohen, J.D. (2004) Dorsal anterior cingulate cortex shows fMRI response to internal and external error signals. *Nature Neuroscience*, **7**, 497–498.

Hopkins, D.A. & Niessen, L.W. (1976) Substantia nigra projections to the reticular formation, superior colliculus and central gray in the rat, cat and monkey. *Neuroscience Letters*, **2**, 253–259.

Hornykiewicz, O. (1975) Brain monoamines and parkinsonism. *Natl Inst Drug Abuse Res Monogr Ser*, 13–21.
Hutchison, W.D., Allan, R.J., Opitz, H., Levy, R., Dostrovsky, J.O., Lang, A.E., & Lozano, A.M. (1998) Neurophysiological identification of the subthalamic nucleus in surgery for Parkinson's disease. *Annals of Neurology*, **44**, 622–628.
Hutchison, W.D., Lozano, A.M., Davis, K.D., Saint-Cyr, J.A., Lang, A.E., & Dostrovsky, J.O. (1994) Differential neuronal activity in segments of globus pallidus in Parkinson's disease patients. *NeuroReport*, **5**, 1533–1537.
Ilinsky, I.A., Jouandet, M.L., & Goldman-Rakic, P.S. (1985) Organization of the nigrothalamocortical system in the rhesus monkey. *Journal of Comparative Neurology*, **236**, 315–330.
Inase, M., Sakai, S.T., & Tanji, J. (1996) Overlapping corticostriatal projections from the supplementary motor area and the primary motor cortex in the macaque monkey: An anterograde double labeling study. *The Journal of Comparative Neurology*, **373**, 283–296.
Ito, M. & Doya, K. (2015) Distinct Neural Representation in the Dorsolateral, Dorsomedial, and Ventral Parts of the Striatum during Fixed- and Free-Choice Tasks. *The Journal of Neuroscience*, **35**, 3499–3514.
Ito, S., Stuphorn, V., Brown, J.W., & Schall, J.D. (2003) Performance Monitoring by the Anterior Cingulate Cortex During Saccade Countermanding. *Science*, **302**, 120–122.
Izquierdo, A., Suda, R.K., & Murray, E.A. (2004) Bilateral Orbital Prefrontal Cortex Lesions in Rhesus Monkeys Disrupt Choices Guided by Both Reward Value and Reward Contingency. *The Journal of Neuroscience*, **24**, 7540–7548.
Joel, D., Niv, Y., & Ruppin, E. (2002) Actor–critic models of the basal ganglia: new anatomical and computational perspectives. *Neural Networks*, **15**, 535–547.
Jones, E.G. & Leavitt, R.Y. (1974) Retrograde axonal transport and the demonstration of non-specific projections to the cerebral cortex and striatum from thalamic intralaminar nuclei in the rat, cat and monkey. *Journal of Comparative Neurology*, **154**, 349–377.
Joshua, M., Adler, A., Mitelman, R., Vaadia, E., & Bergman, H. (2008) Midbrain Dopaminergic Neurons and Striatal Cholinergic Interneurons Encode the Difference between Reward and Aversive Events at Different Epochs of Probabilistic Classical Conditioning Trials. *The Journal of Neuroscience*, **28**, 11673–11684.
Joshua, M., Adler, A., Prut, Y., Vaadia, E., Wickens, J.R., & Bergman, H. (2009) Synchronization of Midbrain Dopaminergic Neurons Is Enhanced by Rewarding Events. *Neuron*, **62**, 695–704.
Joshua, M., Adler, A., Rosin, B., Vaadia, E., & Bergman, H. (2009) Encoding of Probabilistic Rewarding and Aversive Events by Pallidal and Nigral Neurons. *Journal of Neurophysiology*, **101**, 758–772.
Kable, J.W. & Glimcher, P.W. (2007) The neural correlates of subjective value during intertemporal choice. *Nature Neuroscience*, **10**, 1625–1633.
Kable, J.W. & Glimcher, P.W. (2009) The Neurobiology of Decision: Consensus and Controversy. *Neuron*, **63**, 733–745.
Kahneman, D. & Tversky, A. (1979) Prospect Theory: An Analysis of Decision under Risk. *Econometrica*, **47**, 263–292.
Kaplan, A., Mizrahi-Kliger, A.D., Israel, Z., Adler, A., & Bergman, H. (2020) Dissociable roles of ventral pallidum neurons in the basal ganglia reinforcement learning network. *Nature Neuroscience*, **23**, 556–564.
Katabi, S., Adler, A., Deffains, M., & Bergman, H. (2023) Dichotomous activity and function of neurons with low- and high-frequency discharge in the external globus pallidus of non-human primates. *Cell Reports*, **42**, 111898.
Kawaguchi, Y. (1993) Physiological, morphological, and histochemical characterization of three classes of interneurons in rat neostriatum. *The Journal of Neuroscience*, **13**, 4908–4923.
Kawaguchi, Y., Wilson, C.J., Augood, S.J., & Emson, P.C. (1995) Striatal interneurones: chemical, physiological and morphological characterization. *Trends in Neurosciences*, **18**, 527–535.
Kawaguchi, Y., Wilson, C.J., & Emson, P.C. (1990) Projection subtypes of rat neostriatal matrix cells revealed by intracellular injection of biocytin. *The Journal of Neuroscience*, **10**, 3421–3438.
Kemp, J.M. & Powell, T.P.S. (1970) The Cortico-Striate Projection in the Monkey. *Brain*, **93**, 525–546.
Kennerley, S.W., Dahmubed, A.F., Lara, A.H., & Wallis, J.D. (2009) Neurons in the frontal lobe encode the value of multiple decision variables. *Journal of Cognitive Neuroscience*, **21**, 1162–1178.
Kennerley, S.W. & Wallis, J.D. (2009) Evaluating choices by single neurons in the frontal lobe: outcome value encoded across multiple decision variables. *European Journal of Neuroscience*, **29**, 2061–2073.
Kennerley, S.W., Walton, M.E., Behrens, T.E.J., Buckley, M.J., & Rushworth, M.F.S. (2006) Optimal decision making and the anterior cingulate cortex. *Nature Neuroscience*, **9**, 940–947.
Kerns, J.G., Cohen, J.D., MacDonald, A.W., Cho, R.Y., Stenger, V.A., & Carter, C.S. (2004) Anterior Cingulate Conflict Monitoring and Adjustments in Control. *Science*, **303**, 1023–1026.

Kievit, J. & Kuypers, H.G.J.M. (1977) Organization of the thalamo-cortical connexions to the frontal lobe in the rhesus monkey. *Experimental Brain Research*, **29**, 299–322.

Kim, H., Sul, J.H., Huh, N., Lee, D., & Jung, M.W. (2009) Role of Striatum in Updating Values of Chosen Actions. *J. Neurosci.*, **29**, 14701–14712.

Kim, R., Nakano, K., Jayaraman, A., & Carpenter, M.B. (1976) Projections of the globus pallidus and adjacent structures: An autoradiographic study in the monkey. *Journal of Comparative Neurology*, **169**, 263–290.

Kimura, M. (1986) The role of primate putamen neurons in the association of sensory stimuli with movement. *Neuroscience Research*, **3**, 436–443.

Kimura, M. (1992) Behavioral modulation of sensory responses of primate putamen neurons. *Brain Research*, **578**, 204–214.

Kimura, M., Kato, M., & Shimazaki, H. (1990) Physiological properties of projection neurons in the monkey striatum to the globus pallidus. *Experimental Brain Research*, **82**, 672–676.

Kimura, M., Kato, M., Shimazaki, H., Watanabe, K., & Matsumoto, N. (1996) Neural information transferred from the putamen to the globus pallidus during learned movement in the monkey. *Journal of Neurophysiology*, **76**, 3771–3786.

Kimura, M., Rajkowski, J., & Evarts, E. (1984) Tonically discharging putamen neurons exhibit set-dependent responses. *Proc. Natl. Acad. Sci. U.S.A.*, **81**, 4998–5001.

Kincaid, A.E., Zheng, T., & Wilson, C.J. (1998) Connectivity and Convergence of Single Corticostriatal Axons. *The Journal of Neuroscience*, **18**, 4722–4731.

Kita, H. (2007) Globus pallidus external segment. In *Progress in Brain Research*. Elsevier, Volume 160, pp. 111–133.

Kita, H. & Kita, S.T. (1994) The morphology of globus pallidus projection neurons in the rat: an intracellular staining study. *Brain Research*, **636**, 308–319.

Kita, H. & Kitai, S.T. (1987) Efferent projections of the subthalamic nucleus in the rat: Light and electron microscopic analysis with the PHA-L method. *Journal of Comparative Neurology*, **260**, 435–452.

Kita, T. & Kita, H. (2012) The Subthalamic Nucleus Is One of Multiple Innervation Sites for Long-Range Corticofugal Axons: A Single-Axon Tracing Study in the Rat. *The Journal of Neuroscience*, **32**, 5990–5999.

Kitai, S.T. & Deniau, J.M. (1981) Cortical inputs to the subthalamus: intracellular analysis. *Brain Research*, **214**, 411–415.

Kjær, S.W., Damholdt, M.F., & Callesen, M.B. (2018) A systematic review of decision-making impairments in Parkinson's Disease: Dopaminergic medication and methodological variability. *Basal Ganglia*, **14**, 31–40.

Klein-Flügge, M.C., Hunt, L.T., Bach, D.R., Dolan, R.J., & Behrens, T.E.J. (2011) Dissociable Reward and Timing Signals in Human Midbrain and Ventral Striatum. *Neuron*, **72**, 654–664.

Knutson, B., Adams, C.M., Fong, G.W., & Hommer, D. (2001) Anticipation of Increasing Monetary Reward Selectively Recruits Nucleus Accumbens. *The Journal of Neuroscience*, **21**, RC159.

Knutson, B., Taylor, J., Kaufman, M., Peterson, R., & Glover, G. (2005) Distributed Neural Representation of Expected Value. *The Journal of Neuroscience*, **25**, 4806–4812.

Kobayakawa, M., Koyama, S., Mimura, M., & Kawamura, M. (2008) Decision making in Parkinson's disease: Analysis of behavioral and physiological patterns in the Iowa gambling task. *Movement Disorders*, **23**, 547–552.

Koshimizu, Y., Fujiyama, F., Nakamura, K.C., Furuta, T., & Kaneko, T. (2013) Quantitative analysis of axon bouton distribution of subthalamic nucleus neurons in the rat by single neuron visualization with a viral vector. *Journal of Comparative Neurology*, **521**, 2125–2146.

Krack, P., Hariz, M.I., Baunez, C., Guridi, J., & Obeso, J.A. (2010) Deep brain stimulation: from neurology to psychiatry? *Trends in Neurosciences*, **33**, 474–484.

Kühn, A.A., Kempf, F., Brücke, C., Gaynor Doyle, L., Martinez-Torres, I., Pogosyan, A., Trottenberg, T., Kupsch, A., Schneider, G.-H., Hariz, M.I., Vandenberghe, W., Nuttin, B., & Brown, P. (2008) High-Frequency Stimulation of the Subthalamic Nucleus Suppresses Oscillatory Activity in Patients with Parkinson's Disease in Parallel with Improvement in Motor Performance. *Journal of Neuroscience*, **28**, 6165–6173.

Kühn, A.A., Williams, D., Kupsch, A., Limousin, P., Hariz, M., Schneider, G., Yarrow, K., & Brown, P. (2004) Event-related beta desynchronization in human subthalamic nucleus correlates with motor performance. *Brain*, **127**, 735–746.

Künzle, H. (1975) Bilateral projections from precentral motor cortex to the putamen and other parts of the basal ganglia. An autoradiographic study in Macaca fascicularis. *Brain Research*, **88**, 195–209.

Künzle, H. (1977) Projections from the primary somatosensory cortex to basal ganglia and thalamus in the monkey. *Exp Brain Res*, **30**, 481–492.

Künzle, H. (1978) An Autoradiographic Analysis of the Efferent Connections from Premotor and Adjacent Prefrontal Regions (Areas 6 and 9) in Macaca fascicularis. *Brain Behavior and Evolution*, **15**, 185–234.

Künzle, H. & Akert, K. (1977) Efferent connections of cortical, area 8 (frontal eye field) in *Macaca fascicularis*. A reinvestigation using the autoradiographic technique. *Journal of Comparative Neurology*, **173**, 147–164.

Kupferschmidt, D.A., Juczewski, K., Cui, G., Johnson, K.A., & Lovinger, D.M. (2017) Parallel, but Dissociable, Processing in Discrete Corticostriatal Inputs Encodes Skill Learning. *Neuron*, **96**, 476-489.e5.

Lanciego, J.L., Luquin, N., & Obeso, J.A. (2012) Functional Neuroanatomy of the Basal Ganglia. *Cold Spring Harbor Perspectives in Medicine*, **2**, a009621.

Lardeux, S., Pernaud, R., Paleressompoulle, D., & Baunez, C. (2009) Beyond the Reward Pathway: Coding Reward Magnitude and Error in the Rat Subthalamic Nucleus. *Journal of Neurophysiology*, **102**, 2526–2537.

Lau, B. & Glimcher, P.W. (2008) Value Representations in the Primate Striatum during Matching Behavior. *Neuron*, **58**, 451–463.

Lawrence, A.D., Goerendt, I.K., & Brooks, D.J. (2011) Apathy blunts neural response to money in Parkinson's disease. *Social Neuroscience*, **6**, 653–662.

Lazaridis, I., Crittenden, J.R., Ahn, G., Hirokane, K., Wickersham, I.R., Yoshida, T., Mahar, A., Skara, V., Loftus, J.H., Parvataneni, K., Meletis, K., Ting, J.T., Hueske, E., Matsushima, A., & Graybiel, A.M. (2024) Striosomes control dopamine via dual pathways paralleling canonical basal ganglia circuits. *Current Biology*, **34**, 5263-5283.e8.

Le Bouc, R., Rigoux, L., Schmidt, L., Degos, B., Welter, M.-L., Vidailhet, M., Daunizeau, J., & Pessiglione, M. (2016) Computational Dissection of Dopamine Motor and Motivational Functions in Humans. *The Journal of Neuroscience*, **36**, 6623–6633.

Le Heron, C., Plant, O., Manohar, S., Ang, Y.-S., Jackson, M., Lennox, G., Hu, M.T., & Husain, M. (2018) Distinct effects of apathy and dopamine on effort-based decision-making in Parkinson's disease. *Brain*, **141**, 1455–1469.

Lederman, J., Lardeux, S., & Nicola, S.M. (2021) Vigor Encoding in the Ventral Pallidum. *eNeuro*, **8**, ENEURO.0064-21.2021.

Lee, S.W., Shimojo, S., & O'Doherty, J.P. (2014) Neural Computations Underlying Arbitration between Model-Based and Model-free Learning. *Neuron*, **81**, 687–699.

Lehéricy, S., Benali, H., Van De Moortele, P.-F., Pélégrini-Issac, M., Waechter, T., Ugurbil, K., & Doyon, J. (2005) Distinct basal ganglia territories are engaged in early and advanced motor sequence learning. *Proc. Natl. Acad. Sci. U.S.A.*, **102**, 12566–12571.

Lévesque, M. & Parent, A. (2005) The striatofugal fiber system in primates: A reevaluation of its organization based on single-axon tracing studies. *Proc. Natl. Acad. Sci. U.S.A.*, **102**, 11888–11893.

Levy, D.J. & Glimcher, P.W. (2012) The root of all value: a neural common currency for choice. *Current Opinion in Neurobiology*, **22**, 1027–1038.

Lewicki, M.S. (1998) A review of methods for spike sorting: the detection and classification of neural action potentials. *Network: Computation in Neural Systems*, **9**, R53-78.

Mackey, S. & Petrides, M. (2010) Quantitative demonstration of comparable architectonic areas within the ventromedial and lateral orbital frontal cortex in the human and the macaque monkey brains. *European Journal of Neuroscience*, **32**, 1940–1950.

Mah, A., Golden, C.E.M., & Constantinople, C.M. (2024) Dopamine transients encode reward prediction errors independent of learning rates. *Cell Reports*, **43**, 114840.

Mallet, N., Micklem, B.R., Henny, P., Brown, M.T., Williams, C., Bolam, J.P., Nakamura, K.C., & Magill, P.J. (2012) Dichotomous Organization of the External Globus Pallidus. *Neuron*, **74**, 1075–1086.

Mallet, N., Pogosyan, A., Sharott, A., Csicsvari, J., Bolam, J.P., Brown, P., & Magill, P.J. (2008) Disrupted Dopamine Transmission and the Emergence of Exaggerated Beta Oscillations in Subthalamic Nucleus and Cerebral Cortex. *The Journal of Neuroscience*, **28**, 4795–4806.

Matsumoto, M. & Hikosaka, O. (2009) Two types of dopamine neuron distinctly convey positive and negative motivational signals. *Nature*, **459**, 837–841.

Matsumoto, M., Matsumoto, K., Abe, H., & Tanaka, K. (2007) Medial prefrontal cell activity signaling prediction errors of action values. *Nature Neuroscience*, **10**, 647–656.

Matsumura, M., Kojima, J., Gardiner, T.W., & Hikosaka, O. (1992) Visual and oculomotor functions of monkey subthalamic nucleus. *Journal of Neurophysiology*, **67**, 1615–1632.

Mazzoni, P., Hristova, A., & Krakauer, J.W. (2007) Why don't we move faster? Parkinson's disease, movement vigor, and implicit motivation. *The Journal of Neuroscience*, **27**, 7105–7116.

McGeorge, A.J. & Faull, R.L.M. (1989) The organization of the projection from the cerebral cortex to the striatum in the rat. *Neuroscience*, **29**, 503–537.

McGregor, M.M. & Nelson, A.B. (2019) Circuit Mechanisms of Parkinson's Disease. *Neuron*, **101**, 1042–1056.
Meissner, W., Leblois, A., Hansel, D., Bioulac, B., Gross, C.E., Benazzouz, A., & Boraud, T. (2005) Subthalamic high frequency stimulation resets subthalamic firing and reduces abnormal oscillations. *Brain*, **128**, 2372–2382.
Mendelsohn, A.I., Nikoobakht, L., Bikoff, J.B., & Costa, R.M. (2025) Segregated basal ganglia output pathways correspond to genetically divergent neuronal subclasses. *Cell Reports*, **44**, 115454.
Meredith, G.E., Pattiselanno, A., Groenewegen, H.J., & Haber, S.N. (1996) Shell and core in monkey and human nucleus accumbens identified with antibodies to calbindin-D28k. *The Journal of Comparative Neurology*, **365**, 628–639.
Middleton, F.A. & Strick, P.L. (1994) Anatomical Evidence for Cerebellar and Basal Ganglia Involvement in Higher Cognitive Function. *Science*, **266**, 458–461.
Miller, E.K. & Cohen, J.D. (2001) An Integrative Theory of Prefrontal Cortex Function. *Annual Review of Neuroscience*, **24**, 167–202.
Miller, W.C. & DeLong, M.R. (1987) Altered Tonic Activity of Neurons in the Globus Pallidus and Subthalamic Nucleus in the Primate MPTP Model of Parkinsonism. In Carpenter, M.B. & Jayaraman, A. (eds), *The Basal Ganglia II*, *Advances in Behavioral Biology, Vol 32*. Springer US, Boston, MA.
Milstein, D.M. & Dorris, M.C. (2007) The Influence of Expected Value on Saccadic Preparation. *The Journal of Neuroscience*, **27**, 4810–4818.
Milstein, D.M. & Dorris, M.C. (2011) The Relationship between Saccadic Choice and Reaction Times with Manipulations of Target Value. *Frontiers in Neuroscience*, **5**, 122.
Mink, J.W. (1996) The basal ganglia: focused selection and inhibition of competing motor programs. *Progress in Neurobiology*, **50**, 381–425.
Mitchell, S.J., Richardson, R.T., Baker, F.H., & DeLong, M.R. (1987) The primate globus pallidus: neuronal activity related to direction of movement. *Experimental Brain Research*, **68**, 491–505.
Miyachi, S., Hikosaka, O., & Lu, X. (2002) Differential activation of monkey striatal neurons in the early and late stages of procedural learning. *Experimental Brain Research*, **146**, 122–126.
Mogenson, G., Jones, D., & Yim, C. (1980) From motivation to action: Functional interface between the limbic system and the motor system. *Progress in Neurobiology*, **14**, 69–97.
Monakow, K.H., Akert, K., & Künzle, H. (1978) Projections of the precentral motor cortex and other cortical areas of the frontal lobe to the subthalamic nucleus in the monkey. *Experimental Brain Research*, **33**, 395–403.
Monchi, O., Petrides, M., Petre, V., Worsley, K., & Dagher, A. (2001) Wisconsin Card Sorting Revisited: Distinct Neural Circuits Participating in Different Stages of the Task Identified by Event-Related Functional Magnetic Resonance Imaging. *The Journal of Neuroscience*, **21**, 7733–7741.
Morris, G., Arkadir, D., Nevet, A., Vaadia, E., & Bergman, H. (2004) Coincident but Distinct Messages of Midbrain Dopamine and Striatal Tonically Active Neurons. *Neuron*, **43**, 133–143.
Morris, L., O'Callaghan, C., & Le Heron, C. (2022) Disordered Decision Making: A Cognitive Framework for Apathy and Impulsivity in Huntington's Disease. *Movement Disorders*, **37**, 1149–1163.
Nambu, A. (2004) A new dynamic model of the cortico-basal ganglia loop. In *Progress in Brain Research*. Elsevier, Volume 143, pp. 461–466.
Nambu, A. (2007) Globus pallidus internal segment. In *Progress in Brain Research*. Elsevier, Volume 160, pp. 135–150.
Nambu, A. (2011) Somatotopic Organization of the Primate Basal Ganglia. *Frontiers in Neuroanatomy*, **5**, 26.
Nambu, A., Kaneda, K., Tokuno, H., & Takada, M. (2002) Organization of Corticostriatal Motor Inputs in Monkey Putamen. *Journal of Neurophysiology*, **88**, 1830–1842.
Nambu, A., Tachibana, Y., & Chiken, S. (2015) Cause of parkinsonian symptoms: Firing rate, firing pattern or dynamic activity changes? *Basal Ganglia*, **5**, 1–6.
Nambu, A., Takada, M., Inase, M., & Tokuno, H. (1996) Dual somatotopical representations in the primate subthalamic nucleus: evidence for ordered but reversed body-map transformations from the primary motor cortex and the supplementary motor area. *The Journal of Neuroscience*, **16**, 2671–2683.
Nambu, A., Tokuno, H., Hamada, I., Kita, H., Imanishi, M., Akazawa, T., Ikeuchi, Y., & Hasegawa, N. (2000) Excitatory Cortical Inputs to Pallidal Neurons Via the Subthalamic Nucleus in the Monkey. *Journal of Neurophysiology*, **84**, 289–300.
Nambu, A., Tokuno, H., & Takada, M. (2002) Functional significance of the cortico–subthalamo–pallidal 'hyperdirect' pathway. *Neuroscience Research*, **43**, 111–117.
Nauta, H.J.W. & Cole, M. (1978) Efferent projections of the subthalamic nucleus: An autoradiographic study in monkey and cat. *Journal of Comparative Neurology*, **180**, 1–16.

Nauta, H.J.W. & Mehler, W.R. (1966) Projections of the lentiform nucleus in the moneky. *Brain Research*, **1**, 3–42.

Neumann, W.-J., Steiner, L.A., & Milosevic, L. (2023) Neurophysiological mechanisms of deep brain stimulation across spatiotemporal resolutions. *Brain*, **146**, 4456–4468.

Nevet, A., Morris, G., Saban, G., Fainstein, N., & Bergman, H. (2004) Discharge Rate of Substantia Nigra Pars Reticulata Neurons Is Reduced In Non-Parkinsonian Monkeys With Apomorphine-Induced Orofacial Dyskinesia. *Journal of Neurophysiology*, **92**, 1973–1981.

Nini, A., Feingold, A., Slovin, H., & Bergman, H. (1995) Neurons in the globus pallidus do not show correlated activity in the normal monkey, but phase-locked oscillations appear in the MPTP model of parkinsonism. *Journal of Neurophysiology*, **74**, 1800–1805.

Nioche, A., Bourgeois-Gironde, S., & Boraud, T. (2019) An asymmetry of treatment between lotteries involving gains and losses in rhesus monkeys. *Scientific Reports*, **9**, 10441.

Niv, Y. (2019) Learning task-state representations. *Nat Neurosci*, **22**, 1544–1553.

Niv, Y., Daw, N.D., Joel, D., & Dayan, P. (2007) Tonic dopamine: opportunity costs and the control of response vigor. *Psychopharmacology (Berl)*, **191**, 507–520.

Noonan, M.P., Walton, M.E., Behrens, T.E.J., Sallet, J., Buckley, M.J., & Rushworth, M.F.S. (2010) Separate value comparison and learning mechanisms in macaque medial and lateral orbitofrontal cortex. *Proc. Natl. Acad. Sci. U.S.A.*, **107**, 20547–20552.

Nougaret, S., Baunez, C., & Ravel, S. (2022) Neurons in the Monkey's Subthalamic Nucleus Differentially Encode Motivation and Effort. *J Neurosci*, **42**, 2539–2551.

Nougaret, S. & Ravel, S. (2015) Modulation of Tonically Active Neurons of the Monkey Striatum by Events Carrying Different Force and Reward Information. *The Journal of Neuroscience*, **35**, 15214–15226.

Nougaret, S. & Ravel, S. (2018) Dynamic Encoding of Effort and Reward throughout the Execution of Action by External Globus Pallidus Neurons in Monkeys. *Journal of Cognitive Neuroscience*, **30**, 1130–1144.

Nygren, T.E., Isen, A.M., Taylor, P.J., & Dulin, J. (1996) The Influence of Positive Affect on the Decision Rule in Risk Situations: Focus on Outcome (and Especially Avoidance of Loss) Rather Than Probability. *Organizational Behavior and Human Decision Processes*, **66**, 59–72.

Obeso, J.A., Rodríguez-Oroz, M.C., Benitez-Temino, B., Blesa, F.J., Guridi, J., Marin, C., & Rodriguez, M. (2008) Functional organization of the basal ganglia: Therapeutic implications for Parkinson's disease: Therapeutic Implications for Parkinson's Disease. *Movement Disorders*, **23**, S548-559.

O'Doherty, J., Dayan, P., Schultz, J., Deichmann, R., Friston, K., & Dolan, R.J. (2004) Dissociable Roles of Ventral and Dorsal Striatum in Instrumental Conditioning. *Science*, **304**, 452–454.

O'Doherty, J., Kringelbach, M.L., Rolls, E.T., Hornak, J., & Andrews, C. (2001) Abstract reward and punishment representations in the human orbitofrontal cortex. *Nature Neuroscience*, **4**, 95–102.

O'Doherty, J.P., Deichmann, R., Critchley, H.D., & Dolan, R.J. (2002) Neural Responses during Anticipation of a Primary Taste Reward. *Neuron*, **33**, 815–826.

Oertel, W.H. & Mugnaini, E. (1984) Immunocytochemical studies of GABAergic neurons in rat basal ganglia and their relations to other neuronal systems. *Neuroscience Letters*, **47**, 233–238.

Ongür, D. & Price, J. (2000) The Organization of Networks within the Orbital and Medial Prefrontal Cortex of Rats, Monkeys and Humans. *Cerebral Cortex*, **10**, 206–219.

Oorschot, D.E. (1996) Total number of neurons in the neostriatal, pallidal, subthalamic, and substantia nigral nuclei of the rat basal ganglia: A stereological study using the cavalieri and optical disector methods. *The Journal of Comparative Neurology*, **366**, 580–599.

Ottenheimer, D., Richard, J.M., & Janak, P.H. (2018) Ventral pallidum encodes relative reward value earlier and more robustly than nucleus accumbens. *Nature Communications*, **9**, 4350.

Ottenheimer, D.J., Bari, B.A., Sutlief, E., Fraser, K.M., Kim, T.H., Richard, J.M., Cohen, J.Y., & Janak, P.H. (2020) A quantitative reward prediction error signal in the ventral pallidum. *Nature Neuroscience*, **23**, 1267–1276.

Ottenheimer, D.J., Wang, K., Tong, X., Fraser, K.M., Richard, J.M., & Janak, P.H. (2020) Reward activity in ventral pallidum tracks satiety-sensitive preference and drives choice behavior. *Science Advances*, **6**, eabc9321.

Ouchi, Y., Yoshikawa, E., Okada, H., Futatsubashi, M., Sekine, Y., Iyo, M., & Sakamoto, M. (1999) Alterations in binding site density of dopamine transporter in the striatum, orbitofrontal cortex, and amygdala in early Parkinson's disease: Compartment analysis for beta-CFT binding with positron emission tomography. *Annals of Neurology*, **45**, 601–610.

Padoa-Schioppa, C. (2011) Neurobiology of Economic Choice: A Good-Based Model. *Annual Review of Neuroscience*, **34**, 333–359.

Padoa-Schioppa, C. (2013) Neuronal Origins of Choice Variability in Economic Decisions. *Neuron*, **80**, 1322–1336.

Padoa-Schioppa, C. & Assad, J.A. (2006) Neurons in the orbitofrontal cortex encode economic value. *Nature*, **441**, 223–226.
Padoa-Schioppa, C. & Conen, K.E. (2017) Orbitofrontal Cortex: A Neural Circuit for Economic Decisions. *Neuron*, **96**, 736–754.
Parent, A. (1990) Extrinsic connections of the basal ganglia. *Trends in Neurosciences*, **13**, 254–258.
Parent, A., Bouchard, C., & Smith, Y. (1984) The striatopallidal and striatonigral projections: two distinct fiber systems in primate. *Brain Research*, **303**, 385–390.
Parent, A. & De Bellefeuille, L. (1982) Organization of efferent projections from the internal segment of globus pallidus in primate as revealed by fluorescence retrograde labeling method. *Brain Research*, **245**, 201–213.
Parent, A. & Hazrati, L.-N. (1995a) Functional anatomy of the basal ganglia. I. The cortico-basal ganglia-thalamo-cortical loop. *Brain Research Reviews*, **20**, 91–127.
Parent, A. & Hazrati, L.-N. (1995b) Functional anatomy of the basal ganglia. II. The place of subthalamic nucleus and external pallidum in basal ganglia circuitry. *Brain Research Reviews*, **20**, 128–154.
Parent, A., Mackey, A., & Bellefeuille, L.D. (1983) The subcortical afferents to caudate nucleus and putamen in primate: A fluorescence retrograde double labeling study. *Neuroscience*, **10**, 1137–1150.
Parent, M. & Parent, A. (2006) Single-axon tracing study of corticostriatal projections arising from primary motor cortex in primates. *Journal of Comparative Neurology*, **496**, 202–213.
Parkinson, J. (1817) *An Essay on the Shaking Palsy*. London Printed by Whittingham and Rowland for Sherwood, Neely and Jones.
Parush, N., Tishby, N., & Bergman, H. (2011) Dopaminergic Balance between Reward Maximization and Policy Complexity. *Frontiers in Systems Neuroscience*, **5**, 22.
Pasquereau, B., Nadjar, A., Arkadir, D., Bezard, E., Goillandeau, M., Bioulac, B., Gross, C.E., & Boraud, T. (2007) Shaping of Motor Responses by Incentive Values through the Basal Ganglia. *The Journal of Neuroscience*, **27**, 1176–1183.
Pasquereau, B. & Turner, R.S. (2017) A selective role for ventromedial subthalamic nucleus in inhibitory control. *eLife*, **6**, e31627.
Pastor-Bernier, A., Tremblay, E., & Cisek, P. (2012) Dorsal premotor cortex is involved in switching motor plans. *Frontiers in Neuroengineering*, **5**, 5.
Pauli, W.M., Nili, A.N., & Tyszka, J.M. (2018) A high-resolution probabilistic in vivo atlas of human subcortical brain nuclei. *Scientific Data*, **5**, 180063.
Paxinos, G., Petrides, M., & Evrard, H.C. (2024) *The Rhesus Monkey Brain in Stereotaxic Coordinates*, Academic press.
Penney, J.B. & Young, A.B. (1981) GABA as the pallidothalamic neurotransmitter: implications for basal ganglia function. *Brain Research*, **207**, 195–199.
Percheron, G., François, C., Yelnik, J., Fénelon, G., & Talbi, B. (1994) The Basal Ganglia Related System of Primates: Definition, Description and Informational Analysis. In *The Basal Ganglia IV*, *Advances in Behavioral Biology, Vol 41*. Springer, Boston, MA, pp. 3–20.
Percheron, G., Yelnik, J., & François, C. (1984) A Golgi analysis of the primate globus pallidus. III. Spatial organization of the striato-pallidal complex. *The Journal of Comparative Neurology*, **227**, 214–227.
Petrides (1991) Functional specialization within the dorsolateral frontal cortex for serial order memory. *Proceedings. Biological Sciences*, **246**, 299–306.
Petrides, M. (1985) Deficits on conditional associative-learning tasks after frontal- and temporal-lobe lesions in man. *Neuropsychologia*, **23**, 601–614.
Plassmann, H., O'Doherty, J., & Rangel, A. (2007) Orbitofrontal Cortex Encodes Willingness to Pay in Everyday Economic Transactions. *The Journal of Neuroscience*, **27**, 9984–9988.
Pochon, J.-B., Riis, J., Sanfey, A.G., Nystrom, L.E., & Cohen, J.D. (2008) Functional Imaging of Decision Conflict. *The Journal of Neuroscience*, **28**, 3468–3473.
Powell, T.P.S. & Cowan, W.M. (1956) A study of thalamo-striate relations in the monkey. *Brain*, **79**, 364–366.
Prasad, A.A. & Wallén-Mackenzie, Å. (2024) Architecture of the subthalamic nucleus. *Communications Biology*, **7**, 78.
Prelec, D. (1998) The Probability Weighting Function. *Econometrica*, **66**, 497–527.
Raghuraman, A.P. & Padoa-Schioppa, C. (2014) Integration of Multiple Determinants in the Neuronal Computation of Economic Values. *Journal of Neuroscience*, **34**, 11583–11603.
Ragsdale, C.W. & Graybiel, A.M. (1981) The fronto-striatal projection in the cat and monkey and its relationship to inhomogeneities established by acetylcholinesterase histochemistry. *Brain Research*, **208**, 259–266.

Rangel, A., Camerer, C., & Montague, P.R. (2008) A framework for studying the neurobiology of value-based decision making. *Nature reviews. Neuroscience*, **9**, 545–556.

Rangel, A. & Hare, T. (2010) Neural computations associated with goal-directed choice. *Current Opinion in Neurobiology*, **20**, 262–270.

Ravel, S., Legallet, E., & Apicella, P. (1999) Tonically active neurons in the monkey striatum do not preferentially respond to appetitive stimuli. *Experimental Brain Research*, **128**, 531–534.

Raz, A., Vaadia, E., & Bergman, H. (2000) Firing Patterns and Correlations of Spontaneous Discharge of Pallidal Neurons in the Normal and the Tremulous 1-Methyl-4-Phenyl-1,2,3,6-Tetrahydropyridine Vervet Model of Parkinsonism. *The Journal of Neuroscience*, **20**, 8559–8571.

Redgrave, P., Rodriguez, M., Smith, Y., Rodriguez-Oroz, M.C., Lehericy, S., Bergman, H., Agid, Y., DeLong, M.R., & Obeso, J.A. (2010) Goal-directed and habitual control in the basal ganglia: implications for Parkinson's disease. *Nature Reviews. Neuroscience*, **11**, 760–772.

Reiner, A., Medina, L., & Veenman, C.L. (1998) Structural and functional evolution of the basal ganglia in vertebrates. *Brain Research Reviews*, **28**, 235–285.

Rey, H.G., Pedreira, C., & Quian Quiroga, R. (2015) Past, present and future of spike sorting techniques. *Brain Research Bulletin*, **119**, 106–117.

Reynolds, J.N.J., Hyland, B.I., & Wickens, J.R. (2001) A cellular mechanism of reward-related learning. *Nature*, **413**, 67–70.

Ribak, C.E., Harris, A.B., Vaughn, J.E., & Roberts, E. (1979) Inhibitory, GABAergic Nerve Terminals Decrease at Sites of Focal Epilepsy. *Science*, **205**, 211–214.

Rich, E.L. & Wallis, J.D. (2016) Decoding subjective decisions from orbitofrontal cortex. *Nature Neuroscience*, **19**, 973–980.

Rigotti, M., Barak, O., Warden, M.R., Wang, X.-J., Daw, N.D., Miller, E.K., & Fusi, S. (2013) The importance of mixed selectivity in complex cognitive tasks. *Nature*, **497**, 585–590.

Rizzolatti, G. & Luppino, G. (2001) The Cortical Motor System. *Neuron*, **27**, 889–901.

Robinson, T.E. & Berridge, K.C. (1993) The neural basis of drug craving: an incentive-sensitization theory of addiction. *Brain Research Reviews*, **18**, 247–291.

Rodrigues-Vaz, I., Athalye, V.R., Peterka, D.S., & Costa, R.M. (2025) Striatal ensembles specify and control granular forelimb actions. *bioRxiv*,.

Roesch, M.R. & Olson, C.R. (2004) Neuronal Activity Related to Reward Value and Motivation in Primate Frontal Cortex. *Science*, **304**, 307–310.

Roesch, M.R., Singh, T., Brown, P.L., Mullins, S.E., & Schoenbaum, G. (2009) Ventral striatal neurons encode the value of the chosen action in rats deciding between differently delayed or sized rewards. *The Journal of Neuroscience*, **29**, 13365–13376.

Roitman, M.F., Wheeler, R.A., & Carelli, R.M. (2005) Nucleus Accumbens Neurons Are Innately Tuned for Rewarding and Aversive Taste Stimuli, Encode Their Predictors, and Are Linked to Motor Output. *Neuron*, **45**, 587–597.

Root, D.H., Melendez, R.I., Zaborszky, L., & Napier, T.C. (2015) The ventral pallidum: Subregion-specific functional anatomy and roles in motivated behaviors. *Progress in Neurobiology*, **130**, 29–70.

Rudebeck, P.H., Behrens, T.E., Kennerley, S.W., Baxter, M.G., Buckley, M.J., Walton, M.E., & Rushworth, M.F.S. (2008) Frontal Cortex Subregions Play Distinct Roles in Choices between Actions and Stimuli. *The Journal of Neuroscience*, **28**, 13775–13785.

Rudebeck, P.H. & Murray, E.A. (2011) Dissociable Effects of Subtotal Lesions within the Macaque Orbital Prefrontal Cortex on Reward-Guided Behavior. *Journal of Neuroscience*, **31**, 10569–10578.

Ryan, L.J. & Clark, K.B. (1991) The role of the subthalamic nucleus in the response of globus pallidus neurons to stimulation of the prelimbic and agranular frontal cortices in rats. *Experimental Brain Research*, **86**, 641–651.

Ryterska, A., Jahanshahi, M., & Osman, M. (2013) What are people with Parkinson's disease really impaired on when it comes to making decisions? A meta-analysis of the evidence. *Neuroscience & Biobehavioral Reviews*, **37**, 2836–2846.

Salamone, J.D., Yohn, S.E., López-Cruz, L., San Miguel, N., & Correa, M. (2016) Activational and effort-related aspects of motivation: neural mechanisms and implications for psychopathology. *Brain*, **139**, 1325–1347.

Salinas, E. & Sejnowski, T.J. (2001) Gain Modulation in the Central Nervous System: Where Behavior, Neurophysiology, and Computation Meet. *The Neuroscientist*, **7**, 430–440.

Salinas, E. & Thier, P. (2000) Gain Modulation: A Major Computational Principle of the Central Nervous System. *Neuron*, **27**, 15–21.

Salvesen, L., Ullerup, B.H., Sunay, F.B., Brudek, T., Løkkegaard, A., Agander, T.K., Winge, K., & Pakkenberg, B. (2015) Changes in total cell numbers of the basal ganglia in patients with multiple system atrophy — A stereological study. *Neurobiology of Disease*, **74**, 104–113.

Samejima, K., Ueda, Y., Doya, K., & Kimura, M. (2005) Representation of action-specific reward values in the striatum. *Science*, **310**, 1337–1340.

Sato, F., Lavallée, P., Lévesque, M., & Parent, A. (2000) Single-axon tracing study of neurons of the external segment of the globus pallidus in primate. *The Journal of Comparative Neurology*, **417**, 17–31.

Saunders, B.T. & Robinson, T.E. (2012) The role of dopamine in the accumbens core in the expression of Pavlovian-conditioned responses. *European Journal of Neuroscience*, **36**, 2521–2532.

Schell, G. & Strick, P. (1984) The origin of thalamic inputs to the arcuate premotor and supplementary motor areas. *The Journal of Neuroscience*, **4**, 539–560.

Schmued, L.C. & Fallon, J.H. (1986) Fluoro-gold: a new fluorescent retrograde axonal tracer with numerous unique properties. *Brain Research*, **377**, 147–154.

Schonberg, T., O'Doherty, J.P., Joel, D., Inzelberg, R., Segev, Y., & Daw, N.D. (2010) Selective impairment of prediction error signaling in human dorsolateral but not ventral striatum in Parkinson's disease patients: evidence from a model-based fMRI study. *NeuroImage*, **49**, 772–781.

Schultz, W. (1998) Predictive Reward Signal of Dopamine Neurons. *Journal of Neurophysiology*, **80**, 1–27.

Schultz, W. (2016) Dopamine reward prediction-error signalling: a two-component response. *Nature Reviews Neuroscience*, **17**, 183–195.

Schultz, W., Apicella, P., & Ljungberg, T. (1993) Responses of monkey dopamine neurons to reward and conditioned stimuli during successive steps of learning a delayed response task. *The Journal of Neuroscience*, **13**, 900–913.

Schultz, W., Apicella, P., Scarnati, E., & Ljungberg, T. (1992) Neuronal activity in monkey ventral striatum related to the expectation of reward. *The Journal of Neuroscience*, **12**, 4595–4610.

Schultz, W., Dayan, P., & Montague, P.R. (1997) A Neural Substrate of Prediction and Reward. *Science*, **275**, 1593–1599.

Selemon, L.D. & Goldman-Rakic, P.S. (1985) Longitudinal Topography and Interdigitation of Corticostriatal Projections in the Rhesus Monkey. *The Journal of Neuroscience*, **5**, 776–794.

Seo, H., Barraclough, D.J., & Lee, D. (2007) Dynamic Signals Related to Choices and Outcomes in the Dorsolateral Prefrontal Cortex. *Cerebral Cortex*, **17**, i110–i117.

Seymour, B., Daw, N., Dayan, P., Singer, T., & Dolan, R. (2007) Differential encoding of losses and gains in the human striatum. *The Journal of Neuroscience*, **27**, 4826–4831.

Shadlen, M.N. & Kiani, R. (2013) Decision Making as a Window on Cognition. *Neuron*, **80**, 791–806.

Shadmehr, R. & Ahmed, A.A. (2021) Précis of Vigor: Neuroeconomics of Movement Control. *Behavioral and Brain Sciences*, **44**, e123.

Shadmehr, R., Reppert, T.R., Summerside, E.M., Yoon, T., & Ahmed, A.A. (2019) Movement Vigor as a Reflection of Subjective Economic Utility. *Trends in Neurosciences*, **42**, 323–336.

Shallice, T. (1982) Specific Impairments of Planning. *Philosophical Transactions of the Royal Society of London*, **298**, 199–209.

Shen, W., Flajolet, M., Greengard, P., & Surmeier, D.J. (2008) Dichotomous Dopaminergic Control of Striatal Synaptic Plasticity. *Science*, **321**, 848–851.

Shenoy, K.V., Sahani, M., & Churchland, M.M. (2013) Cortical Control of Arm Movements: A Dynamical Systems Perspective. *Annual Review of Neuroscience*, **36**, 337–359.

Shimo, Y. & Hikosaka, O. (2001) Role of Tonically Active Neurons in Primate Caudate in Reward-Oriented Saccadic Eye Movement. *The Journal of Neuroscience*, **21**, 7804–7814.

Shin, E.J., Jang, Y., Kim, S., Kim, H., Cai, X., Lee, H., Sul, J.H., Lee, S.-H., Chung, Y., Lee, D., & Jung, M.W. (2021) Robust and distributed neural representation of action values. *eLife*, **10**, e53045.

Shiner, T., Seymour, B., Symmonds, M., Dayan, P., Bhatia, K.P., & Dolan, R.J. (2012) The Effect of Motivation on Movement: A Study of Bradykinesia in Parkinson's Disease. *PLOS One*, **7**, e47138.

Shiner, T., Seymour, B., Wunderlich, K., Hill, C., Bhatia, K.P., Dayan, P., & Dolan, R.J. (2012) Dopamine and performance in a reinforcement learning task: evidence from Parkinson's disease. *Brain*, **135**, 1871–1883.

Slovin, H., Abeles, M., Vaadia, E., Haalman, I., Prut, Y., & Bergman, H. (1999) Frontal Cognitive Impairments and Saccadic Deficits in Low-Dose MPTP-Treated Monkeys. *Journal of Neurophysiology*, **81**, 858–874.

Smith, K.S., Tindell, A.J., Aldridge, J.W., & Berridge, K.C. (2009) Ventral pallidum roles in reward and motivation. *Behavioural Brain Research*, **196**, 155–167.

Smith, Y. & Parent, A. (1986) Differential connections of caudate nucleus and putamen in the squirrel monkey (Saimiri sciureus). *Neuroscience*, **18**, 347–371.
Smith, Y. & Parent, A. (1988) Neurons of the subthalamic nucleus in primates display glutamate but not GABA immunoreactivity. *Brain Research*, **453**, 353–356.
Smith, Y., Wichmann, T., & DeLong, M.R. (1994) Synaptic innervation of neurons in the internal pallidal segment by the subthalamic nucleus and the external pallidum in monkeys. *J of Comparative Neurology*, **343**, 297–318.
Smittenaar, P., Chase, H.W., Aarts, E., Nusselein, B., Bloem, B.R., & Cools, R. (2012) Decomposing effects of dopaminergic medication in Parkinson's disease on probabilistic action selection – learning or performance? *European Journal of Neuroscience*, **35**, 1144–1151.
Spillantini, M.G., Schmidt, M.L., Lee, V.M.-Y., Trojanowski, J.Q., Jakes, R., & Goedert, M. (1997) α-Synuclein in Lewy bodies. *Nature*, **388**, 839–840.
Spooren, W.P.J.M., Lynd-Balta, E., Mitchell, S., & Haber, S.N. (1996) Ventral pallidostriatal pathway in the monkey: Evidence for modulation of basal ganglia circuits. *The Journal of Comparative Neurology*, **370**, 295–312.
Stauffer, W.R., Lak, A., Bossaerts, P., & Schultz, W. (2015) Economic choices reveal probability distortion in macaque monkeys. *The Journal of Neuroscience*, **35**, 3146–3154.
Stauffer, W.R., Lak, A., Kobayashi, S., & Schultz, W. (2016) Components and characteristics of the dopamine reward utility signal. *The Journal of Comparative Neurology*, **524**, 1699–1711.
Stuss, D.T., Levine, B., Alexander, M.P., Hong, J., Palumbo, C., Hamer, L., Murphy, K.J., & Izukawa, D. (2000) Wisconsin Card Sorting Test performance in patients with focal frontal and posterior brain damage: effects of lesion location and test structure on separable cognitive processes. *Neuropsychologia*, **38**, 388–402.
Summerfield, C. & Tsetsos, K. (2012) Building Bridges between Perceptual and Economic Decision-Making: Neural and Computational Mechanisms. *Frontiers in Neuroscience*, **6**, 70.
Surmeier, D.J., Song, W.-J., & Yan, Z. (1996) Coordinated Expression of Dopamine Receptors in Neostriatal Medium Spiny Neurons. *The Journal of Neuroscience*, **16**, 6579–6591.
Sutton, R.S. & Barto, A.G. (1998) Reinforcement Learning: An Introduction. *IEEE Transactions on Neural Networks*, **9**, 1054.
Switzer, R.C., Hill, J., & Heimer, L. (1982) The globus pallidus and its rostroventral extension into the olfactory tubercle of the rat: A cyto- and chemoarchitectural study. *Neuroscience*, **7**, 1891–1904.
Tachibana, Y. & Hikosaka, O. (2012) The primate ventral pallidum encodes expected reward value and regulates motor action. *Neuron*, **76**, 826–837.
Takahashi, K., Lin, J.-S., & Sakai, K. (2006) Neuronal Activity of Histaminergic Tuberomammillary Neurons During Wake–Sleep States in the Mouse. *The Journal of Neuroscience*, **26**, 10292–10298.
Tanaka, S.C., Balleine, B.W., & O'Doherty, J.P. (2008) Calculating Consequences: Brain Systems That Encode the Causal Effects of Actions. *Journal of Neuroscience*, **28**, 6750–6755.
Taswell, C.A., Janssen, M., Murray, E.A., & Averbeck, B.B. (2023) The motivational role of the ventral striatum and amygdala in learning from gains and losses. *Behavioral Neuroscience*, **137**, 268–280.
Taverna, S., Ilijic, E., & Surmeier, D.J. (2008) Recurrent Collateral Connections of Striatal Medium Spiny Neurons Are Disrupted in Models of Parkinson's Disease. *The Journal of Neuroscience*, **28**, 5504–5512.
Tecuapetla, F., Jin, X., Lima, S.Q., & Costa, R.M. (2016) Complementary Contributions of Striatal Projection Pathways to Action Initiation and Execution. *Cell*, **166**, 703–715.
Tepper, J.M. & Bolam, J.P. (2004) Functional diversity and specificity of neostriatal interneurons. *Current Opinion in Neurobiology*, **14**, 685–692.
Thiel, A., Hilker, R., Kessler, J., Habedank, B., Herholz, K., & Heiss, W.-D. (2003) Activation of basal ganglia loops in idiopathic Parkinson's disease: a PET study. *Journal of Neural Transmission*, **110**, 1289–1301.
Thobois, S., Ardouin, C., Lhommee, E., Klinger, H., Lagrange, C., Xie, J., Fraix, V., Coelho Braga, M.C., Hassani, R., Kistner, A., Juphard, A., Seigneuret, E., Chabardes, S., Mertens, P., Polo, G., Reilhac, A., Costes, N., LeBars, D., Savasta, M., Tremblay, L., Quesada, J.L., Bosson, J.L., Benabid, A.L., Broussolle, E., Pollak, P., & Krack, P. (2010) Non-motor dopamine withdrawal syndrome after surgery for Parkinson's disease: predictors and underlying mesolimbic denervation. *Brain*, **133**, 1111–1127.
Thorn, C.A., Atallah, H., Howe, M., & Graybiel, A.M. (2010) Differential Dynamics of Activity Changes in Dorsolateral and Dorsomedial Striatal Loops during Learning. *Neuron*, **66**, 781–795.
Thura, D. (2020) Decision urgency invigorates movement in humans. *Behavioural Brain Research*, **382**, 112477.
Thura, D., Cos, I., Trung, J., & Cisek, P. (2014) Context-Dependent Urgency Influences Speed–Accuracy Trade-Offs in Decision-Making and Movement Execution. *The Journal of Neuroscience*, **34**, 16442–16454.

Tindell, A.J., Berridge, K.C., Zhang, J., Peciña, S., & Aldridge, J.W. (2005) Ventral pallidal neurons code incentive motivation: amplification by mesolimbic sensitization and amphetamine. *European Journal of Neuroscience*, **22**, 2617–2634.

Tindell, A.J., Smith, K.S., Peciña, S., Berridge, K.C., & Aldridge, J.W. (2006) Ventral Pallidum Firing Codes Hedonic Reward: When a Bad Taste Turns Good. *Journal of Neurophysiology*, **96**, 2399–2409.

Tobler, P.N., Dickinson, A., & Schultz, W. (2003) Coding of Predicted Reward Omission by Dopamine Neurons in a Conditioned Inhibition Paradigm. *The Journal of Neuroscience*, **23**, 10402–10410.

Tobler, P.N., Fiorillo, C.D., & Schultz, W. (2005) Adaptive Coding of Reward Value by Dopamine Neurons. *Science*, **307**, 1642–1645.

Tom, S.M., Fox, C.R., Trepel, C., & Poldrack, R.A. (2007) The Neural Basis of Loss Aversion in Decision-Making Under Risk. *Science*, **315**, 515–518.

Tremblay, L., Hollerman, J.R., & Schultz, W. (1998) Modifications of Reward Expectation-Related Neuronal Activity During Learning in Primate Striatum. *Journal of Neurophysiology*, **80**, 964–977.

Tremblay, L. & Schultz, W. (1999) Relative reward preference in primate orbitofrontal cortex. *Nature*, **398**, 704–708.

Tremblay, L. & Schultz, W. (2000) Modifications of Reward Expectation-Related Neuronal Activity During Learning in Primate Orbitofrontal Cortex. *Journal of Neurophysiology*, **83**, 1877–1885.

Tricomi, E., Balleine, B.W., & O'Doherty, J.P. (2009) A specific role for posterior dorsolateral striatum in human habit learning. *European Journal of Neuroscience*, **29**, 2225–2232.

Tsujimoto, S., Genovesio, A., & Wise, S.P. (2009) Monkey Orbitofrontal Cortex Encodes Response Choices Near Feedback Time. *The Journal of Neuroscience*, **29**, 2569–2574.

Turner, K.M., Svegborn, A., Langguth, M., McKenzie, C., & Robbins, T.W. (2022) Opposing Roles of the Dorsolateral and Dorsomedial Striatum in the Acquisition of Skilled Action Sequencing in Rats. *The Journal of Neuroscience*, **42**, 2039–2051.

Turner, R.S. & DeLong, M.R. (2000) Corticostriatal Activity in Primary Motor Cortex of the Macaque. *The Journal of Neuroscience*, **20**, 7096–7108.

Tversky, A. & Kahneman, D. (1992) Advances in prospect theory: Cumulative representation of uncertainty. *Journal of Risk and Uncertainty*, **5**, 297–323.

Ungerleider, L.G. & Haxby, J.V. (1994) 'What' and 'where' in the human brain. *Current Opinion in Neurobiology*, **4**, 157–165.

Ungless, M.A., Magill, P.J., & Bolam, J.P. (2004) Uniform Inhibition of Dopamine Neurons in the Ventral Tegmental Area by Aversive Stimuli. *Science*, **303**, 2040–2042.

Van Der Kooy, D. & Hattori, T. (1980) Single subthalamic nucleus neurons project to both the globus pallidus and substantia nigra in rat. *Journal of Comparative Neurology*, **192**, 751–768.

Vieitas-Gaspar, N., Soares-Cunha, C., & Rodrigues, A.J. (2025) From valence encoding to motivated behavior: A focus on the nucleus accumbens circuitry. *Neuroscience & Biobehavioral Reviews*, **172**, 106125.

von Neumann, J., Morgenstern, O., & Rubinstein, A. (1944) *Theory of Games and Economic Behavior (60th Anniversary Commemorative Edition)*. Princeton University Press.

Voorn, P., Gerfen, C.R., & Groenewegen, H.J. (1989) Compartmental organization of the ventral striatum of the rat: Immunohistochemical distribution of enkephalin, substance P, dopamine, and calcium-binding protein. *Journal of Comparative Neurology*, **289**, 189–201.

Wallis, J.D. & Miller, E.K. (2003) Neuronal activity in primate dorsolateral and orbital prefrontal cortex during performance of a reward preference task. *European Journal of Neuroscience*, **18**, 2069–2081.

Walton, M.E., Devlin, J.T., & Rushworth, M.F.S. (2004) Interactions between decision making and performance monitoring within prefrontal cortex. *Nature Neuroscience*, **7**, 1259–1265.

West, A.R. & Grace, A.A. (2002) Opposite Influences of Endogenous Dopamine D_1 and D_2 Receptor Activation on Activity States and Electrophysiological Properties of Striatal Neurons: Studies Combining *In Vivo* Intracellular Recordings and Reverse Microdialysis. *The Journal of Neuroscience*, **22**, 294–304.

White, I.M. & Wise, S.P. (1999) Rule-dependent neuronal activity in the prefrontal cortex. *Experimental Brain Research*, **126**, 315–335.

Wichmann, T., Bergman, H., & DeLong, M.R. (1994) The primate subthalamic nucleus. I. Functional properties in intact animals. *Journal of Neurophysiology*, **72**, 494–506.

Wichmann, T. & DeLong, M.R. (2003) Pathophysiology of Parkinson's Disease: The MPTP Primate Model of the Human Disorder. *Annals of the New York Academy of Sciences*, **991**, 199–213.

Wilson, C.J. & Groves, P.M. (1980) Fine structure and synaptic connections of the common spiny neuron of the rat neostriatum: A study employing intracellular injection of horseradish peroxidase. *Journal of Comparative Neurology*, **194**, 599–615.

Wu, Y., Richard, S., & Parent, A. (2000) The organization of the striatal output system: a single-cell juxtacellular labeling study in the rat. *Neuroscience Research*, **38**, 49–62.

Yacubian, J., Gläscher, J., Schroeder, K., Sommer, T., Braus, D.F., & Büchel, C. (2006) Dissociable Systems for Gain- and Loss-Related Value Predictions and Errors of Prediction in the Human Brain. *The Journal of Neuroscience*, **26**, 9530–9537.

Yasuda, M. & Hikosaka, O. (2015) Functional territories in primate substantia nigra pars reticulata separately signaling stable and flexible values. *Journal of Neurophysiology*, **113**, 1681–1696.

Yelnik, J. (2002) Functional anatomy of the basal ganglia. *Movement Disorders*, **17**, S15–S21.

Yelnik, J., Francis, C., Percheron, G., & Tandéa, D. (1991) Morphological taxonomy of the neurons of the primate striatum. *Journal of Comparative Neurology*, **313**, 273–294.

Yelnik, J., François, C., Percheron, G., & Heyner, S. (1987) Golgi study of the primate substantia nigra. I. Quantitative morphology and typology of nigral neurons. *The Journal of Comparative Neurology*, **265**, 455–472.

Yelnik, J. & Percheron, G. (1979) Subthalamic neurons in primates: A quantitative and comparative analysis. *Neuroscience*, **4**, 1717–1743.

Yelnik, J., Percheron, G., & François, C. (1984) A Golgi analysis of the primate globus pallidus. II. Quantitative morphology and spatial orientation of dendritic arborizations. *J of Comparative Neurology*, **227**, 200–213.

Yeterian, E.H. & Van Hoesen, G.W. (1978) Cortico-striate projections in the rhesus monkey: The organization of certain cortico-caudate connections. *Brain Research*, **139**, 43–63.

Yin, H.H. & Knowlton, B.J. (2006) The role of the basal ganglia in habit formation. *Nature Reviews Neuroscience*, **7**, 464–476.

Yin, H.H., Mulcare, S.P., Hilário, M.R.F., Clouse, E., Holloway, T., Davis, M.I., Hansson, A.C., Lovinger, D.M., & Costa, R.M. (2009) Dynamic reorganization of striatal circuits during the acquisition and consolidation of a skill. *Nature Neuroscience*, **12**, 333–341.

Yoshida, S., Nambu, A., & Jinnai, K. (1993) The distribution of the globus pallidus neurons with input from various cortical areas in the monkeys. *Brain Research*, **611**, 170–174.

Young, C.B., Reddy, V., & Sonne, J. (2023) Neuroanatomy, Basal Ganglia. In *StatPearls*. StatPearls Publishing, Treasure Island (FL).

Yuste, R. (2015) From the neuron doctrine to neural networks. *Nat Rev Neurosci*, **16**, 487–497.

Zahm, D.S. (1989) The ventral striatopallidal parts of the basal ganglia in the rat—II. Compartmentation of ventral pallidal efferents. *Neuroscience*, **30**, 33–50.

Zahm, D.S. & Heimer, L. (1988) Ventral striatopallidal parts of the basal ganglia in the rat: I. Neurochemical compartmentation as reflected by the distributions of neurotensin and substance P immunoreactivity. *The Journal of Comparative Neurology*, **272**, 516–535.

Zahm, D.S. & Heimer, L. (1990) Two transpallidal pathways originating in the rat nucleus accumbens. *The Journal of Comparative Neurology*, **302**, 437–446.

Zheng, T. & Wilson, C.J. (2002) Corticostriatal Combinatorics: The Implications of Corticostriatal Axonal Arborizations. *Journal of Neurophysiology*, **87**, 1007–1017.

Ziemssen, T. & Reichmann, H. (2007) Non-motor dysfunction in Parkinson's disease. *Parkinsonism & Related Disorders*, **13**, 323–332.